TECHNISCHE UNIVERSITÄT WIEN
Vienna University of Technology

DIPLOMARBEIT

EVALUATION OF IGNITION CONDITIONS FOR A HYDROGEN PEROXIDE BASED MICRO PROPULSION SYSTEM

Ausgeführt am Institut für

Verfahrenstechnik, Umwelttechnik und Technische Biowissenschaften der
Technischen Universität Wien

In Zusammenarbeit mit der
FOTEC Forschungs- und Technologietransfer GmbH

unter Betreuung von
Ao.Univ.Prof. Dipl.-Ing. Dr.techn. Franz Winter
Technische Universität Wien

Dr.-Ing. Alexander Woschnak
FOTEC Forschungs- und Technologietransfer GmbH

durch
Ing. Markus Schiebl, BSc
0225960
Vorgartenstraße 221/5/11, 1020 Wien

_____   _____
Datum   Unterschrift

DECLARATION

I declare that this thesis is my own work and has not been submitted in any form for another degree or diploma at any university or other institution of tertiary education. Information arrived from the published or unpublished work of others has been acknowledged in the text and a list of references is given.

Vienna,

Markus Schiebl

ACKNOWLEDGMENTS

This work is dedicated to Sonja, Lennard Pau and Lilli Marleen, without whose support it would not have been completed.

KURZFASSUNG

Derzeit verwendete Treibstoffe für Mono- und Zweikomponenten-treibstoffsysteme wie Hydrazin, NTO, und MMH sind hochgiftig und daher teuer zu realisieren. Sogenannte grüne Treibstoffe haben zunehmendes Interesse in Zeiten mit abnehmendem Budget für Weltraummissionen geweckt. Sie versprechen eine signifikante Verringerung der gesamten Entwicklungs-und Betriebskosten bei gleicher oder besserer Leistung. FOTEC GmbH entwickelt für die Europäischen Weltraumorganisation ESA ein 1 Newton Flüssigkeits-antriebssystem welches ausschließlich mit grünen Treibstoffen betrieben wird. Eine der wichtigsten Eigenschaften welche untersucht wurde betraf die Zündfähigkeit und Zünd-Bedingungen dieser neuen Treibstoffe. Für das untersuchte System wurde Wasserstoffperoxid (87 Gew.%) als Oxidationsmittel verwendet. Kerosin wurde als Brennstoff ausgewählt und auf seine Eignung für ein solches Antriebssystem untersucht. Die Selbstzündfähigkeit in Gegenwart von zersetztdem Wasserstoffperoxid, dh Wasserdampf und Sauerstoff, wurde experimentell untersucht. Im Gegensatz zu reinen hypergolen Mischungen zündet ein Gemisch aus Kohlenwasserstoff und Sauerstoff nicht spontan bei Kontakt, sondern erfordert gut definierte Randbedingungen hinsichtlich Druck und Temperatur. Selbstzündung ist abhängig von verschiedenen physikalisch-chemischen Parametern wie der Art der Reaktanten, Reaktionskinetik, Vordruck, anfängliche Temperatur und Wärmeübertragungsprozess. Zusätzlich ist für Mikro-Propulsion Systeme die Selbstentzündfähigkeit stark vom Brennkammeroberflächen-zu Brennkammervolumenverhältnis abhängig. Ein analytisches nichtadiabatisches Selbstentzündungsmodell für einen geblockten und nichtgeblockten Durchflussreaktor wurde entwickelt mit der Annahme einer chemischen Ein-Schritt- Reaktion und unter Berücksichtigung einer Verweilzeitverteilung der Treibstoffe. Besonderes Augenmerk liegt auf dem Druck-Temperatur-Zündverhalten in Korrelation zu der Brennraumgeometrie wie Brennraumvolumen und Brennraumdurchmesser. Das analytische Modell zeigt sehr gute Übereinstimmung mit der Druck-Temperatur-Korrelationsfunktion für ein zersetztes Wasserstoffperoxid/Kerosin Gemisch welche von Walder in den frühen 1950er Jahren vorgeschlagen wurde, bei der der Zündverzug proportional zu der charakteristischen Brennkammerlänge, L^*, angenommen wurde. Für die Modellvalidierung, wurde eine Versuchsaufbau und eine segmentierte Brennkammer entwickelt, die es erlaubt, systematisch die Selbstzündbedingungen zu untersuchen, wobei der Brennkammervordruck,

Einspritztemperatur und Massenfluss des Treibstoffgemisches unabhängig voneinander variirt werden konnte.

ABSTRACT

Currently used propellants for mono- and bipropellant systems such as hydrazine, NTO, and MMH are highly toxic and therefore expensive to be implemented. So-called green propellants have drawn increasing interest in times with decreasing budgets for space missions and development tasks. They are promising a significant reduction of the overall development and operational costs at similar or better performance. FOTEC GmbH is developing a 1 N bipropellant thruster system operating exclusively with green propellants under contract of the European Space Agency. One of the main properties to be investigated is the ignition capability and ignition conditions of such new propellants. For the investigated system hydrogen peroxide (87 wt%) is used as oxidizer. Kerosene is selected as fuel and their suitability is investigated for such a propulsion system. Their auto- ignition capability (quasi-hypergolicity) in the presence of decomposed hydrogen peroxide (i.e. steam and oxygen) shall be investigated experimentally. In contrast to pure hypergolic mixtures, the present auto-ignitable mixture of hydrocarbon/oxygen does not spontaneously ignite when they come into contact but necessitates well defined initial conditions with regard to pressure and temperature. Auto-ignition is dependent on various physicochemical parameters such as the type of reactants, reaction kinetics, initial pressure, initial temperature, and heat transfer process. Additionally for Micro-Propulsion systems the auto-ignition phenomenon is a strong function of the combustion chamber surface-to-volume ratio. An analytical non-adiabatic auto-ignition model of the ignition conditions for a choked and non-choked flow reactor has been developed assuming a one-step single forward chemical reaction and with consideration of a residence time distribution of the propellants. Special focus is laid on the pressure temperature ignition behavior in correlation to the combustion chamber geometry. The analytical model shows well accordance to the pressure-temperature correlation function for a decomposed hydrogen peroxide/kerosene fuel mixture proposed by Walder in the early 1950s whereas the ignition delay is proportional to the characteristic chamber length, L^*, of the engine. For the model validation, an experimental setup and a segmented combustion chamber was developed which allows to systematically investigate the auto-ignition conditions whereas the initial pressure, initial temperature and mass flow can

be varied independently and with easy variation of the combustion chamber geometry.

CONTENTS

LIST OF FIGURES

LIST OF TABLES

NOMENCLATURE

Roman

$\vec{a}$	Eigenvector
$\vec{a}^{\mu}$	External force on molecules of kind μ per unit mass
A'	Frequency factor independent from temperature
A''	Empirical constant
A^*	Throat area
A	Area
b	Impact parameter
Bo	Bodenstein number
c_p^{μ}	Specific heat of species μ
$\left\langle c_p\big|_{T_0} \right\rangle_{mix}$	Specific heat of mixture at temperature T_0
C_i	Initial concentration
C_O	Outlet concentration
$C_I,\ C_{II},$	Fit coefficients
d_e	Orifice diameter
$D_C,\ D_3$	Combustion chamber diameter
D_2	Combustion chamber inlet diameter
D_d	Droplet diameter
E_A	Activation energy
$f(t)$	Residence time distribution
f^{μ}	Velocity distribution function of species μ
F_{Th}	Thrust force
$G(\varepsilon_r)$	Boltzmann energy distribution
h	Rearward facing step high
h_i	Specific enthalpy of specie i [J/kg]
$\tilde{h}^{\mu}$	Specific enthalpy of specie μ [J/mol]
I_{sp}	Specific impulse
J,j	Volumetric flow
$\tilde{J}$	Frequency factor
J_j	Frequency factor for species j
k	Specific reaction rate coefficient

k_1	Specific reaction rate coefficient at initiation
k_2, k_3, k_4	Specific reaction rate coefficient at chain-branching
k_g, k_5, k_6	Specific reaction rate coefficient at gas termination
k_w, k_7	Specific reaction rate coefficient at wall termination
k_f	Specific reaction rate coefficient for forward reaction
k_B	Bolzmann constant
L	Reactor length
L^*	Characteristic chamber length
L_r	Reattachment length
L_C	Combustion chamber length
m'	Fit coefficient
$\dot{m}$	Mass flow
$\dot{m}_{evap}$	Evaporated mass flow
$m_I, \ m_{II}$	Fit coefficients
m^μ	Mass of one molecule of species μ
$\mathfrak{M}$	Molar mass
M_i	Chemical species
$[M_i]$	Concentration of species M_i
n'_A, n'_B	Densities of molecules of type A and B (particle density)
n_{M_i}	Amount of substance M_i
N'	Total number of species (reactants+products)
$N_{Avogadro}$	Avogadro constant
N	Number of cells
Nu	Nusselt number
p	Pressure
p_e	Back pressure
P_{st}	Steric factor
Pr	Prandtl number
P_{ij}	Total stress tensor
q_j	Heat flux in j direction
r_d	Droplet radius
r_{inj}	Fuel injector radius
R	Universal gas constant
Re	Reynolds number
R_I	Inner radius of swirl inlet
R_O	Outer radius of swirl inlet

S_i	Inner surface
S_o	Outer surface
S	Swirl number
t	Time
t_{ig}	Ignition time
t_{res}	Residence time
t_{evap}	Remaining evaporation time regarding to combustion chamber
$\widehat{t}_{evap}$	Overall evaporation time
t'_{evap}	Evaporation time prior the combustion chamber
t'	Residence time of a PFR
T	Temperature
T_{ad}	Adiabatic flame temperature
T^*	Minimal temperature
T_w	Wall temperature
T_∞	Ambient temperature
T_{boil}	Boiling point temperature of fuel
U	Perimeter
U'	Fit coefficient
v_e	Exit velocity
v_{rel}	Relative velocity
v_c	Relative velocity along the line of centers
v_r	Radial velocity
$\vec{\boldsymbol{v}}$	Velocity vector
V	Molecular velocity
V_C	Combustion chamber volume
$\dot{V}$	Volumetric flow
$\vec{\boldsymbol{x}}$	Position vector
Y	Mole fraction

Greek

α	Imapct angle
α',β_j	Reaction rate exponent
γ	Adiabatic coefficient of the gas mixture
Γ_{ij}	Viscous stress tensor
Δh_r	Heat of reaction per mole

ΔH_r	Overall heat of reaction
$\Delta h_f^{(i)}$	Standard enthalpy of formation
ε	Nondimensional energy
ε_c	Energy associated with motion along the line of centers
ε_{rel}	Energy of relative motion
ε^*	Threshold energy
ζ	Recirculation number
ζ'	Longitudinal diffusion coefficient
η, η', η''	Multiplication factor in the chain branching cycle
η_{cr}	Critical multiplication factor
η_C	Combustor efficiency
ϑ	Swirl angle
Θ	Nondimensional temperature
λ'	Eigenvalue
λ	Heat conduction
μ	Reduced mass
μ'	Viscosity coefficient
μ''	Second viscosity coefficient
μ'''	Bulk viscosity coefficient
ν_i'	Stoichiometric coefficient of the reactants
ν_i''	Stoichiometric coefficient of the products
ϖ	Rel. wt% H_2O_2
ρ	Density
σ_c	Collision cross section
$\sigma_{reaction}$	Reaction cross section
τ	Nondimensional time
τ_{ig}	Nondimensinal ignition time
τ_{sh}	Shear layer residence time
τ_η^*	Kinetic time for fuel and CO oxidation
τ_{eb}	Droplet evaporation time
Φ	Residence time factor
ϕ	Equivalence ratio
χ	Heat transfer coefficient
χ_o	Heat transfer coefficient from chamber surface to ambient
ω	Reaction rate

Subscripts & Superscripts

max	Maximum
0	Initial
mix	Mixture
F	Fuel
O_2	Oxygen
Ox	Oxidizer
$stoich$	Stoichiometric
μ	Species

Acronyms

LEO	Low Earth Orbit
NTO	Nitrogen Tetroxide
MMH	Mono Methyl Hydrazine
NTC	Negative Temperature Coefficient
CSTR	Continuous Stirred Tank Reactor
PFR	Plug Flow Reactor
RTD	Residence Time Distribution

1

INTRODUCTION

1.1 Motivation

Micro chemical propulsion is a candidate technology with the potential to fill the near term performance gap in the market for micro-satellites, defined by the lack of proposed systems providing an I_{sp} in the range 100-300s Such a system could conceivably be used for such tasks as orbit modification in micro and nano-satellites, end-of-life de-orbit manoeuvring, LEO (low Earth orbit) drag compensation, manoeuvring for satellite inspection and so on. Micro-satellites have very strong constraints in mass, volume, and available electrical power. Therefore, all the subsystems have to be miniaturised, in particular the propulsion systems.

Conventionally engineered miniature propulsion systems does not provide a suitable solution to meet this constraints and subsequently to accomplish above space missions because typically these propulsion systems are expensive solutions, using toxic propellants that, which necessitates special storage requirements and in many cases do not scale favourable to the size demanded by small satellite technology [1]. Thus interests are directed towards toxic-free and environmental benign properties for space propulsion fuels which will become more and more attractive for future space missions.

High concentration hydrogen peroxide and kerosene have been proposed as one of the most promising alternatives for the toxic nitrogen tetroxide (NTO) and mono methyl hydrazine (MMH) bipropellant currently in use, due to the high volumetric specific impulse, low toxicity, as well as abundant and non-expensive supply of hydrogen peroxide and kerosene composite [2]. If this composite can be made auto-ignitable, then it is even more attractive, because in this way the design of engines and the handling of rocket systems can be simplified to a quite greater extent, while at the same time, the rocket engines

can be restarted for a great number of times, without the use of an ignition source which needs power for operation.

Auto-ignition is dependent on various physicochemical parameters such as the type of reactants, rate coefficient, initial pressure, initial temperature, heat transfer process ect. Furthermore for micro propulsion systems the auto-ignition phenomenon becomes strongly dependent on the combustion chamber surface to volume ratio. The rate of heat generated by the chemical reaction is dependent on the heat of formation of the reactants and products, temperature regime where the reaction takes place and the activation energy. The ignition delay consists of two separated delays. The physical delay controlled by the boiling point, the volatility and the droplet size of the reactants and the chemical delay controlled by the rate coefficient, activation energy and temperature. For instance Qasim Sarwar Khan et. al. [3], studied experimentally the effects of high ambient pressure and temperatures on the auto ignition delay times of isolated kerosene fuel droplets. They showed that the auto ignition delay times decreases with an increase in both temperature and pressure and the delay times follows a exponential function similar to the Arrhenius expression. All this facts makes a deeper study of the ignition and chemical process necessary particularly for the design of micro propulsion systems.

2

CHEMICAL KINETICS

2.1 Rates of reaction

A stoichiometric relation describing a one-step single forward chemical reaction of arbitrary complexity can be represented by the equation [4]
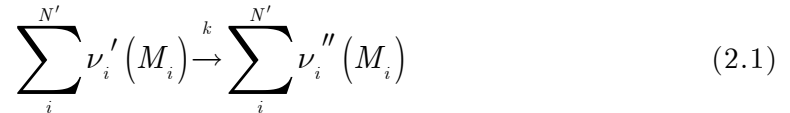
$$\sum_i^{N'} \nu_i' \left(M_i \right) \xrightarrow{k} \sum_i^{N'} \nu_i'' \left(M_i \right) \tag{2.1}$$

where ν_i' ist he stoichiometric coefficient of the reactants, ν_i'' is the stoichiometric coefficient of the products, M is an arbitrary specification of all chemical species, and N' is the total number of species. If a species represented by M_i does not occur as a reactant or product, its ν_i equals zero. For the reaction in equation (2.1) there exists a relationship among changes in amount of substance for all species. If $\mathrm{d}n_{M_i}$ denotes the change of the amount of substance M_i, then equation (2.1) states that,

$$\frac{\mathrm{d}n_{M_i}}{\left(\nu_i'' - \nu_i' \right)} = \frac{\mathrm{d}n_{M_j}}{\left(\nu_j'' - \nu_j' \right)}$$

$$\Rightarrow \frac{1}{\left(\nu_i'' - \nu_i' \right)} \frac{\mathrm{d}n_{M_i}}{\mathrm{d}t} = \frac{1}{\left(\nu_j'' - \nu_j' \right)} \frac{\mathrm{d}n_{M_j}}{\mathrm{d}t} \tag{2.2}$$

$$\Rightarrow \frac{1}{\left(\nu_i'' - \nu_i' \right)} \frac{\mathrm{d}\left[M_i \right]}{\mathrm{d}t} = \frac{1}{\left(\nu_j'' - \nu_j' \right)} \frac{\mathrm{d}\left[M_j \right]}{\mathrm{d}t} = \omega$$

where $[M_i]$ and $[M_j]$ represents the concentration of species M_i respectively M_j. Since ω is species independent, it can be defined as the reaction rate of equation (2.1). Then the phenomenological law of mass action, which is

confirmed experimentally, states that ω is proportional to the product of the concentrations of the reacting chemical species, where each concentration is raised to a power equal to the corresponding stoichiometric coefficient; that is,

$$\omega = k(T) \prod_{i}^{N'} [M_i]^{\nu_i'} \qquad (2.3)$$

where k is the specific reaction rate coefficient. The overall order of the reaction is given by $\sum_{i}^{N'} \nu_i'$. Then with equation (2.3) the rate of change of the concentration of a given species i is given by,

$$\frac{d[M_i]}{dt} = (\nu_i'' - \nu_i')k(T) \prod_{j}^{N'} [M_j]^{\nu_j'} = \tilde{\omega}_i \qquad (2.4)$$

Since ν_i'' moles of M_i are formed for every ν_i' moles of M_i consumed. In many systems M_i can be formed not only from a single-step reaction, but also from many different steps, leading to a rather complex formulation of the overall rate. However, for a single step reaction, $\sum_{i}^{N'} \nu_i'$ not only represents the overall order of the reaction, but also the molecularity, which is defined as the number of molecules that interact in the reaction step. If a complex reaction scheme is approximated by a global one step reaction (equation 2.5) the concept of molecularity is not appropriate and the overall order can take various values including fractional ones.

$$\begin{bmatrix} A + B \rightarrow I_1 \\ I_1 + A \rightarrow I_2 \\ I_2 + I_1 \rightarrow I_3 \\ . \\ . \\ . \\ I_i + I_{i-1} \rightarrow C \end{bmatrix} \Rightarrow [A + B \rightarrow C] \qquad (2.5)$$
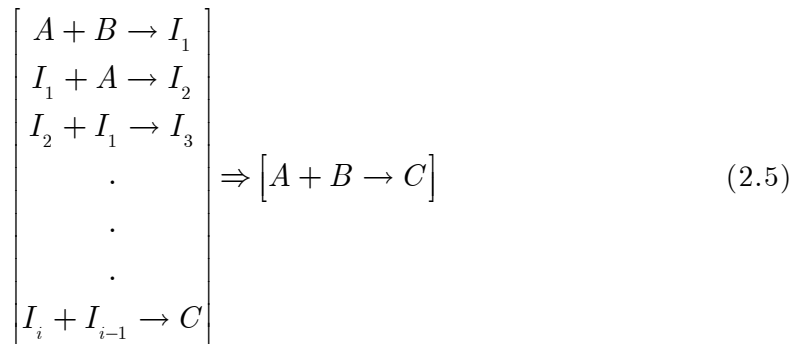
Therefore if a complex reaction scheme is approximated by a global one step reaction the rate of change of the concentration of a given species i can be approximated by,

$$\frac{\mathrm{d}[M_i]}{\mathrm{d}t} = \tilde{J}'(\phi)k(T)\prod_{j}^{N'}[M_j]^{\alpha'_j}$$
$$\tilde{J}'(\phi) = f(\phi)$$

(2.6)

where the rate of change of the concentration of a given species i can be dependent on the equivalence ration, e.g. the chain branching process of Jet-A is strongly controlled by hydrocarbon hydroperoxide species which is directly proportional to the fuel concentration.

2.2 Determination of the specific reaction-rate coefficient by collision theory

The specific reaction rate coefficient can be derived quantitatively from simple collision theory. It is the simplest explanation of the Arrhenius expression and it shows that chemical reactions take place via collisions [5,6]. The collision rate between two dissimilar species per unit volume is given by,

$$Z_{AB} = \sigma_c v_{rel} n'_A n'_B = N^2_{Avogadro}\sigma_c v_{rel}[A][B]$$

(2.7)

where v_{rel} is the relative velocity and n'_A, n'_B are the densities of molecules of type A and B, $[A]$ and $[B]$ are the concentrations of type A and B, and σ_c is given by the collision cross section. The chemical reaction rate assuming a bimolecular reaction $(A + B \rightarrow D)$ is given by the empirical equation (see equation 2.3),

$$\mathrm{reaction\ rate} = k[A][B]$$

(2.8)

If it is assumed that a chemical reaction takes place via molecular collisions, the rate constant is defined as (equation 2.7),

$$k = N^2_{Avogadro} \sigma_{reaction} v_{rel} \tag{2.9}$$

where σ_c is replaced by $\sigma_{reaction}$ to account the fact that not all collisions will lead to a reaction. The reaction cross section can be written as,

$$\sigma_{reaction} = \sum_i \sigma_c \left(b_i + \Delta b \right) - \sigma_c \left(b_i \right) = \sum_i^{b_{max}} \frac{\sigma_c \left(b_i + \Delta b \right) - \sigma_c \left(b_i \right)}{\Delta b} \Delta b$$

$$\Rightarrow \sigma_{reaction} = \int_0^b \frac{d\sigma_c \left(b' \right)}{d b'} d b' \tag{2.10}$$

where b is equal to the impact parameter. For simplicity the reactants can be approximated as spheres. Furthermore it is assumed that a reaction will occur only if the energy, when evaluated using the relative velocity along the line between the centers of the spheres, exceed a particular value, ε^*, because glancing collisions for a given velocity will be less effective in causing reaction than head-on collisions (figure 1).
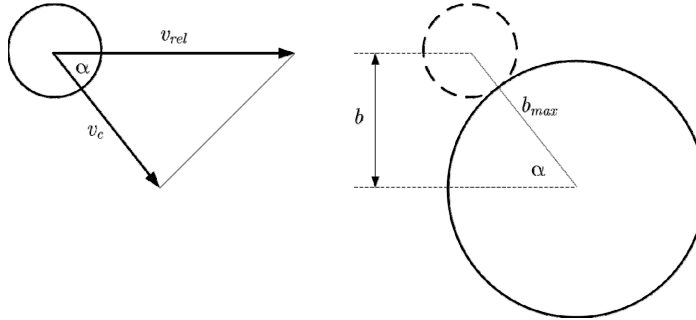
Fig. 1: Energy dependence of the reaction cross section

From figure 1 follows that the velocity along the line of centers is given by,

$$v_c = v_{rel} \cos \alpha \tag{2.11}$$

The energy associated with motion along the line of centers is then,

$$\varepsilon_c = \frac{1}{2} \mu v_c^2 = \frac{1}{2} \mu v_{rel}^2 \cos^2 \alpha = \frac{1}{2} \mu v_{rel}^2 \left(1 - \sin^2 \alpha \right) = \varepsilon_{rel} \left(1 - \frac{b^2}{b_{max}^2} \right) \tag{2.12}$$

where μ represents the reduced mass. Reaction occurs only if $\varepsilon_c \geq \varepsilon^*$. Therefore from equation (2.12) follows for b,

$$b^2 \leq b_{max}^2 \left(1 - \frac{\varepsilon^*}{\varepsilon_{rel}}\right) \tag{2.13}$$

The hard-sphere cross section is given by,

$$\sigma_c = \pi b^2 \Rightarrow \frac{d\sigma_c(b)}{db} = 2\pi b \tag{2.14}$$

Hence the reaction cross section becomes (equation 2.10),

$$\sigma_{reaction} = \int_0^{b_{max}\sqrt{\left(1-\frac{\varepsilon^*}{\varepsilon_r}\right)}} 2\pi b' db' = \pi b_{max}^2 \left(1 - \frac{\varepsilon^*}{\varepsilon_{rel}}\right) \tag{2.15}$$

Thus the reaction rate constant is given by,

$$k(\varepsilon_r) = N_{Avogadro}^2 \pi b_{max}^2 \left(1 - \frac{\varepsilon^*}{\varepsilon_{rel}}\right) v_{rel} \tag{2.16}$$

The mean reaction rate constant $k(T)$ then is given by averaging over the Boltzmann energy distribution which is given by,

$$G(\varepsilon_{rel}) d\varepsilon_{rel} = 2\pi \left(\frac{1}{\pi k_B T}\right)^{3/2} \sqrt{\varepsilon_{rel}} \exp\left(-\frac{\varepsilon_{rel}}{k_B T}\right) d\varepsilon_{rel} \tag{2.17}$$

Therefore $k(T)$ is given by noting that $\frac{1}{2}\mu v_{rel}^2 = \varepsilon_{rel}$,

$$k\left(T\right) = N_{Avogadro}^2 \, 2\pi \left(\frac{1}{\pi k_B T}\right)^{3/2} \int\limits_{\varepsilon^*}^{\infty} \pi b_{\max}^2 \left(1 - \frac{\varepsilon^*}{\varepsilon_{rel}}\right)\sqrt{\frac{2\varepsilon_{rel}}{\mu}} \sqrt{\varepsilon_{rel}} \, \exp\left(-\frac{\varepsilon_{rel}}{k_B T}\right) \mathrm{d}\varepsilon_{rel}$$

$$k\left(T\right) = N_{Avogadro}^2 \, 2\pi^2 b_{\max}^2 \left(\frac{1}{\pi k_B T}\right)^{3/2} \left(\frac{2}{\mu}\right)^{1/2} \int\limits_{\varepsilon^*}^{\infty} \left(\varepsilon_{rel} - \varepsilon^*\right)\exp\left(-\frac{\varepsilon_{rel}}{k_B T}\right) \mathrm{d}\varepsilon_{rel}$$

$$k\left(T\right) = N_{Avogadro}^2 \, \pi b_{\max}^2 \left(\frac{8 k_B T}{\pi \mu}\right)^{1/2} \int\limits_{\varepsilon^*}^{\infty} \frac{\left(\varepsilon_{rel} - \varepsilon^*\right)}{k_B T}\exp\left(-\frac{\varepsilon_{rel}}{k_B T}\right)\frac{\mathrm{d}\varepsilon_{rel}}{k_B T}$$

$$(2.18)$$

Premultiply the integral by $\exp(-\varepsilon^*/k_B T)$, multiplay the integrand by $\exp(+\varepsilon^*/k_B T)$, and transform variables by letting $x \equiv \left(\varepsilon_{rel} - \varepsilon^*\right)/k_B T$, the specific rate constant becomes,

$$k\left(T\right) = N_{Avogadro}^2 \, \pi b_{\max}^2 \left(\frac{8 k_B T}{\pi \mu}\right)^{1/2} \exp\left(-\frac{\varepsilon^*}{k_B T}\right)\int\limits_{0}^{\infty} x \exp\left(-x\right)\mathrm{d}x \qquad (2.19)$$

The integral in equation (2.19) can be shown to be unity. Hence the specific rate constant is given by,

$$k\left(T\right) = N_{Avogadro}^2 \, \pi b_{\max}^2 \left(\frac{8 k_B T}{\pi \mu}\right)^{1/2} \exp\left(-\frac{\varepsilon^*}{k_B T}\right) \qquad (2.20)$$

Simple collision theory suffers, however, in that it usually overestimates the absolut magnitude of k. The reason is that for most reactions, the reactants must have favourable orientations for reaction, even when the collision supplies sufficient energy along the line of centers. For this reason a so-called steric factor, P_{st}, with $P_{st} < 1$, is included to equation (2.20). Thus the specific rate constant becomes,

$$k\left(T\right) = N_{Avogadro}^2 \, P_{st} \, \pi b_{\max}^2 \left(\frac{8 k_B T}{\pi \mu}\right)^{1/2} \exp\left(-\frac{\varepsilon^*}{k_B T}\right) \qquad (2.21)$$

From equation (2.21) it is noted that the result in equation (2.21) is very similar to the Arrhenius form, $k = A\exp\left(-E_A{}'\big/k_B T\right)$ except that ε^* is not exactly equal to E_A, which can be shown as follows.

The activation energy E_A, can be defined from the Arrhenius expression as,

$$E_A{}' = k_B T^2 \frac{\partial \ln k(T)}{\partial T} \tag{2.22}$$

Inserting equation (2.21) into equation (2.22) leads to,

$$\varepsilon^* = E_A{}' - \frac{1}{2} k_B T \tag{2.23}$$

Hence the specific reaction rate constant becomes,

$$
\begin{aligned}
k(T) &= N_{Avogadro}^2 P_{st} \pi b_{max}^2 \left(\frac{8k_B T}{\pi\mu}\right)^{1/2} \exp\left(\frac{1}{2}\right)\exp\left(-\frac{E_A{}'}{k_B T}\right) \\
&= \tilde{J}\exp\left(-\frac{E_A{}'}{k_B T}\right) \\
&= \tilde{J}\exp\left(-\frac{E_A{}' N_{Avogadro}}{RT}\right) = \tilde{J}\exp\left(-\frac{E_A}{RT}\right)
\end{aligned}
\tag{2.24}
$$

3

IGNITION THEORY

Ignitions have been studied extensive in the past both theoretically and experimentally in approximately homogeneous chemical system by introducing reactants into a preheated vessel, by use of shock-tube techniques in which a shock wave produces compression, and by a piston-driven adiabatic compression to achieve a rapid increase of temperature. Several publications [7-26] gives a selected overview of combustion and ignition studies in the past 40 years. In these experiments measurable rates of reaction, and reaction histories are recorded which are initiated by a temperature increase with the objective of ascertaining, for example, whether the heat-release rate eventually experiences an abrupt increase that would be classified as an ignition, and –if so- the time that elapses before this increase occurs (the ignition time).

3.1 Branched-chain ignition

In most reaction mechanisms there are present small concentration of highly reactive intermediate species that participate and are regenerated in a sequence of reactions. It is through the participation of these species, called the chain carriers, that the reactants are converted to the products. Chain reactions can be further classified into straight-chain and branched-chain reaction. Branched chain reactions are characterised by a net production of chain carriers for each cycle of reaction instead of a straight chain reaction where a net production of chain carriers does not occur. This accumulation of chain carriers in the case of a branched chain reaction, leads to an extremely rapid rate of the overall reaction, which may eventually culminate into an ignition. To illustrate the conditions under which a system that includes chain propagating, chain branching, and chain termination steps can generate an ignition, a simplified generalized kinetic model is introduced which describes the behaviour of an

explosive mixture in response to changes in pressure and temperature. It can be given by [4],

$$
\begin{aligned}
nR &\xrightarrow{k_1} C & &\text{Initiation} \\
R+C &\xrightarrow{k_2} \eta C + P & &\text{Chain-branching cycle} \\
C+R+R &\xrightarrow{k_g} P & &\text{Gas termination} \\
C &\xrightarrow{k_w} I & &\text{Surface termination}
\end{aligned}
\tag{3.1}
$$
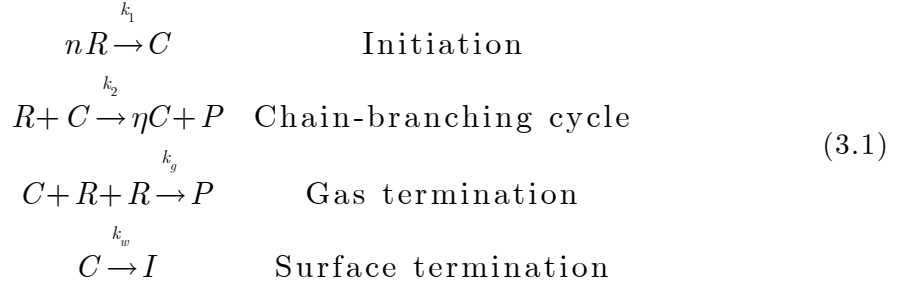
where C represents the chain carrier, R is equal to any arbitrary reactant species, P signifies a product species, I are minor intermediates and η is the multiplication factor in the chain branching cycle which is greater than one , $\eta > 1$, for chain branching reaction. The gas termination reaction is a three-body process while that of surface termination is a one-body process, e.g. the recombination of radicals which is given by $2O \rightarrow O_2$ or $2H \rightarrow H_2$. The rate of production of C is then given by,

$$
\frac{\mathrm{d}[C]}{\mathrm{d}t} = k_1 [R]^n + (\eta - 1)k_2 [R][C] - k_g [R]^2 [C] - k_w [C]
\tag{3.2}
$$

which becomes after further algebra,

$$
\frac{\mathrm{d}[C]}{\mathrm{d}t} = k_1 [R]^n + (\eta - \eta_{cr})k_2 [R][C]
\tag{3.3}
$$

with,

$$
\eta_{cr} = 1 + \frac{k_g [R]^2 + k_w}{k_2 [R]}
\tag{3.4}
$$

Equation (3.3) shows that $[C]$ varies exponentially with time, growing for $(\eta - \eta_{cr}) > 0$ and decaying otherwise.

Consequently the condition for the occurance of branched-chain ignition corresponds to the situation of[†],

$$\eta > \eta_{cr} \qquad (3.5)$$

where η_{cr} is the critical multiplication factor at which the mixture becomes explosive. Equation (3.4) and (3.5) show that ignition is favored for small η_{cr}, which corresponds to situations of fast chain-branching reactions (large k_2) and/or slow chain-termination reactions (small k_g and k_w), as is physically reasonable. Furthermore, since $[R]$ is proportional to the system pressure p, η_{cr} shows following behaviour,

$$\eta_{cr} = \begin{cases} 1 + \dfrac{k_w}{k_2[R]} = \infty & p \to 0 \\ 1 + \dfrac{k_g[R]}{k_2} = \infty & p \to \infty \end{cases} \qquad (3.6)$$

Thus ignition is not possible at either very low or very high pressures. The reason is that as the gas density decreases with $p \to 0$, the chain cycle becomes less efficient because it requires the collision between two molecules. The wall termination reaction, however, depends only on the concentration of the chain carrier and therefore becomes more efficient. The net effect is the tendency to inhibit ignition. Similar, as $p \to \infty$, the increase in density favors the three-body gas termination reaction as compared to the two-body chain-branching reaction, hence again inhibiting ignition. Since the creation of chain carriers requires energy, the chain-branching reaction is endothermic and is more sensitive to temperature variation in that it is characterizes by a large activation energy. On the other hand, the gas and wall termination reactions are not temperature sensitive, implying that k_g and k_w are nearly constants and therefore the associated activation energies can be taken to be identically zero. Thus with increasing temperature, η_{cr} decreases and the gas becomes more explosive. It should be noted that the termination reactions are highly

---

[†] It is also possible to determine the ignition condition by the rate of formation of the products and using the steady-state approximation for the chain carrier concentration [27], since this is accompanied by an extensive heat release. The necessary η is then determined by building the limit of $[C] = \infty$

exothermic because of the release of energy from the activated radicals. The above behaviour can be represented by a schematic C-shaped ignition limit curve shown in figure 2.
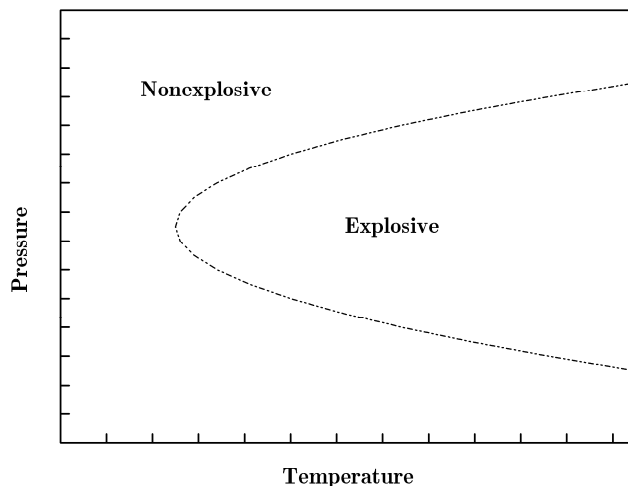
Fig. 2: C-shaped pressure-temperature ignition limits due to chain mechanisms

It demonstrates that, at a given temperature, continuously increasing the pressure of an initially non-explosive gas will cause it to become first explosive (1st limit) and then non-explosive again (2nd limit). Increasing temperature widens the range of explosivity. Usually there exists a 3rd ignition limit given by the thermal ignition process which is somewhat different from the chain ignition mechanism. Presently the requirement for ignition is the presence of some chain carriers that multiply through the branched-chain steps, leading to an explosive acceleration of the overall reaction rate. For the thermal ignition mechanism a critical mass of the reactive mixture has to be heated to a sufficient high temperature such that the rate of chemical heat generation exceeds that of heat loss through various transport mechanisms. The net heat accumulated further enhances the reaction rate and eventually leads to a thermal runaway situation. It should be noted, however, that the chain and thermal mechanisms are usually related in that the creation of chain carriers through the endothermic chain-branching reactions requires energy and therefore the presence of heating. Furthermore, the rapid increase in the radical concentration will lead to the initiation of some highly exothermic, chain-termination reactions and hence the eventual thermal runaway.

Pressure-temperature ignition limits for higher hydrocarbons shows usually a much more complex behaviour because of the tremendous number of reaction propagation and termination steps, e. g., the reaction mechanism of n-decane consist of 209 species and 1673 reversible reactions [28]

3.1.1 Hydrocarbon oxidation at low to intermediate temperatures

In this section the oxidation of hydrocarbons at low- to intermediate temperatures ($<$1000 K) are described because of its relevance to ignition. Figure 3 shows the complex ignition limits in a schematic pressure-temperature diagram.
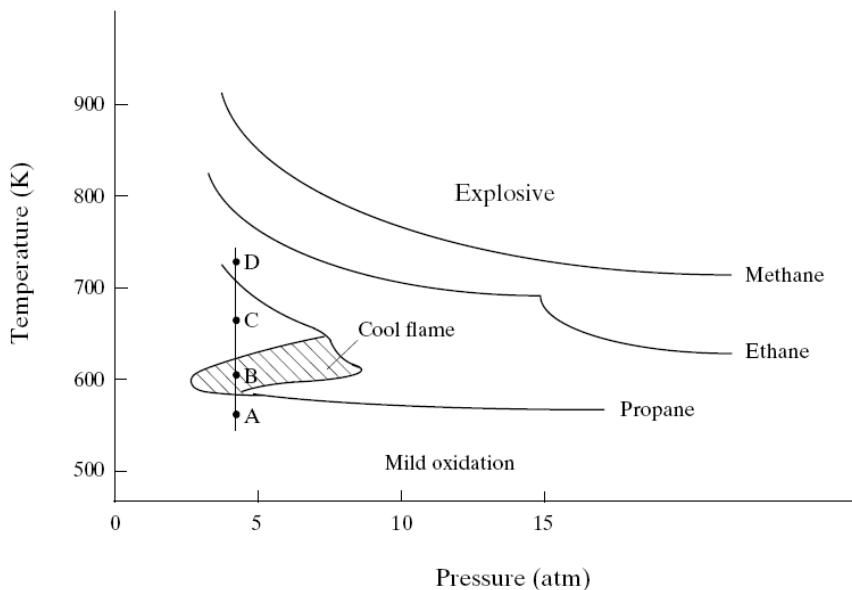
Fig. 3: Ignition limits of methane, ethane, and propane [21]

As demonstrated in figure 3 two physical properties of an explosive gas mixture can be determined. First, the homogeneous ignition temperature decreases with increasing aliphatic hydrocarbon size, indicating that the tendency of ignition is higher for higher hydrocarbons. This can be explained by examining the C-H bond dissociation energy of methane, ethane, and higher aliphatic hydrocarbons. The C-H bonds in methane are 4 kcal/mol stronger than those of ethane, whereas the C-H bonds in ethane are 2-3 kcal/mol stronger than the secondary C-H bonds, which exists only in propane and higher aliphatic

36

hydrocarbons. Since the ignition process depends on the initial attack of the hydrocarbon molecules by O_2 and consequently by active radicals, the difference in bond energy is translated into the difference in the activation energy of these reactions. As a result, it is more difficult to abstract an hydrogen atom from methane than from ethane, and from ethane than from the higher hydrocarbons. A higher temperature is thus needed to make a methane-oxygen mixture explosive. Second, the ignition boundary varies from simple p-T relationship in methane oxidation, to more complex behaviours in higher hydrocarbon oxidation. For methane, the ignition temperature varies smoothly and decreases monotonically with increasing pressure. In the case of ethane, the ignition temperature first shows a slow decrease as pressure increases, then a sharp decline with further increase in pressure. For higher aliphatic hydrocarbons, the ignition p-T diagram is more complex. For a fixed pressure, e.g., along ABCD, the following is observed with increasing temperature. First, there is no observable change in the mixture at A, where the temperature is below T≈530 K. This low-temperature regime is one of chemical synthesis that produces oxygen-containing organic molecules. Oxidation in this regime can only occure through the agency of initiators or catalyst; without them the homogeneous oxidation rates are negligible slow. With increasing temperature the "cool flame" regime is reached, point B. Their reaction rates are generally much lower than those of high-temperature oxidation, and the reaction consume only 5-10% of hydrocarbons. Cool flames may also occure in periodic manner. That is, during the passage of a cool flame, the temperature can be raised by 100-200K. The increase in temperature, however, rapidly slows down the reaction. With simultaneous heat loss, e.g., due the walls of the vessel, the mixture is then cooled. This continues until a sufficient low temperature is reached such that the reaction is again facilitated. The cycle thus repeats itself. Consistent with the periodic behaviour of the cool flame is that when the system temperature is increased from B to C, the reactions slow down until a complete stop. Such a temperature dependence is often called the negative temperature coefficient (NTC) for the reaction rate. With further increase in temperature from C to D at around 700K, the spontaneous thermal ignition is preceded. Figure 4 shows experimental data [12] on the ignition delay of heptane-oxygen-nitrogen mixtures behind reflected shock waves, demonstrating the existence and influence of the NTC regime.
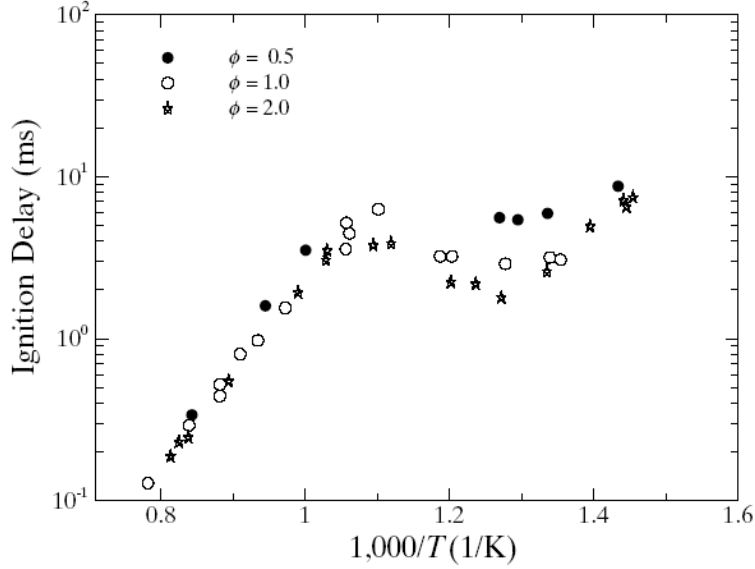
Fig. 4: n-Heptane oxidation behind reflected shock waves [12]

The cool flame behaviour, and the associated negative temperature coefficient for the reaction rate, can be described by following mechanism. Initiation comes from the reaction between fuel and molecular oxygen where R is a function group (e.g., C_3H_7),

$$RH + O_2 \rightarrow R + HO_2 \quad (S1) \tag{3.7}$$
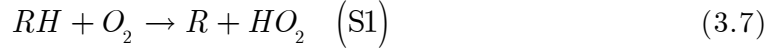
producing R, which further reacts with oxygen according to

$$
\begin{align}
R + O_2 + M &\rightleftharpoons RO_2 + M & (S2) \\
R + O_2 &\rightarrow olefin + HO_2 & (S3) \\
RO_2 + RH &\rightarrow RO_2H + R & (S4) \\
\end{align}
$$

$$RO_2H + M \rightarrow RO + OH + M \quad (S5)$$

$$RH + (OH, HO_2, RO) \rightarrow R + (H_2O, H_2O_2, ROH) \quad (S6)$$

(3.8)
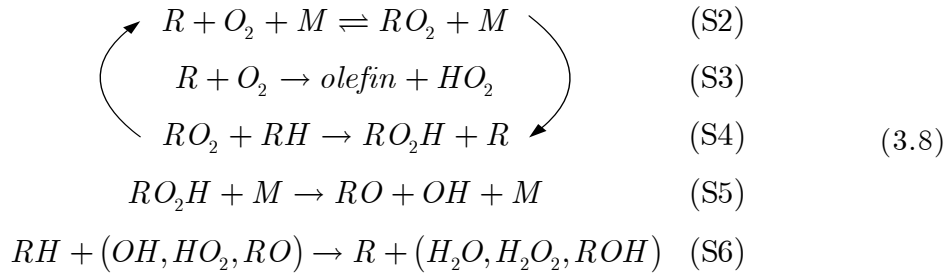
Thus it is seen that the reaction between R and O_2 can proceed in two path. The first is a radical propagation path, involving an exothermic step (S2) with 39 kcal/mol energy release, followed by equation (S4), which generates the radicals R to feed step two (S2). The RO_2H decomposes readily to two radical species, RO and OH, and therefore produces a degenerate chain branching. This path is responsible for the oxidation process in a cool flame. Owing to its high endothermicity, the chain initiating reaction is not an important route to

formation of the radical R. The important generation step of R is a radical attack on the fuel, and the fastest rate of attack is by the hydroxyl radical, OH, since this reaction step is highly exothermic owing to the creation of water as a product (S6). Generally the hydroxyl radical, OH, becomes the predominant attacker of the fuel which leads to ignition. Therefore the ignition mechanism is governed by the building process of the OH pool. In the second path involving equation (S3), an olefin forms with 9 kcal/mol heat release. The hydoperoxyl radical, HO_2 reacts with RH to form H_2O_2, which is a metastable species below 750K, and hence does not contribute to chain branching. When the temperature is increased to above 600 K, reaction step three (S3) becomes increasingly fast, but step two (S2) slows down because k_{S2} tends to decrease with increasing temperature, and its reverse reaction also becomes progressively more important. As a result, the amount of RO_2 that can be fed to step four (S4) decreases rapidly. The production rate of RO_2H decreases to the extent that the subsequent chain-branching step five (S5) which produces the necessary hydroxyl radical stops, and the overall reaction will eventually shut itself off. Generally the competition between the reactions,

$$
\begin{aligned}
R + O_2 + M &\rightleftharpoons RO_2 + M \quad \text{(S2)} \\
R + O_2 &\rightarrow olefin + HO_2 \quad \text{(S3)}
\end{aligned}
\tag{3.9}
$$
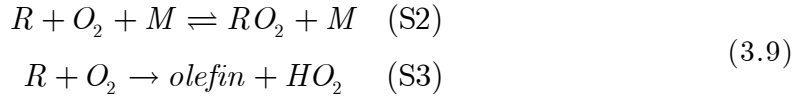
determine the behaviour of the cool flame, i.e., whether the sequence given as reaction (S1)-(S6) becomes chain branching or not. This explains the negative temperature coefficient for the reaction rate. Basically reaction step 3 (S3) becomes more dominate with increasing temperature and thus reaction step 2 (S2) becomes inhibit. With increasing temperature about 750 K, following branching reaction leads to massive build up of hydroxyl radical,

$$
\begin{aligned}
R + O_2 &\rightarrow olefin + HO_2 \quad &\text{(S3)} \\
RH + HO_2 &\rightarrow H_2O_2 + R \quad &\text{(S6)} \\
H_2O_2 + M &\rightarrow OH + OH + M \quad &\text{(S7)}
\end{aligned}
\tag{3.10}
$$
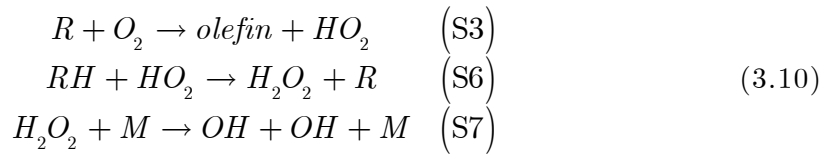
where the OH radicals can reproduce the HO_2, e.g. by [29],

$$
\begin{aligned}
H_2 + OH &\rightarrow H_2O + H \quad \text{(S8)} \\
H + O_2 + M &\rightarrow HO_2 + M \quad \text{(S9)}
\end{aligned}
\tag{3.11}
$$
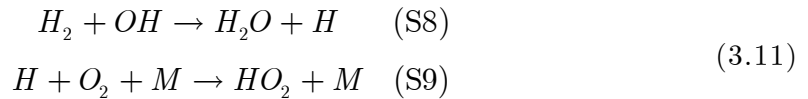
which leads to a full ignition and combustion of the mixture in contrast to the cool flame combustion.

3.1.1.1 Ignition limits

As mentioned in section 3.1 (figure 2) the p-T ignition diagram of a large hydrocarbon-air mixture is more complex than as given by figure 2. The real ignition behaviour of a large hydrocarbon-air mixture with respect to the pressure and temperature is schematically given by figure 5.
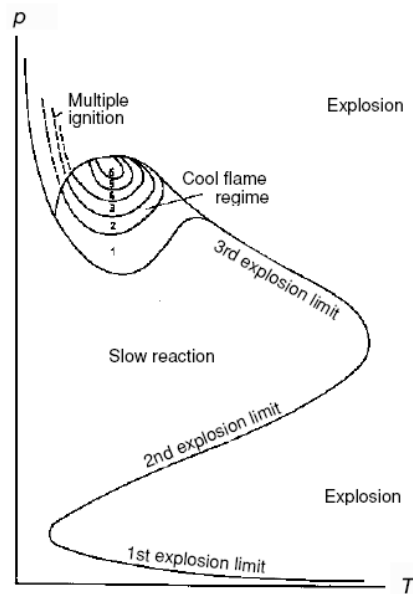
Fig. 5: Schematic ignition limits for hydrocarbons [24]

Certain general characteristics of this curve can be stated. First, the third limit of this curve can be explained by simple density considerations. The first limit reflects the wall effect and its role in chain destruction and the second limit can be explained by gas-phase production and destruction of radicals. Although the quantitative description of the shape of the boundaries of a p-T diagram for a specific gas mixture can only be performed by huge effort, the general shape of the three limits can be explained by reasonable hypotheses of mechanism. Since the reaction mechanism given by equation (3.1) cannot explain a p-T diagram as given by figure 5, the following phenomenological mechanism is introduced,

$$
\left.\begin{array}{l}
R + R' \xrightarrow{k_1} C_1 \quad \left(\text{S1}\right)
\end{array}\right\} \qquad \text{Initiation}
$$

$$
\left.\begin{array}{ll}
R + C_1 \xrightarrow{k_2} \eta C_1 + P & \left(\text{S2}\right) \\
R + R' + C_1 \xrightarrow{k_3} \eta' C_2 + I' & \left(\text{S3}\right) \\
\eta' C_2 \xrightarrow{k_4} \eta'' C_3 & \left(\text{S4}\right)
\end{array}\right\} \quad \text{Carrier generation}
$$

$$
\left.\begin{array}{ll}
C_{1,2,3} + R + R \xrightarrow{k_5} P & \left(\text{S5}\right) \\
C_{1,2,3} + R' \xrightarrow{k_6} P & \left(\text{S6}\right)
\end{array}\right\} \quad \text{Gas termination}
$$

$$
\left.\begin{array}{l}
C_{1,2,3} \xrightarrow{k_7} I \quad \left(\text{S7}\right)
\end{array}\right\} \quad \text{Surface termination}
$$

(3.12)
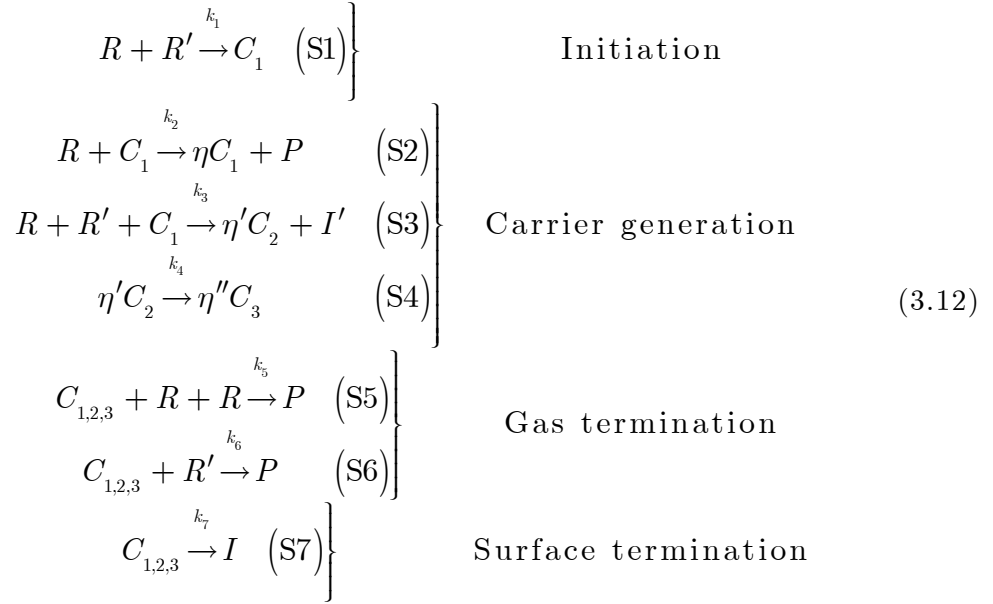
where $C_{1,2,3}$ represents the chain carriers, e.g. HO_2, H_2, OH, R and R' is equal to any arbitrary reactant species, e.g. C_3H_8, O_2, P is equal to a product species, I and I' are minor intermediates, η, η' and η'' are the multiplication factor in the chain branching cycle which $\eta > 1, \eta' > 1, \eta'' > \eta'$. Since the initiation step is high endothermic it is not an important route to form the chain carriers once the reaction system has created chain carriers by chain branching. Thus if one considers the different chain carriers as one global chain carrier $\left([C] = [C_1] = [C_2] = [C_3]\right)$ the chain carrier generation-, gas termination- and surface termination rate becomes,

$$
\frac{\mathrm{d}[C]}{\mathrm{d}t}\bigg|_{gen} = (\eta - 1) k_2(T)[R][C] + (\eta' - 1) k_3(T)[R][R'][C] + k_4(T)(\eta'' - \eta')[C]
$$

$$
\frac{\mathrm{d}[C]}{\mathrm{d}t}\bigg|_{gas} = k_5(T)[R][R][C] + k_6(T)[R'][C]
$$

$$
\frac{\mathrm{d}[C]}{\mathrm{d}t}\bigg|_{sur} = k_7(T)[C]
$$

(3.13)

Since the concentrations of the reactants are related to the pressure according to the ideal gas law $\left([R, R'] \propto a p_0\right)$

where a is a constant[†], equation (3.13) becomes with

$$k_3' = a^2 \left(\eta' - 1\right) k_3, k_2' = a \left(\eta - 1\right) k_2, k_4' = \left(\eta'' - \eta'\right) k_4, k_5' = a^2 k_5 \text{ and } k_6' = a k_6$$

$$\frac{1}{[C]} \frac{\mathrm{d}[C]}{\mathrm{d}t}\bigg|_{gen} = k_3'\left(T\right) p_0^2 + k_2'\left(T\right) p_0 + k_4'\left(T\right)$$

$$\frac{1}{[C]} \frac{\mathrm{d}[C]}{\mathrm{d}t}\bigg|_{gas} = k_5'\left(T\right) p_0^2 + k_6'\left(T\right) p_0 \qquad (3.14)$$

$$\frac{1}{[C]} \frac{\mathrm{d}[C]}{\mathrm{d}t}\bigg|_{sur} = k_7'\left(T\right)$$

Graphs for the carrier generation and carrier destruction are useful to explain the three ignition limits which depend on pressure. A plot of this type is schematically shown in figure 6.
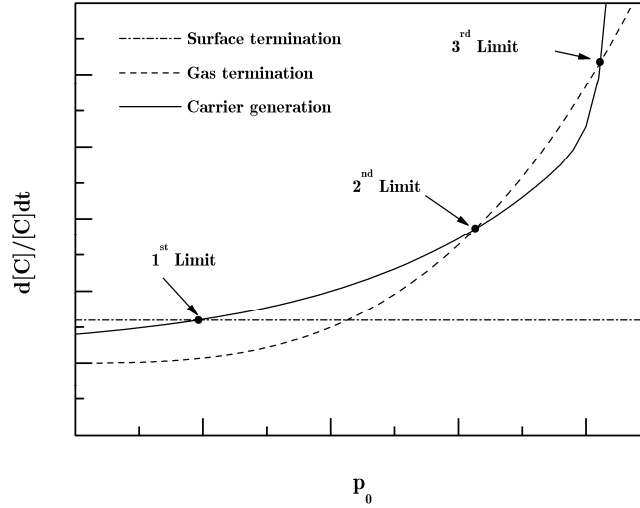
Fig. 6: Determination of ignition limits

The first ignition limit is given by,

$$k_3'\left(T\right) p_0^2 + k_2'\left(T\right) p_0 + k_4'\left(T\right) = k_7'\left(T\right) \qquad (3.15)$$

[†] Actually the reactant concentration decreases during the chemical reaction process, thus $[R, R'] \propto a p_0$ is a little bit misleading. However, this assumption is valid if one assumes a reactant flow into the reaction volume so that the reactant concentration is kept constant

Hence the first ignition limit becomes,

$$p_0 = \frac{-k_2'(T) \pm \sqrt{k_2'^2(T) - 4k_3'(T)\left[k_4'(T) - k_7'(T)\right]}}{2k_3'(T)} \qquad (3.16)$$

A real positive value for the initial pressure is only given if $k_4' < k_7'$. Hence the first ignition limit exists only if $k_4' < k_7'$. Since the carrier generation term is strictly monotonic increasing with pressure ($p_0 \in [0, \infty]$) ignition cannot be observed for initial pressures below the first ignition limit. This lack of ignition is the result of the free radicals being recombined to stable species by reactions on the walls of the vessel. These wall reactions break the chain, preventing the rapid buildup of radicals that leads to ignition. At lower pressures surface collisions become much more predominant than molecular collisions. The first ignition limit is a strong function of the vessel geometry and the chemical nature of the surface. When the pressure is above the first ignition limit the mixture ignites. This is a direct result of the gas phase chain carrier generation prevailing over the radical destruction. The second and third ignition limit are given similarily by,

$$k_3'(T)p_0^2 + k_2'(T)p_0 + k_4'(T) = k_5'(T)p_0^2 + k_6'(T)p_0 \qquad (3.17)$$

Thus the second and third ignition limit becomes,

$$p_0 = \frac{-\left[k_2'(T) - k_6'(T)\right] \pm \sqrt{\left[k_2'(T) - k_6'(T)\right]^2 - 4\left[k_3'(T) - k_5'(T)\right]k_4'(T)}}{2\left[k_3'(T) - k_5'(T)\right]}$$

$$(3.18)$$

Two real positive values for the initial pressure are only given if

$$\left[k_2'(T) - k_6'(T)\right]^2 > 4\left[k_3'(T) - k_5'(T)\right]k_4'(T), k_2' < k_6', k_3' > k_5' \qquad (3.19)$$

The second and third ignition limit is governed by the competition of chain branching and chain termination in the gas phase. Since the rates of carrier generation and destruction are functions of the temperature, the ignition limits

becomes a function of temperature as well. This behaviour is reflected in the p-T ignition diagram (figure 5) as following. The second and third limit comes closer with increasing temperature and above a critical temperature the carrier generation rate always prevails and the mixture is explosive for the complete pressure range. As mentioned above the third limit can be explained by simple density consideration. This can be understood as following. Reaction step (S3) and (S5) in equation (3.12) represents a three body collision (trimolecular reaction). For low pressures and since the density depends on pressure, for low densities, the production rate of chain carriers (S3) and consequently (S4), and the termination rate of chain carriers (S5) are insignificant for the reaction mechanism since the probability of a three body collision is very low for low pressures. Thus if reaction (S5) dominates in contrast to reaction (S2) the mixture will not ignite ($k_6' > k_2'$). Until the pressure is increased to a critical pressure, reaction step (S3) and subsequently (S4) rules the reaction mechanism which leads to an ignition for high pressures. A simpler explanation of the three ignition limits can be given if it is assumed that the trimolecular reaction (S5) is substituted by a bimolecular reaction as following,

$$C + R + R \xrightarrow{k_5} P \Rightarrow C + R \xrightarrow{k_5} P \tag{3.20}$$
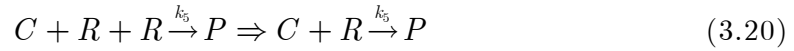
Therefore the gas termination rate in equation (3.14) becomes,

$$\frac{1}{[C]} \frac{\mathrm{d}[C]}{\mathrm{d}t}\bigg|_{gas} = k_6'(T) \, p_0 \tag{3.21}$$

Figure 7 shows schematic graphs of the new situation for the carrier production and termination rates.
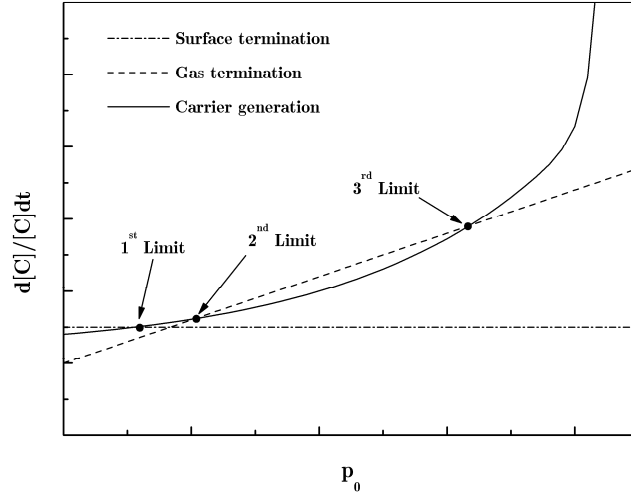
Fig. 7: Determination of ignition limits for the simplified reaction mechanism

Thus the second and third ignition limit are given by,

$$k_3'\left(T\right)p_0^{\ 2} + k_2'\left(T\right)p_0 + k_4'\left(T\right) = k_6'\left(T\right)p_0 \qquad (3.22)$$

Thus the second and third ignition limit becomes,

$$p_0 = \frac{-\left[k_2'\left(T\right) - k_6'\left(T\right)\right] \pm \sqrt{\left[k_2'\left(T\right) - k_6'\left(T\right)\right]^2 - 4k_3'\left(T\right)k_4'\left(T\right)}}{2k_3'\left(T\right)} \qquad (3.23)$$

Similar to the reaction mechanism given by equation (3.12) the production rate of chain carriers (S3) and consequently (S4) are insignificant for reaction mechanism since the probability of a three body collision is very low for low pressures. Therefore (S5) and (S6) together inhibit reaction step 2 (S2) and ignition fails. Until for high enough pressures the trimolecular reaction (S3) dominates and ignition occurs. The difference between the two hypothetic reaction mechanisms is given by the behaviour of the necessary pressure to reach the third limit. As it can be shown if the temperature decreases to a lower limit, T^*, the pressure becomes,

$$\lim_{T \to T^*} p_0 = \infty \qquad (3.24)$$

Where T^* is given by,

45

$$k_3{}'\left(T^*\right) = k_5{}'\left(T^*\right) \tag{3.25}$$

for the reaction mechanism given by equation (3.12). And for the simpler mechanism follows,

$$\lim_{T \to 0} p_0 = \infty \tag{3.26}$$

Basically although even the reaction mechanism is not known in detail, the three ignition limits can be explained by a hypothetic reaction mechanism given by equation (3.12).

3.2 Thermal ignition and model representation of the auto-ignition conditions for a flow reactor

In combustion, the definition of thermal ignition has been specialized to describe the spontaneous development of rapid rates of heat release by chemical reactions in initially nearly homogeneous systems. Pressure-wave generation usually follows but is not relevant to the definition. In addition to the branched-chain ignitions, there are thermal ignitions, which do not require complex chemical kinetics for their explanation but instead can be understood on the basis of a one-step approximation for the chemical reaction. They occur for high initial pressures typically above the magnitude of 10^5 Pa. Since overall rates of chemical reactions generally increase with increasing temperature, the heat release from an exothermic process may accelerate the rate by rising the temperature of the reacting mixture. The increased rate of reaction further increases the rate of heat release, leading to a rapid buildup of thermal energy in the system. The importance of the dependence of the rate upon temperature distinguishes thermal ignition from branched-chain ignition which may occur in isothermal systems. Thermal ignition has been discussed in various books and review articles [30-35]. These ignitions have been studied for both gaseous and condensed-phase reactants. In addition to being of fundamental interest to chemical kinetics, they are of practical concern in wide-ranging problems of fire and explosion safety. Statement of an appropriate model for describing thermal ignitions necessitates introduction of an energy balance. As a basis for a

simplified model that preserves homogeneity, the loss effect will be approximated by the employment of a phenomenological heat-transfer coefficient. Furthermore the concentrations of the fuel-oxidizer mixture are assumed to be constant.

3.2.1 The conservation equations for multicomponent chemically reacting gas mixtures

Most textbooks that present the conservation equations for multicomponent reacting gas mixtures without giving kinetic-theory derivations lack the generality needed for application to combustions. A notable expectation, recommended for study is [35]. Therefore the conservation equations for a multicomponent chemically reaction gas mixture based on kinetic theory derivations will be given in the proceeding section.

3.2.1.1 The generalized Bolzmann equation and the velocity distribution function

The kinetic theory derivation of a the fluid dynamical conservation equations fo a multicomponent chemically reacting gas mixture will be obtained from a physical derivation of the Bolzmann transport equation, followed by the identification of the hydrodynamic variables and the development of the equation of change [35]. In defining the velocity distribution function for molecules of species μ,

$$f^{\mu}\left(\vec{\boldsymbol{x}},\vec{\boldsymbol{v}},t\right)\mathrm{d}^3x\mathrm{d}^3v \tag{3.27}$$

will denote the probable number of molecules of type μ in the position range $\mathrm{d}^3x = \mathrm{d}x\mathrm{d}y\mathrm{d}z$ about the spatial position $\vec{\boldsymbol{x}}$ and with velocities in the range $\mathrm{d}^3v = \mathrm{d}v_x\mathrm{d}v_y\mathrm{d}v_z$ about the velocity $\vec{\boldsymbol{v}}$ at time t. The six dimensional space consisting of the coordinates $\left(\vec{\boldsymbol{x}},\vec{\boldsymbol{v}}\right)$ is called phase space. Molecules of species μ at position $\vec{\boldsymbol{x}}$ with velocity $\vec{\boldsymbol{v}}$ at time t would move in such a way that at a short time later $t+\mathrm{d}t$ its position would be $\vec{\boldsymbol{x}} + \vec{\boldsymbol{v}}\mathrm{d}t$ and its velocity would be

$\vec{v} + \vec{a}^{\mu}\mathrm{d}t$, where $\vec{a}^{\mu}$ is the external force on molecules of kind μ per unit mass of molecules of kind μ assuming no intermolecular collisions, unimolecular reactions, radiative transitions, ect. [35]. Therefore, the only μ molecules arriving at the phase-space position $\left(\vec{x} + \vec{v}\mathrm{d}t, \vec{v} + \vec{a}^{\mu}\mathrm{d}t\right)$ at time $t+\mathrm{d}t$ would be those at $\left(\vec{x}, \vec{v}\right)$ at time $t^{\dagger}$.

$$f^{\mu}\left(\vec{x} + \vec{v}\mathrm{d}t, \vec{v} + \vec{a}^{\mu}\mathrm{d}t, t + \mathrm{d}t\right)\mathrm{d}^{3}x\mathrm{d}^{3}v = f^{\mu}\left(\vec{x}, \vec{v}, t\right)\mathrm{d}^{3}x\mathrm{d}^{3}v \tag{3.28}$$

Since collisions and other similar events cause some molecules of type μ in the range $\left(\mathrm{d}^{3}x, \mathrm{d}^{3}v\right)$ about $\left(\vec{x}, \vec{v}\right)$ at time t to arrive at a phase space position outside of the range $\left(\mathrm{d}^{3}x, \mathrm{d}^{3}v\right)$ about $\left(\vec{x} + \vec{v}\mathrm{d}t, \vec{v} + \vec{a}^{\mu}\mathrm{d}t\right)$ at time $t+\mathrm{d}t$ denote by $\left(\delta f^{\mu}/\delta t\right)^{(-)}\mathrm{d}^{3}x\mathrm{d}^{3}v\mathrm{d}t$, and these events also cause some μ molecules not in $\left(\mathrm{d}^{3}x, \mathrm{d}^{3}v\right)$ about $\left(\vec{x}, \vec{v}\right)$ at time t to arrive in $\left(\mathrm{d}^{3}x, \mathrm{d}^{3}v\right)$ about $\left(\vec{x} + \vec{v}\mathrm{d}t, \vec{v} + \vec{a}^{\mu}\mathrm{d}t\right)$ at time $t+\mathrm{d}t$ denoted by $\left(\delta f^{\mu}/\delta t\right)^{(+)}\mathrm{d}^{3}x\mathrm{d}^{3}v\mathrm{d}t$ equation (3.28) is not valid and must be replaced by [35],

$$f^{\mu}\left(\vec{x} + \vec{v}\mathrm{d}t, \vec{v} + \vec{a}^{\mu}\mathrm{d}t, t + \mathrm{d}t\right)\mathrm{d}^{3}x\mathrm{d}^{3}v = f^{\mu}\left(\vec{x}, \vec{v}, t\right)\mathrm{d}^{3}x\mathrm{d}^{3}v + \frac{\delta f^{\mu}}{\delta t}\mathrm{d}^{3}x\mathrm{d}^{3}v\mathrm{d}t \tag{3.29}$$

where

$$\frac{\delta f^{\mu}}{\delta t} := \left(\frac{\delta f^{\mu}}{\delta t}\right)^{(+)} - \left(\frac{\delta f^{\mu}}{\delta t}\right)^{(-)} \tag{3.30}$$

is the net time rate of change of f^{μ} caused by collisions and other molecular processes. Passing to the limit $\mathrm{d}t \to 0$ in equation (3.29) shows that,

$$\frac{\partial f^{\mu}}{\partial t} + \vec{v} \cdot \vec{\nabla}_{x}f^{\mu} + \vec{a}^{\mu} \cdot \vec{\nabla}_{v}f^{\mu} = \frac{\delta f^{\mu}}{\delta t} \tag{3.31}$$

---

†It must be assumed that $\vec{a}$ is independent of $\vec{v}$ for the volume elements on both sides of this equation to be equal.

In which the subscripts x and v on the gradient operator distinguish derivatives with respect to spatial and velocity coordinates. Equtaion (3.31) is a generalization of Bolzmann transport equation.

3.2.1.2 Definition of fluid dynamical variables

The conventional variables of fluid dynamics are be defined as suitable integral over velocity space, weighted by the distribution function. For example, the total number of molecules of kind μ per unit spatial volume at $\left(\vec{x}, t\right)$ is given by,

$$n^{\mu}\left(\vec{x}, t\right) = \int_{-\infty}^{+\infty} f^{\mu}\left(\vec{x}, \vec{v}, t\right) \mathrm{d}^3 v \tag{3.32}$$

Thus the local average value of any property G of species μ is defined as,

$$\left\langle G^{\mu}\left(\vec{x}, t\right)\right\rangle = \frac{1}{n^{\mu}} \int_{-\infty}^{+\infty} G^{\mu}\left(\vec{x}, \vec{v}, t\right) f^{\mu}\left(\vec{x}, \vec{v}, t\right) \mathrm{d}^3 v \tag{3.33}$$

Therefore the average velocity of molecules of type μ is given by,

$$\left\langle \vec{v}\left(\vec{x}, t\right)\right\rangle^{\mu} = \frac{1}{n^{\mu}} \int_{-\infty}^{+\infty} \vec{v} f^{\mu}\left(\vec{x}, \vec{v}, t\right) \mathrm{d}^3 v \tag{3.34}$$

The mass weighted average velocity $\vec{v}^0$ of the mixture is given by,

$$\rho \vec{v}^0 = \sum_{\mu=1}^{N'} \rho^{\mu} \left\langle \vec{v}\right\rangle^{\mu} \tag{3.35}$$

where the total density is given by,

$$\rho = \sum_{\mu=1}^{N'} \rho^\mu = \sum_{\mu=1}^{N'} n^\mu m^\mu \tag{3.36}$$

where m^μ is the mass of one molecule of species μ. The mass weighted average velocity of the mixture is identified by the ordinary flow velocity of fluid mechanics. The difference between the molecular velocity $\vec{v}$ and the flow velocity $\vec{v}^0$ is,

$$\vec{V}\left(\vec{x},\vec{v},t\right) = \vec{v} - \vec{v}^0 \tag{3.37}$$

and the average value of $\vec{V}\left(\vec{x},\vec{v},t\right)$ which is equivalent to the diffusion velocity for species μ is given by,

$$
\begin{aligned}
\left\langle \vec{V}\left(\vec{x},\vec{v},t\right)\right\rangle^\mu &= \frac{1}{n^\mu}\int_{-\infty}^{+\infty} \vec{V}\left(\vec{x},\vec{v},t\right)f^\mu\left(\vec{x},\vec{v},t\right)\mathrm{d}^3v \\
&= \frac{1}{n^\mu}\int_{-\infty}^{+\infty}\left(\vec{v} - \vec{v}^0\right)f^\mu\left(\vec{x},\vec{v},t\right)\mathrm{d}^3v \\
&= \frac{1}{n^\mu}\int_{-\infty}^{+\infty}\vec{v}f^\mu\left(\vec{x},\vec{v},t\right)\mathrm{d}^3v - \vec{v}^0\frac{1}{n^\mu}\int_{-\infty}^{+\infty}f^\mu\left(\vec{x},\vec{v},t\right)\mathrm{d}^3v \\
&= \left\langle \vec{v}\right\rangle^\mu - \vec{v}^0
\end{aligned}
\tag{3.38}
$$

From equation (3.35) and (3.38) follows,

$$
\begin{aligned}
\sum_{\mu=1}^{N'} \rho^{\mu} \left\langle \vec{\boldsymbol{V}} \right\rangle^{\mu} &= \sum_{\mu=1}^{N'} \rho^{\mu} \left(\left\langle \vec{\boldsymbol{v}} \right\rangle^{\mu} - \vec{\boldsymbol{v}}^{0} \right) \\
&= \sum_{\mu=1}^{N'} \rho^{\mu} \left\langle \vec{\boldsymbol{v}} \right\rangle^{\mu} - \vec{\boldsymbol{v}}^{0} \sum_{\mu=1}^{N'} \rho^{\mu} \\
&= \rho \vec{\boldsymbol{v}}^{0} - \rho \vec{\boldsymbol{v}}^{0} \\
\\
&= 0
\end{aligned}
\tag{3.39}
$$

Unlike solids, in which transmission of forces between molecules is the dominant contributor to surface stresses, gases experience surface stresses primarily by migration of molecules with differing momenta across surfaces. The momentum of one molecule of type μ with the mass m^{μ} moving in the i direction relative to a coordinate system which moves with the velocity $\vec{\boldsymbol{v}}^{0}$ is given by,

$$
p_i^{\mu} = m^{\mu} V_i
\tag{3.40}
$$

Therefore the momentum per second of one molecule of type μ transported relative to $\vec{\boldsymbol{v}}^{0}$ in the j direction is given by,

$$
\left. \frac{dp_i^{\mu}}{dt} \right|_j = \left(m^{\mu} V_i \right) V_j
\tag{3.41}
$$

Thus the total momentum per second per spatial volume of μ molecules transported in the j direction is,

$$
\begin{aligned}
\left. \frac{d\tilde{p}_i^{\mu}}{dt} \right|_j &= \int_{-\infty}^{+\infty} m^{\mu} V_i V_j f^{\mu} \left(\vec{\boldsymbol{x}}, \vec{\boldsymbol{v}}, t \right) \mathrm{d}^3 v \\
&= n^{\mu} m^{\mu} \left\langle V_i V_j \right\rangle^{\mu}
\end{aligned}
\tag{3.42}
$$

This is equivalent to a momentum diffusion flux. From that follows that equation (3.42) has the physical meaning of a stress tensor for gases. Thus the stress tensor for species μ is defined by [38],

$$P_{ij}^{\mu} = n^{\mu}m^{\mu}\left\langle V_i V_j \right\rangle^{\mu} \tag{3.43}$$

The diagonal elements represent normal stresses and the off-diagonal elements are shear stresses. The total stress tensor is defined as,

$$P_{ij} = \sum_{\mu}^{N'} P_{ij}^{\mu} = \sum_{\mu}^{N'} n^{\mu}m^{\mu}\left\langle V_i V_j \right\rangle^{\mu} \tag{3.44}$$

The total absolute internal energy of one molecule of type μ travelling with velocity $\vec{V}$ relative to a coordinate system moving with velocity $\vec{v}^0$ is given by,

$$U^{\mu} = m^{\mu}\frac{1}{2}V_i V_i + U_{\dagger}^{\mu} \tag{3.45}$$

where $U_{\dagger}^{\mu}$ is the contribution to U^{μ} from rotational, vibrational and electronic degrees of freedom. The internal energy per unit mass of species μ is given by,

$$u^{\mu} = \frac{\left\langle U^{\mu} \right\rangle}{m^{\mu}} \tag{3.46}$$

where $\left\langle U^{\mu} \right\rangle$ is,

$$\left\langle U^{\mu} \right\rangle = \frac{1}{n^{\mu}}\left[\int_{-\infty}^{+\infty} m^{\mu}\frac{1}{2}V_i V_i f^{\mu}\left(\vec{x},\vec{v},t\right)\mathrm{d}^3 v + \int_{-\infty}^{+\infty} U_{\dagger}^{\mu} f^{\mu}\left(\vec{x},\vec{v},t\right)\mathrm{d}^3 v\right] \tag{3.47}$$

The definition of the energy diffusion flux in the j direction is similar to the definition of the momentum diffusion flux, equation (3.42), and becomes,

$$
\begin{aligned}
q_j^\mu &= \int_{-\infty}^{+\infty} U^\mu V_j f^\mu \left(\vec{x}, \vec{v}, t \right) \mathrm{d}^3 v \\
&= \int_{-\infty}^{+\infty} \left[m^\mu \frac{1}{2} V_i V_i \right] V_j f^\mu \left(\vec{x}, \vec{v}, t \right) \mathrm{d}^3 v + \int_{-\infty}^{+\infty} U_\dagger^\mu V_j f^\mu \left(\vec{x}, \vec{v}, t \right) \mathrm{d}^3 v \qquad (3.48) \\
&= n^\mu \left\langle U^\mu V_j \right\rangle^\mu
\end{aligned}
$$

q_j^μ is also called the heat flux for species μ in the j direction. Therefore the total heat flux is given by,

$$
q_j = \sum_{\mu=1}^{N'} q_j^\mu = \sum_{\mu=1}^{N'} n^\mu \left\langle U^\mu V_j \right\rangle^\mu \qquad (3.49)
$$

The final variable needed in the fluid equations is the mass of species μ per unit volume per second produced by chemical reactions $\tilde{\omega}^\mu$. From the definition of $\left(\delta f^\mu / \delta t \right)$, it is clear that the number of molecules of species μ per unit spatial volume per second produced by chemical processes is,

$$
\int_{-\infty}^{+\infty} \frac{\delta f^\mu}{\delta t} \mathrm{d}^3 v \qquad (3.50)
$$

whence it follows that,

$$
\tilde{\omega}^\mu = m^\mu \int_{-\infty}^{+\infty} \frac{\delta f^\mu}{\delta t} \mathrm{d}^3 v \qquad (3.51)
$$

3.2.1.3   Fluid equations derived from the Bolzmann transport equation

The fluid equations are obtained by multiplying the Bolzmann transport equation, equation (3.31), by an arbitrary function depending on velocity for species μ and integrating over velocity space. It is noted that $\vec{x}, \vec{v}$, and t are all independent variables in equation (3.31). Thus following equation of change is obtained,

$$
\int_{-\infty}^{+\infty} \frac{\delta f^{\mu}}{\delta t} \Psi^{\mu}\left(\vec{v}\right) \mathrm{d}^3 v = \int_{-\infty}^{+\infty} \frac{\partial f^{\mu}}{\partial t} \Psi^{\mu}\left(\vec{v}\right) \mathrm{d}^3 v
$$
$$
+ \int_{-\infty}^{+\infty} \vec{v} \cdot \left(\vec{\nabla}_{x} f^{\mu}\right) \Psi^{\mu}\left(\vec{v}\right) \mathrm{d}^3 v \qquad (3.52)
$$
$$
+ \int_{-\infty}^{+\infty} \vec{a}^{\mu} \cdot \left(\vec{\nabla}_{v} f^{\mu}\right) \Psi^{\mu}\left(\vec{v}\right) \mathrm{d}^3 v
$$

With the identity,

$$
\frac{\partial}{\partial t}\left(f^{\mu} \Psi^{\mu}\left(\vec{v}\right)\right) = \Psi^{\mu}\left(\vec{v}\right) \frac{\partial f^{\mu}}{\partial t} \qquad (3.53)
$$

the first term on the right hand side of equation (3.52) becomes,

$$
\int_{-\infty}^{+\infty} \frac{\partial f^{\mu}}{\partial t} \Psi^{\mu}\left(\vec{v}\right) \mathrm{d}^3 v = \frac{\partial}{\partial t} \int_{-\infty}^{+\infty} f^{\mu} \Psi^{\mu}\left(\vec{v}\right) \mathrm{d}^3 v = \frac{\partial}{\partial t}\left[n^{\mu} \left\langle \Psi^{\mu} \right\rangle\right] \qquad (3.54)
$$

With the identities,

$$
\begin{aligned}
\vec{\nabla}_{x} \cdot \left(f^{\mu} \vec{v}\right) &= \vec{v} \cdot \vec{\nabla}_{x} f^{\mu} \\
\vec{\nabla}_{x} \cdot \left(f^{\mu} \vec{v} \Psi^{\mu}\left(\vec{v}\right)\right) &= \Psi^{\mu}\left(\vec{v}\right) \vec{\nabla}_{x} \cdot \left(f^{\mu} \vec{v}\right) \\
&= \Psi^{\mu}\left(\vec{v}\right)\left(\vec{v} \cdot \vec{\nabla}_{x} f^{\mu}\right)
\end{aligned} \qquad (3.55)
$$

54

the second term on the right hand side of equation (3.52) becomes,

$$
\begin{aligned}
\int_{-\infty}^{+\infty} \vec{v} \cdot \left(\vec{\nabla}_{x} f^{\mu} \right) \Psi^{\mu} \left(\vec{v} \right) \mathrm{d}^3 v \;=\;& \int_{-\infty}^{+\infty} \vec{\nabla}_{x} \cdot \left(f^{\mu} \vec{v} \Psi^{\mu} \left(\vec{v} \right) \right) \mathrm{d}^3 v \\[2ex]
=\;& \vec{\nabla}_{x} \cdot \int_{-\infty}^{+\infty} \vec{v} \Psi^{\mu} \left(\vec{v} \right) f^{\mu} \mathrm{d}^3 v \\[2ex]
=\;& \vec{\nabla}_{x} \cdot \left[n^{\mu} \left\langle \Psi^{\mu} \vec{v} \right\rangle^{\mu} \right]
\end{aligned}
\tag{3.56}
$$

The third term on the right hand side of equation (3.52) becomes (considering that $\vec{a}^{\mu}$ is independent from velocity,

$$
\begin{aligned}
a_{j}^{\mu} \int_{-\infty}^{+\infty} \left(\partial_{v}^{j} f^{\mu} \right) \Psi^{\mu} \left(\vec{v} \right) \mathrm{d}^3 v \;=\;& a_{1}^{\mu} \iiint \left(\partial_{v}^{1} f^{\mu} \right) \Psi^{\mu} \left(v_1, v_2, v_3 \right) \mathrm{d}v_1 \mathrm{d}v_2 \mathrm{d}v_3 \\[2ex]
+\;& a_{2}^{\mu} \iiint \left(\partial_{v}^{2} f^{\mu} \right) \Psi^{\mu} \left(v_1, v_2, v_3 \right) \mathrm{d}v_1 \mathrm{d}v_2 \mathrm{d}v_3 \\[2ex]
+\;& a_{3}^{\mu} \iiint \left(\partial_{v}^{3} f^{\mu} \right) \Psi^{\mu} \left(v_1, v_2, v_3 \right) \mathrm{d}v_1 \mathrm{d}v_2 \mathrm{d}v_3 \\[2ex]
=\;& a_{1}^{\mu} \iint \left\{ \left[f^{\mu} \Psi^{\mu} \right]_{-\infty}^{+\infty} - \int_{-\infty}^{+\infty} f^{\mu} \partial_{v}^{1} \Psi^{\mu} \mathrm{d}v_1 \right\} \mathrm{d}v_2 \mathrm{d}v_3 \\[2ex]
+\;& ...
\end{aligned}
$$

$$
(3.57)
$$

with $\lim\limits_{\vec{v} \to \infty} f\left(\vec{v} \right) = 0$ follows,

$$a_j^\mu \int\limits_{-\infty}^{+\infty} \left(\partial_v^j f^\mu\right) \Psi^\mu\left(\vec{v}\right)\mathrm{d}^3 v \;=\; -a_j^\mu \int\limits_{-\infty}^{+\infty} f^\mu \partial_v^j \Psi^\mu\left(\vec{v}\right)\mathrm{d}^3 v$$

$$=\; -\vec{a}^\mu \cdot \left[n^\mu \left\langle \vec{\nabla}_v \Psi^\mu \right\rangle^\mu \right] \tag{3.58}$$

Thus the equation of change becomes for species μ,

$$\frac{\partial}{\partial t}\left[n^\mu \left\langle \Psi^\mu \right\rangle\right] + \partial_x^j\left[n^\mu \left\langle \Psi^\mu v_j \right\rangle^\mu\right] - n^\mu a_j^\mu\left[\left\langle \partial_v^j \Psi^\mu \right\rangle^\mu\right] = \int\limits_{-\infty}^{+\infty} \frac{\delta f^\mu}{\delta t}\Psi^\mu\left(\vec{v}\right)\mathrm{d}^3 v \tag{3.59}$$

The toatal equation of change for a fluid mixture is then given by,

$$\sum_{\mu=1}^{N'} \int\limits_{-\infty}^{+\infty} \frac{\delta f^\mu}{\delta t}\Psi^\mu\left(\vec{v}\right)\mathrm{d}^3 v \;=\; \sum_{\mu=1}^{N'} \frac{\partial}{\partial t}\left[n^\mu \left\langle \Psi^\mu \right\rangle\right]$$

$$+\; \sum_{\mu=1}^{N'} \partial_x^j\left[n^\mu \left\langle \Psi^\mu v_j \right\rangle^\mu\right] \tag{3.60}$$

$$-\; \sum_{\mu=1}^{N'} n^\mu a_j^\mu\left[\left\langle \partial_v^j \Psi^\mu \right\rangle^\mu\right]$$

Due to the linearity of the derivation operators, equation (3.60) is equivalent to,

$$\int\limits_{-\infty}^{+\infty} \sum_{\mu=1}^{N'} \frac{\delta f^\mu}{\delta t}\Psi^\mu\left(\vec{v}\right)\mathrm{d}^3 v \;=\; \frac{\partial}{\partial t}\left[\sum_{\mu=1}^{N'} n^\mu \left\langle \Psi^\mu \right\rangle\right]$$

$$+\; \partial_x^j\left[\sum_{\mu=1}^{N'} n^\mu \left\langle \Psi^\mu v_j \right\rangle^\mu\right] \tag{3.61}$$

$$-\; \sum_{\mu=1}^{N'} n^\mu a_j^\mu\left[\left\langle \partial_v^j \Psi^\mu \right\rangle^\mu\right]$$

For all microscopic processes certain quantities may be conserved. If Ψ^μ is such a quantity, then it is called a summational invariant which is given by,

$$\int\limits_{-\infty}^{+\infty} \sum_{\mu=1}^{N'} \frac{\delta f^\mu}{\delta t} \Psi^\mu\left(\vec{v}\right) = 0 \tag{3.62}$$

Equation (3.62) means that the change in the total Ψ^μ per unit volume per second due to microscopic processes vanishes. This will be valid for the total mass, momentum and energy of a macroscopic system if energy removed by radiation in collisions is neglected.

3.2.1.4   Macroscopic conservation equations

3.2.1.4.1   Species conservation

In deriving the species conservation, Ψ^μ will be set equal to unity, which is not a summational invariant, since the number of molecules need not be conserved in chemical reactions. With $\Psi^\mu = 1$ and equation (2.4) following relations are obtained,

$$\begin{aligned}
\left\langle \Psi^\mu \right\rangle &= \frac{1}{n^\mu} \int\limits_{-\infty}^{+\infty} f^\mu \mathrm{d}^3 v = 1 \\
\left\langle \Psi^\mu v_j \right\rangle^\mu &= \frac{1}{n^\mu} \int\limits_{-\infty}^{+\infty} v_j f^\mu \mathrm{d}^3 v = \left\langle v_j \right\rangle^\mu \\
\left\langle \partial_v^j \Psi^\mu \right\rangle^\mu &= \frac{1}{n^\mu} \int\limits_{-\infty}^{+\infty} \left(\partial_v^j 1 \right) f^\mu \mathrm{d}^3 v = 0 \\
\int\limits_{-\infty}^{+\infty} \frac{\delta f^\mu}{\delta t} \mathrm{d}^3 v &= \tilde{\omega}^\mu N_{Avogadro}
\end{aligned} \tag{3.63}$$

where $\tilde{\omega} N_{Avogadro}$ is the rate of change of the total number of molecules of species μ. Hence the equation of change, equation (3.61) for molecules of type μ becomes,

$$\frac{\partial}{\partial t}\left[n^{\mu}\right] + \partial_x^j \left[n^{\mu} \left\langle v_j \right\rangle^{\mu}\right] = \tilde{\omega}^{\mu} N_{Avogadro} \tag{3.64}$$

Multiplying equation (3.64) by the mass of one molecule of species μ gives,

$$\frac{\partial}{\partial t}\left[n^{\mu} m^{\mu}\right] + \partial_x^j \left[n^{\mu} m^{\mu} \left\langle v_j \right\rangle^{\mu}\right] = m^{\mu} \tilde{\omega}^{\mu} N_{Avogadro} \tag{3.65}$$

With equation (3.36) the species conservation becomes,

$$\frac{\partial}{\partial t}\left[\rho^{\mu}\right] + \partial_x^j \left[\rho^{\mu} \left\langle v_j \right\rangle^{\mu}\right] = \mathfrak{M}^{\mu} \tilde{\omega}^{\mu} \tag{3.66}$$

From equation (3.38) follows,

$$\left\langle V_j \right\rangle^{\mu} = \left\langle v_j \right\rangle^{\mu} - v_j^0 \tag{3.67}$$

With euation (3.67) the final species conservation becomes,

$$\frac{\partial}{\partial t}\left[\rho^{\mu}\right] + \partial_x^j \left[\rho^{\mu} v_j^0\right] = \mathfrak{M}^{\mu} \tilde{\omega}^{\mu} - \partial_x^j \left[\rho^{\mu} \left\langle V_j \right\rangle^{\mu}\right] \tag{3.68}$$

where the term $\partial_x^j \left[\rho^{\mu} \left\langle V_j \right\rangle^{\mu}\right]$ represents the divergence of a species diffusion flux.

3.2.1.4.2 Mass conservation

Summing equation (3.68) over μ and considering the linearity of the derivation operators the mass conservation is given by,

$$\frac{\partial}{\partial t}\sum_{\mu=1}^{N'}\rho^{\mu} + \partial_x^j \sum_{\mu=1}^{N'}\rho^{\mu} v_j^0 = \sum_{\mu=1}^{N'}\mathfrak{M}^{\mu} \tilde{\omega}^{\mu} - \partial_x^j \sum_{\mu=1}^{N'}\rho^{\mu} \left\langle V_j \right\rangle^{\mu} \tag{3.69}$$

Since mass is neither created nor destroyed by chemical reactions but only converted from one species to another, it follows,

$$\sum_{\mu=1}^{N'} \mathfrak{M}^{\mu} \tilde{\omega}^{\mu} = 0 \tag{3.70}$$

The last term on the right hand side of equation (3.69) becomes,

$$
\begin{aligned}
\partial_x^j \sum_{\mu=1}^{N'} \rho^{\mu} \left\langle V_j \right\rangle^{\mu} &= \partial_x^j \left[\sum_{\mu=1}^{N'} \rho^{\mu} \left(\left\langle v_j \right\rangle^{\mu} - v_j^0 \right) \right] \\
&= \partial_x^j \left[\sum_{\mu=1}^{N'} \rho^{\mu} \left\langle v_j \right\rangle^{\mu} - v_j^0 \sum_{\mu=1}^{N'} \rho^{\mu} \right] \\
&= \partial_x^j \left[\rho v_j^0 - v_j^0 \rho \right] = 0
\end{aligned} \tag{3.71}
$$

Therefore the final mass conservation equation becomes,

$$\frac{\partial}{\partial t} \rho + \partial_x^j \left(\rho v_j^0 \right) = 0 \tag{3.72}$$

3.2.1.4.3 Momentum conservation

In deriving the momentum conservation, Ψ^{μ} will be set equal to $m^{\mu} v_i$ in equation (3.61). Considering that the left hand side vanishes, following relations are obtained,

$$
\begin{aligned}
\left\langle \Psi^{\mu} \right\rangle &= \frac{1}{n^{\mu}} \int_{-\infty}^{+\infty} m^{\mu} v_i f^{\mu} \mathrm{d}^3 v = m^{\mu} \left\langle v_i \right\rangle^{\mu} \\
\left\langle \Psi^{\mu} v_j \right\rangle^{\mu} &= \frac{1}{n^{\mu}} \int_{-\infty}^{+\infty} m^{\mu} v_i v_j f^{\mu} \mathrm{d}^3 v = m^{\mu} \left\langle v_i v_j \right\rangle^{\mu} \\
\left\langle \partial_v^j \Psi^{\mu} \right\rangle^{\mu} &= \frac{1}{n^{\mu}} \int_{-\infty}^{+\infty} m^{\mu} \left(\partial_v^j v_i \right) f^{\mu} \mathrm{d}^3 v = m^{\mu} \delta_i^j
\end{aligned} \tag{3.73}
$$

Thus the equation of change becomes,

$$\frac{\partial}{\partial t}\sum_{\mu=1}^{N'} n^{\mu} m^{\mu}\left\langle v_i\right\rangle^{\mu} + \partial_x^j \sum_{\mu=1}^{N'} n^{\mu} m^{\mu}\left\langle v_i v_j\right\rangle^{\mu} - \sum_{\mu=1}^{N'} n^{\mu} a_j^{\mu} m^{\mu} \delta_i^j = 0 \qquad (3.74)$$

This is equivalent to,

$$\frac{\partial}{\partial t}\sum_{\mu=1}^{N'} \rho^{\mu}\left\langle v_i\right\rangle^{\mu} + \partial_x^j \sum_{\mu=1}^{N'} \rho^{\mu}\left\langle v_i v_j\right\rangle^{\mu} - \sum_{\mu=1}^{N'} \rho^{\mu} a_i^{\mu} = 0 \qquad (3.75)$$

With equations (3.67) equation (3.75) becomes,

$$\frac{\partial}{\partial t}\sum_{\mu=1}^{N'} \rho^{\mu}\left(\left\langle V_i\right\rangle^{\mu} + v_i^0\right) + \partial_x^j \sum_{\mu=1}^{N'} \rho^{\mu}\left\langle \left(\left\langle V_i\right\rangle^{\mu} + v_i^0\right)\left(\left\langle V_i\right\rangle^{\mu} + v_i^0\right)\right\rangle^{\mu} - \sum_{\mu=1}^{N'} \rho^{\mu} a_i^{\mu} = 0$$

$$(3.76)$$

The first term on the left hand side of equation (3.76) becomes,

$$
\begin{aligned}
\frac{\partial}{\partial t}\sum_{\mu=1}^{N'} \rho^{\mu}\left(\left\langle V_i\right\rangle^{\mu} + v_i^0\right) &= \frac{\partial}{\partial t}\left[\sum_{\mu=1}^{N'} \rho^{\mu}\left\langle V_i\right\rangle^{\mu} + v_i^0 \sum_{\mu=1}^{N'} \rho^{\mu}\right] \\
&= \frac{\partial}{\partial t}\left[\sum_{\mu=1}^{N'} \rho^{\mu}\left(\left\langle v_i\right\rangle^{\mu} - v_i^0\right) + v_i^0 \sum_{\mu=1}^{N'} \rho^{\mu}\right] \\
&= \frac{\partial}{\partial t}\left[\rho v_i^0 - \rho v_i^0 + v_i^0 \rho\right] \\
&= \frac{\partial}{\partial t}\left[v_i^0 \rho\right]
\end{aligned}
\qquad (3.77)
$$

The second term on the left hand side of equation (3.76) becomes,

$$\partial_x^j \sum_{\mu=1}^{N'} \rho^\mu \left\langle \left(\langle V_i \rangle^\mu + v_i^0 \right) \left(\langle V_i \rangle^\mu + v_i^0 \right) \right\rangle^\mu = \partial_x^j \left[\sum_{\mu=1}^{N'} \rho^\mu \left\langle V V_j \right\rangle^\mu + \sum_{\mu=1}^{N'} \rho^\mu v_i^0 v_j^0 \right]$$

$$+ \quad \partial_x^j \left[v_j^0 \sum_{\mu=1}^{N'} \rho^\mu \left\langle V_i \right\rangle^\mu + v_i^0 \sum_{\mu=1}^{N'} \rho^\mu \left\langle V_j \right\rangle^\mu \right]$$

$$= \quad \partial_x^j \left[\sum_{\mu=1}^{N'} P_{ij}^\mu + v_i^0 v_j^0 \sum_{\mu=1}^{N'} \rho^\mu \right]$$

$$(3.78)$$

Thus the equation of change becomes,

$$\frac{\partial}{\partial t} \left[\rho v_i^0 \right] + \partial_x^j \left[P_{ij} + \rho v_i^0 v_j^0 \right] - \sum_{\mu=1}^{N'} \rho^\mu a_i^\mu = 0 \tag{3.79}$$

applying the derivation operators and using the mass conservation equation, the final momentum conservation is given by,

$$\rho \left[\frac{\partial}{\partial t} + v_j^0 \partial_x^j \right] v_i^0 = -\partial_x^j P_{ij} + \sum_{\mu=1}^{N'} \rho^\mu a_i^\mu = \rho \frac{\mathrm{D}}{\mathrm{D}t} v_i^0 \tag{3.80}$$

This is equivalent to the mechanical energy conservation given by,

$$\rho \frac{\mathrm{D}}{\mathrm{D}t} \left(\frac{1}{2} v_i^0 v_i^0 \right) = -v_i^0 \partial_x^j P_{ij} + v_i^0 \sum_{\mu=1}^{N'} \rho^\mu a_i^\mu \tag{3.81}$$

3.2.1.4.4   Energy conservation

In order to derive the energy conservation equation, Ψ^μ is set equal to $\left(1/2 \right) m^\mu v_i v_i + U_\dagger^\mu$. Thus the following relations are obtained,

$$
\begin{aligned}
\langle \Psi^\mu \rangle &= \int_{-\infty}^{+\infty} \left(\frac{m^\mu}{2} v_i v_i + U_\dagger^\mu \right) \frac{f^\mu}{n^\mu} \mathrm{d}^3 v = \frac{m^\mu}{2} \langle v_i v_i \rangle^\mu + \langle U_\dagger^\mu \rangle = m^\mu \left(\frac{v_i^0 v_i^0}{2} + v_i^0 \langle V_i \rangle^\mu + u^\mu \right) \\
\langle \Psi^\mu v_j \rangle^\mu &= \frac{1}{n^\mu} \int_{-\infty}^{+\infty} \left(\frac{1}{2} m^\mu v_i v_i v_j + U_\dagger^\mu v_j \right) f^\mu \mathrm{d}^3 v = m^\mu \frac{1}{2} \langle v_i v_i v_j \rangle^\mu + \langle U_\dagger^\mu v_j \rangle \\
&= \frac{1}{n^\mu} q_j^\mu + \frac{1}{n^\mu} P_{ij}^\mu v_i^0 + m^\mu u^\mu v_j^0 + \frac{m^\mu}{2} \langle V_j \rangle^\mu v_i^0 v_i^0 + \frac{m^\mu}{2} v_i^0 v_i^0 v_j^0 + m^\mu \langle V_i \rangle^\mu v_i^0 v_j^0 \\
\langle \partial_v^j \Psi^\mu \rangle^\mu &= \frac{1}{n^\mu} \int_{-\infty}^{+\infty} \partial_v^j \left(\frac{1}{2} m^\mu v_i v_i + U_\dagger^\mu \right) f^\mu \mathrm{d}^3 v = \frac{m^\mu}{n^\mu} \int_{-\infty}^{+\infty} v_i \delta_i^j f^\mu \mathrm{d}^3 v = m^\mu \delta_i^j \langle v_i \rangle^\mu \\
&= m^\mu \langle V_j + v_j^0 \rangle
\end{aligned}
$$

$$(3.82)$$

Thus the equation of change becomes with $\rho^\mu = n^\mu m^\mu$, $\displaystyle\sum_{\mu=1}^{N'} \rho^\mu \langle V_i \rangle^\mu = 0$

$$
\begin{aligned}
0 = &\ \frac{\partial}{\partial t} \left[\frac{1}{2} \rho v_i^0 v_i^0 + \sum_{\mu=1}^{N'} \rho^\mu u^\mu \right] \\
&+ \partial_x^j \left[q_j + P_{ij} v_i^0 + v_j^0 \sum_{\mu=1}^{N'} \rho^\mu u^\mu + \frac{1}{2} \rho v_i^0 v_i^0 v_j^0 \right] \\
&- \sum_{\mu=1}^{N'} \rho^\mu a_i^\mu \langle V_i \rangle^\mu - \sum_{\mu=1}^{N'} \rho^\mu a_i^\mu v_i^0
\end{aligned}
$$

$$(3.83)$$

This is equivalent to,

$$
\begin{aligned}
0 = &\ \frac{\partial}{\partial t} \left[\frac{1}{2} \rho v_i^0 v_i^0 \right] + \partial_x^j \left[\frac{1}{2} \rho v_i^0 v_i^0 v_j^0 \right] + \frac{\partial}{\partial t} \left[\sum_{\mu=1}^{N'} \rho^\mu u^\mu \right] \\
&+ \partial_x^j \left[q_j + P_{ij} v_i^0 + v_j^0 \sum_{\mu=1}^{N'} \rho^\mu u^\mu \right] - \sum_{\mu=1}^{N'} \rho^\mu a_i^\mu \langle V_i \rangle^\mu - \sum_{\mu=1}^{N'} \rho^\mu a_i^\mu v_i^0
\end{aligned}
$$

$$(3.84)$$

The fist and second term on the right hand side becomes with the mass conservation (3.68),

$$\frac{\partial}{\partial t}\left[\frac{1}{2}\rho v_i^0 v_i^0\right] + \partial_x^j\left[\frac{1}{2}\rho v_i^0 v_i^0 v_j^0\right] = \rho\left[\frac{\partial}{\partial t} + v_j^0 \partial_x^j\right]\left(\frac{1}{2}v_i^0 v_i^0\right) = \rho\frac{\mathrm{D}}{\mathrm{D}t}\left(\frac{1}{2}v_i^0 v_i^0\right) \quad (3.85)$$

Using the mechanical energy conservation (3.81) the energy conservation becomes,

$$\frac{\partial}{\partial t}\sum_{\mu=1}^{N'}\rho^\mu u^\mu + \partial_x^j\left[v_j^0\sum_{\mu=1}^{N'}\rho^\mu u^\mu\right] = -\partial_x^j q_j - \partial_x^j\left(P_{ij}v_i^0\right) + v_i^0\partial_x^j P_{ij} + \sum_{\mu=1}^{N'}\rho^\mu a_i^\mu\left\langle V_i\right\rangle^\mu$$

$$(3.86)$$

The first and second term on the left hand side of equation becomes with the species conservation (3.72),

$$\begin{aligned}\sum_{\mu=1}^{N'}\frac{\partial}{\partial t}\left(\rho^\mu u^\mu\right) + \sum_{\mu=1}^{N'}\partial_x^j\left(\rho^\mu v_j^0 u^\mu\right) &= \sum_{\mu=1}^{N'} u^\mu\left[\frac{\partial}{\partial t}\rho^\mu + \partial_x^j\left(\rho^\mu v_j^0\right)\right]\\ &\quad + \sum_{\mu=1}^{N'}\rho^\mu\left[\frac{\partial}{\partial t} + v_j^0\partial_x^j\right]u^\mu\\ &= \sum_{\mu=1}^{N'} u^\mu\left\{\mathfrak{M}^\mu\tilde{\omega}^\mu - \partial_x^j\left[\rho^\mu\left\langle V_j\right\rangle^\mu\right]\right\}\\ &\quad + \sum_{\mu=1}^{N'}\rho^\mu\left[\frac{\partial}{\partial t} + v_j^0\partial_x^j\right]u^\mu\end{aligned} \quad (3.87)$$

Therefore the final energy conservation equation is given by,

$$\begin{aligned}\sum_{\mu=1}^{N'}\rho^\mu\frac{\mathrm{D}}{\mathrm{D}t}u^\mu &= -\sum_{\mu=1}^{N'} u^\mu\mathfrak{M}^\mu\tilde{\omega}^\mu + \sum_{\mu=1}^{N'} u^\mu\partial_x^j\left(\rho^\mu\left\langle V_j\right\rangle^\mu\right) - \partial_x^j q_j\\ &\quad - \partial_x^j\left(P_{ij}v_i^0\right) + v_i^0\partial_x^j P_{ij} + \sum_{\mu=1}^{N'}\rho^\mu a_i^\mu\left\langle V_i\right\rangle^\mu\end{aligned} \quad (3.88)$$

3.2.1.5 Transport properties and constitutive laws

The diffusion velocities, stresses, and heat fluxes appearing in the conservation equations of fluid dynamics, which are determined by the molecular transport of mass, momentum, and energy respectively, must be calculable in order to render the conservation equations soluble. Instead of a rigorous derivation of the transport vectors and tensors for gas mixtures, a general mean-free-path description of molecular transport leads to suitable expressions for the transport vectors and tensors in terms of the gradients of the dependent variables of fluid dynamics, although in the case of mass diffusion results by using this method are rather over simplified and other techniques has to be utilized to achieve a closer agreement with the exact theory [35]. Therefore and from the fact that mass diffusion flux becomes irrelevant in the proceeding sections it will be omitted and only expressions for the stress tensor and thermal conductivity will be given.

3.2.1.5.1 Stress tensor

Since the diagonal elements of the stress tensor represents normal stresses and the off-diagonal elements are shear stresses, the stress tensor, equation (3.44), can be expressed as the sum of a mean pressure tensor and a viscous stress tensor,

$$P_{ij} = p\delta_{ij} + \Gamma_{ij} \tag{3.89}$$

Where p is the hydrostatic pressure. For gases the pressure is given by the ideal gas law. For arbitrary geometries in multicomponent mixtures the shear stress tensor is given by [35],

$$\Gamma_{ij} = -\mu' \left(\partial_x^i v_j^0 + \partial_x^j v_i^0 \right) + \mu'' \partial_x^m v_m^0 \delta_{ij} \tag{3.90}$$

where μ'' is the second viscosity coefficient. The second viscosity coefficient is expressed as,

$$\mu'' = \frac{2}{3}\mu' - \mu''' \qquad (3.91)$$

where μ''' is the coefficient of bulk viscosity. For monoatomic gas mixtures, kinetic theory shows that $\mu''' = 0$. For polyatomic gases, relaxation effects between the translational motion and the various internal degrees of freedom leads to a positive value of μ'''. Nevertheless the bulk viscosity is usually negligible in combustion processes [35]. For multicomponent mixtures of gases the viscosity coefficient μ' depent on the concentrations, and the results of accurate kinetic theory are quite complicated. Nevertheless the viscosity of gas mixtures is usually adequately described by semi-empirical mixing rules such as the square-root rule which is applicable for the most engineering calculations [37],

$$\mu'_{mix} = \frac{\displaystyle\sum_{\mu=1}^{N'} \sqrt{\mathfrak{M}^{\mu}} Y^{\mu} \mu'^{\mu}}{\displaystyle\sum_{\mu=1}^{N'} \sqrt{\mathfrak{M}^{\mu}} Y^{\mu}} \qquad (3.92)$$

where $\mathfrak{M}^{\mu}$ and Y^{μ} are the molar mass and mole fraction of species μ.

3.2.1.5.2 Thermal conductivity

From the mean-free-path description of molecular transport, the heat flux, equation (3.49) for one component gas is given by,

$$q_j = -\lambda \partial_x^j T \qquad (3.93)$$

where λ is the thermal conductivity. Again for multicomponent mixtures the theoretical formalism to calculate the thermal conductivity coefficient is very complicated. For engineering estimates it is often sufficient to use the cube-rule-law which is [37],

$$\lambda_{mix} = \frac{\displaystyle\sum_{\mu=1}^{N'} \sqrt[3]{\mathfrak{M}^\mu} Y^\mu \lambda^\mu}{\displaystyle\sum_{\mu=1}^{N'} \sqrt[3]{\mathfrak{M}^\mu} Y^\mu} \tag{3.94}$$

3.2.1.6 Conservation equation governing the temperature field

The conservation equation governing the temperature field is readily obtained from the energy conservation equation (3.88), the expression for the stress tensor, equation (3.89), and the specific enthalpy which is,

$$h^\mu = u^\mu + \frac{p}{\rho} \tag{3.95}$$

Furthermore from the mass continuity equation follows,

$$\frac{\mathrm{D}}{\mathrm{D}t}\rho = \frac{\partial}{\partial t}\rho + v_j^0 \partial_x^j \rho = -\rho \partial_x^j v_j^0 \tag{3.96}$$

and,

$$\sum_{\mu=1}^{N'} \rho^\mu \frac{\mathrm{D}}{\mathrm{D}t}\left(\frac{p}{\rho}\right) = \rho\left(\frac{1}{\rho}\frac{\mathrm{D}}{\mathrm{D}t}p + p\frac{\mathrm{D}}{\mathrm{D}t}\left(\frac{1}{\rho}\right)\right) = \frac{\mathrm{D}}{\mathrm{D}t}p - \frac{p}{\rho}\frac{\mathrm{D}}{\mathrm{D}t}\rho \tag{3.97}$$

Thus the left hand side of equation (3.88) becomes,

$$\begin{aligned}
\sum_{\mu=1}^{N'} \rho^\mu \frac{\mathrm{D}}{\mathrm{D}t}u^\mu &= \sum_{\mu=1}^{N'} \rho^\mu \frac{\mathrm{D}}{\mathrm{D}t}\left(h^\mu - \frac{p}{\rho}\right) \\
&= \sum_{\mu=1}^{N'} \rho^\mu \frac{\mathrm{D}}{\mathrm{D}t}h^\mu - \frac{\mathrm{D}}{\mathrm{D}t}p - p\partial_x^j v_j^0
\end{aligned} \tag{3.98}$$

On the right hand side of equation (3.88) follows,

$$-\partial_x^j q_j + \sum_{\mu=1}^{N'} u^\mu \partial_x^j \left(\rho^\mu \left\langle V_j \right\rangle^\mu \right) = -\partial_x^j \left(q_j - \sum_{\mu=1}^{N'} u^\mu \rho^\mu \left\langle V_j \right\rangle^\mu \right)$$
$$- \sum_{\mu=1}^{N'} \rho^\mu \left\langle V_j \right\rangle^\mu \partial_x^j u^\mu \qquad (3.99)$$

with equation (3.95), equation (3.99) becomes with $\displaystyle\sum_{\mu=1}^{N'} \rho^\mu \left\langle V_i \right\rangle^\mu = 0$,

$$-\partial_x^j q_j + \sum_{\mu=1}^{N'} \left(h^\mu - \frac{p}{\rho} \right) \partial_x^j \left(\rho^\mu \left\langle V_j \right\rangle^\mu \right) = -\partial_x^j \left(q_j - \sum_{\mu=1}^{N'} h^\mu \rho^\mu \left\langle V_j \right\rangle^\mu \right)$$
$$- \sum_{\mu=1}^{N'} \rho^\mu \left\langle V_j \right\rangle^\mu \partial_x^j h^\mu \qquad (3.100)$$

Furthermore,

$$\sum_{\mu=1}^{N'} u^\mu \mathfrak{M}^\mu \tilde{\omega}^\mu = \sum_{\mu=1}^{N'} \left(h^\mu - \frac{p}{\rho} \right) \mathfrak{M}^\mu \tilde{\omega}^\mu = \sum_{\mu=1}^{N'} h^\mu \mathfrak{M}^\mu \tilde{\omega}^\mu \qquad (3.101)$$

since $\displaystyle\frac{p}{\rho} \sum_{\mu=1}^{N'} \tilde{\omega}^\mu = 0$. Thus the energy equation becomes in terms of the enthalpy,

$$\sum_{\mu=1}^{N'} \rho^\mu \frac{\mathrm{D}}{\mathrm{D}t} h^\mu = \frac{\mathrm{D}}{\mathrm{D}t} p + p \partial_x^j v_j^0 - \sum_{\mu=1}^{N'} h^\mu \mathfrak{M}^\mu \tilde{\omega}^\mu - \partial_x^j \left(q_j - \sum_{\mu=1}^{N'} h^\mu \rho^\mu \left\langle V_j \right\rangle^\mu \right)$$
$$- \sum_{\mu=1}^{N'} \rho^\mu \left\langle V_j \right\rangle^\mu \partial_x^j h^\mu - \partial_x^j \left(P_{ij} v_i^0 \right) + v_i^0 \partial_x^j P_{ij} + \sum_{\mu=1}^{N'} \rho^\mu a_i^\mu \left\langle V_i \right\rangle^\mu$$
$$(3.102)$$

From equation (3.89) follows that,

$$
\begin{aligned}
p\partial_x^j v_j^0 - \partial_x^j\left(P_{ij}v_i^0\right) + v_i^0\partial_x^j P_{ij} &= p\partial_x^j v_j^0 - P_{ij}\partial_x^j v_i^0 \\
&= p\partial_x^j v_j^0 - \left(p\delta_{ij} + \Gamma_{ij}\right)\partial_x^j v_i^0 \qquad (3.103)\\
&= \Gamma_{ij}\partial_x^j v_i^0
\end{aligned}
$$

which is equivalent to the energy dissipation rate. The energy production term respectively the enthalpy production term becomes,

$$
\sum_{\mu=1}^{N'} h^\mu \mathfrak{M}^\mu \tilde{\omega}^\mu = \sum_{\mu=1}^{N'} h^\mu \mathfrak{M}^\mu \frac{\mathrm{d}\left[M^\mu\right]}{\mathrm{d}t} \qquad (3.104)
$$

With the stoichiometric relation describing a forward one-step chemical reaction of arbitrary complexity, equation (2.1), the change in amount of substance of species i is uniquely related to the change in amount of substance of species j, equation (2.2). If one species is defined as the fuel which is consumed by chemical reaction following relation can be given,

$$
\frac{\mathrm{d}\left[M^\mu\right]}{\mathrm{d}t} = \frac{\nu_2^\mu - \nu_1^\mu}{\nu_2^{Fuel} - \nu_1^{Fuel}} \frac{\mathrm{d}\left[M^{Fuel}\right]}{\mathrm{d}t} \qquad (3.105)
$$

Then equation (3.104) becomes,

$$
\begin{aligned}
\sum_{\mu=1}^{N'} h^\mu \mathfrak{M}^\mu \tilde{\omega}^\mu &= \frac{1}{\nu_2^{Fuel} - \nu_1^{Fuel}} \frac{\mathrm{d}\left[M^{Fuel}\right]}{\mathrm{d}t} \sum_{\mu=1}^{N'}\left(\nu_2^\mu - \nu_1^\mu\right)\tilde{h}^\mu \\
&= \frac{1}{\nu_2^{Fuel} - \nu_1^{Fuel}} \frac{\mathrm{d}\left[M^{Fuel}\right]}{\mathrm{d}t}\left(\sum_{\mu=1}^{Products}\nu_2^\mu\tilde{h}^\mu - \sum_{\mu=1}^{Reactants}\nu_1^\mu\tilde{h}^\mu\right)
\end{aligned} \qquad (3.106)
$$

where $\tilde{h}^\mu$ is the specific enthalpy of species μ given in J/mol. Defining the energy released by the chemical reaction per mole of fluid which is consumed as,

$$
\Delta h_r = \frac{1}{\nu_2^{Fuel} - \nu_1^{Fuel}}\left(\sum_{\mu=1}^{Products}\nu_2^\mu\tilde{h}^\mu - \sum_{\mu=1}^{Reactants}\nu_1^\mu\tilde{h}^\mu\right) \qquad (3.107)
$$

where the term in the parantheses is equal to the difference of the heat of formation of the products and the reactants. For conclusions it is important to note that the heat of reaction is independent from the equivalence ratio. For exothermic reactions the specific enthalpy of reaction is defined conventionally negative. Therefore it is convenient to define the specific enthalpy of reaction by $Q_r = -\Delta h_r$. Assuming a global one step chemical reaction, equation (2.6) the energy production term is given by,

$$\sum_{\mu=1}^{N'} h^\mu \mathfrak{M}^\mu \tilde{\omega}^\mu = -Q_r \tilde{J}'(\phi) k(T) \prod_{\mu=1}^{N'} \left[M^\mu \right]^{\alpha_\mu'} = -Q_r \tilde{J}'(\phi) k(T) \left[Fuel \right]^{\alpha'} \prod_{\mu \neq Fuel}^{N'-1} \left[C^\mu \right]^{\beta_\mu}$$

$$(3.108)$$

Thus with $\mathrm{d}h^\mu = c_p^\mu \mathrm{d}T$ the final temperature field equation becomes,

$$
\begin{aligned}
\sum_{\mu=1}^{N'} \rho^\mu c_p^\mu \frac{\mathrm{D}}{\mathrm{D}t} T \;=\; & \frac{\mathrm{D}}{\mathrm{D}t} p + Q_r \tilde{J}'(\phi) k(T) \prod_{\mu=1}^{N'} \left[M^\mu \right]^{\alpha_\mu'} \\
& - \partial_x^j \left(q_j - \sum_{\mu=1}^{N'} h^\mu \rho^\mu \left\langle V_j \right\rangle^\mu \right) + \sum_{\mu=1}^{N'} \rho^\mu a_i^\mu \left\langle V_i \right\rangle^\mu \\
& - \sum_{\mu=1}^{N'} \rho^\mu c_p^\mu \left\langle V_j \right\rangle^\mu \partial_x^j T + \Gamma_{ij} \partial_x^j v_i^0
\end{aligned}
\quad (3.109)
$$

3.2.2 Steady one-dimensional inviscid chemically reacting flow with negligible molecular transport in a duct of constant flow area

There are a number of combustion problems in which transport phenomena are negligible [35]. For example, in flows at high subsonic or supersonic speeds, transport effects are usually unimportant except in thin regions, such as shock waves and boundary layers, where the flow variables change very rapidly with position. Furthermore to develop an analytical model for the auto-ignition of a gas mixture, it is assumed that the flow is steady, one-dimensional and inviscid, figure 8.
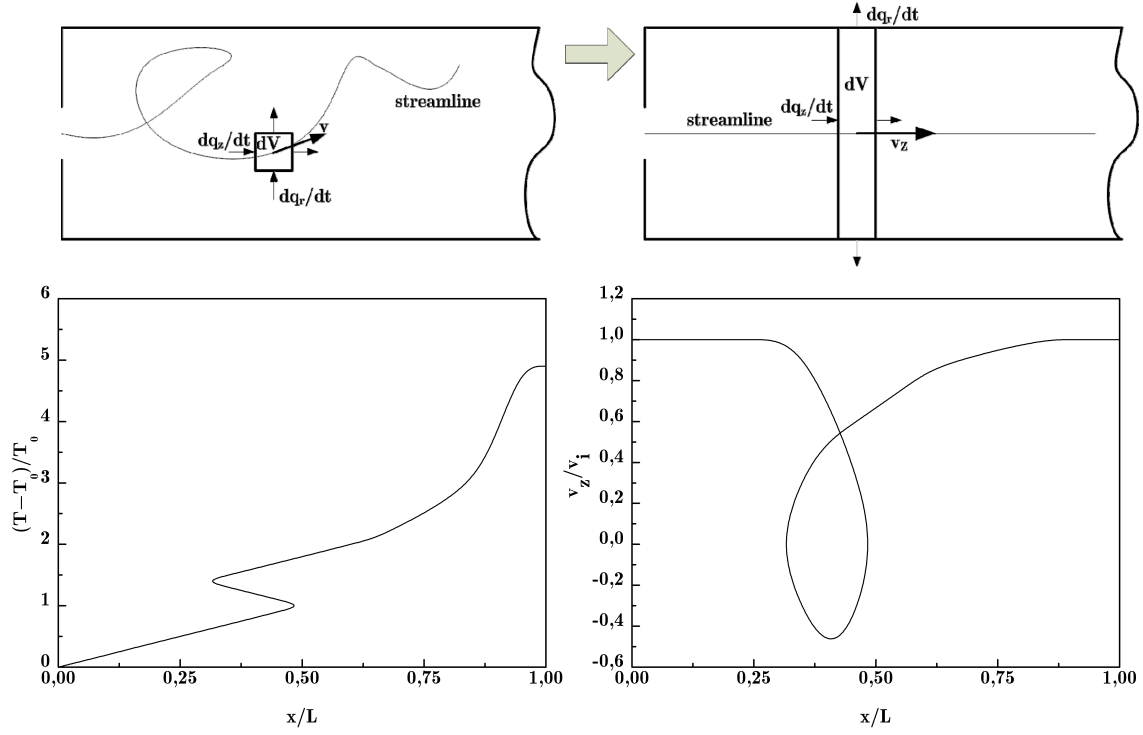
Fig. 8: Approximation of a three-dimensional flow to a one-dimensional flow

The bottom of figure 8 shows a hypothetical dimensonless temperature and velocity characteristic due to recirculation effects of the one dimensional flow field relative to the dimensionless position where L is equivalent to the combustion chamber length and v_i is the initial velocity. Particular the flow velocity along the longitudinal axis can take positive and negative values (recirculation). Therefore it should be noted that by the simplification to a one dimensional flow the correlation between $x \rightarrow f(x) := T(x)$ and $x \rightarrow f(x) := v_z(x)$ is not bijective in contrast to $\vec{x} \rightarrow f(\vec{x}) = T(x, y, z)$ and $\vec{x} \rightarrow f(\vec{x}) = \vec{v}(x, y, z)$.

3.2.2.1 Simplified energy, momentum, mass, and species equations

Assuming an inviscid flow with negligible molecular transport and negligible body forces the temperature field equation (3.109) becomes,

$$\sum_{\mu=1}^{N'} \rho^{\mu} c_p^{\mu} \frac{\mathrm{D}}{\mathrm{D}t} T = \frac{\mathrm{D}}{\mathrm{D}t} p + Q_r \tilde{J}'(\phi) k(T) \prod_{\mu=1}^{N'} \left[M^{\mu} \right]^{\alpha_{\mu}'} - \partial_x^j q_j \qquad (3.110)$$

70

With $\rho\left\langle c_p \right\rangle_{mix} = \sum\limits_{\mu=1}^{N'} \rho^\mu c_p^\mu$ and integrating over a infinitesimal volume, equation (3.110) becomes with Gauss Theorem,

$$\int\limits_V \rho\left\langle c_p \right\rangle_{mix} \frac{\mathrm{D}}{\mathrm{D}t} T \mathrm{d}V = \int\limits_V \frac{\mathrm{D}}{\mathrm{D}t} p \mathrm{d}V + \int\limits_V Q_r \tilde{J}'(\phi) k(T) \prod_{\mu=1}^{N'} \left[M^\mu \right]^{\alpha_\mu'} \mathrm{d}V - \int\limits_A q_j \mathrm{d}A_j$$

(3.111)

The last term on the right hand side of equation (3.111) can be written as,

$$\int\limits_A q_j \mathrm{d}A_j = \int\limits_{LS} q_j \mathrm{d}A_j + \int\limits_B q_j \mathrm{d}A_j + \int\limits_C q_j \mathrm{d}A_j \qquad (3.112)$$

where the first, second, and third term on the right hand side is the integral over the lateral, base, and cover surface. Assuming negligible heat flux along the flow direction, equation (3.112) becomes,

$$\int\limits_A q_j \mathrm{d}A_j = \int\limits_{LS} q_j \mathrm{d}A_j = q(R) 2\pi R \mathrm{d}x = q(R) U \mathrm{d}x \qquad (3.113)$$

where U is the perimeter of the duct. The heat flux between the gas mixture and the surface of the flow reactor is linearly approximated by,

$$q(R) = \chi\left(T - T_w\right) \qquad (3.114)$$

Thus with $\mathrm{d}V = A\mathrm{d}x$, equation (3.113), and equation (3.114), equation (3.111) becomes assuming steady flow conditions,

$$\rho\left\langle c_p \right\rangle_{mix} v \frac{\mathrm{d}T}{\mathrm{d}x} = v\frac{\mathrm{d}p}{\mathrm{d}x} + Q_r \tilde{J}'(\phi) k(T) \prod_{\mu=1}^{N'} \left[M^\mu \right]^{\alpha_\mu'} - \chi\left(T - T_w\right)\frac{U}{A} \qquad (3.115)$$

The momentum equation becomes with negligible body forces and with $P_{ij} = p\delta_{ij}$,

$$\rho v \frac{\mathrm{d}v}{\mathrm{d}x} = -\frac{\mathrm{d}p}{\mathrm{d}x} \tag{3.116}$$

For the mass conservation follows,

$$
\begin{aligned}
\int_V \partial_x^j \left(\rho v_j\right) \mathrm{d}V &= \int_A \rho v_j \mathrm{d}A_j \\
&= \rho\left(x+\mathrm{d}x\right) v\left(x+\mathrm{d}x\right) A\left(x+\mathrm{d}x\right) \\
&\quad - \rho\left(x\right) v\left(x\right) A\left(x\right) \\
&= \frac{\mathrm{d}\left(\rho v A\right)}{\mathrm{d}x} = 0
\end{aligned}
\tag{3.117}
$$

The species conservation becomes,

$$
\begin{aligned}
\int_V \partial_x^j \left(\rho^\mu v_j\right) \mathrm{d}V &= \int_A \rho^\mu v_j \mathrm{d}A_j \\
&= \rho^\mu\left(x+\mathrm{d}x\right) v\left(x+\mathrm{d}x\right) A\left(x+\mathrm{d}x\right) \\
&\quad - \rho^\mu\left(x\right) v\left(x\right) A\left(x\right) \\
&= \frac{\mathrm{d}\left(\rho^\mu v A\right)}{\mathrm{d}x} = \mathfrak{M}^\mu \tilde{J}'\left(\phi\right) k\left(T\right) \prod_{\mu=1}^{N'} \left[M^\mu\right]^{\alpha_\mu'}
\end{aligned}
\tag{3.118}
$$

3.2.2.2 Governing equations for the flow field

With the equations in section (3.2.2.1) the basic equations describing the flow field are given by,

$$\rho \left\langle c_p \right\rangle_{mix} v \frac{\mathrm{d}T}{\mathrm{d}x} = v \frac{\mathrm{d}p}{\mathrm{d}x} + Q_r \tilde{J}'(\phi) k(T) \prod_{\mu=1}^{N'} \left[M^\mu \right]^{\alpha'_\mu} - \chi \left(T - T_w \right) \frac{U}{A}$$

$$\rho v \frac{\mathrm{d}v}{\mathrm{d}x} = - \frac{\mathrm{d}p}{\mathrm{d}x}$$

$$\frac{\mathrm{d} \left(\rho v A \right)}{\mathrm{d}x} = 0 \tag{3.119}$$

$$\frac{\mathrm{d} \left(\rho^\mu v A \right)}{\mathrm{d}x} = \mathfrak{M}^\mu \tilde{J}'(\phi) k(T) \prod_{\mu=1}^{N'} \left[M^\mu \right]^{\alpha'_\mu}$$

$$\rho = \frac{p \left\langle \mathfrak{M} \right\rangle_{mix}}{RT} = \frac{p}{T \left\langle R \right\rangle_{mix}}$$

From the last equation in (3.119) follows,

$$\frac{\mathrm{d}\rho}{\mathrm{d}x} = \frac{1}{T \left\langle R \right\rangle_{mix}} \frac{\mathrm{d}p}{\mathrm{d}x} - p \frac{1}{T^2 \left\langle R \right\rangle_{mix}} \frac{\mathrm{d}T}{\mathrm{d}x} \tag{3.120}$$

From the third equation of (3.119) follows for dA=0,

$$v \frac{\mathrm{d}\rho}{\mathrm{d}x} + \rho \frac{\mathrm{d}v}{\mathrm{d}x} = 0 \tag{3.121}$$

Combining the momentum equation (second equation in (3.119)), the density euation (last equation in equation in (3.119)), equation (3.120) and equation (3.121) leads to,

$$\frac{\mathrm{d}v}{\mathrm{d}x} = \frac{v \left\langle R \right\rangle_{mix}}{T \left\langle R \right\rangle_{mix} - v^2} \frac{\mathrm{d}T}{\mathrm{d}x} \tag{3.122}$$

Furthermore the species equation in (3.119) can be written as,

$$\frac{\mathrm{d} \left(\rho^\mu v A \right)}{\mathrm{d}x} = \rho^\mu \frac{\mathrm{d}v}{\mathrm{d}x} + v \frac{\mathrm{d}\rho^\mu}{\mathrm{d}x} = \left[M^\mu \right] \mathfrak{M}^\mu \frac{\mathrm{d}v}{\mathrm{d}x} + v \mathfrak{M}^\mu \frac{\mathrm{d} \left[M^\mu \right]}{\mathrm{d}x}$$

$$= v \frac{\mathrm{d} \left[M^\mu \right]}{\mathrm{d}x} + \left[M^\mu \right] \frac{\mathrm{d}v}{\mathrm{d}x} = \tilde{J}'(\phi) k(T) \prod_{\mu=1}^{N'} \left[M^\mu \right]^{\alpha'_\mu} \tag{3.123}$$

Therefore the final equations describing the flow field becomes,

$$\rho \left\langle c_p \right\rangle_{mix} \frac{\mathrm{d}T}{\mathrm{d}x} \quad = \quad -\rho v \frac{\mathrm{d}v}{\mathrm{d}x} + \frac{1}{v} Q_r \tilde{J}'(\phi) k(T) \prod_{\mu=1}^{N'} \left[M^\mu \right]^{\alpha_\mu'} - \frac{1}{v} \chi (T - T_w) \frac{U}{A}$$

$$v \frac{\mathrm{d}\left[M^\mu \right]}{\mathrm{d}x} + \left[M^\mu \right] \frac{\mathrm{d}v}{\mathrm{d}x} = \tilde{J}'(\phi) k(T) \prod_{\mu=1}^{N'} \left[M^\mu \right]^{\alpha_\mu'}$$

$$\frac{\mathrm{d}v}{\mathrm{d}x} = \frac{v \left\langle R \right\rangle_{mix}}{T \left\langle R \right\rangle_{mix} - v^2} \frac{\mathrm{d}T}{\mathrm{d}x}$$

$$\frac{\mathrm{d}p}{\mathrm{d}x} = -\rho v \frac{\mathrm{d}v}{\mathrm{d}x}$$

$$\frac{\mathrm{d}\rho}{\mathrm{d}x} = \frac{1}{T \left\langle R \right\rangle_{mix}} \frac{\mathrm{d}p}{\mathrm{d}x} - p \frac{1}{T^2 \left\langle R \right\rangle_{mix}} \frac{\mathrm{d}T}{\mathrm{d}x}$$

$$(3.124)$$

3.2.2.2.1 Parameterization and simplification of the flow field equations

The object is to derive an analytical model for the auto ignition conditions based on the simplified thermal ignition theory which explains the p-T ignition behaviour of a chemical system above the 3rd ignition limit (refer to chapter 3.1). In order to achieve an analytical relation between pressure and temperature the temperature is linearized about T_0 (Fig. 8) which is equivalent to a Taylor series up to the linear term.
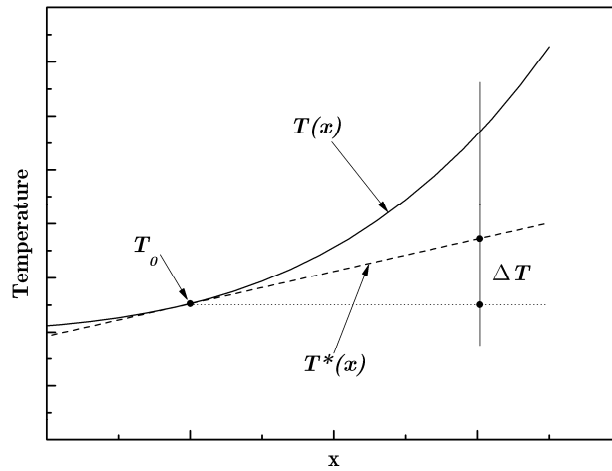
Fig. 9: Linearization of the temperature

From figure 9 follows,

$$T^*\left(x_0 + \Delta x\right) = T_0 + \left.\frac{\mathrm{d}T}{\mathrm{d}x}\right|_{x_0} \left(x - x_0\right) = T_0 + \Delta T = T_0 + T^*\left(x_0 + \Delta x\right) - T_0$$

(3.125)

If small changes of the temperature are assumed it can be approximated by,

$$
\begin{aligned}
T\left(x_0 + \Delta x\right) &\approx T^*\left(x_0 + \Delta x\right) \\[2mm]
&\approx T_0 + T^*\left(x_0 + \Delta x\right) - T_0 \\[2mm]
&\approx T_0 + \frac{T^*\left(x_0 + \Delta x\right) - T_0}{T_0} T_0 \\[2mm]
&\approx T_0\left(1 + \psi\right)
\end{aligned}
$$

(3.126)

Research [39] has identified efficient nondimensional variables by introducing Θ as nondimensional temperature variable as follows,

$$
\begin{aligned}
\Theta &= \frac{\psi}{\varepsilon} \Rightarrow \psi = \varepsilon\Theta \\[2mm]
\varepsilon &= \frac{RT_0}{E_A}
\end{aligned}
$$

(3.127)

Thus,

$$
\begin{aligned}
T &\approx T_0\left(1 + \varepsilon\Theta\right) \\[2mm]
\frac{\mathrm{d}T}{\mathrm{d}x} &= T_0\varepsilon\frac{\mathrm{d}\Theta}{\mathrm{d}x}
\end{aligned}
$$

(3.128)

The specific reaction rate constant, equation (2.24), becomes,

$$k\left(T\right) = \tilde{J}\exp\left(-\frac{E_A}{RT}\right) = \tilde{J}\exp\left(-\frac{E_A}{RT_0\left(1+\varepsilon\Theta\right)}\right)$$

$$= \tilde{J}\exp\left(-\frac{E_A}{RT_0}\right)\exp\left(\frac{\frac{E_A}{RT_0}\varepsilon\Theta}{1+\varepsilon\Theta}\right) \qquad (3.129)$$

$$= \tilde{J}\exp\left(-\frac{1}{\varepsilon}\right)\exp\left(\frac{\Theta}{1+\varepsilon\Theta}\right)$$

Therefore the final flow fiel equations becomes,

$$\rho\left\langle c_p\right\rangle_{mix}T_0\varepsilon\frac{\mathrm{d}\Theta}{\mathrm{d}x} = -\rho v\frac{\mathrm{d}v}{\mathrm{d}x}+\frac{1}{v}Q_r\tilde{J}'\left(\phi\right)\tilde{J}\exp\left(-\frac{1}{\varepsilon}\right)\exp\left(\frac{\Theta}{1+\varepsilon\Theta}\right)\prod_{\mu=1}^{N'}\left[M^\mu\right]^{\alpha_\mu'}$$

$$-\frac{1}{v}\chi\left(T_0\left(1+\varepsilon\Theta\right)-T_w\right)\frac{U}{A}$$

$$v\frac{\mathrm{d}\left[M^\mu\right]}{\mathrm{d}x}+\left[M^\mu\right]\frac{\mathrm{d}v}{\mathrm{d}x} = \tilde{J}'\left(\phi\right)\tilde{J}\exp\left(-\frac{1}{\varepsilon}\right)\exp\left(\frac{\Theta}{1+\varepsilon\Theta}\right)\prod_{\mu=1}^{N'}\left[M^\mu\right]^{\alpha_\mu'}$$

$$\frac{\mathrm{d}v}{\mathrm{d}x} = \frac{v\left\langle R\right\rangle_{mix}}{T_0\left(1+\varepsilon\Theta\right)\left\langle R\right\rangle_{mix}-v^2}\frac{\mathrm{d}T}{\mathrm{d}x}$$

$$\frac{\mathrm{d}p}{\mathrm{d}x} = -\rho v\frac{\mathrm{d}v}{\mathrm{d}x}$$

$$\frac{\mathrm{d}\rho}{\mathrm{d}x} = \frac{1}{T_0\left(1+\varepsilon\Theta\right)\left\langle R\right\rangle_{mix}}\frac{\mathrm{d}p}{\mathrm{d}x}-p\frac{1}{\left[T_0\left(1+\varepsilon\Theta\right)\right]^2\left\langle R\right\rangle_{mix}}T_0\varepsilon\frac{\mathrm{d}\Theta}{\mathrm{d}x}$$

$$(3.130)$$

Assuming that $\varepsilon\ll 1$ and bearing in mind that the specific heat becomes a function of the temperature, then follows,

$$\frac{\mathrm{d}v}{\mathrm{d}x} \approx 0 \Rightarrow \frac{\mathrm{d}p}{\mathrm{d}x} \approx 0 \Rightarrow \frac{\mathrm{d}\rho}{\mathrm{d}x} \approx 0 \Rightarrow \frac{\mathrm{d}\left[M^{\mu}\right]}{\mathrm{d}x} \approx 0$$

$$\left\langle c_{p} \right\rangle_{mix}(T) = \left\langle c_{p} \right\rangle_{mix}\left(T_{0}\left(1 + \varepsilon\Theta\right)\right) = \left\langle c_{p}\big|_{T_{0}} \right\rangle_{mix}$$

(3.131)

Thus if $\varepsilon \ll 1$ which is satisfied for high activation energies (typically for hydrocarbons) the change in velocity, pressure, density and reactant depletion is negligible except in late stages of the process. It is only essential to take it into account if post-ignition phenomena are to be described with any accuracy [35]. Hence the chemical composition of the system is essentially defined by the initial values as long as the temperature increase during the process till ignition is small -which is an intrinsic property of thermal ignition phenomenon if the activation energy, E_{A}, is large. This assumption which leads to a strong simplification may lead to wrong predictions for the necessary conditions such as the initial pressure to achieve thermal ignition but at least it is a good approximation if the activation energies E_{A}, are large. Furthermore by the assumption $\varepsilon \ll 1$ the mathematical description of the mechanism of thermal ignition becomes simplified and only a single differential equation for Θ remains, which is,

$$\begin{aligned}
\rho_{0} \left\langle c_{p}\big|_{T_{0}} \right\rangle_{mix} \frac{\mathrm{d}\Theta}{\mathrm{d}x} &= \frac{1}{v} Q_{r} \tilde{J}'(\phi) \tilde{J} \frac{1}{T_{0}\varepsilon} \exp\left(-\frac{1}{\varepsilon}\right) \exp\left(\frac{\Theta}{1 + \varepsilon\Theta}\right) \prod_{\mu=1}^{N'} \left[M^{\mu}\right]_{0}^{\alpha_{\mu}'} \\
&- \frac{1}{v} \frac{1}{T_{0}\varepsilon} \chi\left(T_{0}\left(1 + \varepsilon\Theta\right) - T_{w}\right) \frac{U}{A}
\end{aligned}$$

(3.132)

Further algebra leads to,

$$\begin{aligned}
\rho_{0} \left\langle c_{p}\big|_{T_{0}} \right\rangle_{mix} v \frac{\mathrm{d}\Theta}{\mathrm{d}x} &= \frac{Q_{r}}{T_{0}\varepsilon} \tilde{J}'(\phi) \tilde{J} \exp\left(-\frac{1}{\varepsilon}\right) \exp(\Theta) \prod_{\mu=1}^{N'} \left[M^{\mu}\right]_{0}^{\alpha_{\mu}'} \\
&- \chi\left[\Theta + \frac{1}{T_{0}\varepsilon}\left(T_{0} - T_{w}\right)\right]
\end{aligned}$$

(3.133)

From figure 8 one can expect that the correlation $x \to f(x) := \Theta(x)$ is not bijective and therefore equation (3.133) can not be solved a priori relative to the axial position. To overcome this problem equation (3.133) is rewritten in terms of the

time. The eventually recirculating motion of a particle (top left hand side of figure 8) respectively the oscillating motion caused by a oscillating longitudinal flow velocity (top right hand side of figure 8) is then accounted by a statistical residence time distribution. Furthermore if the wall temperature distribution with respect to the spatial coordinate x is nearly constant, the mean wall temperature $<T_w>$ which is given by,

$$\left\langle T_w \right\rangle = \frac{1}{x} \int_0^x T_w\left(x'\right)\mathrm{d}x' \tag{3.134}$$

is a good approximation for $T_w(x)$. Therefore by substituting for $\mathrm{d}x = v\mathrm{d}t$ the thermal ignition equation becomes,

$$
\begin{aligned}
\rho_0 \left\langle c_p\big|_{T_0} \right\rangle_{mix} \frac{\mathrm{d}\Theta}{\mathrm{d}t} &= \frac{Q_r A'\left(\phi\right)}{\varepsilon T_0} \exp\left(-\frac{1}{\varepsilon}\right)\left[Fuel\right]_0^{\alpha'} \prod_{\mu \neq Fuel}^{N'-1} \left[C^\mu\right]_0^{\beta_\mu} \exp\left(\Theta\right) \\
&\quad - \chi \frac{U}{A}\left[\Theta\left(t\right) + \frac{1}{\varepsilon T_0}\left(T_0 - \left\langle T_w \right\rangle\right)\right]
\end{aligned}
\tag{3.135}
$$

3.2.3 Solution of the simplified adiabatic thermal ignition equation

The simplest method to describe thermal ignition is given by the assumption of negligible heat losses by $\chi = 0$. That means that the loss term always remains negligible in comparison with the generation term thus the thermal ignition equation becomes,

$$\rho_0 \left\langle c_p\big|_{T_0} \right\rangle_{mix} \frac{\mathrm{d}\Theta}{\mathrm{d}t} = \frac{Q_r A'\left(\phi\right)}{\varepsilon T_0} \exp\left(-\frac{1}{\varepsilon}\right)\left[Fuel\right]_0^{\alpha'} \prod_{\mu \neq Fuel}^{N'-1} \left[C^\mu\right]_0^{\beta_\mu} \exp\left(\Theta\right) \tag{3.136}$$

Further algebra leads to,

$$\frac{\mathrm{d}\Theta}{\mathrm{d}t} = \Omega^* \exp\left(\Theta\right) \tag{3.137}$$

with,

$$\Omega^* = \frac{Q_r E_A A'(\phi)\left[Fuel\right]_0^{\alpha'} \displaystyle\prod_{\mu \neq Fuel}^{N'-1} \left[C^\mu\right]_0^{\beta_\mu}}{R T_0^2 \rho_0 \left\langle c_p\big|_{T_0}\right\rangle_{mix}} \exp\left(-\frac{E_A}{R T_0}\right) \qquad (3.138)$$

The solution of equation (3.144) is given by,

$$\int_{\Theta_0}^{\Theta} \frac{\mathrm{d}\Theta'}{\exp(\Theta')} = \int_0^t \Omega^* \partial t' \qquad (3.139)$$

And becomes,

$$\Theta(t) = -\ln\left[\exp\left(-\Theta_0\right) - \Omega^* t\right] \qquad (3.140)$$

In dimensional variables the temperature-time characteristic are given by $\Theta\left(T = T_0\right) = 0$

$$T(t) = T_0\left[1 - \ln\left(1 - \Omega^* t\right)\frac{R T_0}{E_A}\right] \qquad (3.141)$$

3.2.3.1   Ideal ignition condition and ignition delay time

Figure 10 shows the nondimensional temperature-time histories for several values of Ω^* for thermal ignition assuming negligible heat losses according to equation (3.140).The ignition occurs at the point where a rapid increase of the temperature is developed and reaches infinity. The infinite nondimensional temperature, Θ, at a finite nondimensional time, t, is contradictory to the physical behaviour of ignition and combustion and is a consequence of the approximations that lead to equation (3.140). If reactant depletion is taken into account then the maximum temperature is limited by the adiabatic flame temperature. Anyway, reactant depletion can be neglected except for late stages of the process and if ε is small the ignition time obtained from the study

of equation (3.141) assuming negligible heat loss remains valid, except for corrections that are small when ε is small.
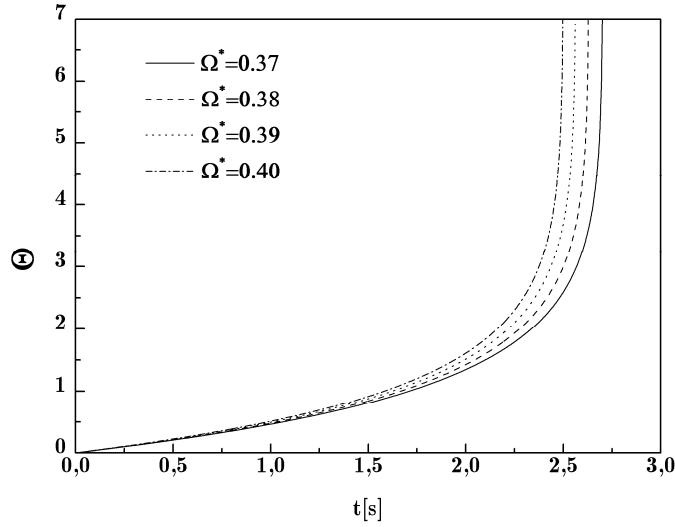
Fig. 10: Nondimensional temperature time-histories for the simplified thermal ignition model assumeing negligible loss effects

The ignition delay time, t_{ig}, is defined as the maximum value of t at which T rapidly increases and approaches infinity.

$$\lim_{t \to t_{ig}} T(t) = \lim_{t \to t_{ig}} \left\{ T_0 \left[1 - \ln\left(1 - \Omega^* t\right) \frac{R T_0}{E_A} \right] \right\} = \infty \tag{3.142}$$

Hence for the nondimensional ignition delay time follows,

$$1 - \Omega^* t_{ig} = 0$$
$$\Rightarrow t_{ig} = \frac{1}{\Omega^*} \tag{3.143}$$

and for the ignition condition respectively,

$$\Omega^* \geq \frac{1}{t_{ig}} \tag{3.144}$$

3.2.4 Solution of simplified non-adiabatic thermal ignition equation

The thermal ignition equation accounting loss effects is given by equation (3.135)

$$
\begin{aligned}
\rho_0 \left\langle c_p\big|_{T_0} \right\rangle_{mix} \frac{\mathrm{d}\Theta}{\mathrm{d}t} = \quad & \frac{Q_r A'(\phi)}{\varepsilon T_0} \exp\left(-\frac{1}{\varepsilon}\right) [Fuel]_0^{\alpha'} \prod_{\mu \neq Fuel}^{N'-1} [C^\mu]_0^{\beta_\mu} \exp(\Theta) \\
& - \chi \frac{U}{A}\left[\Theta(t) + \frac{1}{\varepsilon T_0}\left(T_0 - \langle T_w \rangle\right)\right]
\end{aligned}
$$
(3.145)

After further alegebra the energy balance equation becomes,

$$
\frac{\mathrm{d}\Theta}{\mathrm{d}\tau} = \Omega \exp(\Theta) - (\Theta + \xi)
$$
(3.146)

with,

$$
\begin{aligned}
\Omega &= \frac{Q_r E_A A'(\phi)[Fuel]_0^{\alpha'} \prod_{\mu \neq Fuel}^{N'-1} [C^\mu]_0^{\beta_\mu} A}{RT_0^2 \chi U} \exp\left(-\frac{E_A}{RT_0}\right) \\
\xi &= \frac{1}{\varepsilon T_0}\left(T_0 - \langle T_w \rangle\right) \\
\tau &= \frac{\chi U}{\rho_0 \left\langle c_p\big|_{T_0} \right\rangle_{mix} A} t \\
\varepsilon &= \frac{RT_0}{E_A}
\end{aligned}
$$
(3.147)

where $\Omega \exp(\Theta)$ represents the heat generation term and the second term on the right hand side of equation (3.153) represents the heat loss term. Graphs of heat generation and heat loss terms as functions of Θ are useful in defining necessary conditions for the occurrence of thermal ignition. A plot of this type is shown schematically in figure 11.
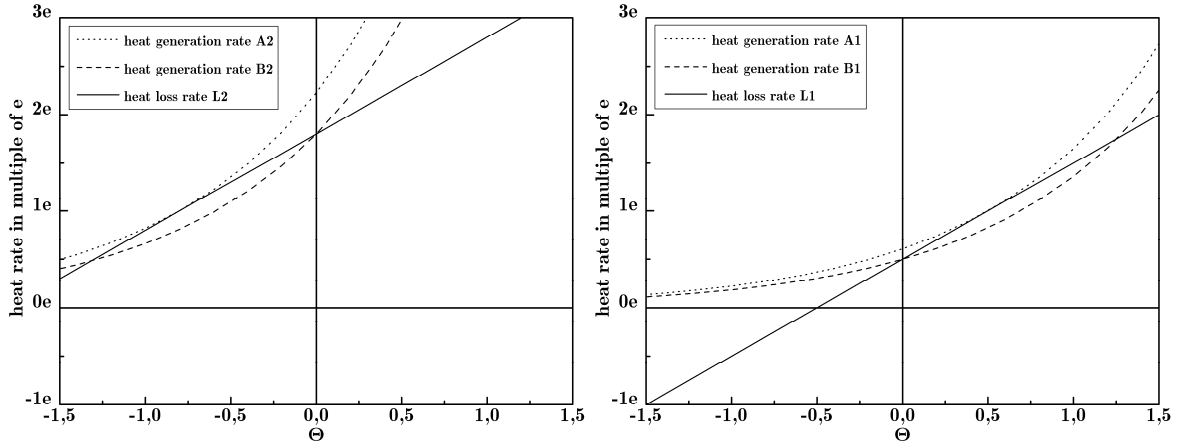
Fig. 11: Illustration of rates for heat generation and losses
as a function of nondimensionall temperature

3.2.4.1   Criteria for thermal ignition

Consider first the diagram on the right hand side of figure 11 where the offset of the heat loss rate is small. If Ω is small enough, then there are two intersections of the loss line with the generation curve labeld B1. The lower intersection defines a stable, slow reaction at $\Theta=0$ which is equivalent with $T=T_0$, while the upper intersection corresponds to an unstable steady state. It should be noted that the initial value of the dimensionless temperature Θ is zero. The instability is evident from the fact that a small increase in temperature causes the generation to exceed the loss, and therefore Θ will increase even more according to equation (3.153), similarly, a decrease in Θ causes the loss to exceed the generation, so that Θ decreases further. Thus at sufficiently small Ω, there exists one stable state, and a steady, slow reaction is possible. If Ω is large enough, then there is one intersection which defines the critical value of Ω where a rapid increase of the temperature is possible (heat generation curve labeled A1). Above the critical value for Ω the heat generation rate always prevails. Thus in the case of small ξ thermal ignition can occur at the critical value of Ω for which the loss line is tangent to the generation curve (B1). Consider now the diagram on the left hand side of figure 11 where the offset of the loss rate is large. The critical value of Ω for which the loss line is tangent to the generation curve (A2) leads to a too large value

for Ω to achieve auto ignition because as already mentioned the initial value of the dimensionless temperature is given by $\Theta=0$. In that case the critical value for Ω becomes decreased (heat generation curve labeled B2) compared to the critical value for which the loss line is tangent to the generation curve. Thus two cases exist where thermal ignition can occur. The behaviour of the balance equation assuming loss effects becomes essential for combustion chambers with high surface to volume ratios according to equation (3.145). For high surface to volume ratios, U/A, the loss term has a major influence for successful auto ignition occurrence since the heat generation term may be limited in all parameters except for the concentrations. Nevertheless the concentration are given by the partial pressures of the reactants and therefore high partial pressures are required to counteract the loss rate due to high surface to volume ratios to achieve auto ignition which may either technically difficult or it is not desired for the combustion system.

Mathematical identification of the first ignition constraint is given by the tangency condition which is straight forward when equation (3.153) applies. Equality of generation and loss rates requires,

$$\Omega_{\min} \exp(\Theta) = \Theta + \xi \tag{3.148}$$

and the equality of slopes requires,

$$\frac{\mathrm{d}}{\mathrm{d}\Theta}\left[\Omega_{\min}\exp(\Theta)\right] = \frac{\mathrm{d}}{\mathrm{d}\Theta}(\Theta + \xi) \tag{3.149}$$

Thus after algebraic manipulation follows,

$$\Omega_{\min} = \frac{1}{e}\exp(\xi)$$
$$\Theta_{crit} = 1 - \xi \tag{3.150}$$

Which can properly be interpreted as the critical measure of the ratio of the generation rate to the loss rate, above which thermal ignition occurs. Figure 12 shows the numerical solution of equation (3.153) for different cases for the value of Ω.and ξ with $\Theta_0 = 0$.
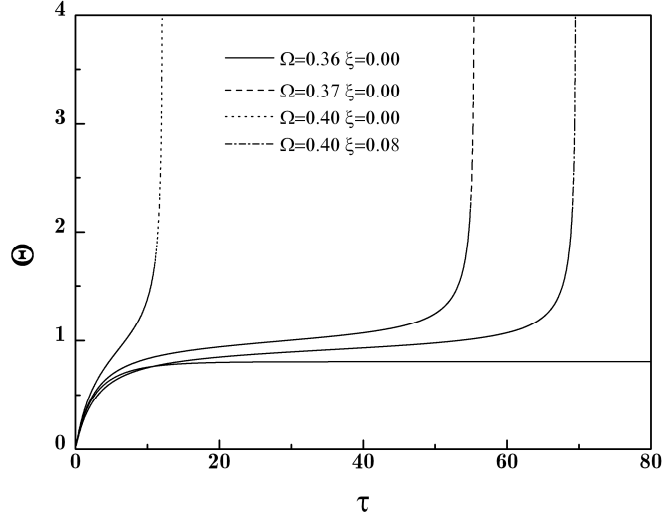
Fig. 12: Nondimensional temperature time histories for the simplified thermal ignition model assuming loss effects

Figure 12 gives the nondimensional temperature time histories for several values of Ω and ξ. The nondimensional ignition delay time, τ_{ig}, is defined as the maximum value of τ at which Θ rapidly increases and approaches infinity. The results of the simplified thermal ignition equation assuming negligible loss effects, figure 10, and non negligible loss effects, figure 12, demonstrate indeed a similar curve progression between the two cases although the two different ansatz shows a large discrepance particularly for values of Ω near Ω_{min}. For $\Omega < \Omega_{min}$, the system frezzes at the stationary point (first intersection) according to figure 11 and no ignition occurs (line with square label). Furthermore the solution of equation (3.153) shows a tremendous dependency on ξ.

Mathematical identification of the second ignition constraint is given by,

$$
\begin{aligned}
\Omega_{min} \exp\left(\Theta_0\right) &= \Theta_0 + \xi \\
\Rightarrow \Omega_{min} &= \frac{\Theta_0 + \xi}{\exp\left(\Theta_0\right)}
\end{aligned}
\tag{3.151}
$$

Thus with $\Theta_0 = 0$ the minimum value for Ω becomes,

$$
\Omega_{min} = \xi
\tag{3.152}
$$

The critical value of ξ at which the second ignition condition must be used instead of the first ignition condition is given with $\Theta_{\mathrm{crit}}=0$ by $\xi=1$ (equation (3.150) Thus the criterion for thermal ignition is given by equation (3.157) and (3.152),

$$\Omega_{\mathrm{min}} = \begin{cases} \exp(\xi-1) & \xi \leq 1 \\ \xi & \xi > 1 \end{cases} \qquad (3.153)$$

Figure 13 shows the necessary values of Ω for which thermal ignition occur. For ξ between 0 and 1 the minimal value of Ω increases exponentially respectively linear for ξ greater than 1.
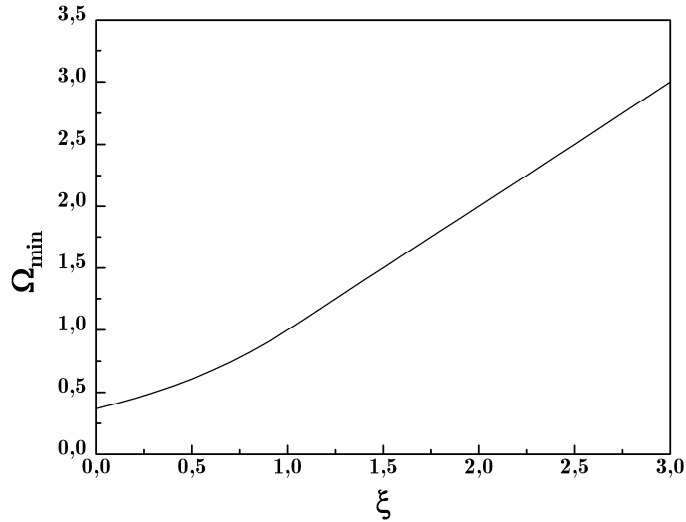
Fig. 13: Ω_{min} for the occurance of thermal ignition for a given ξ

3.2.4.2 Auto ignition condition considering heat loss effects and ignition delay time

Equation (3.153) gives the condition to achieve auto ignition in principle. To determine the time dependency of Ω similar to equation (3.144) in case of an adiabatic chemically reacting flow, equation (3.146) must be integrated. Since no analytical solution exists following ansatz is made. It is clear that Ω should fulfil in the limit of $\tau\to\infty$,

$$\lim_{\tau_{ig} \to \infty} \Omega = \begin{cases} \exp(\xi - 1) & \xi \leq 1 \\ \xi & \xi > 1 \end{cases} \tag{3.154}$$

Furthermore it is obvious that Ω becomes infinity if $\tau_{ig} \to 0$. Thus it is essential,

$$\lim_{\tau_{ig} \to 0} \Omega = \begin{cases} \infty & \xi \leq 1 \\ \infty & \xi > 1 \end{cases} \tag{3.155}$$

Therefore it is convenient to represent Ω as a hyperbolic function as follows,

$$\Omega \geq \begin{cases} \exp(\xi - 1) + \dfrac{C_I(\xi)}{\tau_{ig}^{m_I(\xi)}} & \xi \leq 1 \\[3mm] \xi + \dfrac{C_{II}(\xi)}{\tau_{ig}^{m_{II}(\xi)}} & \xi > 1 \end{cases} \tag{3.156}$$

where m_I, m_{II}, C_I and C_{II} are unknown parameters. It is assumed that they are depending on ξ. They are specified in section 3.4

3.2.5 Thermal ignition theory vs. Branched chain ignition theory

In section 3.1.1.1 the ignition limits were quantitative explained by using a hypothetic branched chain mechanism. Ignition occurs by an excessive generation of chain carries (radicals) which convert the reactants to product. Whether if an accumulation of chain carriers occur or not is strongly dependent on the initial temperature and initial pressure which leads to the three ignition limits. In either case a conversion of the reactants to products occurs (slow or fast reaction dependent on the initial state) except below the first ignition limit where intermediates are generated. By definition ignition is characterized by a rapid increase of temperature although the production of chain carriers and subsequently the conversion of reactants to products which requires the existence of chain carriers occurs at a constant temperature (isothermal). But it is this phenomenon which creates new chain carrier generation steps, e.g., equation (3.10), leading to a massive build up of chain carriers (accumulation) and subsequently the ignition of the mixture. In contrast the thermal ignition

theory assumes a one step global reaction without a need of a deeper understanding of the actual reaction process where the quantitative description is correlated with ignition delay studies. Thus the correlated thermal ignition mechanism assumes a chemical reaction which leads to ignition, i.e., the thermal ignition mechanism describes a approximated reaction process above the first or third ignition limit (usually the third) which can be explained by branched chain ignition mechanism. Thus thermal ignition theory can be seen as an approximation of the branched chain ignition theory. It links external influences (ambient conditions) to the chemical reaction and thus gives an explanation of the criterion for a monotone increasing temperature which is necessary for the excessive accumulation of chain carriers leading to ignition. Actually the correlated thermal ignition mechanism is strictly limited to the range of values (initial pressure and temperature) which are used for the correlation process and extrapolation and prediction of the system behaviour for initial values outside the margin is only conditionally feasible (consideration of the second ignition limit). Furthermore with the branched chain ignition theory the phenomenon of the temperature dependent activation energy can be explained which is alluded e.g. in the study of Dean [40]. For high initial temperatures further chain carrier generation steps are involved in the chemical reaction mechanisms which are suppressed at low and intermediate temperatures. This leads to a faster accumulation of chain carriers. This behaviour is reflected by a temperature dependent global activation energy[†].

3.3 Principles of chemical reactor theory

3.3.1 Residence time

To achieve thermal ignition the reactants have to spend a sufficient time, t_{res}, in the combustion chamber for a given Θ_0 and Ω respectively Ω^* (see equation (3.144) and (3.163)). But particles which reach the combustion chamber at the

---

[†] The activation energy for a global one step reaction is correlated by using the approximated thermal ignition theory.

same time remain there for varying periods of time. One particle moves to the exit immediately while another remains in the combustion chamber longer. This is why the residence time in the combustion chamber is a probable value and can be characterized by a distribution function [41, 42, 43].

3.3.1.1 Residence time distribution (RTD) and mean residence time

As mentioned above, the residence time becomes a probable value due to different residence times for each particle. Therefore the mean residence time, $<t_{res}>$ is given by a residence time distribution function as follows [41,42],

$$\left\langle t_{res} \right\rangle = \int\limits_{0}^{\infty} t f\left(t\right) \mathrm{d}t \tag{3.157}$$

where,

$$\int\limits_{0}^{\infty} f\left(t\right) \mathrm{d}t = 1 \tag{3.158}$$

For ideal reactors such as the ideal mixing continuous stirred tank reactor (CSTR) and the ideal plug flow reactor (PFR) a residence time distribution function can be mathematically derived from corresponding mathematical equations of the rate laws of the concentrations of a substance. In real conditions the flows differ from the ideal flows due to many factors. These factors include: immobility (stagnant) zones, inner bypass-flow, molecular and turbulent diffusion, the nonuniform velocity, recirculation zones, ect. The mathematical description of real reactors can be stated by two methods. The first treats a real reactor as a combination of ideal reactors. The second is based on the description of real physical phenomena in the apparatus by applying the corresponding mathematical equations. Both methods of compiling of the mathematical descriptions are brought into correlations with the experimental data with the help of numerical coefficients which are the parameters of the model. The most commonly used one parameter models are the cell model and the diffusion model.

3.3.1.2 The cell model

The method of treating a real rector as a combination of ideal reactors is used for describing the cell model. The real reactor is conceptually divided into a number, N, of consecutively connected cells of ideal mixing reactors. The sum of the volumes of the divided cells is the same as the volume of the real reactor. A CSTR is described when $N=1$ and for $N\to\infty$, a PFR. The number of the cells, N, is the one parameter of the cell model. The residence time distribution function for the cell model is given by [43],

$$f\left(t\right) = \frac{N^N}{\left(N-1\right)!} \frac{t^{\left(N-1\right)}}{t'^N} \exp\left(-\frac{Nt}{t'}\right) \tag{3.159}$$

where t' is the mean residence time of the reagents in a ideal rector. It is defined as the ratio between the reactor volume V_C and the volume flow rate, $\dot{V}$ -which is given by the mass flow rate, $\dot{m}$, and the gas density, ρ.

$$t' = \frac{V_C}{\dot{V}} = \frac{\rho V_C}{\dot{m}} \tag{3.160}$$

The curves for $f(t)$ are shown in figure 14.
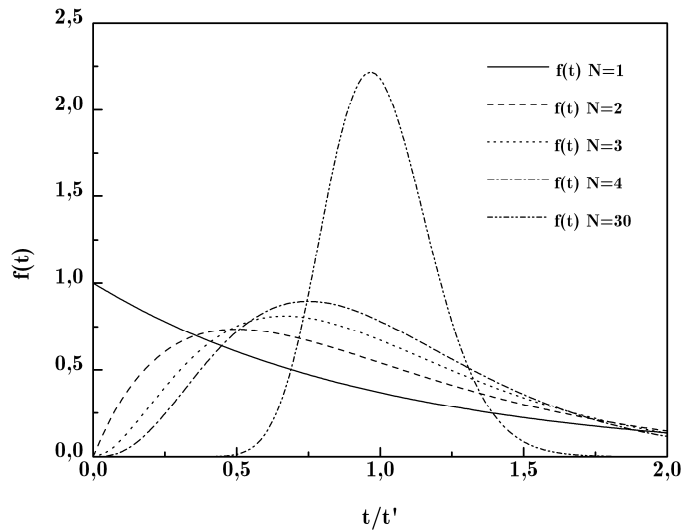
Fig. 14: RTD function vs t/t' for a cascade of N perfectly mixed reactors

These curves can be used to define the meaning of N according to the experimental curves of response for the real regimes in the reactor.

3.3.1.3   The diffusion model

This model describes the flow between two ideal flows which are mixing by diffusion. Because it is difficult to experimentally differentiate the transvers and longitudinal diffusion, the mixing is attributed to the longitudinal diffusion. The coefficient of this diffusion is the only parameter of the model. In contrast to the ideal reactor, the transfer of mass is made not only by convection but also by molecular diffusion which can be determined with the help of the Fick's Law and turbulent diffusion. The residence time distribution for the diffusion model is given by [41],

$$f\left(\delta\right) = \sqrt{\frac{Bo}{4\pi\delta}} \exp\left(-\frac{Bo\left(1-\delta\right)^2}{4\delta}\right)$$

$$Bo = \frac{v_z L}{\zeta'} \quad \delta = \frac{t}{t'}$$

(3.161)

where Bo is known as the Bodenstein number which is a dimensionless number. It is given by the flow velocity, v, the reactor length, L, and the longitudinal diffusion coefficient, ζ'.
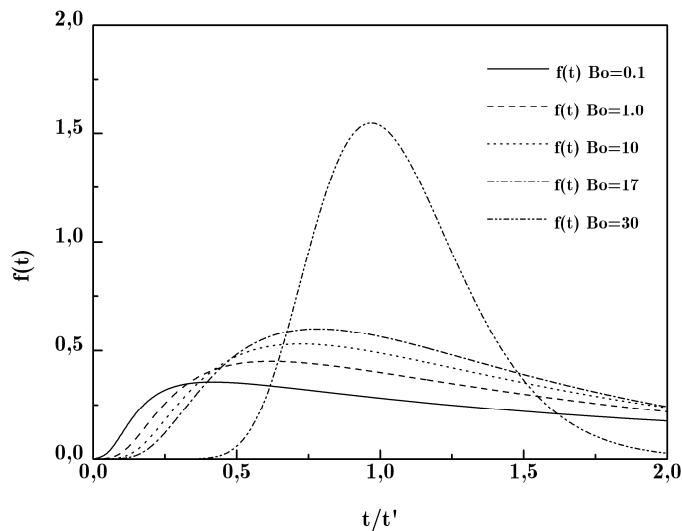
Fig. 15: RTD function vs t/t' for the diffusion model

Figure 15 shows the RTD function for the diffusion model with different values for the parameter *Bo*.

3.3.1.4 Non-ideal reactors

To determine the mean residence time it is necessary to know the exact RTD function of a given reactor. For real reactors the one-parametric models introduced above are only rudimentary practical[†]. It is necessary to introduce multi-parametric models to characterize a real reactor which are on the basis of either axially dispersed plug flow concept or perfect mixers in series model[‡].This is especially the case with processes involving exchanges between a main flow and a stagnant fluid. A commonly used multi-parametric model in residence time distribution applications is the perfect mixers in series with exchange. The conceptional representation of this model is given in figure 15 with $N = 6$.
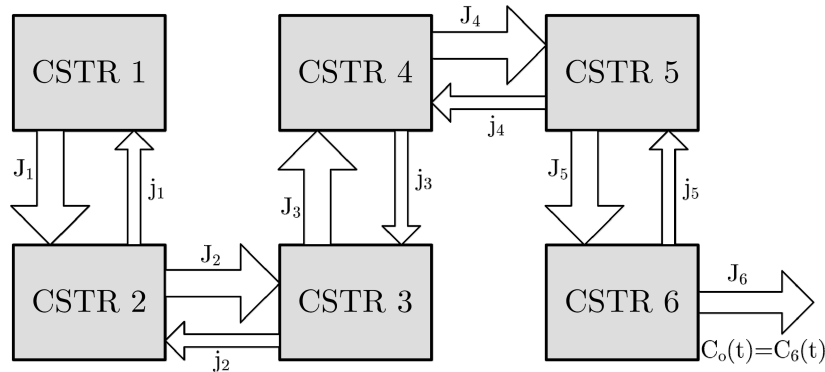
Fig. 16: CSTR in series with back mixing

J is equivalent to the volumetric flow rate passing through the system, j is the recycling volumetric flow rate between two CSTR and $C_O(t)$ is the outlet concentration. For example the recycling flow is formed due to a swirl injector

---

[†] For gas turbine combustion chambers with a swirl injector which consists of 8 blades and swirl angle of 45° degrees three experimental, geometrically similar combustion chambers were manufactured and tested [41]. The authors correlated the results according to a CSTR model without back mixing. The results showed a best fit for the RTD function by using the cell model with $N=4$. It is assumed that a CSTR model with back mixing provides a better fit for the data.

[‡] It should be noted, that these two approaches can be shown to be equivalent

or a rearward facing step induced recirculation. (see chapter 5). The volume of each CSTR is given by the overall reactor volume, V_R, devided by N. The residence time distribution density function is given by the outlet concentration by,

$$f(t) = \frac{C_O(t)}{\int\limits_0^\infty C_O(t)\mathrm{d}t} \tag{3.162}$$

The system of the six CSTR in series with back mixing builds a system of coupled differential equations (CDES) which is given by,

$$\begin{pmatrix} \partial_t c_1 \\ \partial_t c_2 \\ \partial_t c_3 \\ \partial_t c_4 \\ \partial_t c_5 \\ \partial_t c_6 \end{pmatrix} = \frac{6}{V_R} \begin{pmatrix} -J_1 & +j_1 & 0 & 0 & 0 & 0 \\ +J_1 & -(J_2+j_1) & j_2 & 0 & 0 & 0 \\ 0 & +J_2 & -(J_3+j_2) & j_3 & 0 & 0 \\ 0 & 0 & +J_3 & -(J_4+j_3) & j_4 & 0 \\ 0 & 0 & 0 & +J_4 & -(J_5+j_4) & j_5 \\ 0 & 0 & 0 & 0 & +J_5 & -(J_6+j_5) \end{pmatrix} \begin{pmatrix} c_1 \\ c_2 \\ c_3 \\ c_4 \\ c_5 \\ c_6 \end{pmatrix} \tag{3.163}$$

The initial conditions are given by,

$$c_1(0) = C_i \quad c_2(0) = c_3(0) = c_4(0) = c_5(0) = c_6(0) = 0 \tag{3.164}$$

The CDES can be solved with the ansatz,

$$\vec{c} = \exp(\lambda' t)\vec{a} \tag{3.165}$$

Thus the eigenvalues, λ', are given by,

$$\det(\boldsymbol{J} - \lambda'\boldsymbol{I}) = 0 \quad \boldsymbol{I} = \delta_{kl} \tag{3.166}$$

and the eigenvectors, $\vec{a}$, are given by,

$$(\boldsymbol{J} - \lambda'\boldsymbol{I})\vec{a} = 0 \tag{3.167}$$

Therefore the outlet concentration $C_O(t)$ becomes a function of,

$$C_O(t) = c_6(t) = f\left(J_1, ..., J_N, j_1, ..., j_{N-1}, N\right) \tag{3.168}$$

Hence the system is characterised by 2N parameters.

3.4 Detailed definition of the ignition condition

With the equations derived in the previous sections, an analytical model for spontaneous thermal ignition can be developed within the fundamental assumptions that firstly molecular transport and heat conduction along the flow axis is negligible, secondly the flow is one dimensional (uniform temperature transversal to the flow direction), and thirdly the physical properties of the gas mixture are dominated by the initial state and reactant depletion is assumed to be evanescent small (large activation energy).

Furthermore the model focuses in particular onto the prediction of the needed initial combustion chamber pressure to achieve spontaneous thermal ignition (auto ignition). As a basic result of the previous sections the ignition conditions are given by equation (3.144) and equation (3.163) with $\tau_{ig} = X\chi t_{ig}$ and $X = U \Big/ \rho_0 \left\langle c_p \big|_{T_0} \right\rangle_{mix} A$,

$$\Omega^* \geq \frac{1}{t_{ig}} \quad \Omega \geq \begin{cases} \exp\left(\xi - 1\right) + \dfrac{C_I\left(\xi\right)}{\left(X\chi t_{ig}\right)^{m_I(\xi)}} & \xi \leq 1 \\[4mm] \xi + \dfrac{C_{II}\left(\xi\right)}{\left(X\chi t_{ig}\right)^{m_{II}(\xi)}} & \xi > 1 \end{cases} \tag{3.169}$$

For a detailed definition of the ignition condition the fit coefficients, C_I, C_{II}, m_I, m_{II}, the heat transfer coefficient, χ, and the ignition time, t_{ig}, must be specified.

3.4.1 Determination of the fit coefficients for the ignition condition in case of a significant heat loss coefficient

To determine the unknown parameters in equation (3.156), equation (3.146) was solved numerically for several values of Ω and ξ. The nondimensional ignition delay time, τ_{ig}, was identified as the maximum value of τ at which Θ rapidly increases and approaches infinity. In the numerical procedure this was perceivable by a singularity for a given step size. Table 1 and table 2 summarizes the nondimensional ignition delay times, τ_{ig}, dependent of Ω for several ξ between 0.0 and 3.2 and figure 17 shows exemplarily a typical plot of Ω depending on τ_{ig} for ξ=0.

$\Omega,\xi=0$	$\tau,\ \xi=0$	$\Omega,\xi=0.2$	$\tau,\ \xi=0.2$	$\Omega,\xi=0.4$	$\tau,\ \xi=0.4$	$\Omega,\xi=0.8$	$\tau,\ \xi=0.8$
1228.8000000 00000000	0.000813967 529809	1228.8000000 00000000	0.000814033 788329	1280.0000000 00000000	0.000781524 605915	1433.6000000 00000000	0.000697861 000000
614.40000000 0000000	0.001628266 436150	614.40000000 0000000	0.001628531 594936	640.00000000 0000000	0.001563599 147503	716.80000000 0000000	0.001396360 000000
307.20000000 0000000	0.003257859 338303	307.20000000 0000000	0.003258920 972310	320.00000000 0000000	0.003129400 519722	358.40000000 0000000	0.002795250 000000
153.60000000 0000000	0.006521030 000000	153.60000000 0000000	0.006525286 779570	160.00000000 0000000	0.006267629 848323	179.20000000 0000000	0.005600678 453755
76.800000000 000000	0.013063400 000000	76.800000000 000000	0.013080463 032893	80.000000000 000000	0.012570735 079141	89.600000000 000000	0.011242329 170275
38.400000000 000000	0.026212522 620177	38.400000000 000000	0.026281372 987895	40.000000000 000000	0.025284666 899064	44.800000000 000000	0.022650545 147824
19.200000000 000000	0.052772132 262164	19.200000000 000000	0.053051775 725646	20.000000000 000000	0.051152712 438348	22.400000000 000000	0.045981101 186920
9.6000000000 00000	0.106965900 557288	9.6000000000 00000	0.108119769 809321	10.000000000 000000	0.104727535 545371	11.200000000 000000	0.094822200 000000
4.8000000000 00000	0.219901171 938171	4.8000000000 00000	0.224822792 811471	5.0000000000 00000	0.219920579 463579	5.6000000000 00000	0.202355115 336923
2.4000000000 00000	0.466246278 930894	2.4000000000 00000	0.488841459 635053	2.5000000000 00000	0.489271929 109085	2.8000000000 00000	0.468995778 222697
1.2000000000 00000	1.065404072 139080	1.2000000000 00000	1.190357035 295090	1.0000000000 00000	1.883515626 835240	1.4000000000 00000	1.416083869 175570
0.5000000000 00000	4.746628785 891420	0.5500000000 00000	6.097057529 466440	0.6600000000 00000	5.874089531 175620	0.9000000000 00000	6.830824002 672660
0.4000000000 00000	12.09975023 1527600	0.4800000000 00000	13.44058686 2429100	0.5900000000 00000	11.80426466 1131600	0.8570000000 00000	11.82650423 3591300
0.3900000000 00000	15.14466618 5494000	0.4700000000 00000	17.09878724 8740700	0.5700000000 00000	18.03904415 2935700	0.8380000000 00000	19.06174467 6251000

0.380000000000000	21.459657249600800	0.453000000000000	45.431460663547800	0.555000000000000	37.123521661393300	0.825000000000000	39.545093011326900
0.370000000000000	55.441127610492200	0.451000000000000	69.113885281448600	0.552000000000000	53.538904152960300	0.823000000000000	50.019716949321000
0.369000000000000	77.413692141577100	0.450000000000000	111.214935168300000	0.550000000000000	90.699666549489000	0.820000000000000	100.852805526827000

Tab. 1: Ignition delay times τ_{ig} for several ξ between 0.0 and 0.8 vs. Ω

$\Omega,\xi=1.2$	$\tau, \xi=1.2$	$\Omega,\xi=1.6$	$\tau, \xi=1.6$	$\Omega,\xi=2.4$	$\tau, \xi=2.4$	$\Omega,\xi=3.2$	$\tau, \xi=3.2$
1638.40000000000000	0.000610668277423	1843.20000000000000	0.000542843880375	2539.52000000000000	0.000394000113084	3307.52000000000000	0.000302510496229
819.200000000000000	0.001221970975372	921.600000000000000	0.001086307114160	1269.76000000000000	0.000788450824430	1653.76000000000000	0.000605359907850
409.600000000000000	0.002446484131202	460.800000000000000	0.002175096583552	634.880000000000000	0.001578707764971	826.880000000000000	0.001212078276809
204.800000000000000	0.004903173128879	230.400000000000000	0.004360162318276	317.440000000000000	0.003164669935341	413.440000000000000	0.002429612913005
102.400000000000000	0.009847457430361	115.200000000000000	0.008760522278626	158.720000000000000	0.006358599552554	206.720000000000000	0.004881230000000
51.2000000000000000	0.019861734802244	57.6000000000000000	0.017684455712117	79.3600000000000000	0.012836215814273	103.360000000000000	0.009851980000000
25.6000000000000000	0.040410443781882	28.8000000000000000	0.036044396303024	39.6800000000000000	0.026165000000000	51.6800000000000000	0.020074500000000
12.8000000000000000	0.083738353486552	14.4000000000000000	0.074980840308177	19.8400000000000000	0.054444875880001	25.8400000000000000	0.041739764617357
6.40000000000000000	0.180731182603732	7.20000000000000000	0.163351341856196	9.92000000000000000	0.118749175229837	12.9200000000000000	0.090899552148603
3.20000000000000000	0.432525584180800	3.60000000000000000	0.402483098557118	4.96000000000000000	0.294615887376219	6.46000000000000000	0.224927764300220
1.60000000000000000	1.555153373212140	1.80000000000000000	1.897302416638160	2.48000000000000000	1.891310264707330	3.23000000000000000	1.855456487158380
1.24000000000000000	5.890218192551510	1.61000000000000000	5.840163497840500	2.40040000000000000	5.568987484448520	3.20001000000000000	5.475297578846850
1.23000000000000000	6.710484891072540	1.60100000000000000	9.536264164358310	2.40000400000000000	8.851756920276030	3.20000000100000000	9.581357002823950
1.22000000000000000	7.971401311199780	1.60010000000000000	13.350373050413000	2.40000040000000000	13.701240303038600	3.20000000010000000	12.673382183500100
1.21000000000000000	10.393022109361300	1.60000010000000000	24.776033114013100	2.40000000040000000	16.940339251311500	3.20000000000100000	13.705263443611100
1.20100000000000000	20.223682483680700	1.60000000010000000	39.894656112986600	2.40000000004000000	18.559961441768800	3.20000000000060000	13.930493588788900
1.20001000000000000	42.810581707047300	1.60000000000100000	47.457873838325700	2.40000000000040000	21.798020536347000	3.20000000000050000	14.017183856935300

Tab. 2: Ignition delay times τ_{ig} for several ξ between 1.2 and 3.2 vs. Ω
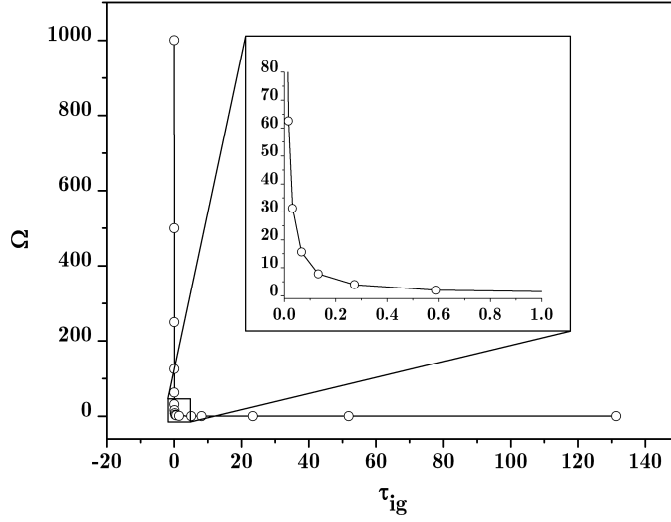
Fig. 17: Ω vs. τ_{ig}

The main graph shows the fit domain for Ω and the inset shows the characteristics of Ω for low nondimensional ignition delay times, τ_{ig}. The circles represent the values of Ω where the thermal energy equation accounting loss effects was solved numerically (equation (3.146). The solid line gives the relationship between Ω and τ_{ig} according to a fit procedure where equation (3.156) was used as a fit function. The fit procedure provides values for C_I, C_{II}, m_I and m_{II} as shown in table 3. At the first iteration it becomes obvious that the exponent m_I and m_{II} differs from unity imperceptibly and secondly, it is assumed m_I and m_{II} does not depend on ξ. Thus for the second iteration the exponent m_I and m_{II} were defined to be unity. Furthermore values of R^2, the coefficient of determination are displayed which indicates the quality of a fit. It is defined as,

$$R^2 = 1 - \frac{\sum_i \left(y_{i,data} - y_{i,fit}\right)^2}{\sum_i \left(y_{i,data} - \overline{y_{i,data}}\right)^2} \tag{3.170}$$

where, $y_{i,data}$ is given by the data, $y_{i,fit}$ is equal to the fitted data and $\overline{y_{i,data}}$ is equal to the mean of the observed data. An $R^2=1$ indicates a perfectly model fit.

96

ξ	$C_{I,1}$	$C_{II,1}$	$m_{I,1}$	$m_{II,1}$	R^2	$C_{I,2}$	$C_{II,2}$	$m_{I,2}$	$m_{II,2}$	R^2
0	0.99		1.00031		1	0.99		1		1
0.2	0.99		1.00026		1	0.99		1		1
0.4	0.99		1.00025		1	0.99		1		1
0.8	0.99		1.00037		1	0.99		1		1
1.2		0.99		1.00068	1		0.99		1	1
1.6		0.99		1.00094	1		0.99		1	1
2.4		0.99		1.00118	1		0.99		1	1
3.2		0.99		1.00129	1		0.99		1	1

Tab. 3: Fit parameters for ξ between 0.0 and 3.2

It is also evident that C_I and C_{II} do not depend on ξ. Furthermore for analogousness between the adiabatic ignition condition, equation (3.144) and the non-adiabatic ignition condition, C_I and C_{II} are defined to unity.

$$C_I = C_{II} = 1 \tag{3.171}$$

Thus the ignition condition for a real system, equation (3.156) becomes

$$\Omega = \begin{cases} \exp\left(\xi - 1\right) + \dfrac{1}{X\chi t_{ig}} & \xi \leq 1 \\[2ex] \xi + \dfrac{1}{X\chi t_{ig}} & \xi > 1 \end{cases} \tag{3.172}$$

3.4.2 Determination of the ignition time

The ignition delay time defines the time within the reactant have to be ignite before they are expelled. It can be defined as the difference of the residence time, t_{res}, and the evaporation time, t_{evap}, which is needed for evaporation of the reactants,

$$t_{ig} = t_{res} - t_{evap} \tag{3.173}$$

As mentioned in section 3.3 the particles which reach the combustion chamber at the same time remain there for varying periods of time. One particle moves

to the exit immediately while another remains in the combustion chamber longer. This is why the residence time in the combustion chamber is a probable value and can be characterized by a distribution function. If a plug flow reactor (PFR) is assumed the residence time is easily given by the definition of the mass flow,

$$\dot{m} = \rho A \frac{\mathrm{d}s}{\mathrm{d}t} \Rightarrow \dot{m} t_{res} = \rho V_C \Rightarrow t_{res} = \frac{\rho V_C}{\dot{m}} \tag{3.174}$$

The same result for the residence time of a PFR is obtained by calculating the mean value of the residence time with the PFR-RTD function

$$t_{res} = \frac{\rho V_C}{\dot{m}} = \int_0^\infty t\delta\left(t - \frac{\rho V_C}{\dot{m}}\right)\mathrm{d}t \Rightarrow t = \frac{\rho V_C}{\dot{m}} \tag{3.175}$$

Basically it is imperative that the residence time becomes a function of the combustion chamber volumen, $t_{res} = f\left(V_C\right)$. In fact that if the volume becomes larger the residence time becomes longer. Therefore for a real reactor one can phenomenological propose for the residence time,

$$t_{res} = \Phi \frac{\rho V_C}{\dot{m}} \tag{3.176}$$

where Φ is a dimensionless parameter which defines the difference of the behaviour between a PFR and a real rector. For consistency the same result should be obtained according to the PFR by,

$$t_{res} = \Phi \frac{\rho V_C}{\dot{m}} = \int_0^\infty t f\left(t\right)\mathrm{d}t \tag{3.177}$$

This can be shown as follows. For simplification purpose the residence time distribution function, $f(t)$, is derived assuming two CSTR in series with back mixing and using the assumption $J_1 = J_2 = J$, $J/V_R = 1/t'$ and $j = \zeta J$. Therefore equation (3.163) becomes,

$$\begin{pmatrix} \partial_t c_1 \\ \partial_t c_2 \end{pmatrix} = \begin{pmatrix} -2t'^{-1} & +2\zeta t'^{-1} \\ +2t'^{-1} & -2t'^{-1}\left(1+\zeta\right) \end{pmatrix}\begin{pmatrix} c_1 \\ c_2 \end{pmatrix} \tag{3.178}$$

The eigenvalues are given by equation (3.167),

$$\det\begin{pmatrix} -2t'^{-1}-\lambda' & +2\zeta t'^{-1} \\ +2t'^{-1} & -2t'^{-1}\left(1+\zeta\right)-\lambda' \end{pmatrix} = 0 \tag{3.179}$$

Further algebra results for the eigenvalues,

$$\begin{aligned} \lambda_1' &= -\frac{2+\zeta+\sqrt{4\zeta+\zeta^2}}{t'} \\ \lambda_2' &= -\frac{2+\zeta-\sqrt{4\zeta+\zeta^2}}{t'} \end{aligned} \tag{3.180}$$

and the eigenvectors becomes,

$$\begin{aligned} \vec{a}_1 &= \begin{pmatrix} \frac{1}{2}\left(\zeta-\sqrt{4\zeta+\zeta^2}\right) \\ 1 \end{pmatrix} \\ \vec{a}_2 &= \begin{pmatrix} \frac{1}{2}\left(\zeta+\sqrt{4\zeta+\zeta^2}\right) \\ 1 \end{pmatrix} \end{aligned} \tag{3.181}$$

Thus the concentrations are given by,

$$\vec{c}\left(t\right) = k_1'\exp\left(\lambda_1't\right)\frac{\vec{a}_1}{\left|\vec{a}_1\right|} + k_2'\exp\left(\lambda_1't\right)\frac{\vec{a}_2}{\left|\vec{a}_2\right|} \tag{3.182}$$

Hence

$$
\begin{aligned}
c_1\left(t\right) &= \frac{k_1'\left(\zeta - \sqrt{4\zeta + \zeta^2}\right)}{2\left|\vec{a}_1\right|}\exp\left(-\frac{2+\zeta+\sqrt{4\zeta+\zeta^2}}{t'}t\right) \\
&+ \frac{k_2'\left(\zeta + \sqrt{4\zeta + \zeta^2}\right)}{2\left|\vec{a}_2\right|}\exp\left(-\frac{2+\zeta-\sqrt{4\zeta+\zeta^2}}{t'}t\right) \\
c_2\left(t\right) &= \frac{k_1'}{\left|\vec{a}_1\right|}\exp\left(-\frac{2+\zeta+\sqrt{4\zeta+\zeta^2}}{t'}t\right) \\
&+ \frac{k_2'}{\left|\vec{a}_2\right|}\exp\left(-\frac{2+\zeta-\sqrt{4\zeta+\zeta^2}}{t'}t\right)
\end{aligned}
\tag{3.183}
$$

With the initial conditions given by equation (3.164), k_1 and k_2 becomes,

$$
\begin{aligned}
C_i &= \frac{k_1'\left(\zeta - \sqrt{4\zeta + \zeta^2}\right)}{2\left|\vec{a}_1\right|} + \frac{k_2'\left(\zeta + \sqrt{4\zeta + \zeta^2}\right)}{2\left|\vec{a}_2\right|} \\
0 &= \frac{k_1'}{\left|\vec{a}_1\right|} + \frac{k_2'}{\left|\vec{a}_2\right|}
\end{aligned}
\tag{3.184}
$$

which leads to,

$$
k_1' = -\frac{\left|\vec{a}_1\right|C_i}{\sqrt{4\zeta + \zeta^2}} \quad k_2' = \frac{\left|\vec{a}_2\right|C_i}{\sqrt{4\zeta + \zeta^2}}
\tag{3.185}
$$

Therefore the outlet concentration is given by,

$$
C_O\left(t\right) = c_2\left(t\right) = \frac{C_i}{\sqrt{4\zeta + \zeta^2}}\left[\exp\left(-\frac{2+\zeta-\sqrt{4\zeta+\zeta^2}}{t'}t\right) - \exp\left(-\frac{2+\zeta+\sqrt{4\zeta+\zeta^2}}{t'}t\right)\right]
\tag{3.186}
$$

The residence time distribution density function is given with equation (3.162) by,

$$f\left(t\right) = \frac{\exp\left(-\dfrac{2+\zeta-\sqrt{4\zeta+\zeta^2}}{t'}t\right) - \exp\left(-\dfrac{2+\zeta+\sqrt{4\zeta+\zeta^2}}{t'}t\right)}{\displaystyle\int_0^\infty\left[\exp\left(-\dfrac{2+\zeta-\sqrt{4\zeta+\zeta^2}}{t'}t\right) - \exp\left(-\dfrac{2+\zeta+\sqrt{4\zeta+\zeta^2}}{t'}t\right)\right]\mathrm{d}t}$$

$$(3.187)$$

and becomes (for $N=2$),

$$f\left(t\right) = \frac{2}{t'\sqrt{4\zeta+\zeta^2}}\left[\exp\left(-\frac{2+\zeta-\sqrt{4\zeta+\zeta^2}}{t'}t\right) - \exp\left(-\frac{2+\zeta+\sqrt{4\zeta+\zeta^2}}{t'}t\right)\right]$$

$$(3.188)$$

The mean residence time, $<t_{res}>$, becomes with equation (3.157)

$$\left\langle t_{res}\right\rangle = \int_0^\infty tf\left(t\right)\mathrm{d}t = \left(1+\frac{1}{2}\zeta\right)t' = \left(1+\frac{1}{2}\zeta\right)\frac{\rho V_C}{\dot{m}} \qquad (3.189)$$

For $N=3$ the residence time distribution density function can be determined analytically as well which is [44],

$$f\left(t\right) = \frac{1}{4\zeta t'}\exp\left(\frac{-t}{t'}\right)\left[\exp\left(-\sqrt{\frac{2\zeta}{1+2\zeta}}\frac{t}{t'}\right) + \exp\left(\sqrt{\frac{2\zeta}{1+2\zeta}}\frac{t}{t'}\right) - 2\right] \qquad (3.190)$$

where t' is the mean residence time of one CSTR ($V_R/3$). Thus the mean residence time, $<t_{res}>$, becomes,

$$\left\langle t_{res}\right\rangle = \int_0^\infty tf\left(t\right)\mathrm{d}t = \left(3+4\zeta\right)t' = \left(1+\frac{4}{3}\zeta\right)\frac{\rho V_C}{\dot{m}} \qquad (3.191)$$

From equation (3.189) and equation (3.191) follows that the mean residence time can be defined phenomenological as

$$\left\langle t_{res}\right\rangle = \varPhi\,\frac{V_C\rho}{\dot{m}} \qquad (3.192)$$

with $\Phi=[1,\infty]$. Figure 18 shows the mean RTD function of a system with three CSTR ($N=3$) in series with back mixing for different values of ζ and $t'=5$ms. For small values of ζ the probability to find molecules in the time interval $\left(t \gg t', t+\mathrm{d}t\right)$ becomes low. For large values of ζ the RTD function becomes highly asymmetrical and therefore the probability to find molecules in the time interval $\left(t \gg t', t+\mathrm{d}t\right)$ becomes high.
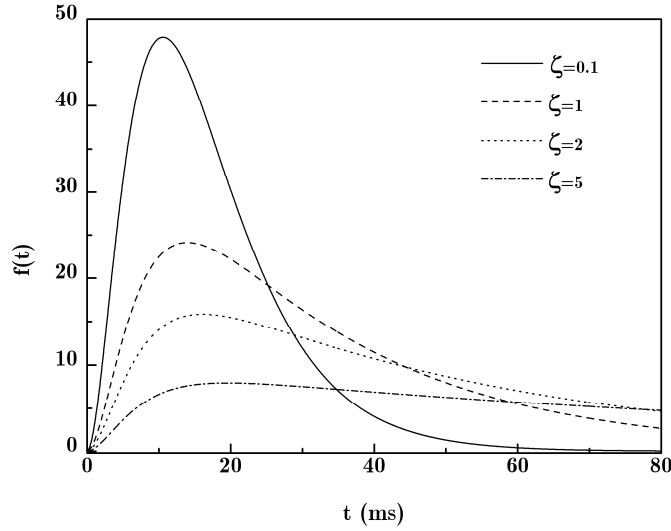

Fig. 18: Theoretical RTD for 3 CSTR in series with back mixing

Therefore the ignition delay time becomes,

$$t_{ig} = \Phi \frac{V_C \rho}{\dot{m}} - t_{evap} \tag{3.193}$$

Therefore it is assumed that the mean value of the residence time of a given reactor is the essential parameter for the determination of the ignition delay time

102

3.4.3 Determination of the heat transfer coefficient

Generally the heat transfer coefficient for a cylindrical flow for one species is given by,

$$\chi = \frac{\lambda Nu}{D_C} \tag{3.194}$$

where λ is equal to the heat conduction coefficient, Nu is known as the Nusselt number and D_C is equal to the combustion chamber diameter. A widely used method to determine the Nusselt number, Nu, is given by the Dittus Boelter relation [45-52].

$$Nu = 0.026 Re^{0.8} Pr^{0.3} \tag{3.195}$$

where Re and Pr are known as the Reynolds number and the Prandtl number respectively. It should be noted that equation (3.195) is only valid for a turbulent pipe flow which is given by $Re>2300$ and for a location far from the pipe entrance ($>$50 pipe diameters) Nevertheless, this heat transfer correlation is used for further calculations and prediction even for $Re<2300$ since the flow pattern inside a combustion chamber is to be assumed turbulent. The Reynolds number and the Prandtl number are given by,

$$Re = \frac{\rho v D_C}{\mu'} \quad Pr = \frac{\mu' c_p}{\lambda} \tag{3.196}$$

where ρ denotes the gas density, v represents the flow velocity, μ' is equal to the dynamic gas viscosity, and c_p is equal to the mean specific heat of the gas By substituting the gas velocity, v, which is dependent on mass flow rate, flow area and density, the Reynolds Number becomes,

$$Re = \frac{4\dot{m}}{\pi \mu' D_C} \tag{3.197}$$

Thus the heat transfer coefficient becomes after further algebra noting that the physical properties, λ, μ', c_p, of a substance depend on temperature

$$\chi(T) = \lambda(T)0.026\left[\frac{4\dot{m}}{\pi\mu'(T)}\right]^{0.8}\left[\frac{\mu'(T)c_p(T)}{\lambda(T)}\right]^{0.3}D_C^{-1.8}$$

$$= 0.026\frac{\lambda(T)^{0.7}c_p(T)^{0.3}}{\sqrt{\mu'(T)}}\left(\frac{4\dot{m}}{\pi}\right)^{0.8}D_C^{-1.8} \tag{3.198}$$

Since the temperature increase till ignition occurs is small for large activation energies the heat transfer coefficient becomes,

$$\chi\big|_{T_0} = 0.026\frac{\left(\lambda\big|_{T_0}\right)^{0.7}\left(c_p\big|_{T_0}\right)^{0.3}}{\sqrt{\mu'\big|_{T_0}}}\left(\frac{4\dot{m}}{\pi}\right)^{0.8}D_C^{-1.8} \tag{3.199}$$

For a mixture of several species the heat transfer coefficient is given by,

$$\left\langle\chi\big|_{T_0}\right\rangle_{mix} = 0.026\frac{\left(\left\langle\lambda\big|_{T_0}\right\rangle_{mix}\right)^{0.7}\left(\left\langle c_p\big|_{T_0}\right\rangle_{mix}\right)^{0.3}}{\sqrt{\left\langle\mu'\big|_{T_0}\right\rangle_{mix}}}\left(\frac{4\dot{m}}{\pi}\right)^{0.8}D_C^{-1.8} \tag{3.200}$$

with the mean physical properties of the mixture given by,

$$\left\langle c_p\big|_{T_0}\right\rangle_{mix} = \frac{\displaystyle\sum_{\mu=1}^{N'}\mathfrak{M}^\mu n^\mu c_p^\mu\big|_{T_0}}{\displaystyle\sum_{i}^{N'}\mathfrak{M}^\mu n^\mu}$$

$$\left\langle \lambda\big|_{T_0}\right\rangle_{mix} = \frac{\displaystyle\sum_{\mu=1}^{N'}\sqrt[3]{\mathfrak{M}^\mu}\, n^\mu\, \lambda^\mu\big|_{T_0}}{\displaystyle\sum_{\mu=1}^{N'}\sqrt[3]{\mathfrak{M}^\mu}\, n^\mu}$$

$$\left\langle \mu'\big|_{T_0}\right\rangle_{mix} = \frac{\displaystyle\sum_{\mu=1}^{N'}\sqrt{\mathfrak{M}^\mu}\, n^\mu\, \mu'^\mu\big|_{T_0}}{\displaystyle\sum_{\mu=1}^{N'}\sqrt{\mathfrak{M}^\mu}\, n^\mu} \tag{3.201}$$

104

If the temperature dependency of the physical properties is small, the heat transfer coefficient can be approximated by,

$$\langle \chi \rangle = \left\langle \left\langle \chi \big|_{T_0} \right\rangle_{mix} \right\rangle_{T_0} = 0.026 \left(\frac{4\dot{m}}{\pi} \right)^{0.8} D_C^{-1.8} \left\langle \frac{\left(\left\langle \lambda \big|_{T_0} \right\rangle_{mix} \right)^{0.7} \left(\left\langle c_p \big|_{T_0} \right\rangle_{mix} \right)^{0.3}}{\sqrt{\left\langle \mu' \big|_{T_0} \right\rangle_{mix}}} \right\rangle_{T_0}$$

$$(3.202)$$

3.4.4 Auto ignition conditions

The general adiabatic and non-adiabatic thermal ignition conditions are given with equation (3.144) and (3.156) by,

$$\text{adiabatic:} \qquad \Omega^* \geq \frac{1}{t_{ig}}$$

$$\text{non-adiabatic:} \quad \Omega \geq \begin{cases} \exp(\xi - 1) + \dfrac{1}{\tau_{ig}} & \xi \leq 1 \\[2mm] \xi + \dfrac{1}{\tau_{ig}} & \xi > 1 \end{cases}$$

$$(3.203)$$

with,

$$\Omega^* = \frac{Q_r E_A A'(\phi) \left[Fuel \right]_0^{\alpha'} \displaystyle\prod_{\substack{\mu \neq Fuel}}^{N'-1} \left[C^\mu \right]_0^{\beta_\mu}}{R T_0^2 \rho_0 \left\langle c_p \big|_{T_0} \right\rangle_{mix}} \exp\left(-\frac{E_A}{R T_0} \right)$$

$$\Omega = \frac{Q_r E_A A'(\phi) \left[Fuel \right]_0^{\alpha'} \displaystyle\prod_{\substack{\mu \neq Fuel}}^{N'-1} \left[C^\mu \right]_0^{\beta_\mu}}{R T_0^2 \left\langle \chi \big|_{T_0} \right\rangle_{mix}} \frac{A}{U} \exp\left(-\frac{E_A}{R T_0} \right)$$
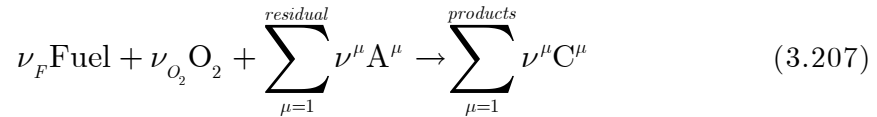
$$(3.204)$$

and,

$$
\begin{aligned}
\tau_{ig} &= \frac{\left\langle \chi\big|_{T_0}\right\rangle_{mix}}{\rho_0 \left\langle c_p\big|_{T_0}\right\rangle_{mix}} \frac{U}{A} t_{ig} \\
\xi &= \frac{1}{\varepsilon T_0}\left(T_0 - \left\langle T_w\right\rangle\right) \\
\varepsilon &= \frac{R T_0}{E_A} \\
t_{ig} &= \left\langle t_{res}\right\rangle - t_{evap} \\
\left\langle t_{res}\right\rangle &= \Phi \frac{V_C \rho_0}{\dot{m}}
\end{aligned}
\tag{3.205}
$$

If ideal gas law is assumed the concentrations, $\left[Fuel\right]_0$ and $\left[C^\mu\right]_0$ can be expressed by

$$
\begin{aligned}
\left[C^\mu\right]_0 &= Y_\mu \frac{p_0}{R T_0} \\
\left[Fuel\right]_0 &= Y_{Fuel} \frac{p_0}{R T_0}
\end{aligned}
\tag{3.206}
$$

Where Y^μ is equivalent to the mole fraction of species μ. The indices 0 denotes initial values. To determine the mole fraction of species μ it is necessary to distinguish between three kinds of combustion processes which are, lean, rich, and stoichiometric Basically for a combustion process the chemical reaction can be written as

$$
\nu_F \text{Fuel} + \nu_{O_2} \text{O}_2 + \sum_{\mu=1}^{residual} \nu^\mu \text{A}^\mu \rightarrow \sum_{\mu=1}^{products} \nu^\mu \text{C}^\mu
\tag{3.207}
$$

where ν_F and ν_{O_2} are the stoichiometric factors of fuel and oxygen and ν^μ is the stoichiometric factor of residual species A^μ. Thus,

$$
\left[Fuel\right]_0^{\alpha'} \prod_{\mu \neq Fuel}^{N'-1} \left[C^\mu\right]_0^{\beta_\mu} = \left[Fuel\right]_0^{\alpha_F} \left[O_2\right]_0^{\alpha_{O_2}} \prod_{\mu \neq Fuel \wedge \mu \neq O_2}^{N'-2} \left[C^\mu\right]_0^{\beta_\mu}
\tag{3.208}
$$

The three different combustion process cases can be given by,

106

$$\text{Stoichiometric :} \qquad \text{Rich :} \qquad \text{Lean :}$$

$$
\begin{aligned}
\nu_F &= \nu_F^{(st)} & \nu_F &= \nu_F^{(st)} + \Delta\nu_F & \nu_F &= \nu_F^{(st)} \\
\nu_{O_2} &= \nu_{O_2}^{(st)} & \nu_{O_2} &= \nu_{O_2}^{(st)} & \nu_{O_2} &= \nu_{O_2}^{(st)} + \Delta\nu_{O_2}
\end{aligned}
\tag{3.209}
$$

Note that the additional amount of substance $(\Delta\nu)$ is not consumed by the chemical reaction. Therefore the mole fractions which contributes in a chemical reaction for the three different cases are given by,

$$
\text{Stoich. :} \quad Y_F = \frac{\nu_F^{(st)}}{\nu_F^{(st)} + \nu_{O_2}^{(st)} + \overset{residual}{\underset{\mu=1}{\sum}} \nu^\mu} \qquad Y_{O_2} = \frac{\nu_{O_2}^{(st)}}{\nu_F^{(st)} + \nu_{O_2}^{(st)} + \overset{residual}{\underset{\mu=1}{\sum}} \nu^\mu}
$$

$$
\text{Rich :} \quad Y_F = \frac{\nu_F^{(st)} + \Delta\nu_F}{\nu_F^{(st)} + \Delta\nu_F + \nu_{O_2}^{(st)} + \overset{residual}{\underset{\mu=1}{\sum}} \nu^\mu} \qquad Y_{O_2} = \frac{\nu_{O_2}^{(st)}}{\nu_F^{(st)} + \Delta\nu_F + \nu_{O_2}^{(st)} + \overset{residual}{\underset{\mu=1}{\sum}} \nu^\mu}
$$

$$
\text{Lean :} \quad Y_F = \frac{\nu_F^{(st)}}{\nu_F^{(st)} + \nu_{O_2}^{(st)} + \Delta\nu_{O_2} + \overset{residual}{\underset{\mu=1}{\sum}} \nu^\mu} \qquad Y_{O_2} = \frac{\nu_{O_2}^{(st)} + \Delta\nu_{O_2}}{\nu_F^{(st)} + \nu_{O_2}^{(st)} + \Delta\nu_{O_2} + \overset{residual}{\underset{\mu=1}{\sum}} \nu^\mu}
$$

$$\tag{3.210}$$

Introducing the equivalence ratio as,

$$
\phi = \frac{\dfrac{m_F}{m_{O_2}}}{\left(\dfrac{m_F}{m_{O_2}}\right)_{stoich}} = \frac{\dfrac{\mathfrak{M}_F \nu_F}{\mathfrak{M}_{O_2} \nu_{O_2}}}{\dfrac{\mathfrak{M}_F \nu_F^{(st)}}{\mathfrak{M}_{O_2} \nu_{O_2}^{(st)}}}
\tag{3.211}
$$

leads to,

$$
\text{Stoich.:} \quad \nu_F = \nu_F^{(st)} \qquad\qquad\qquad , \nu_{O_2} = \nu_{O_2}^{(st)}
$$

$$
\text{Rich:} \quad \nu_F = \nu_F^{(st)} + \Delta\nu_F = \phi\nu_F^{(st)} \quad , \nu_{O_2} = \nu_{O_2}^{(st)}
\tag{3.212}
$$

$$
\text{Lean:} \quad \nu_{O_2} = \nu_{O_2}^{(st)} + \Delta\nu_{O_2} = \frac{\nu_{O_2}^{(st)}}{\phi} \quad , \nu_F = \nu_F^{(st)}
$$

combining with equation (3.210), the mole fractions for the three different cases becomes,

$$
\text{Stoich.}: \quad Y_F = \frac{\nu_F^{(st)}}{\nu_F^{(st)} + \nu_{O_2}^{(st)} + \overset{residual}{\underset{\mu=1}{\sum}} \nu^\mu} \qquad Y_{O_2} = \frac{\nu_{O_2}^{(st)}}{\nu_F^{(st)} + \nu_{O_2}^{(st)} + \overset{residual}{\underset{\mu=1}{\sum}} \nu^\mu}
$$

$$
\text{Rich}: \quad Y_F = \frac{\phi\nu_F^{(st)}}{\phi\nu_F^{(st)} + \nu_{O_2}^{(st)} + \overset{residual}{\underset{\mu=1}{\sum}} \nu^\mu} \qquad Y_{O_2} = \frac{\nu_{O_2}^{(st)}}{\phi\nu_F^{(st)} + \nu_{O_2}^{(st)} + \overset{residual}{\underset{\mu=1}{\sum}} \nu^\mu}
$$

$$
\text{Lean}: \quad Y_F = \frac{\nu_F^{(st)}}{\nu_F^{(st)} + \nu_{O_2}^{(st)}\phi^{-1} + \overset{residual}{\underset{\mu=1}{\sum}} \nu^\mu} \qquad Y_{O_2} = \frac{\nu_{O_2}^{(st)}\phi^{-1}}{\nu_F^{(st)} + \nu_{O_2}^{(st)}\phi^{-1} + \overset{residual}{\underset{\mu=1}{\sum}} \nu^\mu}
$$

$$(3.213)$$

The density ρ_0 can be expressed as

$$
\rho_0 = \overset{reactants}{\underset{\mu=1}{\sum}} \rho_0^\mu = \overset{reactants}{\underset{\mu=1}{\sum}} \mathfrak{M}^\mu \left[C^\mu \right] = \frac{p_0}{T_0 R} \overset{reactants}{\underset{\mu=1}{\sum}} \mathfrak{M}^\mu Y^\mu = \frac{p_0}{T_0 R} \frac{\overset{reactants}{\underset{\mu=1}{\sum}} \mathfrak{M}^\mu \nu^\mu}{\overset{reactants}{\underset{\mu=1}{\sum}} \nu^\mu} = \frac{p_0 \left\langle \mathfrak{M} \right\rangle}{T_0 R}
$$

$$(3.214)$$

with the mean molar mass given by,

$$
\left\langle \mathfrak{M} \right\rangle_{mix} = \left(\frac{\mathfrak{M}_F \nu_F + \mathfrak{M}_{O_2} \nu_{O_2} + \overset{residual}{\underset{\mu=1}{\sum}} \mathfrak{M}^\mu \nu^\mu}{\nu_F + \nu_{O_2} + \overset{residual}{\underset{\mu=1}{\sum}} \nu^\mu} \right) \qquad (3.215)
$$

With equation (3.212) the mean molar mass depents on the equivalent ratio,

$$\left\langle \mathfrak{M} \right\rangle_\phi^{mix} = \begin{cases} \dfrac{\mathfrak{M}_F \nu_F^{(st)} + \mathfrak{M}_{O_2} \nu_{O_2}^{(st)} + \displaystyle\sum_{\mu=1}^{\text{residual}} \mathfrak{M}^\mu \nu^\mu}{\nu_F^{(st)} + \nu_{O_2}^{(st)} + \displaystyle\sum_{\mu=1}^{\text{residual}} \nu^\mu} & \phi = 1 \\[4em] \dfrac{\mathfrak{M}_F \phi \nu_F^{(st)} + \mathfrak{M}_{O_2} \nu_{O_2}^{(st)} + \displaystyle\sum_{\mu=1}^{\text{residual}} \mathfrak{M}^\mu \nu^\mu}{\phi \nu_F^{(st)} + \nu_{O_2}^{(st)} + \displaystyle\sum_{\mu=1}^{\text{residual}} \nu^\mu} & \phi > 1 \\[4em] \dfrac{\mathfrak{M}_F \nu_F^{(st)} + \mathfrak{M}_{O_2} \phi^{-1} \nu_{O_2}^{(st)} + \displaystyle\sum_{\mu=1}^{\text{residual}} \mathfrak{M}^\mu \nu^\mu}{\nu_F^{(st)} + \phi^{-1} \nu_{O_2}^{(st)} + \displaystyle\sum_{\mu=1}^{\text{residual}} \nu^\mu} & \phi < 1 \end{cases} \quad (3.216)$$

The mean specific heat is given by,

$$\left\langle c_p\big|_{T_0} \right\rangle_\phi^{mix} = \begin{cases} \dfrac{\mathfrak{M}_F \nu_F^{(st)} c_p^F\big|_{T_0} + \mathfrak{M}_{O_2} \nu_{O_2}^{(st)} c_p^{O_2}\big|_{T_0} + \displaystyle\sum_{\mu=1}^{\text{residual}} \mathfrak{M}^\mu \nu^\mu c_p^\mu\big|_{T_0}}{\mathfrak{M}_F \nu_F^{(st)} + \mathfrak{M}_F \nu_{O_2}^{(st)} + \displaystyle\sum_{i}^{\text{residual}} \mathfrak{M}^\mu \nu^\mu} & \phi = 1 \\[4em] \dfrac{\mathfrak{M}_F \phi \nu_F^{(st)} c_p^F\big|_{T_0} + \mathfrak{M}_{O_2} \nu_{O_2}^{(st)} c_p^{O_2}\big|_{T_0} + \displaystyle\sum_{\mu=1}^{\text{residual}} \mathfrak{M}^\mu \nu^\mu c_p^\mu\big|_{T_0}}{\mathfrak{M}_F \phi \nu_F^{(st)} + \mathfrak{M}_{O_2} \nu_{O_2}^{(st)} + \displaystyle\sum_{i}^{\text{residual}} \mathfrak{M}^\mu \nu^\mu} & \phi > 1 \\[4em] \dfrac{\mathfrak{M}_F \nu_F^{(st)} c_p^F\big|_{T_0} + \mathfrak{M}_{O_2} \phi^{-1} \nu_{O_2}^{(st)} c_p^{O_2}\big|_{T_0} + \displaystyle\sum_{\mu=1}^{\text{residual}} \mathfrak{M}^\mu \nu^\mu c_p^\mu\big|_{T_0}}{\mathfrak{M}_F \nu_F^{(st)} + \mathfrak{M}_{O_2} \phi^{-1} \nu_{O_2}^{(st)} + \displaystyle\sum_{i}^{\text{residual}} \mathfrak{M}^\mu \nu^\mu} & \phi < 1 \end{cases}$$

$$(3.217)$$

By introducing M as,

$$M = Y_{Fuel}^{\alpha_F} Y_{O_2}^{\alpha_{O_2}} \prod_{\mu=1}^{residual} Y_{\mu}^{\beta_\mu} \tag{3.218}$$

it becomes with equation (3.213),

$$M(\phi) = \begin{cases} \left(\dfrac{\nu_F^{(st)}}{\nu_F^{(st)} + \nu_{O_2}^{(st)} + \sum\limits_{\mu=1}^{residual} \nu^\mu} \right)^{\alpha_F} \left(\dfrac{\nu_{O_2}^{(st)}}{\nu_F^{(st)} + \nu_{O_2}^{(st)} + \sum\limits_{\mu=1}^{residual} \nu^\mu} \right)^{\alpha_{O_2}} \prod\limits_{\mu=1}^{residual} Y_\mu^{\beta_\mu} & \phi = 1 \\[4em] \left(\dfrac{\phi\nu_F^{(st)}}{\phi\nu_F^{(st)} + \nu_{O_2}^{(st)} + \sum\limits_{\mu=1}^{residual} \nu^\mu} \right)^{\alpha_F} \left(\dfrac{\nu_{O_2}^{(st)}}{\phi\nu_F^{(st)} + \nu_{O_2}^{(st)} + \sum\limits_{\mu=1}^{residual} \nu^\mu} \right)^{\alpha_{O_2}} \prod\limits_{\mu=1}^{residual} Y_\mu^{\beta_\mu} & \phi > 1 \\[4em] \left(\dfrac{\nu_F^{(st)}}{\nu_F^{(st)} + \phi^{-1}\nu_{O_2}^{(st)} + \sum\limits_{\mu=1}^{residual} \nu^\mu} \right)^{\alpha_F} \left(\dfrac{\phi^{-1}\nu_{O_2}^{(st)}}{\nu_F^{(st)} + \phi^{-1}\nu_{O_2}^{(st)} + \sum\limits_{\mu=1}^{residual} \nu^\mu} \right)^{\alpha_{O_2}} \prod\limits_{\mu=1}^{residual} Y_\mu^{\beta_\mu} & \phi < 1 \end{cases} \tag{3.219}$$

with,

$$\lim_{\phi \to \phi'} M(\phi) = \begin{cases} 0 & \phi' = \infty \\ 0 & \phi' = 0 \end{cases} \tag{3.220}$$

Furthermore sum of the exponents is defined as,

$$n = \alpha_F + \alpha_{O_2} + \sum_{\mu=1}^{residual} \beta^\mu \tag{3.221}$$

3.4.4.1 General thermal ignition conditions for the ignition pressure for a non choked flow

The ignition pressure is defined as the initial pressure at which thermal ignition occurs. Both the ignition pressure for adiabatic and non adiabatic flow can be derived from the ignition conditions, as follows,

3.4.4.1.1 Adiabatic flow

The thermal ignition condition is given by equation (3.203) and becomes in dimensional variables,

$$\left[Fuel\right]_0^{\alpha_F} \left[O_2\right]_0^{\alpha_{O_2}} \prod_{\mu \neq Fuel \wedge \mu \neq O_2}^{N'-2} \left[C^\mu\right]_0^{\beta_\mu} \geq \frac{\rho_0 \left\langle c_p\big|_{T_0}\right\rangle_\phi^{mix} RT_0^2}{Q_r A'\left(\phi\right) E_A} \exp\left(\frac{E_A}{RT_0}\right)\frac{1}{t_{ig}} \quad (3.222)$$

With equation (3.206), (3.214), (3.218), (3.219), (3.221) the thermal ignition conditions becomes,

$$\Phi \frac{V_C}{\dot{m}} \frac{\left\langle \mathfrak{M}\right\rangle_\phi^{mix}}{T_0 R} p_0^{\ n} - t_{evap} p_0^{\ (n-1)} \geq \frac{\left\langle \mathfrak{M}\right\rangle_\phi^{mix} \left\langle c_p\big|_{T_0}\right\rangle_\phi^{mix} R^n T_0^{(n+1)}}{Q_r A'\left(\phi\right) E_A M\left(\phi\right)} \exp\left(\frac{E_A}{RT_0}\right) \quad (3.223)$$

Equation (3.223) represents a polynomial equation which can only be solved by a appropriate numerical procedure such as the newton's method exept for n=0,1 and 2 for which where a analytical solution can be found[†]. However, if the evaporation time, t_{evap}, is small compared to the mean residence time, $<t_{res}>$, it can be neglected. Thus the final auto ignition condition for the initial pressure becomes,

---

[†] The majority of chemical reactions are bimolecular reactions which is given by n=2 [29]. The approximation of a chemical reaction system by a global one step reaction leads typically to a global reaction order which is in the space of $\mathbb{R}$.

$$p_0 \geq \sqrt[n]{\frac{\dot{m} \left\langle c_p \big|_{T_0} \right\rangle_\phi^{mix} R^{(n+1)} T_0^{(n+2)}}{Q_r A'(\phi) E_A M(\phi) \Phi V_C} \exp\left(\frac{E_A}{R T_0}\right)} \tag{3.224}$$

3.4.4.1.2 Non-adiabatic flow

The thermal ignition condition is given by equation (3.203) and becomes in dimensional variables,

$$\left[Fuel\right]_0^{\alpha_F} \left[O_2\right]_0^{\alpha_{O_2}} \prod_{\mu \neq Fuel \wedge \mu \neq O_2}^{N'-2} \left[C^\mu\right]_0^{\beta_\mu} \geq$$

$$\geq \begin{cases} \left[+ \dfrac{R T_0^2 \left\langle \chi \big|_{T_0} \right\rangle_\phi^{mix} U}{Q_r E_A A'(\phi) A} \exp\left[\dfrac{E_A}{R T_0}\left(1 + \dfrac{T_0 - T_W}{T_0}\right) - 1\right] \\ + \dfrac{\rho_0 \left\langle c_p \big|_{T_0} \right\rangle_\phi^{mix} R T_0^2}{Q_r E_A A'(\phi)} \exp\left(\dfrac{E_A}{R T_0}\right) \dfrac{1}{t_{ig}} \right] \dfrac{E_A}{R T_0^2}\left(T_0 - \left\langle T_w \right\rangle\right) \leq 1 \\[4em] \left[+ \dfrac{\left\langle \chi \big|_{T_0} \right\rangle_\phi^{mix} U \left(T_0 - T_W\right)}{Q_r A'(\phi) A} \exp\left(\dfrac{E_A}{R T_0}\right) \\ + \dfrac{\rho_0 \left\langle c_p \big|_{T_0} \right\rangle_\phi^{mix} R T_0^2}{Q_r E_A A'(\phi)} \exp\left(\dfrac{E_A}{R T_0}\right) \dfrac{1}{t_{ig}} \right] \dfrac{E_A}{R T_0^2}\left(T_0 - \left\langle T_w \right\rangle\right) > 1 \end{cases}$$

$$\tag{3.225}$$

After further algebra and with equation (3.206), (3.214), (3.218), (3.219), (3.221) the thermal ignition conditions becomes

1ˢᵗignition condition given by: $\dfrac{\boldsymbol{E_A}}{\boldsymbol{R T_0^2}}\left(\boldsymbol{T_0} - \left\langle\boldsymbol{T_w}\right\rangle\right) \leq \boldsymbol{1}$

$$\frac{\left\langle\mathfrak{M}\right\rangle_\phi^{mix}}{T_0 R}\left[\Phi\frac{V_C}{\dot m}\left(p_0^{(n+1)} - G_I p_0\right) - Z_I p_0\right] \geq t_{evap}\left(p_0^{\,n} - G_I\right)$$

$$Z_I = \frac{\left\langle c_p\big|_{T_0}\right\rangle_\phi^{mix} R^{(n+1)} T_0^{(n+2)}}{Q_r E_A A'(\phi) M(\phi)}\exp\left(\frac{E_A}{R T_0}\right)$$

$$G_I = \frac{R^{(n+1)} T_0^{(n+2)}}{Q_r E_A A'(\phi) M(\phi)}\frac{\left\langle\chi\big|_{T_0}\right\rangle_\phi^{mix} U}{A}\exp\left[\frac{E_A}{R T_0}\left(1 + \frac{T_0 - \left\langle T_w\right\rangle}{T_0}\right) - 1\right]$$

(3.226)

2ⁿᵈignition condition given by: $\dfrac{\boldsymbol{E_A}}{\boldsymbol{R T_0^2}}\left(\boldsymbol{T_0} - \left\langle\boldsymbol{T_w}\right\rangle\right) > \boldsymbol{1}$

$$\frac{\left\langle\mathfrak{M}\right\rangle_\phi^{mix}}{T_0 R}\left[\Phi\frac{V_C}{\dot m}\left(p_0^{(n+1)} - p_0 G_{II}\right) - p_0 Z_{II}\right] \geq t_{evap}\left(p_0^{\,n} - G_{II}\right)$$

$$Z_{II} = \frac{\left\langle c_p\big|_{T_0}\right\rangle_\phi^{mix} R^{(n+1)} T_0^{(n+2)}}{Q_r E_A A'(\phi) M(\phi)}\exp\left(\frac{E_A}{R T_0}\right)$$

$$G_{II} = \frac{R^n T_0^{\,n}}{Q_r A'(\phi) M(\phi)}\frac{\left\langle\chi\big|_{T_0}\right\rangle_\phi^{mix} U\left(T_0 - \left\langle T_w\right\rangle\right)}{A}\exp\left(\frac{E_A}{R T_0}\right)$$

(3.227)

It is noticed that with the assumption $\left\langle\chi\big|_{T_0}\right\rangle_\phi^{mix} \to 0$, the initial pressure to achieve auto ignition becomes exactly the same as for the adiabatic flow. This behaviour shows the validity of the model. Similar to the adiabatic flow situation the auto ignition equations for the non adiabatic flow represents a polynomial equation which can only be solved by a appropriate numerical procedure such as the newton's method exept for $n=0,1$ and 2 where a analytical solution can be found[†]. However, if the evaporation time, t_{evap}, is small compared to the mean residence time, $<t_{res}>$, it can be neglected. The

---

[†] The majority of chemical reactions are bimolecular reactions which is given by n=2 [29]. The approximation of a chemical reaction system by a global one step reaction leads typically to a global reaction order which is in the space of $\mathbb{R}$.

ignition condition for the initial pressure to achieve ignition assuming a cylindrical combustion chamber ($U/A = 4/D_C$) becomes,

$$1^{\text{st}}\text{ignition condition given by:}\frac{E_A}{RT_0}\left(1 - \frac{\langle T_w \rangle}{T_0}\right) \leq 1$$

$$p_0 \geq \sqrt[n]{\frac{R^{(n+1)}T_0^{(n+2)}}{Q_r E_A A'(\phi) M(\phi)}\left[\frac{\dot{m}\left\langle c_p\big|_{T_0}\right\rangle_\phi^{mix}}{\Phi V_C}\exp\left(\frac{E_A}{RT_0}\right) + \frac{4\left\langle\chi\big|_{T_0}\right\rangle_\phi^{mix}}{D_C}\exp\left[\frac{E_A}{RT_0}\left(2 - \frac{\langle T_w \rangle}{T_0}\right) - 1\right]\right]}$$

$$2^{\text{nd}}\text{ignition condition given by:}\frac{E_A}{RT_0}\left(1 - \frac{\langle T_w \rangle}{T_0}\right) > 1$$

$$p_0 \geq \sqrt[n]{\frac{R^n T_0^n}{Q_r A'(\phi) M(\phi)}\exp\left(\frac{E_A}{RT_0}\right)\left[\frac{\dot{m}\left\langle c_p\big|_{T_0}\right\rangle_\phi^{mix} RT_0^2}{\Phi V_C E_A} + \frac{4\left\langle\chi\big|_{T_0}\right\rangle_\phi^{mix}}{D_C}\left(1 - \frac{\langle T_w \rangle}{T_0}\right)\right]}$$

$$(3.228)$$

3.4.4.2 Thermal ignition conditions for the ignition pressure of a rocket engine (choked nozzle flow)

Basically for an isentropic choked nozzle flow the following relationship holds [36],

$$\dot{m} = p_0 A^*\left[\gamma\left(\frac{2}{\gamma+1}\right)^{\frac{\gamma+1}{\gamma-1}}\frac{\langle\mathfrak{M}\rangle_\phi^{mix}}{T_0 R}\right]^{\frac{1}{2}} \qquad (3.229)$$

Two possibilities exist to treat the ignition condition for a choked nozzle flow. First, the mass flow is considered to be constant, and second the throat area is considered to be constant. The pressure then becomes a function of the throat area respectively of the mass flow,

$$p_0 = \begin{cases} f\left(A^*\right) & \dot{m} = const. \\ f\left(\dot{m}\right) & A^* = const. \end{cases} \qquad (3.230)$$

Since the auto ignition conditions are independent from the throat area, the adiabatic and non-adiabatic choked auto ignition condition assuming a constant mass flow becomes exactly the same as equation (3.224), (3.226), (3.227). Therefore only the case of a not constant mass flow leads to a new auto ignition behaviour.

3.4.4.2.1 Adiabatic choked auto ignition condition

Since the pressure in the combustion chamber is now depending on the mass flow, the mass flow given by equation (3.229) is substituted in the adiabatic auto ignition condition, equation (3.223). Therefore after further algebra the adiabatic auto ignition pressure assuming a choked nozzle flow whereas the mass flow is primarily defined by the pressure becomes,

$$
p_0 \geq \left\{ \frac{\langle \mathfrak{M} \rangle_\phi^{mix} \left\langle c_p |_{T_0} \right\rangle_\phi^{mix} R^n T_0^{(n+1)}}{Q_r A'(\phi) E_A M(\phi) \left\{ \Phi L^* \sqrt{\frac{\langle \mathfrak{M} \rangle_\phi^{mix}}{T_0 R}} \left[\gamma \left(\frac{2}{\gamma+1} \right)^{\frac{\gamma+1}{\gamma-1}} \right]^{-\frac{1}{2}} - t_{evap} \right\}} \exp \left(\frac{E_A}{R T_0} \right) \right\}^{\frac{1}{n-1}}
$$

$$(3.231)$$

where L^* is the characteristic chamber length which are given by,[53]

$$
L^* = \frac{V_C}{A^*}
\tag{3.232}
$$

The substitution for the mass flow rate, $\dot{m}$, leads to an exact definition for the auto ignition pressure without introducing special assumption for the evaporation time, t_{evap}. however if $t_{evap} << t_{res}$, p_0 becomes,

$$
p_0 \geq \left\{ \frac{\left[\gamma \left(\frac{2}{\gamma+1} \right)^{\frac{\gamma+1}{\gamma-1}} \langle \mathfrak{M} \rangle_\phi^{mix} \right]^{\frac{1}{2}} \left\langle c_p |_{T_0} \right\rangle_\phi^{mix} R^{\left(n+\frac{1}{2} \right)}}{Q_r A'(\phi) E_A M(\phi)} \frac{T_0^{\left(n+\frac{3}{2} \right)}}{\Phi L^*} \exp \left(\frac{E_A}{R T_0} \right) \right\}^{\frac{1}{n-1}}
\tag{3.233}
$$

It is noted that for the non-adiabatic auto ignition condition assuming a choked nozzle flow, the relation in equation (3.229), leads to a non analytically solvable problem for the initial auto ignition pressure because of the non linear behaviour of the mass flow rate in equation (3.200). Thus for considering loss effect, equation (3.228) gives the auto ignition condition for the initial pressure but with the disadvantage of the special assumption for a nrgliable evaporation time and further assuming an adiabatic auto ignition process.

3.4.4.3 Analysis of the thermal ignition conditions for the ignition pressure

Table 4 shows the behaviour of the initial pressure to achieve auto ignition on various parameters if they are increased. The symbol "↑" denotes an increase and the symbol "↓" a decrease.

	$\dot{m}$	V_C	T_0	$\left\langle c_p\big|_{T_0}\right\rangle_\phi^{mix}$	$M(\phi)$	D_C	$\langle T_w \rangle$	$\left\langle \chi\big|_{T_0}\right\rangle_\phi^{mix}$	L^*
p_0	↑	↓	↓	↑	↓	↓	↓	↑	↓

Tab. 4: Dependency of p_0

The only arbitrary parameters for designing a combustion system are given by the combustion chamber volume V_C and the combustion chamber diameter D_C respectively the characteristic chamber length L^*. The others are more or less intrinsic parameters which are given by the physical properties of the reactants, the requirements of the combustion system (i.e. thrust, power, ect), and the ambient conditions.

It should be noted that the mean specific heat $\left\langle c_p\big|_{T_0}\right\rangle_\phi^{mix}$ becomes a function of the equivalence ratio, ϕ, as well as the mole fractions given by the parameter $M(\phi)$ Therefore if the composition of the reactants is changed by changing the equivalence ratio, the mean specific heat also changes. If $\phi\rightarrow\infty$, results in $M(\phi)\rightarrow0$ and $<c_p>(\phi)\rightarrow c_{p,F}$ thus $p_0\rightarrow\infty$ and if $\phi\rightarrow0$, results in $M(\phi)\rightarrow0$ and $<c_p>(\phi)\rightarrow c_{p,O2}$ thus $p_0\rightarrow\infty$ Hence, the necessary initial pressure to achieve auto ignition might be less for $\phi\neq1$. For instance the lowest auto ignition

116

temperature, T_0, of a hydrocarbon-air-mixture are given for a slightly rich ($\phi > 1$) combustion condition [54].

Furthermore for small combustion chamber diameters, D_C, the ratio U/A becomes high thus the initial pressure to achieve auto ignition for a non-adiabatic chemically reaction flow differs extensively from the initial pressure to achieve auto ignition assuming an adiabatic chemically reactiong flow. This circumstance must be accounted especially for designing micro propulsion systems.

4

PROPELLANTS

4.1 Kerosene

Kerosene is the name for the lighter end of a group of petroleum streams known as the middle distillates. Kerosene may be obtained either from the distillation of crude oil under atmospheric pressure (straight-run kerosene) or from catalytic, thermal or steam cracking of heavier petroleum streams (cracked kerosene) [55]. The kerosenes, are further treated by a variety of processes (including hydrogenation) to remove or reduce the level of sulfur, nitrogen or olefinic materials [55].

The precise composition of any particular kerosene will depend on the crude oil from which it was derived and on the refinery processes used for its production. Kerosene consists of a large number of hydrocarbons which is shown in figure 19, where the carbon number distribution for aviation kerosene (avgas), jet fuel (Jet A), and rocket fuel (RP-1) is illustrated. The hydrocarbon constituents can be divided into five classes of compounds (figure 20) [56]. The major components of kerosenes are paraffins, isoparafins, cycloparaffins (naphthenes), olefins and aromomatics.
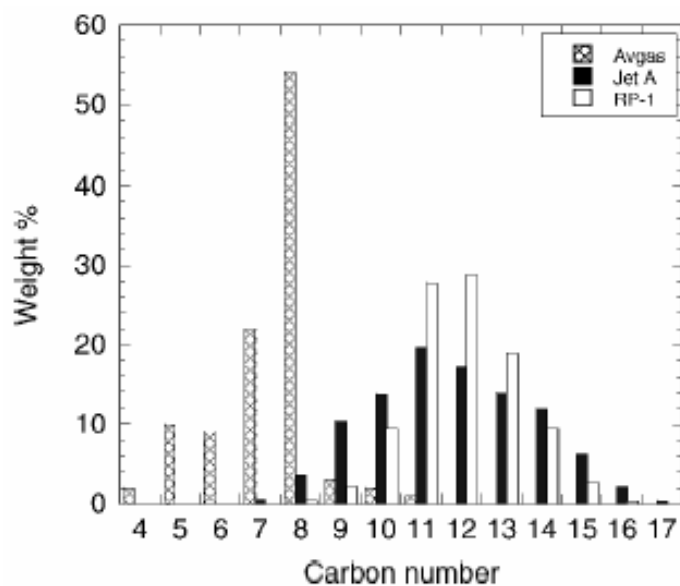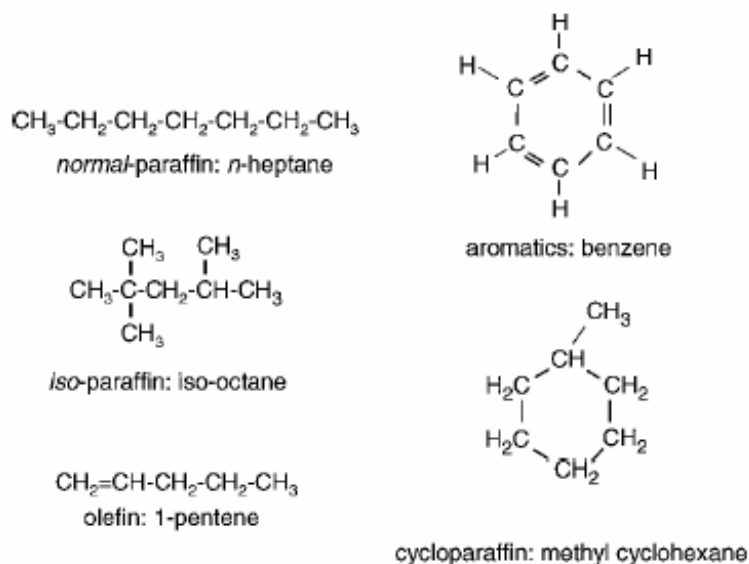
Fig. 19: Carbon number distribution of kerosene [56]

Fig. 20: Classes of hydrocarbons found in hydrocarbon fuels [56]

Common kerosene fuels used in aviation and rocket industries are RP-1, JP-4, JP-5, JP-8 and Jet-A. A brief information about the differences is given by Edwards [56].

4.1.1 Jet-A1

Jet-A1 is a complex mixture of paraffins (50-65% vol.), mono- and poly-aromatics (10-20% vol.) and cycloparaffins (mono- and polycyclic, 20-30% vol.) which is widely used in aircraft engines [57]. Dean and Penyazkov et. al. [40] applied a chromatographic technique to characterize the composition of Jet-A1 (figure 21). N-alkanes (paraffins) up to n-Tricosane , $C_{23}H_{48}$, have been identified during the test. Paraffins and iso-parafins contents are 27.1 % by volume. Aromatics are 21.5 % by volume; Naphthenes are 2.9 % by volume; Olefins are 1.1 % by volume. 50% of the fractional contents were unknown. The averaged formula for studied Jet-A deduced from 167 identified compounds was $C_{10.84}H_{19.65}$.
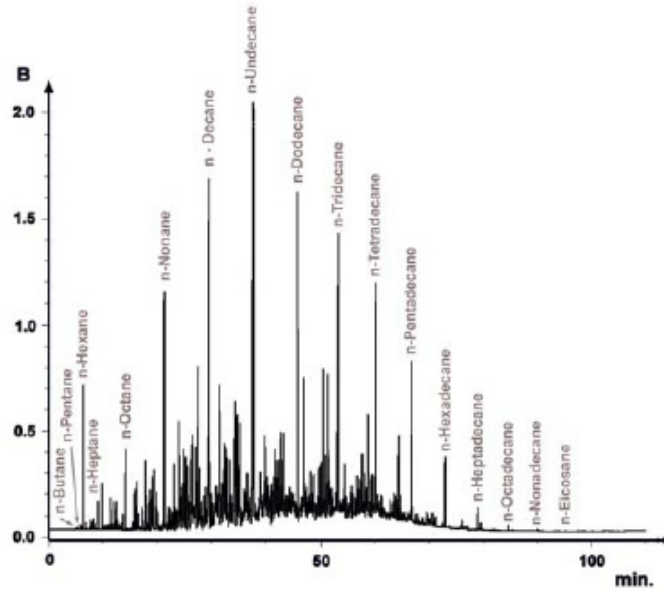
Fig. 21: Chromatogram of Jet-A [40]

A summary if the physical properties of Jet-A1 fuel are given in table 5.

Property	Jet-A1	Family Name	Molecular Formula	C-C Bonding	Structure
Approx. formula [58]	C_nH_{2n}				
H/C ratio [58]	1.91				
Boiling range, F [59]	330-510				
Freeze point, F [59]	-60				
Flash point, F [59]	127				
Net heating value, BTU/lb [60]	18580				
Critical T, F [61,62]	770				
Critical p, psia [61,62]	340				
Avg composition [63,58,64]					
Benzene, vol% [60]	18	Aromatics	C_nH_{2n-6}	Resonance hybrid bonds	Closed rings
Naphthenes	20	Cyclanes	C_2H_{2n} or $(CH_2)_n$	Single bonds only	Closed rings
Paraffins	60	Alkanes	C_nH_{2n+2}	Single bonds only	Straight or branched open rings
Olefins	2	Alkenes	C_nH_{2n}	Double bonds	Straight or branched open rings
Sulfur, ppm [60]	490				

Tab. 5: Properties of Jet-A1 fuel

4.1.2 Ignition delay studies of Jet-A in air

Since research into the auto ignition characteristic of kerosene fuel in decomposed hydrogen peroxide and particularly for Jet-A/O_2/H_2O(g) mixture has not been as substantial as it has been in air the auto ignition behaviour of Jet-A/air is described in this section which is studied since the 1970s. It is idetically to Jet-A1 except the freezing point which is a little bit higher. A lot of these studies were performed using a continuous flow apparatus to simulate ignition and combustion phenomenon in lean, premixed gas turbine engine

combustors [65-68]. The setup usually consisted of a tube or duct through which heated air flows at high subsonic velocity. The fuel is injected into the oxidizer stream (air) where it mixes and reacts. The method of injection is extremely important, especially for liquid fuels, in minimizing effects of vaporization on ignition delay and for obtaining a uniform mixture of fuel and oxidizer. Furthermore the tube diameter also influences the ignition delay due to positive quenching effects of the tube surface (see chapter 3). In the literature it is recommended a minimal tube diameter of greater than 50mm [54]. Ignition is verified through the direct visual observation of a flame inside the tube or exiting the chamber. Ignition is calculated using the air velocity and the distance from the injection point to the position of the visible flame. Ignition delay correlations from these studies are derived from chemical kinetics and make use of the Arrhenius relation. The reaction is treated as a whole using the global activation energy determined from experimental data. Correlations of ignition delay times usually take the following forms [65,69-72]:

$$t_{ig} = B \exp\left(\frac{E_A}{RT}\right) \prod_j \left[C_j\right]^{\alpha_j} p^n$$
$$t_{ig} = B \exp\left(\frac{E_A}{RT}\right) \prod_j \left[C_j\right]^{\alpha_j}$$
$$t_{ig} = B \exp\left(\frac{Z}{T}\right) \prod_j \left[C_j\right]^{\alpha_j} \rho^n \qquad (4.1)$$
$$t_{ig} = \exp\left(A + \frac{Z}{T}\right) \left[\frac{p}{RT}\right]^n$$
$$t_{ig} = B \exp\left(\frac{E_A}{RT}\right) \phi^k p^n$$

where $[C_j]$ are the concentrations and ϕ is the equivalence ratio. The parameters B respectively Z and exponets α_j and n are empirically determined constants. There have been a number of auto ignition studies with kerosene based fuel and air in a continous flow apparatus. Colket, and Spadaccini [73] performed shock tube experiments to measure the ignition delay times of several hydrocarbons in air, namely ethylene, heptane, JP-10, and three model endothermic-fuel/cracked product mixtures for temperatures in the range of 1100-1500K, pressures of 3-8 atm, and equvalence ratios of 0.5-1.5. They found that the ignition delay of hydrocarbons in air is a weak function of the fuel

concentration ($0<\alpha_{Fuel}<0.5$) and a strong function of the oxygen concentration ($\alpha_{Oxigen}<-1$). Data collected by Fieweger et al [74] for iso-octane, methanol and methyl tert-butyl ether showed similar trends. Freeman and Lefebvre [65,67] studied the auto ignition behaviour of Jet-A at atmospheric pressure. Tests were conducted at equivalence ratios from 0.2 to 0.8, velocities from 10 to 40 m/s and temperatures up to 1060 K. They found that the equivalence ratio had a negligible effect on ignition delay for $\phi<1.0$ and the oxygen exponent, was set to -0.65 based on experimental data. Mestre and Ducourneau [68] performed auto ignition tests of kerosene fuel over a wide range of equivalence ratios from approximately 0.8 to 8.0, pressures from 5.5 to 11 bar an average air velocity of 65m/s and temperatures up to 1090 K. Their experimental results showed that the auto ignition temperature becomes a function of the equivalence ratio at constant pressure and the minimum varied with pressure. Data also showed that the auto ignition temperature decreased with increasing pressure. The study also found that the auto ignition temperature decreased with increasing residence time at constant equivalence ratio. Unfortunately they did not correlate their results according to equation (4.1). Spadaccini and TeVelde [66] studied the ignition delay behaviour of Jet-A, Diesel and JP-4 with air for equivalence ratios from 0.3 to 0.7, temperatures from 427 to 732°C, pressures from 10 to 31 bar, and air velocities from 65 to 330 ft/s in a continuous flow apparatus (Fig 22a,Fig. 22b).

The temperature of the air was gradually increased until a visible flame was observed at the exit of the duct while the pressure and velocity of the air were set as well as the duct length. The ignition delay time was calculated by dividing the flow velocity by the duct length. They correlated the experimental data (Fig 22a) of the ignition delay by the use of the Arrhenius form as follows,

$$t_{ig} = \frac{U'}{p^{m'}} \exp\left(\frac{E_A}{RT}\right) \tag{4.2}$$

where t_{ig} is in ms, the coefficient U' is equal to 1.68e-8, m is equal to 2.0, E_A is equal to 155 kJ/mol, p is in atmospheres, and T is the temperature of the incoming air. Results indicated that equivalence ratio did not affect ignition delay.
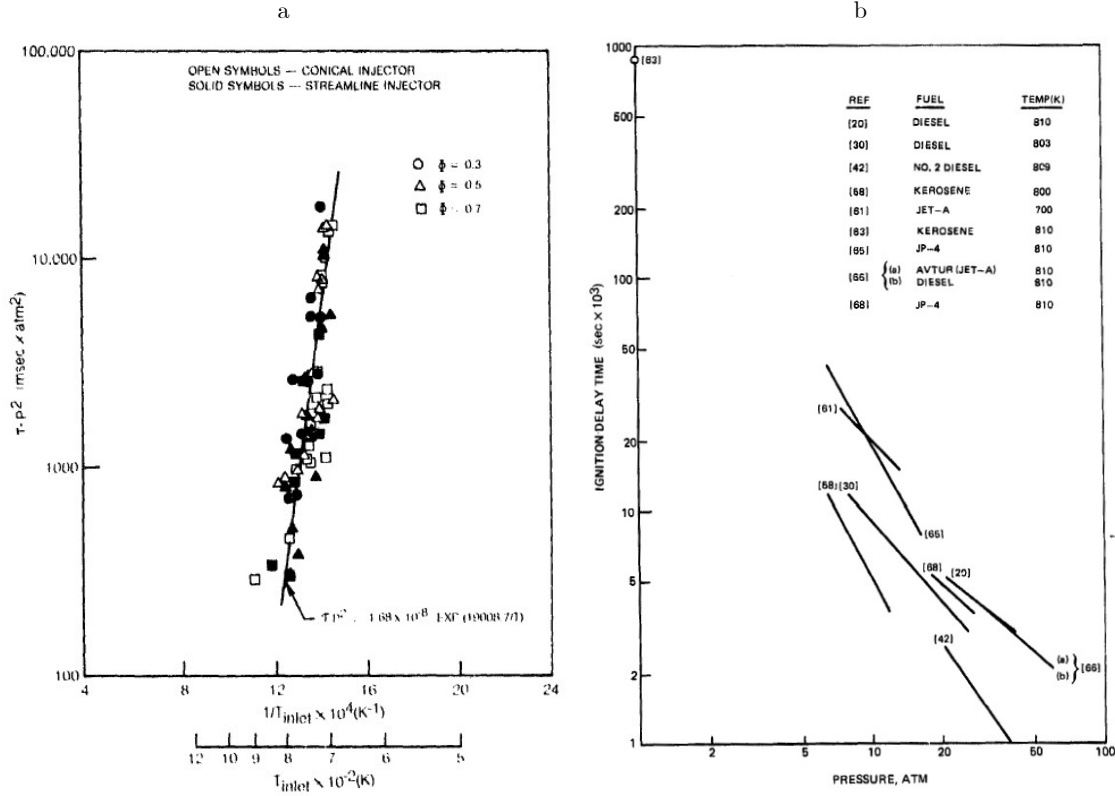
Fig. 22: a) Autoignition characteristic of Jet-A Fuel in air [66] b) Correlation of ignition delay data [66]

Furthermore they noted that most ignition delay correlations are fitted with a pressure exponent of unity (m'=1.0), but their data suggested that an exponent of 2.0 is a better fit particularly at high temperatures. Dean et. al. [40] performed shock tube experiments to study the ignition behaviour of Jet-A/air at elevated temperatures and pressures. The test were done within the temperature range of 1000-1700K at mean post shock pressures of 8.5±1 atm and stoichiometries of ϕ=0.5, ϕ=1, and ϕ=2 (Fig. 23). They found the shortest ignition for a rich mixture ϕ=2 due to the chain branching process for large hydrocarbons which is controlled by hydrocarbon hydroperoxide species. Its production rate is directly proportional to the fuel concentration. Similar trends were observed by the study of Vasu et. al. [75] (Fig 24a). In contrast to Spadaccini and TeVelde they found a NTC (Negative Temperature Coefficient) -type behaviour of Jet-A/air mixture for ϕ=1 at low temperatures in which the ignition delay time remains nearly constant and becomes shorter as the temperature decreases (Fig. 24b).
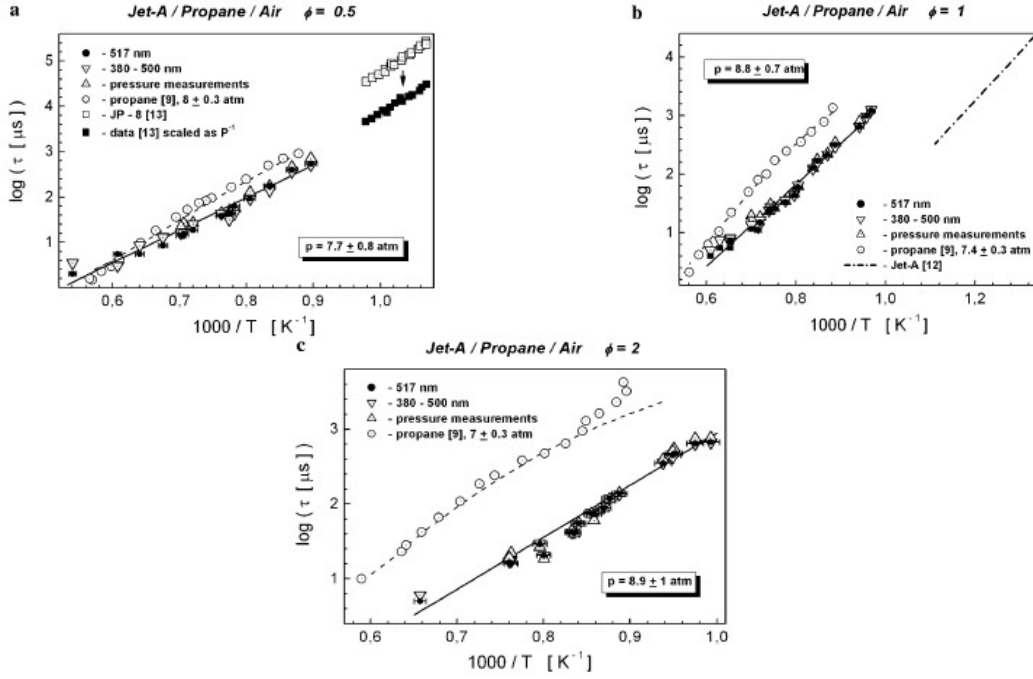
Fig. 23: Ignition delay times of Jet-A/air mixtures at equivalent post-shock conditions [40]

Interestingly, this more or less S-shaped dependence (NTC) is similar to that reported in n-heptane in air, and mixtures of iso-octane and heptane in air, by Fieweger et al. [74].
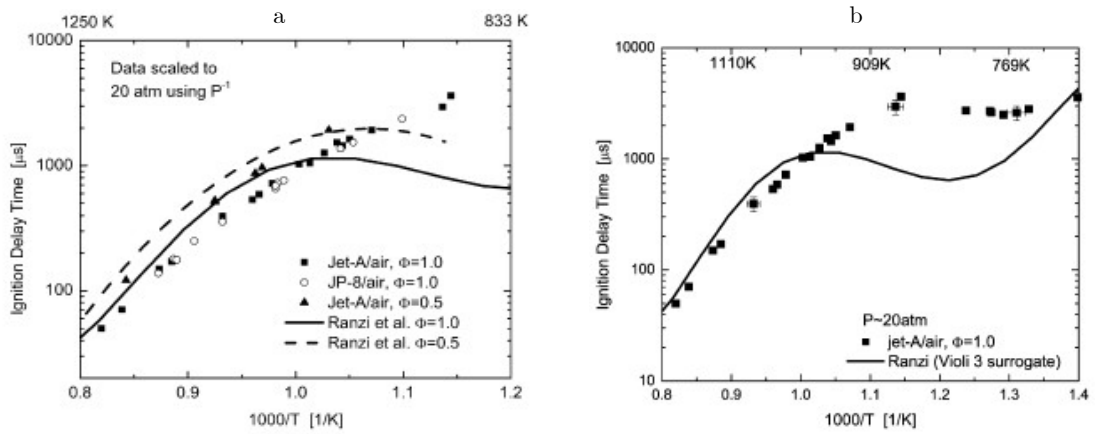

Fig. 24: a) Effect of equivalence ratio ϕ [75] b) Ignition delay times including NTC region data [75]

According to Vasu et. al. the NTC region (non linear behaviour of the logarithmic ignition delay time) begins at temperatures of approx. 869K. It should be noted that this temperature depends on pressure, e.g. n-heptane, $\ln(T)$ grows in a quasi linear way, with T^{-1} for temperatures above: 850K at

5bar, 900K at 14 bar, 1000K at 40bar [77]. Beneath this temperature complex chain branching mechanism becomes important which leads to a low temperature oxidation (cool flame). Cool flame reactions occur when organic compounds are heated in the presence of oxygen and involve the formation of intermediate species such as peroxides and aldehydes. No carbon is formed in the products of the cool flame and only a small fraction of the reactants is consumed. Therefore it is not accompanied by a high heat release ($\Delta T \approx 300K$). This phenomenon is out of the scope of thermal ignition theory and has to be explained by branched chain ignition theory.

Generally the results of the ignition delay studies showed if the pressure and/or the temperature are increased the probability of auto ignition also increases for a given residence time and equivalence ratio. Also these studies show if the residence time is increased the temperature required for auto ignition decreases at constant pressure and equivalence ratio. There is only a discrepance concerning the influence of the equivalence ratio.

4.1.3 Ignition characteristic of Jet-A in air

4.1.3.1 Correlated thermal ignition conditions for the ignition pressure

Equation (4.2) can be used to determine the unknown parameters such as the frequency factor, A', and the activation energy, E_A. If loss effects are negligible the equation for the adiabatic ignition delay time, equation (3.203) can be correlated with equation (4.2). Thus,

$$\frac{1}{\Omega^*} = \frac{U'}{p_0^{m'}} \exp\left(\frac{E_A}{RT_0}\right)$$

$$\Rightarrow \frac{RT_0^2 \rho_0 \left\langle c_p\big|_{T_0}\right\rangle_{mix}}{Q_r E_A A'(\phi)[Fuel]_0^{\alpha'} \prod_{\mu \neq Fuel}^{N'-1} \left[C^\mu\right]_0^{\beta_\mu}} \exp\left(\frac{E_A}{RT_0}\right) = 10^{-3} \frac{U'}{\left(\dfrac{p_0}{1.0133x10^5}\right)^{m'}} \exp\left(\frac{E_A}{RT_0}\right)$$

$$(4.3)$$

The factor 10^{-3} and $1.0133\text{x}10^5$ assures SI units (conversion from milli seconds to seconds and respectively from atm to Pa). Since Jet A and air is considered in the study performed by Spadaccini and TeVelde, equation (4.3) becomes,

$$\frac{\rho_0 \left\langle c_p \big|_{T_0} \right\rangle_{mix} RT_0^2}{Q_r E_A A'(\phi) \left[JetA \right]_0^{\alpha'} \left[Air \right]_0^{\beta}} \exp\left(\frac{E_A}{RT_0}\right) = 10^{-3} \frac{U'}{\left(\dfrac{p_0}{1.0133x10^5}\right)^{m'}} \exp\left(\frac{E_A}{RT_0}\right) \quad (4.4)$$

Using the relationship for the density, equation (3.214) and for the concentrations, equation (3.206), the frequency factor is given by,

$$A'(\phi) = \frac{\left\langle \mathfrak{M} \right\rangle \left\langle c_p \big|_{T_0} \right\rangle_{mix} R^{(n)} T_0^{(1+n)}}{\left(1.0133x10^5\right)^{m'} 10^{-3} U' Q_r E_A M} \quad (4.5)$$

with,

$$\begin{aligned} \alpha + \beta - 1 &= m' \\ n &= m' + 1 \end{aligned} \quad (4.6)$$

Inserting equation (4.5) into equation (3.224) the initial pressure to achieve auto ignition for an adiabatic chemically reactiong flow becomes,

$$p_0 = \sqrt[(m'+1)]{\frac{\left(1.0133x10^5\right)^{m'} 10^{-3} U' \dot{m} RT_0}{\left\langle \mathfrak{M} \right\rangle \Phi V_C} \exp\left(\frac{E_A}{RT_0}\right)} \quad (4.7)$$

and for the real system assuming isobaric flow situation follows,

1st ignition condition given by: $\dfrac{\boldsymbol{E_A}}{\boldsymbol{RT_0}}\left(\boldsymbol{1} - \dfrac{\left\langle\boldsymbol{T_w}\right\rangle}{\boldsymbol{T_0}}\right) \leq \boldsymbol{1}$

$$p_0 \geq {}_{(m'+1)}\sqrt{\frac{\left(1.0133x10^5\right)^{m'}10^{-3}U'RT_0}{\left\langle\mathfrak{M}\right\rangle_\phi^{mix}}\left[\frac{\dot{m}}{\varPhi V_C}\exp\left(\frac{E_A}{RT_0}\right) + \frac{4\left\langle\chi\big|_{T_0}\right\rangle_\phi^{mix}}{D_C\left\langle c_p\big|_{T_0}\right\rangle_\phi^{mix}}\exp\left[\frac{E_A}{RT_0}\left(2 - \frac{\left\langle T_w\right\rangle}{T_0}\right) - 1\right]\right]}$$

2nd ignition condition given by: $\dfrac{\boldsymbol{E_A}}{\boldsymbol{RT_0}}\left(\boldsymbol{1} - \dfrac{\left\langle\boldsymbol{T_w}\right\rangle}{\boldsymbol{T_0}}\right) > \boldsymbol{1}$

$$p_0 \geq {}_{(m'+1)}\sqrt{\frac{\left(1.0133x10^5\right)^{m'}10^{-3}U'RT_0}{\left\langle\mathfrak{M}\right\rangle_\phi^{mix}}\exp\left(\frac{E_A}{RT_0}\right)\left\{\frac{\dot{m}}{\varPhi V_C} + \frac{4E_A\left\langle\chi\big|_{T_0}\right\rangle_\phi^{mix}}{RT_0^2D_C\left\langle c_p\big|_{T_0}\right\rangle_{mix}}\left(1 - \frac{\left\langle T_w\right\rangle}{T_0}\right)\right\}}$$

$$(4.8)$$

It is noted that equation (4.7) and equation (4.8) are only valid in the experimental validated pressure-temperature regime.

4.1.3.2 Correlated thermal ignition conditions for the ignition pressure of a rocket engine (choked nozzle flow)

A alternative correlation function for the ignition delay behaviour of a system was proposed by Walder who studied auto ignition of kerosene fuel in decomposed hydrogen peroxide in the early 1950s [78,79,80]. He supposed that the ignition delay was proportional to L^* of the engine. The basic form of the correlation is as follows,

$$\ln\left(L^*p^{m'}\right) = \frac{K}{T_0} + L' \tag{4.9}$$

where K, L', and m are empirical constants. Walder found m to be equal to 1.15 based on test data. This value is close to unity, which Spadaccini and TeVelde suggested worked well for auto ignition of kerosene in air at low temperatures. If equation (3.233) is rearranged to the form of equation (4.9) and assuming $t_{evap} \simeq 0$ then follows,

$$\ln\left[L^* p_0^{(n-1)}\right] \geq \frac{E_A}{RT_0} + \ln\left\{\frac{\sqrt{\gamma\left(\frac{2}{\gamma+1}\right)^{\frac{\gamma+1}{\gamma-1}}}\langle\mathfrak{M}\rangle_\phi^{mix}\langle c_p\big|_{T_0}\rangle_\phi^{mix} R^{\left(n+\frac{1}{2}\right)}}{Q_r A'(\phi) E_A M(\phi)}\frac{T_0^{\left(n+\frac{3}{2}\right)}}{\Phi}\right\} \quad (4.10)$$

which indicates that equation (4.9) is on the basis of thermal ignition theory. In contrast to Walders suggestion the empirical constant L' depends on the initial gas temperature as well as on the equivalence ration, specific heat, mean molar mass and isentropic exponent. In the recent literature the correlation function of Walder can be found as a basis of designing rocket combustion chambers using hydrogen peroxide and kerosene as propellants [93,124]. By comparison with equation (4.10) it is noticed that this correlation is not applicable a priori for very small combustion chambers with a high surface to volume ratio since the correlation neglects the influence of the heat loss effect which is high for a high surface to volume ratio and additionally since the specific heat and molar mass depends on the mixture ratio the constant L' depends on the mixture ratio as well. .For reasons of comparability the necessary ignition pressure for a choked nozzle flow is correlated with equation (4.2). Thus it becomes,

$$p_0 \geq \left\{\frac{\left(1.0133x10^5\right)^{m'}10^{-3}U'}{\left[\Phi L^*\sqrt{\frac{\langle\mathfrak{M}\rangle_\phi^{mix}}{T_0 R}}\left[\gamma\left(\frac{2}{\gamma+1}\right)^{\frac{\gamma+1}{\gamma-1}}\right]^{-\frac{1}{2}} - t_{evap}\right]}\exp\left(\frac{E_A}{RT_0}\right)\right\}^{\frac{1}{n-1}} \quad (4.11)$$

4.1.3.3   Determination of the physical properties of a Jet-A/air mixture

The combustion of Kerosene in air is given by,

$$\nu_F^{(st)}C_{11}H_{21} + \nu_{Air}^{(st)}Air \rightarrow \sum_i^{products}\nu_i P_i \quad (4.12)$$
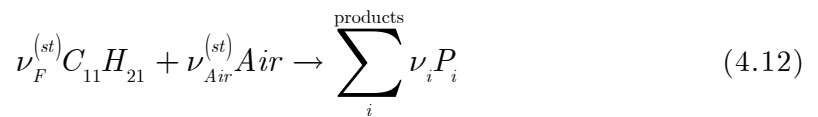
If air is considered as a mixture of oxygen and nitrogen, 1 mol of air is given by,

$$1\text{mol}(Air) = 0.21\text{mol}(O_2) + 0.78\text{mol}(N_2) \tag{4.13}$$

Thus equation (4.13) becomes,

$$\nu_F^{(st)} C_{11}H_{21} + \nu_{Air}^{(st)}\left(0.21 O_2 + 0.78 N_2\right) \rightarrow \sum_i^{\text{products}} \nu_i P_i \tag{4.14}$$

The stoichiometric composition of Jet-A/air can be derived by using CEA [81] which leads to

$$\begin{aligned} \nu_F^{(st)} &= 1\text{mol} & \mathfrak{M}_F &= 153\,{}^{\text{g}}\!/\!_{\text{mol}} \\ \nu_{Air}^{(st)} &= 84\text{mol} & \mathfrak{M}_{Air} &= 28\,{}^{\text{g}}\!/\!_{\text{mol}} \end{aligned} \tag{4.15}$$

Therefore the mean molecular mass becomes,

$$\langle \mathfrak{M} \rangle = \frac{\mathfrak{M}_F \nu_F^{(st)} + \mathfrak{M}_{Air}\nu_{Air}^{(st)}}{\nu_F^{(st)} + \nu_{Air}^{(st)}} = \frac{153\,{}^{\text{g}}\!/\!_{\text{mol}}\,1\text{mol} + 28\,{}^{\text{g}}\!/\!_{\text{mol}}\,84\text{mol}}{1 + 84} \approx 29\,{}^{\text{g}}\!/\!_{\text{mol}} \tag{4.16}$$

The physical properties of the mixture i.e., the mean specific heat , the mean viscosity, equation (3.92) , and the mean thermal conductivity, equation (3.94) are given by,

$$\left\langle c_p\big|_{T_0}\right\rangle_{mix} = \frac{\mathfrak{M}_F \nu_F^{(st)} c_{p,F}\big|_{T_0} + \nu_{Air}^{(st)}\left(0.21\mathfrak{M}_{O_2} c_{p,O_2}\big|_{T_0} + 0.78\mathfrak{M}_{N_2} c_{p,N_2}\big|_{T_0}\right)}{\mathfrak{M}_F \nu_F^{(st)} + \nu_{Air}^{(st)}\left(0.21\mathfrak{M}_{O_2} + 0.78\mathfrak{M}_{N_2}\right)}$$

$$\left\langle \mu\big|_{T_0}\right\rangle_{mix} = \frac{\sqrt{\mathfrak{M}_F}\nu_F^{(st)} \mu_F\big|_{T_0} + \nu_{Air}^{(st)}\left(0.21\sqrt{\mathfrak{M}_{O_2}} \mu_{O_2}\big|_{T_0} + 0.78\sqrt{\mathfrak{M}_{N_2}} \mu_{N_2}\big|_{T_0}\right)}{\sqrt{\mathfrak{M}_F}\nu_F^{(st)} + \nu_{Air}^{(st)}\left(0.21\sqrt{\mathfrak{M}_{O_2}} + 0.78\sqrt{\mathfrak{M}_{N_2}}\right)}$$

$$\left\langle \lambda\big|_{T_0}\right\rangle_{mix} = \frac{\sqrt[3]{\mathfrak{M}_F}\nu_F^{(st)} \lambda_F\big|_{T_0} + \nu_{Air}^{(st)}\left(0.21\sqrt[3]{\mathfrak{M}_{O_2}} \lambda_{O_2}\big|_{T_0} + 0.78\sqrt[3]{\mathfrak{M}_{N_2}} \lambda_{N_2}\big|_{T_0}\right)}{\sqrt[3]{\mathfrak{M}_F}\nu_F^{(st)} + \nu_{Air}^{(st)}\left(0.21\sqrt[3]{\mathfrak{M}_{O_2}} + 0.78\sqrt[3]{\mathfrak{M}_{N_2}}\right)}$$

$$(4.17)$$

The physical properties of O_2 and N_2 can be found at the National Institute of Standards and Technology (NIST) respectively in the thermodynamic data file of CAE [81]. Since the viscosity and thermal conductivity is not available for Jet-A, dodecane ($C_{12}H_{26}$) is considered as fuel although unfortunately μ and λ are only given up to 700K (Table 6).

T_0 [K]	c_p Jet A [J/g]	c_p O_2 [J/g]	c_p N_2 [J/g]	†μ $C_{12}H_{26}$ [Pas]	μ O_2 [Pas]	μ N_2 [Pas]	†λ $C_{12}H_{26}$ [W/mK]	λ O_2 [W/mK]	λ N_2 [W/mK]	$<c_p>$ [J/g]	$<\mu>$ [Pas]	$<\lambda>$ [W/m K]
700	3.48	1.03	1.10	1.12E-05	3.87E-05	3.29E-05	5.11E-02	0.058574	0.049736	1.2502	3.35E-05	0.0510
800	3.75	1.05	1.12	1.30E-05	4.24E-05	3.60E-05	5.95E-02	0.065996	0.055312	1.2858	3.67E-05	0.0570
900	3.98	1.07	1.14	1.47E-05	4.59E-05	3.89E-05	6.78E-02	0.073052	0.060768	1.3190	3.97E-05	0.0627
1000	4.18	1.09	1.16	1.65E-05	4.92E-05	4.16E-05	7.61E-02	0.079733	0.066082	1.3504	4.25E-05	0.0683

Tab. 6: Physical properties of Jet-A/Air mixture

Since the temperature dependency of the heat transfere coefficient is small for the temperature interval [700K,1000K] and furthermore for simplification reasons, the heat transfer coefficient was calculated according to equation (3.203) by

$$\langle\chi\rangle = \left\langle\left\langle\chi\big|_{T_0}\right\rangle_{mix}\right\rangle_{T_0} = 0.026\left(\frac{4\dot{m}}{\pi}\right)^{0.8} D_C^{-1.8}\left\langle\frac{\left(\left\langle\lambda\big|_{T_0}\right\rangle_{mix}\right)^{0.7}\left(\left\langle c_p\big|_{T_0}\right\rangle_{mix}\right)^{0.3}}{\sqrt{\left\langle\eta\big|_{T_0}\right\rangle_{mix}}}\right\rangle_{T_0}$$

$$(4.18)$$

† extrapolated

Furthermore it is convenient to parameterise the wall temperature according
to,

$$\left\langle T_w \right\rangle = \frac{\omega' T_0 + T_\infty}{1 + \omega'} \quad 0 \leq \omega' \leq \infty$$
$$\omega' = \frac{S_i \chi}{S_o \chi_o}$$

(4.19)

where S_i and S_o are equivalent to the inner and outer surface of the combustion
chamber, χ and χ_o are equivalent to the inner and outer heat transfer
coefficient and T_∞ is equivalent to the ambient temperature.

4.1.3.4   Ignition diagrams for Jet-A/Air

From equation (4.8) follows that the auto ignition pressure becomes a function
of numerous parameters. To account the influence of these parameters on the
ignition pressure, pressure diagrams for a Jet-A/air mixture are listed below
based on equation (4.8) and with specific values given by table 7

U	E_A [J/mol]	$\dot{m}$ [g/s]	$\mathfrak{M}$ [g/mol]	c_p [J/g]	μ [Pas]	λ [W/mK]	χ_o [W/m²K]	R [J/molK]	Φ	m
1.68e-8	155000	1	29	1.3	3.81e-5	0.06	20	8.31	1	2

Tab. 7: Physical mean properties and ignition parameters of Jet-A/Air mixture

4.1.3.4.1 p_0-T_0 diagram

Figure 25 and figure 26 show the dependency of the necessary initial pressure,
p_0, to achieve auto ignition on the initial temperature, T_0, for several values of
the combustion chamber volume, V_C, and combustion chamber diameter, D_C.
Figure 27 gives a detailed view of figure 26 in the temperature interval between
850K and 900K. According to equation (4.8) a discontinuity of p_0 occurs. If
both the volume and the diameter are increased, p_0, decreases and if the letter
becomes infinity, the p_0-T_0 graph converges to the ideal adiabatic ignition
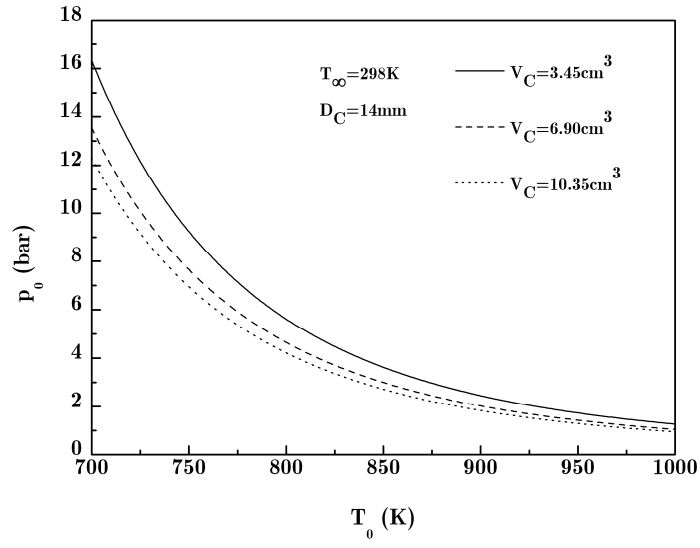behaviour.

Fig. 25: Necessary initial pressure to achieve ignition vs. initial temperature for a constant combustion chamber diameter and several combustion chamber volume
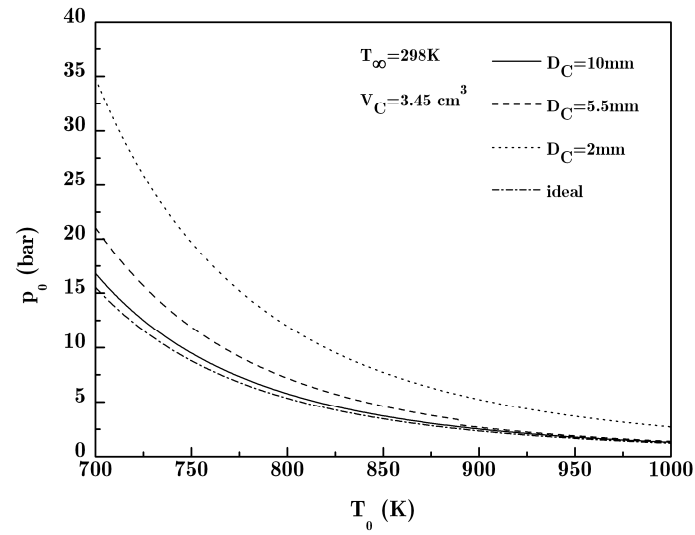

Fig. 26: Necessary initial pressure to achieve ignition vs. initial temperature for a constant combustion chamber volume and several combustion chamber diameters
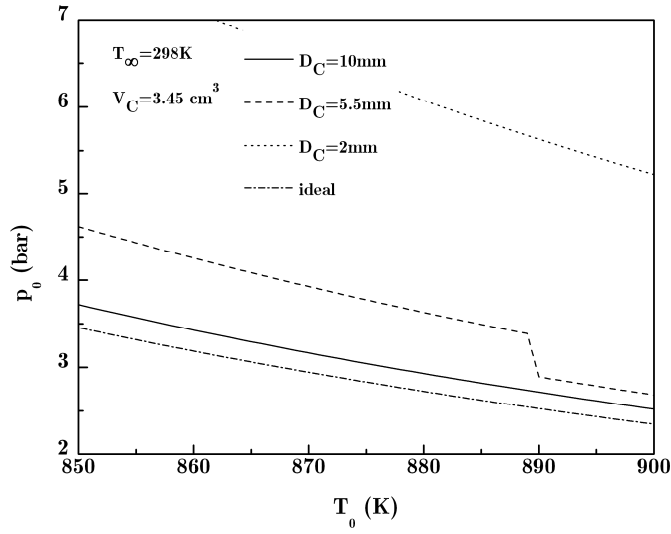
Fig. 27: Detailed view of the necessary initial pressure to achieve ignition vs. initial temperature for a constant combustion chamber volume and several combustion chamber diameters

4.1.3.4.2 p_0-V_C diagram

Figure 28 and 29 shows the dependency of the necessary initial pressure, p_0, to achieve auto ignition on the combustion chamber volume, V_C, for several values of the initial temperarue, T_0, and the combustion chamber diameter, D_C.
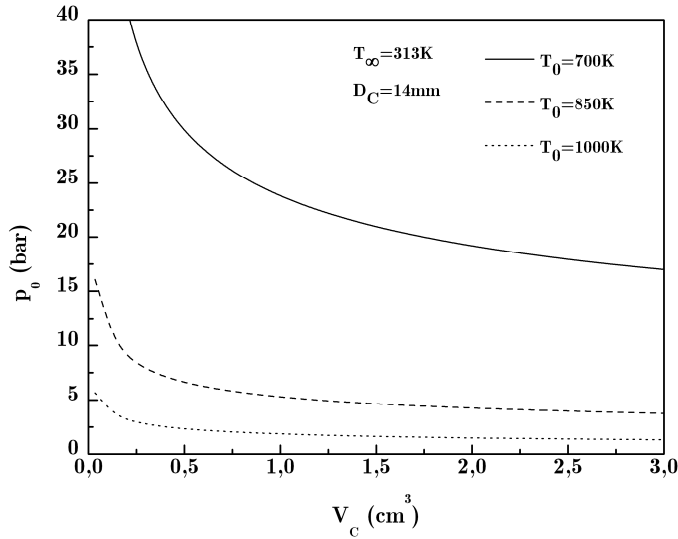

Fig. 28: Necessary initial pressure to achieve ignition vs. combustion chamber volume for a constant combustion chamber diameter and several initial temperatures

The influence of the combustion chamber volume on p_0 becomes significant for small volumes and is negligible for large values of V_C.
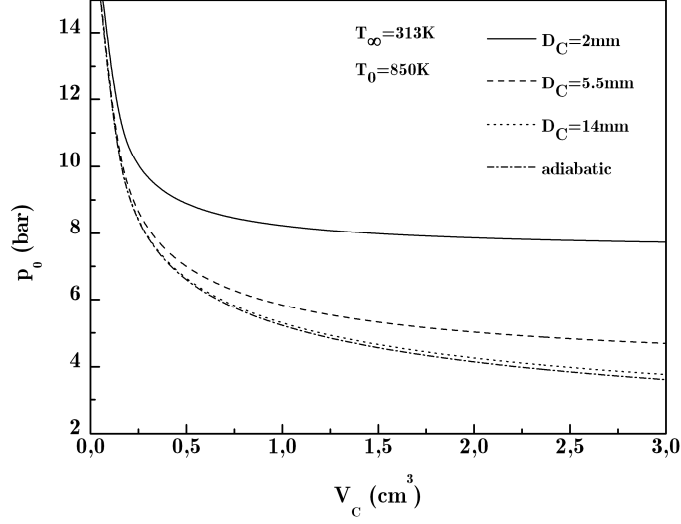

Fig. 29: Necessary initial pressure to achieve ignition vs. combustion chamber volume for a constant initial temperature and several combustion chamber diameters

If V_C becomes very large, p_0 reaches a lower limit in contrast to the adiabatic case, equation 4.7, which is given for the 1st and 2nd ignition (thermal) condition by,

$$\lim_{V_C \to \infty} p_0 \geq \sqrt[(m'+1)]{\frac{\left(1.0133x10^5\right)^{m'} 10^{-3} U' R T_0}{\left\langle \mathfrak{M} \right\rangle_\phi^{mix}} \frac{4 \left\langle \chi\big|_{T_o} \right\rangle_\phi^{mix}}{D_C \left\langle c_p\big|_{T_o} \right\rangle_\phi^{mix}} \exp\left[\frac{E_A}{R T_0}\left(1 + \frac{1 - \frac{T_\infty}{T_0}}{1 + \omega'}\right) - 1\right]}$$

(4.20)

and for the 2nd ignition (thermal) condition,

$$\lim_{V_C \to \infty} p_0 \geq \sqrt[(m'+1)]{\frac{\left(1.0133x10^5\right)^{m'} 10^{-3} U'}{\left\langle \mathfrak{M} \right\rangle_\phi^{mix}} \exp\left(\frac{E_A}{R T_0}\right) \frac{4 E_A \left\langle \chi\big|_{T_o} \right\rangle_\phi^{mix}}{T_0 D_C \left\langle c_p\big|_{T_o} \right\rangle_{mix}} \left(\frac{1 - \frac{T_\infty}{T_0}}{1 + \omega'}\right)}$$

(4.21)

4.1.3.4.3 p_0-D_C diagram

Figure 30 and 31 show the dependency of the necessary initial pressure, p_0, to achieve auto ignition on the combustion chamber diameter, D_C, for several values of the initial temperarue, T_0, and the combustion chamber volume, V_C,.
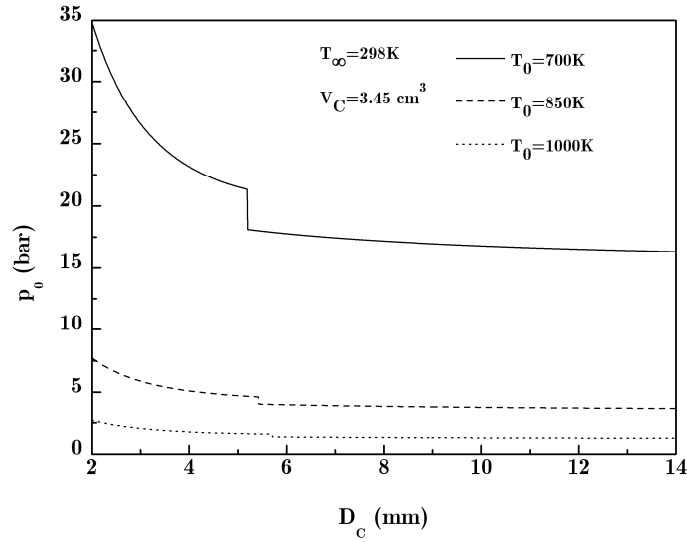

Fig. 30: Necessary initial pressure to achieve ignition vs. combustion chamber diameter for a constant combustion chamber volume and several initial temperatures
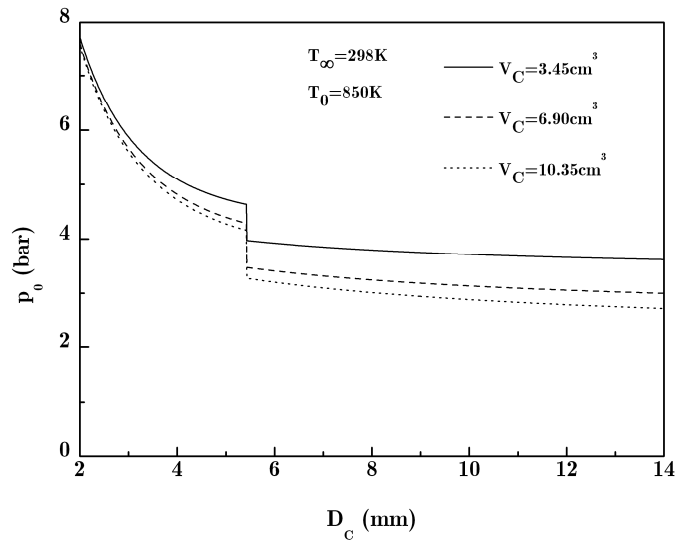

Fig. 31: Necessary initial pressure to achieve ignition vs. combustion chamber diameter for a constant initial temperature and several combustion chamber volume

136

The discontinuity of p_0 is given by the fact that two possible ignition conditions exist and further by the fact that the heat transfer coefficient dependents on D_C. Similar to the combustion chamber volume the influence of the combustion chamber diameter on p_0 becomes significant for small values and becomes negligible for large values.

If D_C becomes very large, p_0 reaches a lower limit which is given by,

$$\lim_{D_C \to \infty} p_0 = \sqrt[(m'+1)]{\frac{\left(1.0133x10^5\right)^m 10^{-3} U' R T_0}{\langle \mathfrak{M} \rangle_\phi^{mix}} \frac{\dot{m}}{\Phi V_C} \exp\left(\frac{E_A}{R T_0}\right)} \qquad (4.22)$$

which is equal to the ideal ignition pressure (equation 4.7).

4.1.3.4.4 p_0-T_∞ diagram

Figure 32 shows the dependency of the necessary initial pressure, p_0, to achieve auto ignition on the ambient temperature, T_∞. for V_C=3.45cm^3, D_C=14mm and T_0=850K.
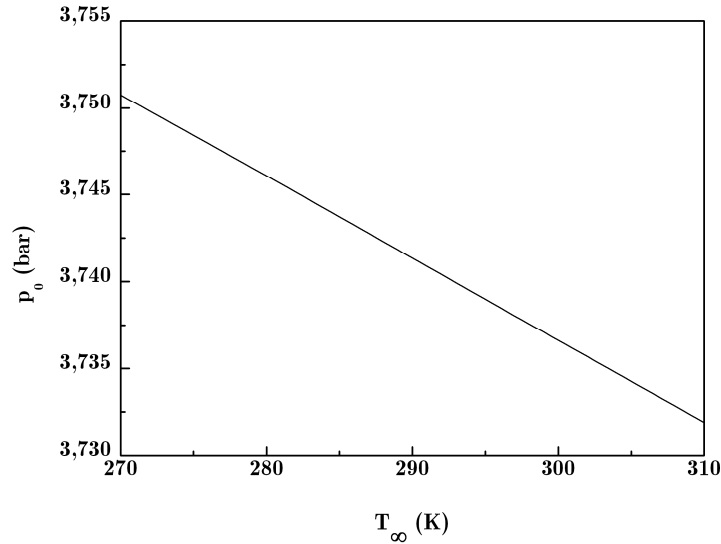

Fig. 32: Necessary initial pressure to achieve ignition vs. ambient temperature

The influence of T_∞ might seem negligible but it is significant particular for auto ignitable propulsion systems if the nominal ignition pressure is close to the necessary initial pressure, p_0, according to equation (4.8) and (4.9).

Wernimont and Durant [82] reported weather effects have considerable influence on start-up performance of their bipropellant thruster and cannot be ignored.

4.1.3.4.5 p_0-T_w diagram

If it is assumed that the rate of change of the wall temperature, $\left[T_w\left(t+t_{ig}\right)-T_w\left(t\right)\right]\big/t_{ig}$ within in time interval $\left[t,t+t_{ig}\right]$ which is the time till ignition is small, the physical system can be described in the quasi equilibrium state and therefore the ignition process can be described as stationary. Thus the wall temperature can be considered as an arbitrary parameter. With equation (4.8) following influence of the wall temperature on the ignition behaviour can be shown.
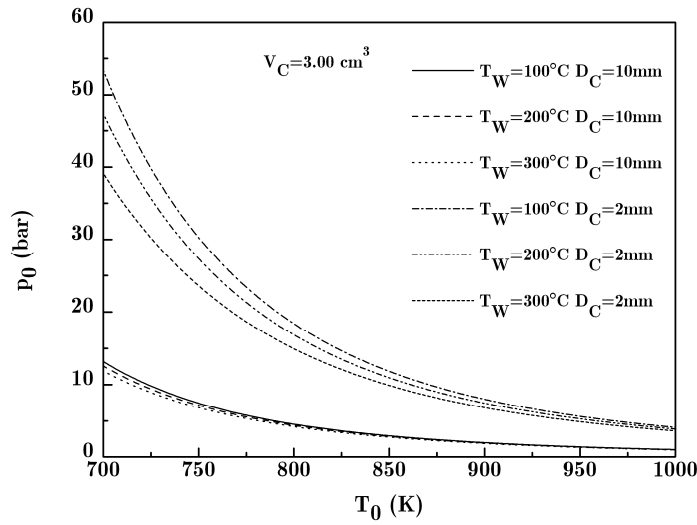

Fig. 33: Necessary initial pressure to achieve ignition vs. initial temperature for a constant combustion chamber volume and several wall temperatures and combustion chamber diameters

Figure 33 shoes that the influence of the wall temperature can be neglected in the complete temperature regime for diameters equal or greater than 10mm. Only for small combustion chamber diameters and for low injection temperatures, T_0, the influence of the wall temperature becomes significant.

4.2   Hydrogen peroxide

Hydrogen peroxide is a chemical compound which is inherently unstable that reacts exothermically, or decomposes, into hot oxygen gas and water vapor. The decomposition rate of propellant-grade H_2O_2 is less than 0.1% per year over normal atmospheric temperature and pressure ranges under proper storage conditions [83]. The decomposition rate is significantly accelerated as the temperature of the H_2O_2 and/or its environment is increased and/or when the liquid is in contact with certain materials or contaminants. Table 8 shows some liquid physical properties of hydrogen peroxide [83,53].

Concentration	70% H_2O_2	80% H_2O_2	90% H_2O_2	98% H_2O_2
Molecular Weight, g/mol	26.86	28.89	31.29	33.42
Specific Gravity	1.283	1.333	1.387	1.432
Boiling Point, F	257		287	299
Vapor Pressure, psia	0.137		0.065	0.045
Heat Capacity, Btu/lbm-R	0.738		0.663	0.633

Tab. 8: Physical properties of liquid H_2O_2 [53,76,112]

4.2.1   Thermal decomposition mechanism of hydrogen peroxide

Although, some theoretical and experimental works have been reported, a complete mechanism for H_2O_2 decomposition has not reported so far since the thermal decomposition of H_2O_2 is a complex process which involves many intermediate radical species. Sengupta, Mazumder, Cole and Lowry [84] proposed a comprehensive mechanism for thermal decomposition of H_2O_2 which is given in table 9 with the complete mechanism and the rate constants for each reaction step.
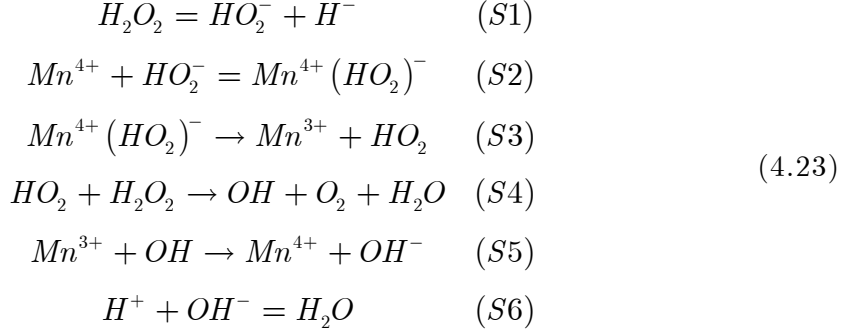
	Reactions	A	n	Ea/R	ΔH
1	2O + M ↔ O2 + M	0.120E+12	-1.00	0.0	-4.9832E+08
2	O + H + M ↔ OH + M	0.500E12	-1.00	0.0	-4.2780E+08
3	O + H2 ↔ H + OH	0.387E+02	2.70	0.32E+04	8.1700E+06
4	O + HO2 ↔ O2 + OH	0.200E+11	0.00	0.0	-2.2237E+08
5	O + H2O2 ↔ OH + HO2	0.963E+04	2.00	0.20E+04	-6.1392E+07
6	O2 + H + M ↔ HO2 + M	0.280E+13	-0.86	0.0	-2.0543E+08
7	2O2 + H ↔ O2 + HO2	0.208E+14	-1.24	0.0	-2.0543E+08
8	O2 + H + H2O ↔ HO2 + H2O	0.113E+14	-0.76	0.0	-2.0543E+08
9	O2 + H ↔ O + OH	0.265E+14	-0.67	0.86E+04	-7.0519E+07
10	2H + M ↔ H2 + M	0.100E+13	-1.00	0.0	-4.3597E+08
11	2H + H2 ↔ 2 H2	0.900E+11	-0.60	0.0	-4.3597E+08
12	2H + H2O ↔ H2 + H2O	0.600E+14	-1.25	0.0	-4.3597E+08
13	H + OH + M ↔ H2O + M	0.220E+17	-2.00	0.0	-4.9914E+08
14	H + HO2 ↔ O + H2O	0.397E+10	0.00	0.34E+03	-2.2319E+08
15	H + HO2 ↔ O2 + H2	0.448E+11	0.00	0.54E+03	-2.3054E+08
16	H + HO2 ↔ 2 OH	0.840E+11	0.00	0.32E+03	-1.5185E+08
17	H + H2O2 ↔ H2 + HO2	0.121E+05	2.00	0.26E+04	-6.9562E+07
18	H + H2O2 ↔ OH + H2O	0.100E+11	0.00	0.18E+04	-2.8458E+08
19	OH + H2 ↔ H + H2O	0.216E+06	1.51	0.17E+04	-6.3171E+07
20	2OH + M ↔ H2O2 + M	0.740E+08	-0.37	0.0	-2.1456E+08
21	2OH ↔ O + H2O	0.357E+02	2.40	-0.11E+04	-7.1341E+07
22	OH + HO2 ↔ O2 + H2O	0.145E+11	0.00	-0.25E+03	-2.9371E+08
23	OH + H2O2 ↔ HO2 + H2O	0.200E+10	0.00	0.21E+03	-1.3273E+08
24	OH + H2O2 ↔ HO2 + H2O	0.170E+16	0.00	0.15E+05	-1.3273E+08
25	2HO2 ↔ O2 + H2O2	0.130E+09	0.00	-0.82E+03	-1.6097E+08
26	2HO2 ↔ O2 + H2O2	0.420E+12	0.00	0.60E+04	-1.6097E+08
27	OH + HO2 ↔ O2 + H2O	0.500E+13	0.00	0.87E+04	-2.9371E+08

Tab. 9: Reaction mechanism of H_2O_2 decomposition [23]

where the rate constants are expressed in Arrhenius form with SI units. ΔH is given in Joule/kmol. M represents a third body. The most important reaction is step 20. This reaction represents the first step of H_2O_2 decomposition to produce two OH radicals. The OH radicals initiate other reactions and produce some intermediate species, such as HO_2, H and O.

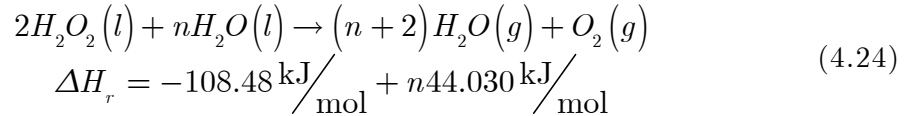## 4.2.2 Catalytic decomposition mechanism of hydrogen peroxide

Similar to the thermal decomposition of hydrogen peroxide the detailed catalytic decomposition mechanism is very complex and furthermore the mechanism depends on the catalyst material. Sorge, Turco, Pilone, and Bagnasco [85] proposed a mechanism of hydrogen peroxide on MnO_2/TiO_2 catalysts. They suggested that the activity of manganese-based catalysts is due to surface Mn^{4+} cations [86,87] and suggested following mechanism.
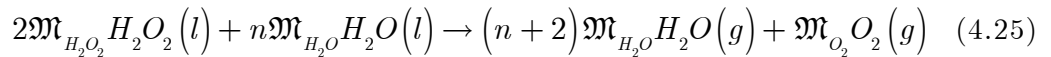
$$H_2O_2 = HO_2^- + H^- \qquad (S1)$$
$$Mn^{4+} + HO_2^- = Mn^{4+}\left(HO_2\right)^- \qquad (S2)$$
$$Mn^{4+}\left(HO_2\right)^- \rightarrow Mn^{3+} + HO_2 \qquad (S3)$$
$$HO_2 + H_2O_2 \rightarrow OH + O_2 + H_2O \qquad (S4)$$
$$Mn^{3+} + OH \rightarrow Mn^{4+} + OH^- \qquad (S5)$$
$$H^+ + OH^- = H_2O \qquad (S6)$$

$$(4.23)$$

The first step corresponds to the ionization equilibrium of H_2O_2, which is very fast. Reaction step 2 (S2) represents the adsorption of HO_2^-, which is also assumed to be very fast and, thus, to exist in pseudoequilibrium conditions. The rate dominat step is probably the formation of the hydroperoxyl radical $HO_2 \cdot$ (S3).

4.2.3 Decomposition temperature of hydrogen peroxide

Although the real reaction mechanism of hydrogen peroxide is complex it can be stated as a global one step reaction considering standard conditions and diluted hydrogen peroxide as follows [53],

$$2H_2O_2\left(l\right) + nH_2O\left(l\right) \rightarrow \left(n+2\right)H_2O\left(g\right) + O_2\left(g\right)$$
$$\Delta H_r = -108.48\,{}^{\text{kJ}}\!\!\diagup\!\!_{\text{mol}} + n44.030\,{}^{\text{kJ}}\!\!\diagup\!\!_{\text{mol}}$$

$$(4.24)$$

The letters in parentheses following the chemical symbol are state symbols and represent the physical state of the chemical species. The term $n44.030$kJ/mol represents the vaporization of n moles of H_2O. Multiplying equation (4.26) with the molecular weight of each species, equation (4.26) becomes,

$$2\mathfrak{M}_{H_2O_2}H_2O_2\left(l\right) + n\mathfrak{M}_{H_2O}H_2O\left(l\right) \rightarrow \left(n+2\right)\mathfrak{M}_{H_2O}H_2O\left(g\right) + \mathfrak{M}_{O_2}O_2\left(g\right) \quad (4.25)$$

By introducing the concentration ϖ which is given in rel. wt% of the diluted hydrogen peroxide by,

$$\varpi = \frac{2\mathfrak{M}_{H_2O_2}}{2\mathfrak{M}_{H_2O_2} + n\mathfrak{M}_{H_2O}} \qquad (4.26)$$

and with the consideration that,

$$\frac{2\mathfrak{M}_{H_2O_2}}{2\mathfrak{M}_{H_2O_2} + n\mathfrak{M}_{H_2O}} + \frac{n\mathfrak{M}_{H_2O}}{2\mathfrak{M}_{H_2O_2} + n\mathfrak{M}_{H_2O}} = 1 \qquad (4.27)$$

follows,

$$\begin{aligned}
n\mathfrak{M}_{H_2O} &= \left(1 - \varpi\right)\left(2\mathfrak{M}_{H_2O_2} + n\mathfrak{M}_{H_2O}\right) \\
2\mathfrak{M}_{H_2O_2} &= \varpi\left(2\mathfrak{M}_{H_2O_2} + n\mathfrak{M}_{H_2O}\right) \\
n &= \frac{2\mathfrak{M}_{H_2O_2}}{\mathfrak{M}_{H_2O}}\left(\frac{1}{\varpi} - 1\right)
\end{aligned} \qquad (4.28)$$

Thus the hydrogen peroxide reaction becomes,

$$\varpi H_2O_2\left(l\right) + \left(1 - \varpi\right)H_2O\left(l\right) \rightarrow \left[\varpi\left(\frac{\mathfrak{M}_{H_2O}}{\mathfrak{M}_{H_2O_2}} - 1\right) + 1\right]H_2O\left(g\right) + \frac{\varpi}{2}\frac{\mathfrak{M}_{O_2}}{\mathfrak{M}_{H_2O_2}}O_2\left(g\right)$$

$$\Delta H_r = \varpi\frac{-54.24\,\text{kJ}\big/\text{mol}}{\mathfrak{M}_{H_2O_2}} + \left(1 - \varpi\right)\frac{44.030\,\text{kJ}\big/\text{mol}}{\mathfrak{M}_{H_2O}}$$

$$(4.29)$$

The adiabatic decomposition temperature can be determined according to [88] or by using the CEA-Code [81].
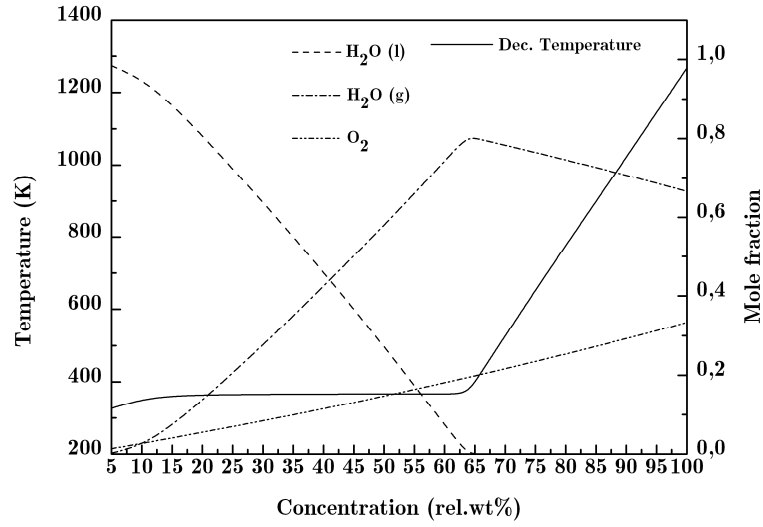
Fig. 34: Decomposition temperature and mole fraction of the products

Figure 34 shows the adiabatic decomposition temperature and the mole fraction of the products with respect to the concentration of the diluted hydrogen peroxide. Around the concentration of 63%wt liquid water in addition to the water steam appears and increases with decreasing concentration until solely water is present (what is evident for $\varpi=0\%$wt). Consequently for concentrations lower than 63%wt the released energy is too small to vaporize the entire water

.

5

PROPULSION SYSTEM DESIGN

5.1 Rocket performance and mass flow

The primary measure of performance of a rocket engine is its specific impulse, I_{sp}, which is defined by,

$$I_{sp} = \frac{\int F_{Th} \mathrm{d}t}{\int \dot{m} \mathrm{d}t} = \frac{\int \dot{m} v_e \mathrm{d}t}{\int \dot{m} \mathrm{d}t} = v_e \tag{5.1}$$

Where F_{Th} is given by the thrust force, and v_e is given by the exit velocity of the propellant. For a given chamber pressure and propellant mixture ratio, the I_{sp} and the adiabatic flame temperature, T_C, are determined using CEA, a NASA code developed by Gordon and McBride [81]. Table 10 summarizes the design parameters for the calculation of the adiabatic flame temperature and specific impulse.

H_2O_2 Concentration	Adiabatic temperature oxidizer [K]	Initial temperature fuel [K]	Pressure [bar]	Expansion ratio ε
87.5%	968	293	1,10	100

Tab. 10: Parameters for the calculation of adiabatic flame temperature and Isp for Jet-A1/H_2O_2

Figure 35 and 36 show the adiabatic flame temperature of Jet-A1/H_2O_2 respectively the specific impulse depending on the oxidizer/fuel ratio.
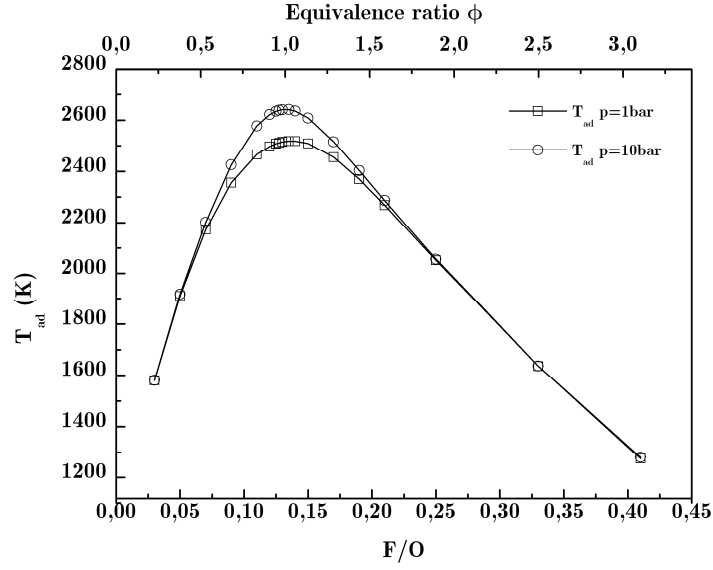
Fig. 35: Adiabatic flame temperature vs fuel/oxidizer ratio respectively equivalence ratio
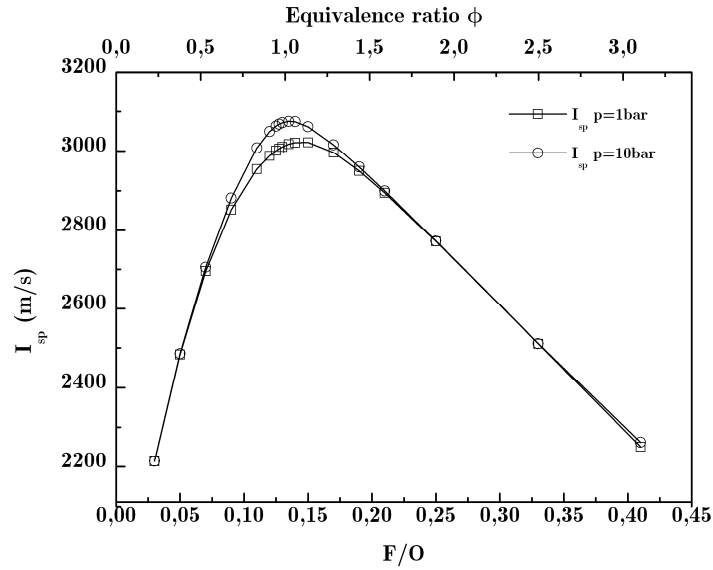

Fig. 36: Specific impulse vs. fuel/oxidizer ratio respectively equivalence ratio

The specific impulse calculation performed assumes equilibrium chemistry up to the throat, and frozen chemistry in the expansion nozzle. The results of these calculations are idealized in the sense that they are adiabatic, assume the combustion reactions proceed completely to equilibrium, and do not account for friction effects on the chamber and nozzle. The variation in the adiabatic flame temperature and specific impulse is therefore due only to the effect of pressure on the equilibrium composition, and not due to its potential impact on the

kinetic rates of the combustion reactions. The mass flow rates now are calculated as follows,

$$\left.\begin{array}{l} \dot{m}_{Ox} + \dot{m}_{F} = \dfrac{F_{Th}}{I_{sp}\left(\phi\right)} \\[2ex] \dot{m}_{F} = \phi\left(F/O\right)_{stoich}\ \dot{m}_{Ox} \end{array}\right\} \Rightarrow \left\{\begin{array}{l} \dot{m}_{Ox} = \dfrac{F_{Th}}{I_{sp}\left(\phi\right)\left[\phi\left(F/O\right)_{stoich} + 1\right]} \\[3ex] \dot{m}_{F} = \dfrac{\phi\left(F/O\right)_{stoich}\ F_{Th}}{I_{sp}\left(\phi\right)\left[\phi\left(F/O\right)_{stoich} + 1\right]} \end{array}\right. \qquad (5.2)$$

5.2 Combustor design

The combustion chamber design for rocket based combustors is a major task to ensure high combustion efficiencies, avoiding poor flame stabilisation and combustion instability. To date, a historical empirical value L^* (characteristic length) is used to design combustion chambers for rocket engines [89]. The characteristic length, L^*, is rather a crude parameter than a detailed guide line to design combustion chambers because it gives only information of the relation between the combustion chamber volume and the throat diameter to achieve combustion for a specific propellant combination (oxidizer and fuel) and combustion regime (pressure, equivalence ratio, ect.). The answer of an optimal aspect ratio of the combustion chamber is ignored. From this follows that if the combustion parameters (propellants, combustion pressure, propellant injector type, mechanism of chamber cooling, ect) differ from the parameters which led in the past to the empirical value of L^* to achieve combustion, the characteristic length, L^*, is rather a rough parameter to design combustion chambers, although characteristic length values for hydrogen peroxide based bipropellant thrusters can be found in the literature [90-93].

Morover the combustion chamber geometry influences the stability of combustion. Stable combustion in combustors may become unstable due to small changes in operating parameters, geometry configurations, and the manner in which the reactants are introduced [94]. Zucrow an Osborn [95], for instance studied the influence of the chamber length required for combustion instability to occur for gaseous fuels. Key mechanisms of the physiochemical process and operating parameters responsible for combustion instabilities initiation and sustaining have been studied in the past but many aspects of

them are still unresolved [96-100]. The complex interaction between fluid mechanics, energetic process and acoustics in the combustion chamber can produce sound waves which generates velocity and pressure perturbations [101]. An amplifying condition exists, if resonant modes and heat release pertubations are in phase with each other [102] (Rayleigh Criterion).

To overcome this problem in designing combustion chambers models of the combustion process can be used to guide the design to an optimum geometry for the combustion chamber. Nevertheless, finite difference techniques, fuel evaporation, submodels for combustion chemistry, and flow turbulence and their interactions are limited of accurate performance predictions which requires experimental validation leading to increase the time and cost of the development.

If the combustion chamber design is according to a dump combustor configuration which implies a rearward facing step which is a sudden enlargement of the combustor, semi empirical models can be used to guide the design of the combustion chamber. They offer an alternative method which is more useful in the preliminary design focuses only on important regions of the combustor flow field and relates conditions there to the combustor geometry. A common used model is the characteristic time model [103] and an alternative but similar model for combustion efficiencies including combustor length effects was developed by Prior, Fowler and Mellor [104].

For high gas velocities flame holding and stabilisation becomes an important issue to avoid flame blow off, particularly for bipropellant systems using gaseous oxidizer. To provide flame holding and flame stabilisation and to enhance the performance of the combustion a dump combustor design with a rearward facing step and a coaxial swirl injector was chosen (Fig 37).
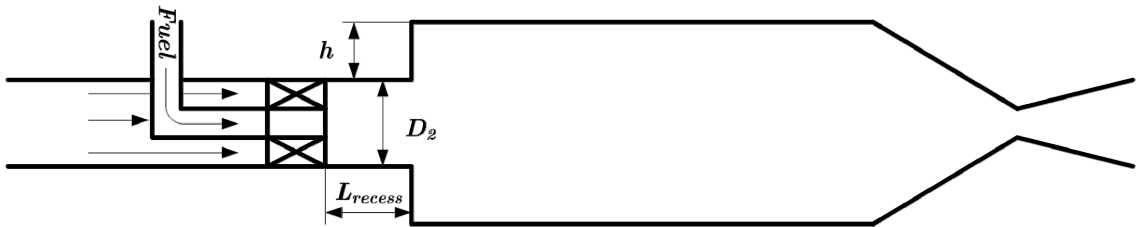

Fig. 37: Schematic of a dump combustor with swirl injector

The fundamentally characteristic of a rearward facing step incorporates the creation of a recirculation zone behind the step that feeds the incoming mixture of fuel and oxidizer with hot combustion products to sustain the

reaction and anchor the flame. Secondary, a turbulent shear layer is developed between the free stream and the recirculating flow creating large scale turbulent eddies (Fig.38). It is assumed that these eddies plays an important role for auto ignition [105]. In this hot eddies a very effective amalgamation of fuel particles and oxidizer particles takes place driving the probability of ignition. Therefore the breakdown time of the eddies is a critical property for achieving auto ignition.
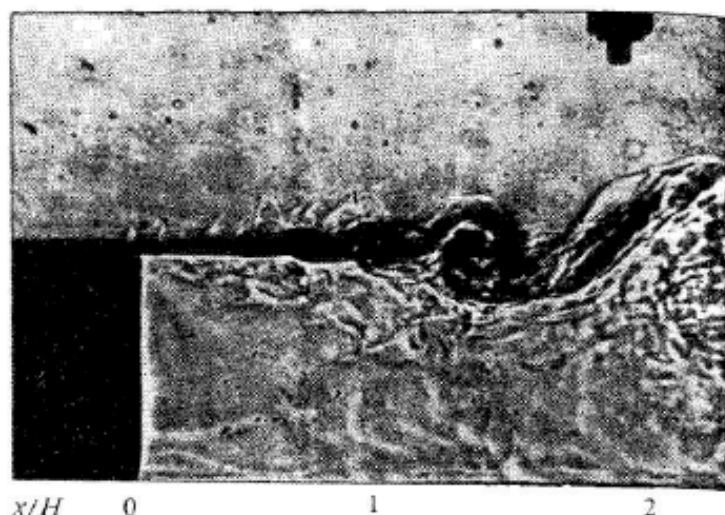

Fig. 38: Flow behind a rearward facing step [114]

In addition a single swirl injector is attached upstream of the reward facing step to enhance the turbulence intensity in the combustion chamber which influences the combustion efficiency, and secondly to assure a perfectly mixed fuel/oxidizer mixture before entering the combustor. In this configuration not only a corner recirculation zone is formed downstream of the backward facing step but also a torodial recirculation zone is established in the wake of the center body under the influence of the swirling flow (Fig 39). The central torodial recirculation zone, a form of vortex breakdown, serves additionally as a flame stabilization region, where hot products are mixed with the incoming mixture of fuel and oxidizer [94].
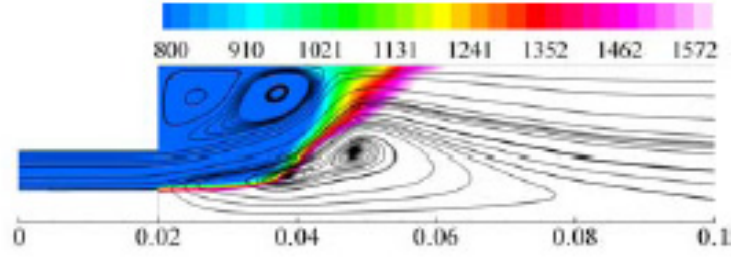
Fig. 39: Mean Temperature contours and streamlinesof stable flame for S = 0.76 [6]

The resulting shape of the flow field in the combustion chamber using a tandem of swirl injector and reward facing step strongly depends on the dimensionless swirl number S which is defined as the ratio between the axial flux of the angular momentum to the product of the axial momentum flux and a characteristic radius, R_O, (equation 5.22).

Figure 40 describes the overal flow development with respect to the inlet swirl number. If there is no swirl, only the wake and corner recirculation zone exists [94]. For low swirl number three recirculation zones are developed in the combustion chamber, including a separation wake recirculation zone behind the centerbody, a corner recirculation zone due to the rearward facing step, and a central toroidal recirculation zone resulting from vortex breakdown [94]. Increasing the swirl number to high values, high positive radial velocity is generated in the main flow passage under the influence of the centrifugal force which spreads the incoming flow from the orifice outwards to the chamber boundary. Thus the central recirculation zone moves upstream and merges with the wake recirculation zone [94]. Subsequently the corner recirculation zone rolls back and becomes diminished for high swirl numbers [94]. Chao et al [106] validate similar results in their experimental study of the flow pattern in a co-annual swirl combustor. The streamline patterns and temperature fields in figure 40 indicate flames anchored at the edge of the centerbody and the corner of the rearward facing step. For high values of swirl number, the flame is much more compact due to the enhanced flame speed resulting from the increased vorticity [94]
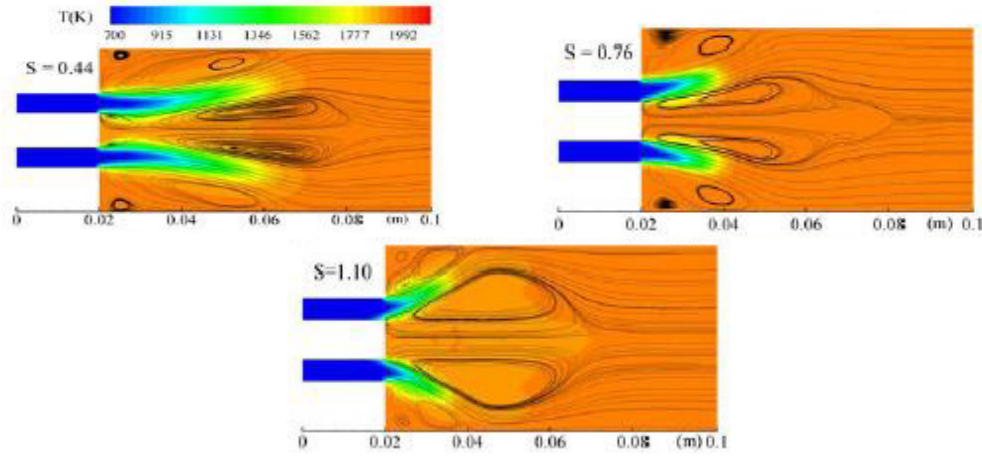
Fig. 40: Mean temperature field and stream line pattern for several values of S [94]

Thus, quality for flow entrainment in the reaction zone, ignition and consequently for flame evolution is dominated by the turbulent intensity of the flow field. Figure 41 shows the vorticity magnitude of the flow pattern for two different swirl numbers. For low swirl number, large vortical structures originate from the shear layer and then evolute into turbulent eddies. For high swirl numbers vortices are shed from the edge of the rearward facing step similar to the low swirl number case, however, the vortex motions become disordered due to the strong central recirculation flow. Generally, high turbulence intensity regions are generated downstream of the centerbody and the rearward facing step where large velocity fluctuations are produced due to the strong turbulent mixing in the shear layers between the recirculation flows and the incoming flow from the orifice. Basically the density of vortices in the flow field is enhanced by high swirl numbers and therefore the turbulence intensity respectively.
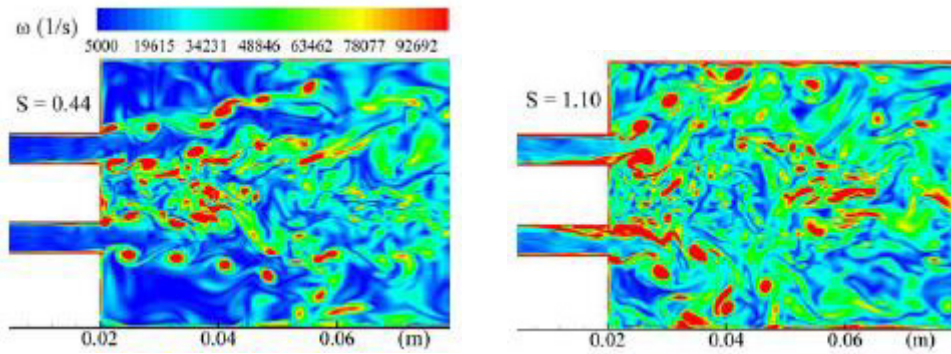

Fig. 41: Vorticity magnitude field for S=0.44 and S=1.10 [94]

150

In order to guide the design of the combustion chamber a semi empirical engineering design model is used to predict the necessary pre mixing chamber geometry (orifice geometry) and combustion chamber geometry although this model does not address the influence of the swirl number to the combustion efficiency [104].

5.2.1 Determination of combustion chamber geometry

Prior, Fowler and Mellor [104] suggested that an efficiency model developed for bluff-body flameholders ca be extended to ramjets (Fig. 421).
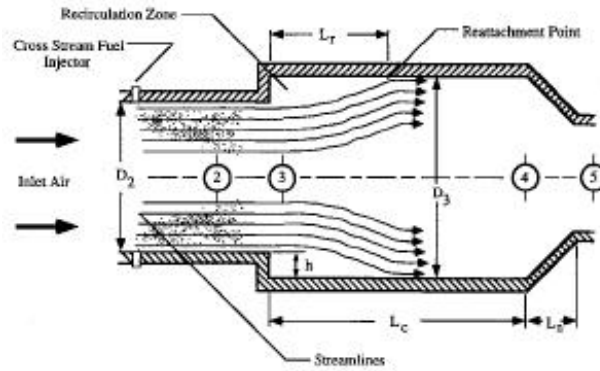

Fig. 42: Liquid fuel ramjet schematic [104]

This model uses the results from Tuttle et. al [107] which treated the shear layer surrounding the bluff-body recirculation zone as the relevant reactor for combustion. Under the consideration of Blazowski and Henderson's [108] results and combining it with Schmidt an Mellor's [109], Prior, Fowler and Mellor proposed an equation for the efficiency of the combustor as follows,

$$\eta_C = 1 - \exp\left(\frac{-A'' \tau_{sl}}{\tau_\eta^* + k\tau_{eb}}\right) \tag{5.3}$$

The shear layer residence time, τ_{sh}, is an important factor for the efficiency of combustion as can be seen in equation (5.3). This is in accordance with the assumption of Plee and Mellor's [110] work that the shear layer residence time, which is usually taken to be equal to the characteristic breakdown time of the eddies plays an important role for combustion. Experimental results have shown that the characteristic length scale of the turbulent eddies for a

151

longitudinal flow is equal to the width of the flameholder ignoring combustor length and exhaust nozzle effects [110]. It is defined by,

$$\tau_{sl} = \frac{D_3 - D_2}{v_2} \tag{5.4}$$

The gas velocity, v_2, is dependent on mass flow rate, flow area and density and is given by in the absence of a swirl to,

$$v_2 = \frac{4\dot{m}}{D_2^{\ 2}\pi\rho} \tag{5.5}$$

Thus, the shear layer residence time becomes,

$$\tau_{sl} = \frac{\left(D_3 - D_2\right)D_2^{\ 2}\pi\rho}{4\dot{m}} \tag{5.6}$$

The maximum of the shear layer residence time is given by the derivation of equation (5.6) with assuming constant mass flow and density.

$$\left(\begin{array}{c}\dfrac{\partial}{\partial D_2} \\[2mm] \dfrac{\partial}{\partial D_3}\end{array}\right)\left[\frac{\left(D_3 - D_2\right)D_2^{\ 2}\pi\rho}{4\dot{m}}\right] = 0 \tag{5.7}$$

Thus

$$\frac{\pi\rho}{4\dot{m}}\left[2D_2\left(D_3 - D_2\right) - D_2^{\ 2}\right] = 0 \tag{5.8}$$

$$\frac{\pi\rho}{4\dot{m}}D_2^{\ 2} = 0 \tag{5.9}$$

Equation (5.9) can be ignored because it gives the trivial result for D_2 and D_3. Thus equation (5.8) gives the optimum relation between the orifice diameter D_2 and the combustion chamber diameter D_3 which is given by,

$$D_3 = \frac{3}{2}D_2 \tag{5.10}$$

152

From equation (5.10) follows for the optimum step size with $D_3\text{-}D_2=2h$,

$$h = \frac{D_3}{6} \qquad (5.11)$$

which has been observed at least for liquid-fueled systems [111]. The shear layer residence time by the ratio of D_2 to D_3 is schematically shown in figure 43.
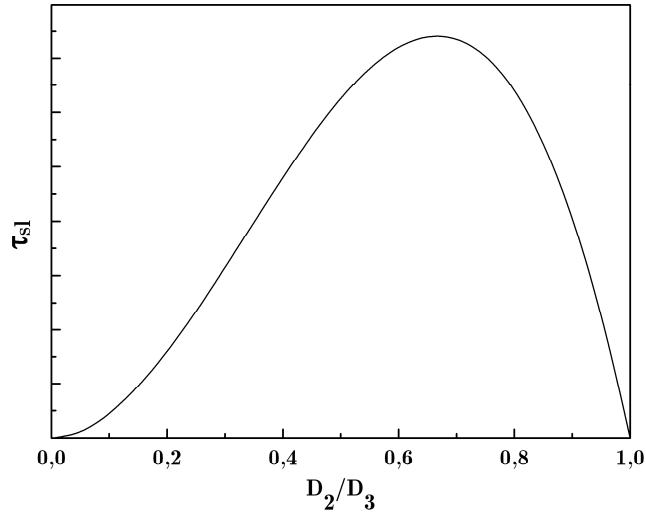

Fig. 43: Schematic view of the shear layer residence time

The previous model does not explicitly account for combustor length effects, however, as Stull et all [111] experimentally determined and Gallagher et al [103] predict that combustion efficiency increases with combustor length, L_C [104]. To account on this results Prior, Fowler and Mellor proposed an alternative approach by substituting the flameholder dimension $(D_3\text{-}D_2)$ which is used as proportional to recirculation zone length by the reattachment length L_r. Thus equation (5.4) becomes,

$$\tau_{sl} = \frac{L_r}{v_2} \qquad (5.12)$$

They derived an equation in the absence of a swirler for the reattachment length, L_r, under the consideration of Drewry's [113] two equations as a defining point and is given by,

$$L_r = 8.72h\left[1 - \exp\left(\frac{-L_C}{D_3}\right)\right] \tag{5.13}$$

With equation (5.12) and (5.13) the combustion efficiency proposed by Prior, Fowler and Mellor becomes assuming negligible evaporation effects to [104],

$$\eta_C = 1 - \exp\left\{-4.36A\frac{2h}{D_3}\left(1 - \frac{2h}{D_3}\right)^2\left[1 - \exp\left(\frac{-L_C}{D_3}\right)\right]\right\} \tag{5.14}$$

where A is proportional to $D_3{}^3$, inlet gas density, and inversely proportional to mass flow rate and the kinetic time for fuel and CO oxidation, $\tau_\eta{}^*$.

$$A = \frac{\pi\rho A'' D_3{}^3}{4\dot{m}\tau_\eta{}^*} \tag{5.15}$$

For the optimum step size $h=D_3/6$, the combustion efficiency is given by,

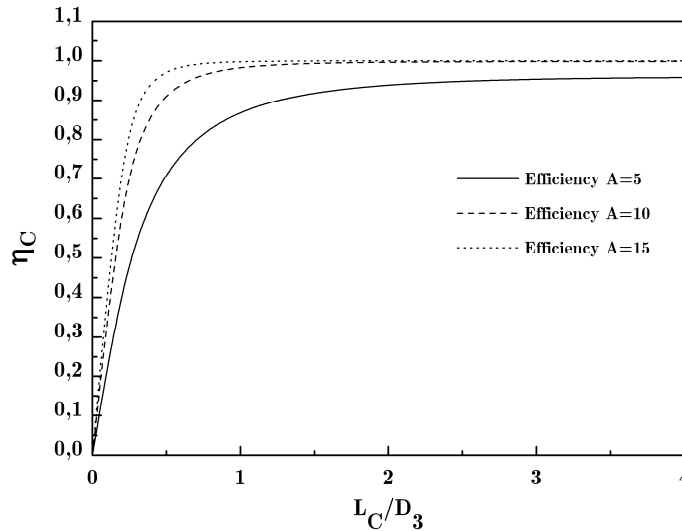$$\eta_C = 1 - \exp\left\{-0.646A\left[1 - \exp\left(\frac{-L_C}{D_3}\right)\right]\right\} \tag{5.16}$$

Fig. 44: Calculated combustor efficiency vs combustor length to diameter ratio

Figure 44 shows the efficiency equation for $h = D_3/6$. The efficiency converges to the maximum value for high L_C/D_3 ratios. Therefore it is suggested to use

high L_C/D_3 ratios for the design of the combustion chamber. The efficiency equation (5.1) respectively equation (5.16) draws only a conclusion how the reattachment length, L_r, the step high of the rearward facing step, h, and the shear layer residence time, τ_{sh} respectively influences the combustion of the fuel/oxidizer mixture for a given characteristic time for fuel and CO oxidation. Thus it is assumed the fuel/oxidizer mixture must spend a defined time period in the combustion chamber which is given by the combustion chamber volume to achieve auto ignition.

The necessary combustion chamber volume can be determined from equation (3.228) which leads to after algebraic manipulation,

$$1^{\text{st}}\text{ignition condition given by:} \frac{\boldsymbol{E_A}}{\boldsymbol{RT_0^2}}\left(\boldsymbol{T_0} - \langle\boldsymbol{T_w}\rangle\right) \leq \boldsymbol{1}$$

$$V_C = \dot{m}\left(\frac{t_{evap}T_0 R}{\langle\mathfrak{M}\rangle_\phi^{mix}\Phi p_0} + \frac{Z_I}{\Phi\left(p_0^{\ n} - G_I\right)}\right)$$

$$Z_I = \frac{\left\langle c_p\big|_{T_0}\right\rangle_\phi^{mix} R^{(n+1)}T_0^{(n+2)}}{Q_r E_A A'(\phi)M(\phi)}\exp\left(\frac{E_A}{RT_0}\right)$$

$$G_I = \frac{R^{(n+1)}T_0^{(n+2)}}{Q_r E_A A'(\phi)M(\phi)}\frac{4\left\langle\chi\big|_{T_0}\right\rangle_\phi^{mix}}{D_3}\exp\left[\frac{E_A}{RT_0}\left(1 + \frac{T_0 - \langle T_w\rangle}{T_0}\right) - 1\right]$$

$$2^{\text{nd}}\text{ignition condition given by:} \frac{\boldsymbol{E_A}}{\boldsymbol{RT_0^2}}\left(\boldsymbol{T_0} - \langle\boldsymbol{T_w}\rangle\right) > \boldsymbol{1}$$

$$V_C = \dot{m}\left(\frac{t_{evap}T_0 R}{\langle\mathfrak{M}\rangle_\phi^{mix}\Phi p_0} + \frac{Z_{II}}{\Phi\left(p_0^{\ n} - G_{II}\right)}\right)$$

$$Z_{II} = \frac{\left\langle c_p\big|_{T_0}\right\rangle_\phi^{mix} R^{(n+1)}T_0^{(n+2)}}{Q_r E_A A'(\phi)M(\phi)}\exp\left(\frac{E_A}{RT_0}\right) \tag{5.17}$$

$$G_{II} = \frac{R^n T_0^{\ n}}{Q_r A'(\phi)M(\phi)}\frac{4\left\langle\chi\big|_{T_0}\right\rangle_\phi^{mix}(T_0 - T_W)}{D_3}\exp\left(\frac{E_A}{RT_0}\right)$$

There exist two cases when designing a combustion chamber. First, no one of the three parameters (D_2, D_3, L_C) are specified. Thus equation (5.10), equation

(5.17) and with a proper assumption for L_C/D_3 according to the results of the efficiency equation (5.16) builds a set of equation with no limitation for the desired ignition pressure, p_0, and with the relation,

$$V_C = L_C \frac{D_C{}^2 \pi}{4} = L_C \frac{D_3{}^2 \pi}{4}$$

(5.18)

And second, if one of the three parameters (D_2, D_3, L_C) are specified. Generally the orifice diameter, D_2, is given due to injector efficiency considerations. Thus the combustion chamber diameter is specified by equation (5.10). This leads to a restriction for the desired ignition pressure, p_0, due to the fact that only positive values of V_C are physical. Thus,

$$p_0{}^n - G_{(j)} \geq 0$$

(5.19)

where "j" is equivalent to I or II. Hence the minimal desirable ignition pressure becomes,

$$p_0 \geq \begin{cases} \sqrt[n]{\dfrac{R^{(n+1)}T_0{}^{(n+2)}}{Q_r E_A A'(\phi) M(\phi)} \dfrac{4 \left\langle \chi|_{T_o} \right\rangle_\phi^{mix}}{D_3} \exp\left[\dfrac{E_A}{RT_0}\left(1 + \dfrac{T_0 - \left\langle T_w \right\rangle}{T_0}\right) - 1\right]} & \dfrac{E_A}{RT_o{}^2}\left(T_o - \left\langle T_w \right\rangle\right) < 1 \\[20pt] \sqrt[n]{\dfrac{R^n T_0{}^n}{Q_r A'(\phi) M(\phi)} \dfrac{4 \left\langle \chi|_{T_o} \right\rangle_\phi^{mix} \left(T_0 - \left\langle T_w \right\rangle\right)}{D_3} \exp\left(\dfrac{E_A}{RT_0}\right)} & \dfrac{E_A}{RT_o{}^2}\left(T_o - \left\langle T_w \right\rangle\right) > 1 \end{cases}$$

(5.20)

5.2.2 Determination of injector recess length, using simple droplet evaporation model

To ensure a fully evaporated fuel/oxidizer mixture prior entering the combustion chamber the recess length, L_{recess}, must equal to a certain value. Generally the evaporation time can be given as,

$$\widehat{t}_{evap} = t'_{evap} + t_{evap} \tag{5.21}$$

where $\widehat{t}_{evap}$ is given by the necessary overall evaporation time to achieve complete evaporation of the fuel, t'_{evap} is equal to the evaporation time prior the combustion chamber and t_{evap} is defined as the remaining necessary evaporation time to achieve a gaseous fuel/oxidizer mixture in the combustion chamber. In order to utilise the advantages of a rearward facing step, the fuel/oxidizer mixture should evaporated completely before entering the combustion chamber. Thus the evaporation time prior the combustion chamber becomes,

$$t'_{evap} = \widehat{t}_{evap} \tag{5.22}$$

The overall evaporation time needed for the complete evaporation of a single droplet can be determined from a simple mass balance equation which is,

$$\frac{\mathrm{d}m_d}{\mathrm{d}t} = -\dot{m}_{evap} \tag{5.23}$$

where m_d defines the mass of the droplet and $\dot{m}_{evap}$ is equal to the evaporated mass per unit time. Since heat is conducted from the hot gas, and if it is assumed that the droplet temperature is uniform at the boiling temperature, all of this heat is used to vaporize the fuel droplet, with no heat flowing into the droplet interior. Thus the evaporation rate becomes,

$$\dot{Q}_{cond} = \dot{m}_{evap} h_{evap} \tag{5.24}$$

where h_{evap} is given by the specific heat of evaporation for the fuel. The heat conduction is given by the Fourier's law and becomes in spherical coordinates,

$$\dot{Q}_{cond} = 4\pi r_d^{\,2} \left.\frac{\mathrm{d}T}{\mathrm{d}r}\right|_{r_d} \tag{5.25}$$

The gas phase temperature distribution for a fluid flow assuming that the evaporation process is quasi steady is given by,

$$\rho c_p \vec{v} \cdot \boldsymbol{\nabla} T = \lambda \boldsymbol{\Delta} T \tag{5.26}$$

Assuming that the temperature distribution is uniform in the elevation and azimuth angle, and substituting for the velocity, $v_r = \dot{m}_{evap}\big/4\pi r^2 \rho$, equation (5.26) becomes,

$$\frac{\dot{m}_{evap} c_p}{4\pi\lambda}\frac{\mathrm{d}T}{\mathrm{d}r} = \frac{\mathrm{d}}{\mathrm{d}r}\left(r^2\frac{\mathrm{d}T}{\mathrm{d}r}\right) \tag{5.27}$$

With the boundary conditions, $T\left(r\to\infty\right) = T_{Ox}$ and $T\left(r\to r_d\right) = T_{boil}$ where r_d is defined as the droplet radius and T_{boil} is equal to the boiling temperature of the fuel, the solution of equation (5.27) is given by,

$$T\left(r\right) = \frac{\left(T_{Ox} - T_{boil}\right)\exp\left(-\dfrac{c_p\dot{m}_{evap}}{4\pi r\lambda}\right) - T_{Ox}\exp\left(-\dfrac{c_p\dot{m}_{evap}}{4\pi r_d\lambda}\right) + T_{boil}}{1 - \exp\left(-\dfrac{c_p\dot{m}_{evap}}{4\pi r_d\lambda}\right)} \tag{5.28}$$

Combining equation (5.24),(5.25) and (5.28) the evaporation rate becomes,

$$\dot{m}_{evap} = \frac{4\pi\lambda r_d}{c_p}\ln\left[\frac{c_p\left(T_{Ox} - T_{boil}\right)}{h_{evap}} + 1\right] \tag{5.29}$$

Equation (5.23) then becomes with $m_d = \rho\pi D_d^3\big/6$

$$\frac{\mathrm{d}D_d}{\mathrm{d}t} = -\frac{4\lambda}{\rho c_p D}\ln\left[\frac{c_p\left(T_{Ox} - T_{boil}\right)}{h_{evap}} + 1\right] \tag{5.30}$$

The droplet diameter variation with time becomes with equation (5.30)

$$D_d^2\left(t\right) = D_{d,0}^2 - \frac{8\lambda}{\rho c_p}\ln\left[\frac{c_p\left(T_{Ox} - T_{boil}\right)}{h_{evap}} + 1\right]t \tag{5.31}$$

where $D_{d,0}$ is given by the initial size of the droplet. The time to evaporate the droplet completely becomes,

$$\widehat{t}_{evap} = \frac{D_{d,0}^2}{\frac{8\lambda}{\rho c_p} \ln\left[\frac{c_p\left(T_{Ox} - T_{boil}\right)}{h_{evap}} + 1\right]} \tag{5.32}$$

The necessary recess length to evaporate the fuel completely becomes,

$$L_{recess} = \frac{\dot{m}_F}{\pi r_{Finj}^2} \frac{c_p D_{d,0}^2}{8\lambda \ln\left[\frac{c_p\left(T_{Ox} - T_{boil}\right)}{h_{evap}} + 1\right]} \tag{5.33}$$

where $\dot{m}_F$ is given by the fuel mass flow and r_{Finj} is equal to the fuel injector radius. In order to predict the necessary recess length, the thermodynamic properties are assumed to be constant and by following the approach of Law and Williams [121] for burning droplets, the following approximations for c_p and λ are suggested,

$$c_p = c_{p,F}\left(\overline{T}\right)$$
$$\lambda = 0.4\lambda_F\left(\overline{T}\right) + 0.6\lambda_{Ox}\left(\overline{T}\right) \tag{5.34}$$

where the subscript F represents the fuel vapour and $\overline{T}$ is the average of the fuel boiling point temperature and that of the free stream,

$$\overline{T} = \frac{T_{boil} + T_{Ox}}{2} \tag{5.35}$$

Assuming that n-Decane/H_2O acts as an surrogate for Jet-A1/(H_2O+O_2) (Fig. 21) and the oxidizer temperature for 87.5% H_2O_2 is equal to 968K (Fig 34) following thermodynamic properties are evaluated,

λ_F [W/mK]	λ_{Ox} [W/mK]	λ [W/mK]	T_{boil} [K]	T_{Ox} [K]	$\overline{T}$ [K]	$c_{p,F}$ [J/kg]	h_{evap} [J/kg]	ρ [kg/m³]
0.0506	0.0579	0.05498	447	968	703	3142	277.000	730

Tab. 11: Thermodynamic properties of n-Decane/H20 based on Turns [122] and NIST

Figure 45 shows the necessary recess length evaluated according to equation (5.33) with the thermodynamic properties given by table 11 as a function of

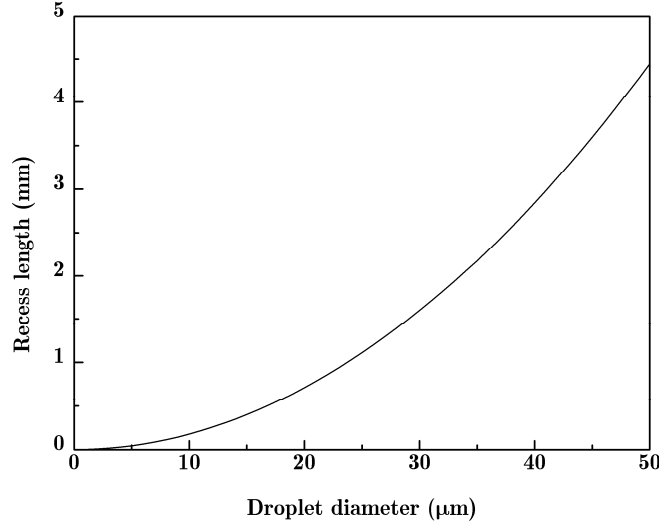the initial droplet diameter $D_{d,0}$ for a fuel mass flow of 0.06g/s and a fuel injector diameter of 0.2mm

Fig. 45: Necessary recess length to achieve complete evaporation vs. initial droplet diameter

5.3 Swirl injector design

The propellant injector has a key role for successfully ignite and stabilize combustion. The major task of an injector is mixing the propellants such as ignition can occure. The best solution is to create a hot recirculation zone which one of the most effective ways to inducing flow recirculation is to fit a swirler around the fuel injector. Many other different ways could be adopted to create a recirculation zone, such as bluff bodies in the flow field. Swirling flow produce stronger shear region, higher turbulence and more rapid mixing rates [116]. Coaxial swirling flows are increasingly used in many industrial configurations such as, cooling systems, fluid mixers, industrial burners and propulsion apparatus [115]. The complex flow structures generated by the swirl increase the turbulence intensity, leading to larger momentum and mass transfer and enhancing the mixing of species. This of course has a crucial impact in combustion processes. Furthermore by incorporating a swirl injector the mean residence time is enlarged by a given combustion chamber volume The main parameters controlling the turbulence intensity and the structure of

the recirculation zone (see section 5.2) near the jet exit plane are given by the swirl number, S, and the streamwise annular velocity. The dimensionless swirl number S is defined as the ratio between the axial flux of the angular momentum to the product of the axial momentum flux and a characteristic radius, R_O, which is given by [116],

$$S = \frac{\dot{m}(\bar{r} \times \bar{v}) \cdot \bar{n}}{\dot{m}\bar{v}} = \frac{\oiint (\rho \bar{v} \cdot \bar{n})(\bar{r} \times \bar{v}) \cdot \bar{n} \mathrm{d}A}{\oiint (\rho \bar{v} \cdot \bar{n})(\bar{v} \cdot \bar{n}) \mathrm{d}A} \tag{5.36}$$

Hence,

$$S = \frac{\oiint \rho v_z r^2 \omega \mathrm{d}A}{R_O \oiint \rho v_z^2 \mathrm{d}A} = \frac{2\pi \int_{R_I}^{R_O} \rho v_z v_\varphi r^2 \mathrm{d}r}{R_O 2\pi \int_{R_I}^{R_O} \rho v_z^2 r \mathrm{d}r} \tag{5.37}$$

Where R_I and R_O are the inner and outer radii of the inlet. If it is assumed that the axial and azimuthal velocities, v_z and v_φ are uniform, the swirl number reduces to,

$$S = \frac{2}{3} \left[\frac{1 - \left(\frac{R_I}{R_O}\right)^3}{1 - \left(\frac{R_I}{R_O}\right)^2} \right] \tan \vartheta \tag{5.38}$$

with,

$$\tan \vartheta = \frac{v_\varphi}{v_z} \tag{5.39}$$

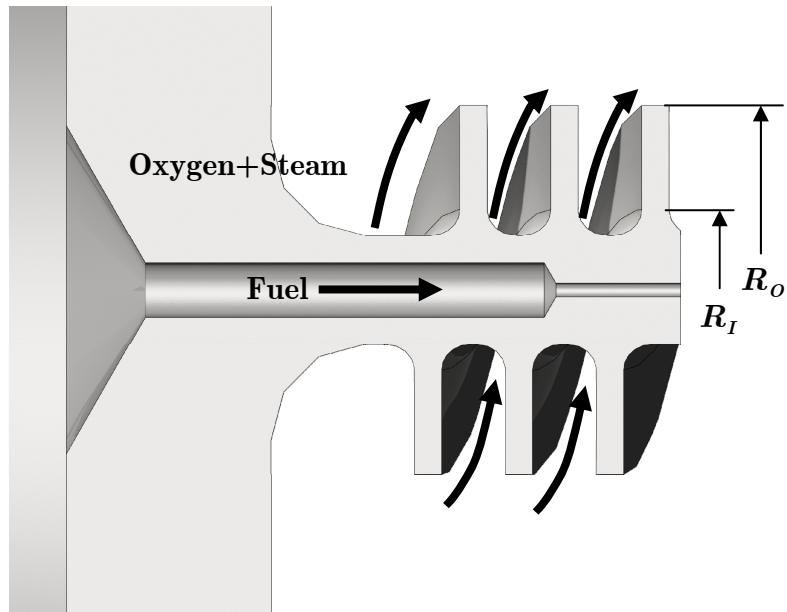Firgure 46 gives a schematic cross section view of a swirl injector.

Fig. 46: Cross section view of a swirl injector

As shown in figure 46, the injection system is made of a central duct, feeding kerosene fuel, and a coaxial annular screw injecting oxygen and water vapour. The angle of the helical flute determines the swirling motion of the oxidizer, which promotes mixing with the inner fuel stream.

6

EXPERIMENTAL SETUP

6.1 Test facility overview and setup

Figure 47 and figure 48 show the test bench for the bi-propellant ignition studies and the flow schematic of the bipropellant test bench respectively. Additionally figure 49 shows the fuel (kerosene) panel of the test bench which is located on the back side of the bench.
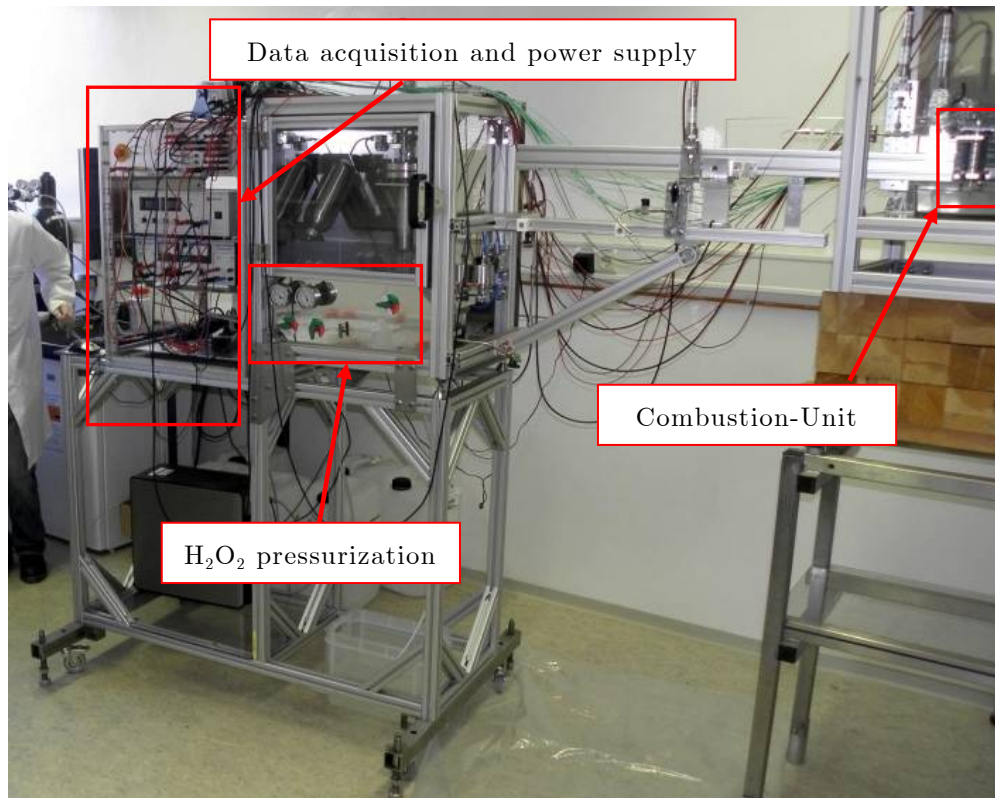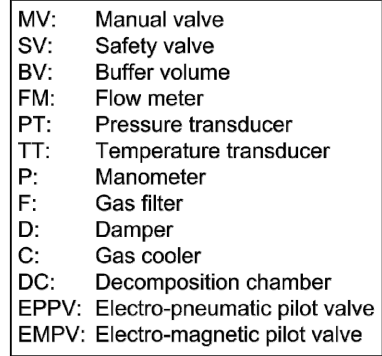

Fig. 47: Bi-propellant test bench
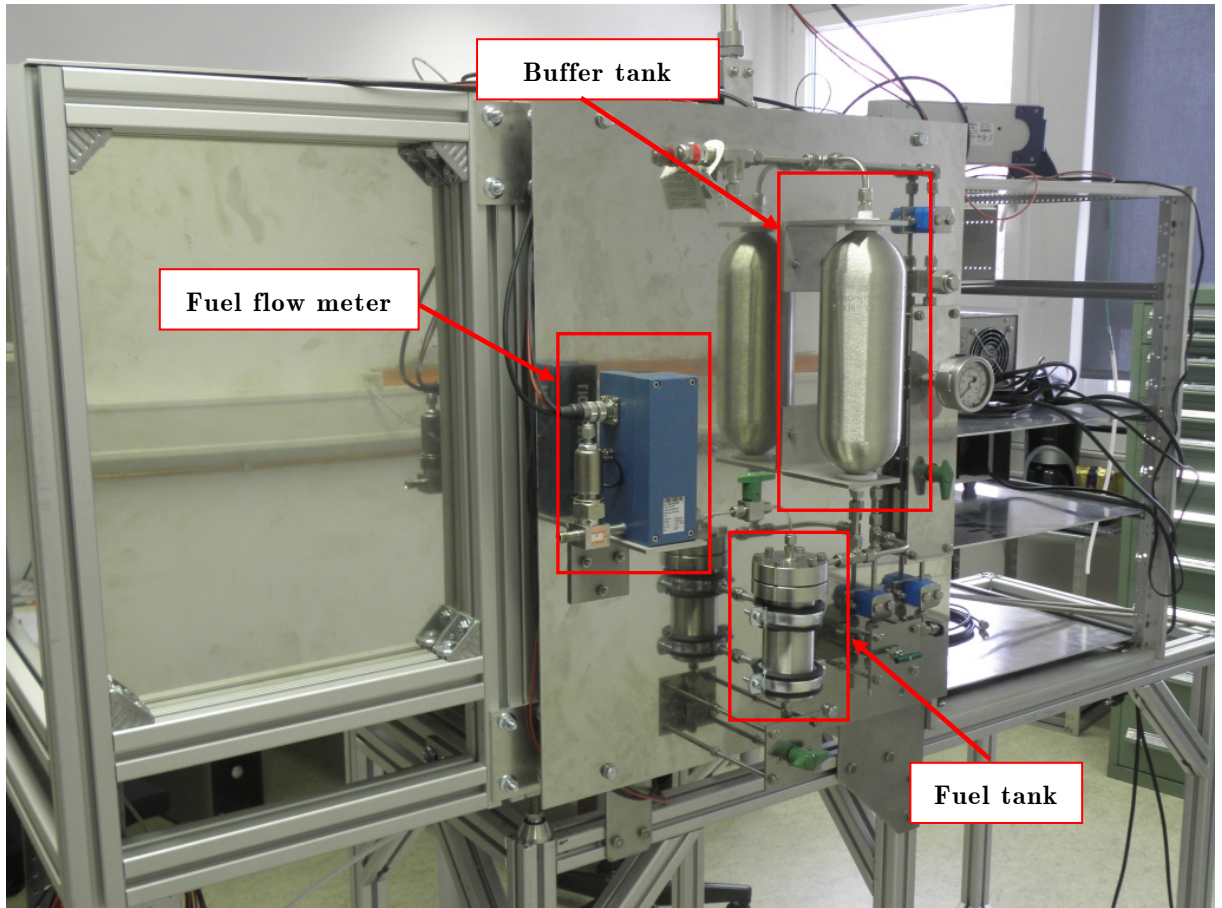
Fig. 48: Test bench

Fig. 49: Fuel panel

The main components of the bipropellant feed system are the tanks for storage of the hydrogen peroxide and kerosene fuel. Additionally two buffer tanks are installed for easy adjustment of the feed pressure by setting the manual valves (MV2, MV3 and MV10, MV12). All elements of the bipropellant feed system are made of stainless steel in order to be compatible with kerosene fuel and hydrogen peroxide such that premature decomposition is avoided. Each of the propellant tanks can store 500ml of hydrogen peroxide respectively kerosene fuel which is enough for a test duration of several hundred seconds and they are rated to a maximum pressure of 40 bar.

The propellant feeding lines between the tanks and the thruster are equipped with various pressure gauges and valves. An electro-pneumatic valve is used to control the hydrogen peroxide flow since a common used solenoid valve is not applicable due to thermal energy release during the operation. This would cause preheating of the hydrogen peroxide before injected into the decomposition chamber which leads to an increased rate of thermal decomposition. The kerosene fuel flow is controlled by an electro-magnetic (solenoid) valve .Nitrogen is used to pressure-feed the propellants to the

thruster and to supply the electro-pneumatic pilot valve. Propellant feed lines as well as nitrogen supply lines consist of a combination of

1/4" and 1/8" diameter stainless steel tubing. Stainless steel, grades 316, is used

throughout the system due its compatibility with hydrogen peroxide and kerosene fuel. Each line (oxidizer, fuel and EPPV supply) are equipped with safety valves which vent the system in case of over-pressure. Ordinary hand activated ball valves (MV4, MV6, MV12, MV14) are installed to drain the system and further to allow the filling and pressurization before initiation of the test. The drainage system allows draining of the propellants if they remain in the tanks following a test or to safely drain the tanks in emergencies. Further elements of the propellant feeding lines are mass flow meters and several temperature sensors. The gas cooler is used to adjust the oxidizer inlet temperature at the thruster in order to determine the ignition pressure at different temperatures. The propellant feeding lines are also equipped with pressure dampers which are stainless steal pipes with an inner pipe diameter of 0.2 mm and a length of several centimetres. These dampers inhibit pressure oscillation to provide a quasi constant mass flow rate.

6.2 Data acquisition

The diagnostic system in the present testing facility include, measurement and control of the mass flow rate of hydrogen peroxide, measurement and control of the mass flow rate of kerosene fuel, measurement of tank and combustion pressure and measurement of up to 4 temperatures. Measurement of the hydrogen peroxide mass flow rate and kerosene mass flow rate was accomplished with a Cori-Flow Meter (Bronkhorst M52) respectively with a liquid flow meter (Bronkhorst LIQUI-FLOW series L1/L2). The former device is based on the measurement of the Coriolis forces which bend or twist internal tubes. The extremely small tube displacements are detected by sensors. The sensor output is proportional to the mass flow and is independent of the density, temperature, viscosity, and conductivity of the fluid. It therefore allows the freedom to change the hydrogen peroxide concentration if whished without the need to send the device to the manufacturer for recalibration. The letter is a thermal mass flow meter which measures the temperature difference

across the in- and outgoing legs of the measuring tube by means of a thermo pile which consists of thousands of thermo couples in series. This mass flow meter is sensitive in density variations and has to be therefore calibrated. The mass flow meters are principally coupled with a mass flow controller. Both systems are computer controlled via an in-house developed Labview program. This software requires a value for the mass flow rate as input. This value is then communicated to the mass flow controller which opens and closes a valve according to the required mass flow rate. The mass flow controller and the mass flow meter are part of a closed loop control system to ensure the accurate delivery of the chosen mass flow rate. Unfortunately it turned out that this system is rather slow and very sensitive to pressure oscillations and it was difficult to supply a constant mass flow rate in spite of the closed loop control of the mass flow meters and controllers. Consequently, the controllers were removed thus the mass flow rates were controlled by the pressurization level. The tank pressures were measured with pressure gauges (Keller, PA 25) which are suitable for a pressure range between 0 and 60 bar and temperatures up to 80 °C and the combustion chamber pressure was measured with a third pressure gauge (Keller, PA 25, HTC) which has a pressure range between 0 and 60 bar and operational temperatures up to 300 °C was installed to measure the combustion chamber pressure. Temperature measurements were made using type K thermocouples and amplified with an integrated circuit (cold junction compensation AD595AQ). The data collected during a test includes the various temperatures, pressures and the mass flow rates. The data acquisition is performed with an in-house developed program running in LabVIEW. A standard NI DAQ device with 16 analog and 8 DIO channels allows the measurement of the mass flow rates and several pressures and temperatures.

6.3 Propulsion system components
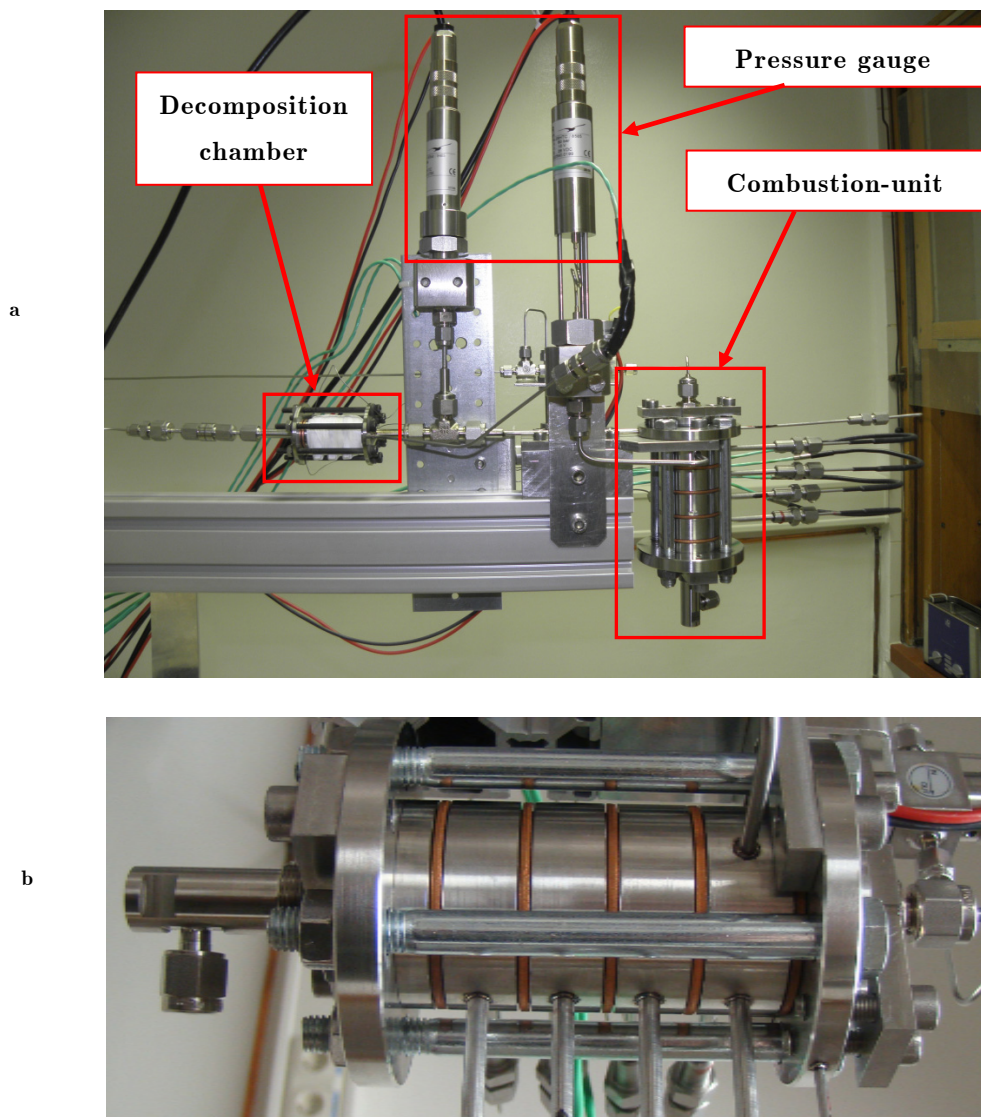
6.3.1 Combustor

Fig. 50: a) Combustion-unit with diagnostic system. 50b) Picture of the combustion-unit with five segments
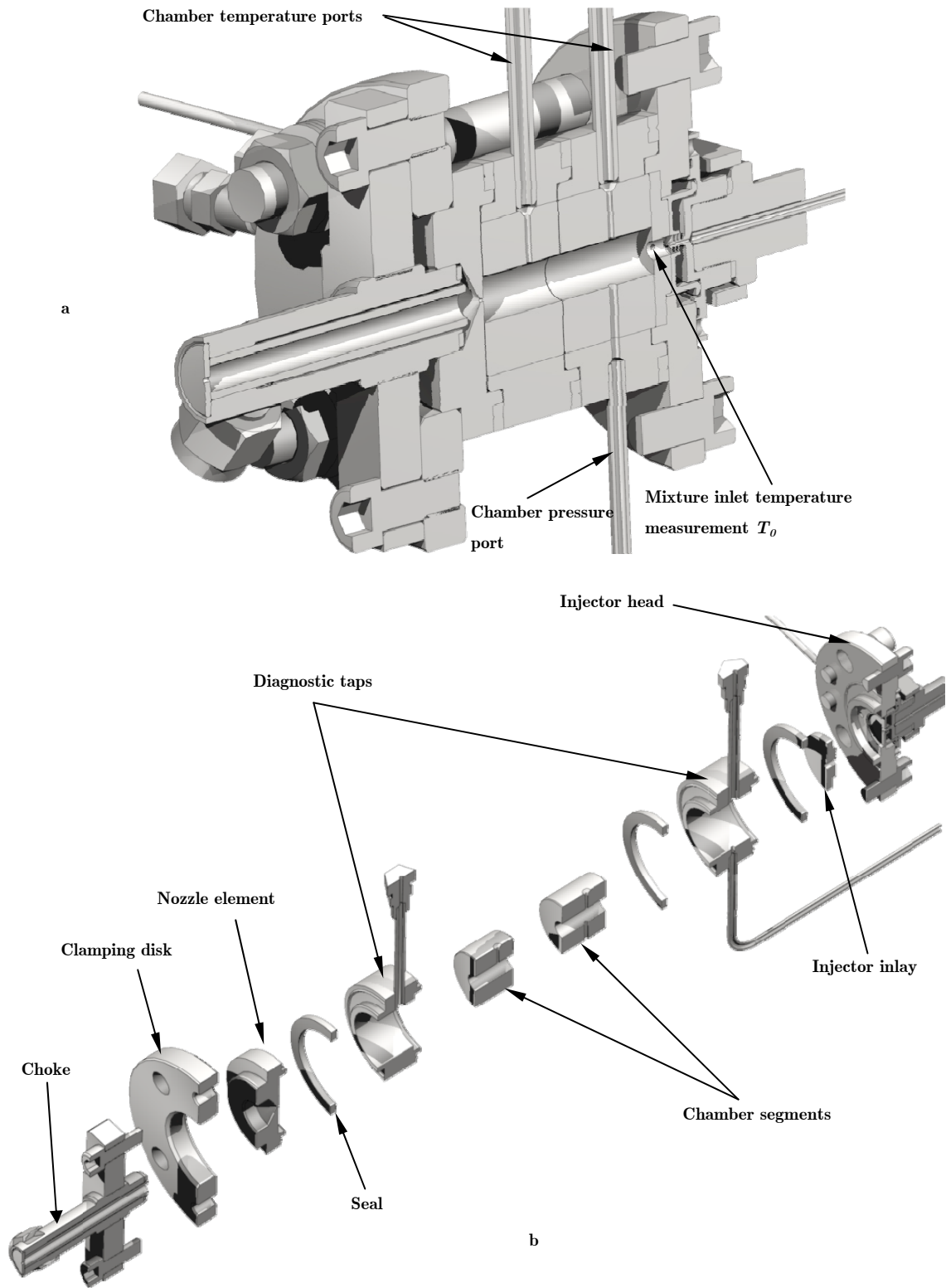
Fig. 51: a) 3D image of the combustion-unit. 51b) Exploded view of the combustor

The combustor features a modular design for easy modification of the test configuration (see figure 50a, 50b and figure 51a, 51b). All sections are tightened together by tie rods and a clamping disk: the injector head, the injector inlay, the chamber segment, the diagnostic taps (pressure and temperature) and the nozzle element, all of them fabricated of stainless steal. The modular design allows an easy variation of the injection inlay, the characteristic length L^*, respectively the combustion chamber length and diameter. The thrust chamber is designed as a pure heat sink combustion chamber that limits the run time up to several seconds. Therefore the injector temperature is measured and monitored to avoid damage due to excessive thermal load because this is the most critical element in the propulsion system which is very complicated end expensive to manufacture. Chamber input conditions are determined by pressure and temperature measurements. The specific propellant injection configuration used for the thrust chamber is realized by a tandem of a swirl injector and a rearward facing step. The former is used to ensure perfect mixing which requires a certain recess length between the swirl injector and the rearward facing step which is guaranteed by the injector inlay section on the one hand and on the other hand to increase the turbulence intensity in the combustion chamber and the latter provides flame stabilisation.

6.3.2 Swirl injector

In order to realise a certain pressure drop which is needed to avoid any back flame from the combustion chamber to the propellant inlet passages the inner and outer swirler diameters plays an important role. In the coaxial swirler injector a pressure drop ranging from 5% to 20% of the nominal combustion chamber pressure is recommended [117]. Furthermore to increase the turbulence intensity which leads not only to a better mixing of the propellants but also leads to a higher mean residence time, a swirl number of 2 was chosen according to section 5. Table 12 summarizes the design parameter of the swirl injector used in this study and figure 52 gives a picture of the swirl injector.

Fuel injector diameter	0.2 [mm]
Swirl outer diameter	1.22 [mm]
Swirl inner diameter	0.8 [mm]
Number fins	4
Fin thickness	0.2 [mm]
Swirl number	2
Swirl angle	67°

Tab. 12: Swirl injector design parameters

Fig. 52: Swirl injector

6.3.3 Decomposition chamber with catalyst bed

The decomposition chamber was developed in the past according to the agreement ESTEC contract no, 22277/09/NL/RA. Figure 53 gives a snap shot of the decomposition chamber and figure 54 shows the three dimensional drawing. The decomposition chamber was designed with diagnostic access to measure the pressure and decomposition temperature of hydrogen peroxide. Its structural design prevents excessive heat loss and facilitates a short warm-up period prior running an auto ignition test. Liquid hydrogen peroxide is injected via an injector head (prepared filter element from Swagelok) and reacts to oxygen and steam under the presence of a catalyst.
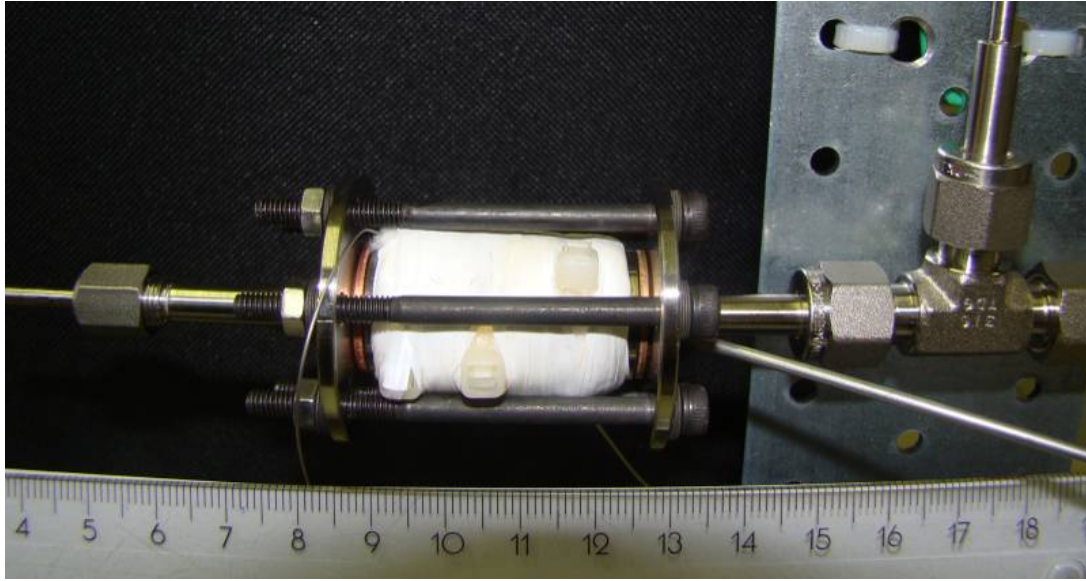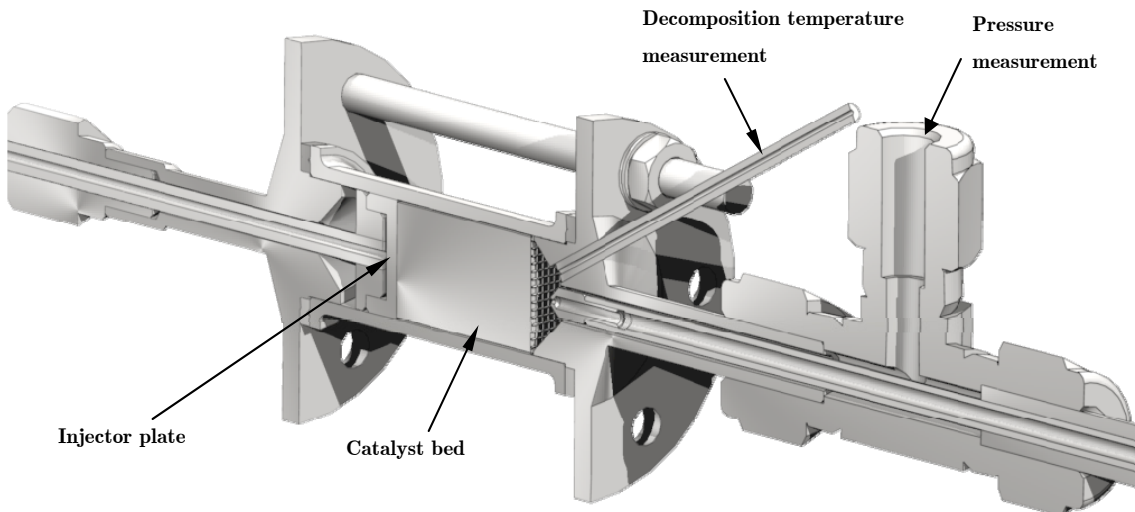
Fig. 53: Decomposition chamber

Fig. 54: 3D drawing of the decomposition chamber

To optimize the decomposition, a monolithic catalyst has to satisfy several requirements such as having a maximum available ratio of active surface to monolith volume and a low pressure drop. At the same time it is important to minimize the monolith volume in order to reduce the thruster's structural mass. Furthermore to maximize the active area to volume ratio, various channel sizes and geometries (square, circular, and hexagonal) have been investigated. The choice of the channel shape influences the total necessary monolith volume which again influences the possible number of channels in the monolith. An analytic model was developed to support the monolith design process. This low fidelity analytic model is capable to include all the geometric

variations and constrains and incorporates also the basic flow dynamics and certain aspects of the phase change and the change in chemistry of the fluid occurring during the decomposition process [119]. Based on this analysis, a square channel shape was chosen with a side wall length, S, of 1.mm. The optimal radius and side length of the monolith was determined to be 13 mm and 20 mm respectively. With this radius, it was possible to accommodate 37 channels. Figure 55 shows a photograph of the catalyst.

Fig. 55: Catalyst

The monolithic cellular ceramics have been manufactured by CTI Company (Céramiques Techniques et Industrielles, France) with two different materials, mullite $(3Al_2O_3 \cdot 2SiO_2)$ and mullite-zirconia $(3Al_2O_3 \cdot 2SiO_2\text{-}ZrO_2)$ using a standard extrusion technique. Mullite-zirconia has the advantage of being suitable for higher temperatures than mullite, but the porosity necessary for a good washcoat adhesion can be more difficult to achieve. The catalyst preparation was performed by LACCO (Laboratory of Catalysis in Organic Chemistry), France [120]. It consists of several steps, the most important being the washcoating and impregnation procedures. The washcoating process increases the low specific surface area of the monolith base material by adding a porous layer on the substrate surface. The wash-coating material is made of transition alumina (γ-alumina) providing a high surface area. The wash-coat layer must be able to resist to thermal shocks during thruster operation. Therefore, its binding to the monolith surface is an important quality criterion. After applying the washcoat layer, the final step of catalyst preparation is the incorporation of the active material precursor into the wash-coat. Aqueous solutions of sodium permanganate $(NaMnO_4)$ were used as catalyst precursor for the present work. The cellular ceramics displays a very low specific surface

area. Hence, a washcoat layer is deposited onto the surface. Most often, this secondary support is a porous alumina layer which allows a good chemical continuity with the substrate. Several different procedures have been used to prepare the alumina washcoat.

6.4 Back pressure device (choke) and nozzle design for the ignition test

In order to adjust the initial combustion chamber pressure, p_0, without varying the mass flow a pressure device (choke) is installed behind the nozzle. If the nozzle operates in the non choked condition the combustion chamber pressure becomes a function of the back pressure. Therefore the combustion chamber pressure increases if the back pressure increases if and only if the mass flow is kept constant. The back pressure, p_e, can be manually adjusted by increasing or decreasing the nitrogen mass flow if the back pressure device operates in the choked condition. Thus the back pressure becomes a function of the total mass flow. It can be assumed that an auto ignition does not occur in the back pressure device because the hot mixture of oxygen, water vapour and eventually fuel is mixed with cold nitrogen. Figure 56 shows a sketch of the back pressure device and its operation principle.
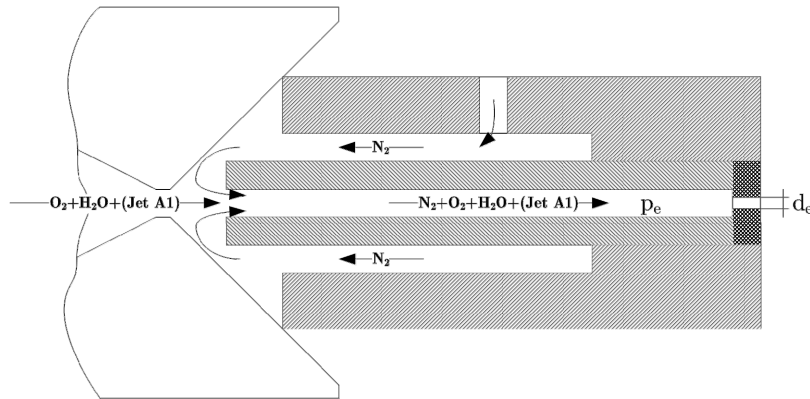

Fig. 56: Back pressure device

Nitrogen is injected into the back pressure device where it is mixed with hot water vapour, oxygen and eventually fuel (if fuel is injected into the combustor). The mixture is then expelled afterwards through a small orifice.

174

6.4.1 Determination of the necessary N$_2$ mass flow and orifice diameter

In order to adjust the back pressure only by increasing or decreasing the nitrogen mass flow for the full N$_2$ mass flow range ($\dot{m}_{N_2} \in \left[0, \dot{m}_{N_2,\max}\right]$), the necessary orifice diameter, d_e, to achieve a choked flow condition for the full N$_2$ mass flow range becomes ($\dot{m}_{N_2} = 0$) [36],

$$d_e = \sqrt{\frac{4\dot{m}_{Ox}}{\pi p_{0,min} \sqrt{\left[\gamma \left(\frac{2}{\gamma+1}\right)^{\frac{\gamma+1}{\gamma-1}} \frac{\langle \mathfrak{M} \rangle}{RT}\right]}}}$$

(6.1)

with,

$$p_{0,min} \geq p_\infty \left(\frac{2}{\gamma+1}\right)^{-\frac{\gamma}{\gamma-1}}$$

(6.2)

whereas p_∞ is given by the ambient pressure. The back pressure, p_e, as a function of the nitrogen mass flow is given by

$$p_e = \frac{4\left(\dot{m}_{Ox} + \dot{m}_{N_2}\right)}{\pi d_e^2 \sqrt{\left[\gamma \left(\frac{2}{\gamma+1}\right)^{\frac{\gamma+1}{\gamma-1}} \frac{\langle \mathfrak{M} \rangle}{RT}\right]}}$$

(6.3)

Combining equation (6.1) with equation (6.3) leads for the necessary N$_2$ mass flow,

$$\dot{m}_{N_2} = \dot{m}_{Ox} \left(\frac{p_e}{p_{0,min}} - 1\right)$$

(6.4)

In order to facilitate a large pressure range of the combustion chamber pressure ($p_0 \in \left[p_{0,min}, p_C\right]$) and on the other hand to keep the nitrogen consumption small, a minimal chamber pressure of four bar, which is equal to zero N$_2$ mass

flow, was defined. The necessary orifice diameter of the back pressure device is then given by table 13 which summarizes the design parameters for the back pressure device

Oxidizer mass flow, $\dot{m}_{Ox}$ [g/s]	Minimal chamber pressure, $p_{0,min}$ [bar][†]	Adiabatic coefficient, γ, [81]	Mean molar mass, $\langle \mathfrak{M} \rangle$ [g/mol][‡], [81]	Temperature, T [K]	Orifice diameter, d, [mm]
0.3	4	1.21	0.21	293	0.743
0.3	4	1.21	0.21	1000	1.001

Tab. 13: Choke design parameters

Because of the indefiniteness of the temperature in the back pressure device the throat diameter is calculated with the lower and upper limit of the gas temperature. Thus the back pressure, p_e, as a function of the nitrogen mass flow for a $d_e = 0.8mm$ is given by figure 57

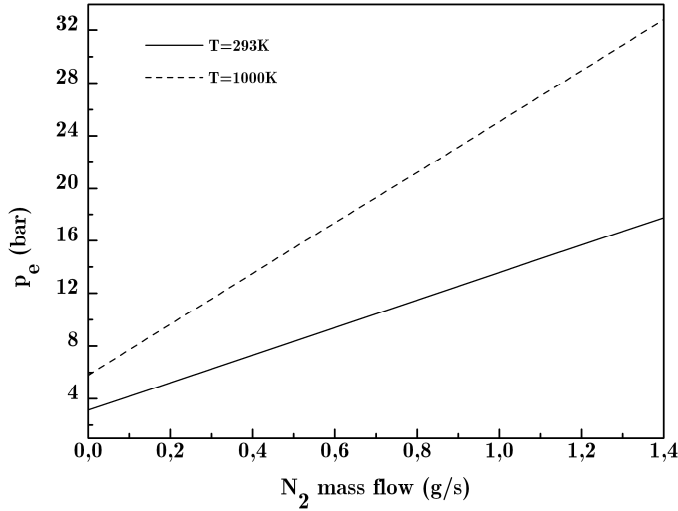Fig. 57: Back pressure vs. nitrogen mass flow

In order to achieve a coupling effect of the back pressure and the combustion chamber pressure the flow density at the nozzle throat must not reach the

---

[†] The minimal chamber pressure is given when the nitrogen mass flow is equal to zero.

[‡] Assuming only an oxidizer mass flow into the combustor, the molar mass is given by the mean molar mass of the oxidizer.

critical value. Therefore the throat diameter of the combustor nozzle must fulfill,

$$A_{nozzle} > \frac{\dot{m}_{Ox}}{p_C} \left[\gamma \left(\frac{2}{\gamma+1} \right)^{\frac{\gamma+1}{\gamma-1}} \frac{\langle \mathfrak{M} \rangle}{RT} \right]^{-\frac{1}{2}} \qquad (6.5)$$

Thus the largest value for the nozzle throat becomes,

$$A_{nozzle} > \frac{\dot{m}_{Ox}}{p_{0,min}} \left[\gamma \left(\frac{2}{\gamma+1} \right)^{\frac{\gamma+1}{\gamma-1}} \frac{\langle \mathfrak{M} \rangle}{RT} \right]^{-\frac{1}{2}} \Rightarrow A_{nozzle} > A_e \qquad (6.6)$$

Hence the nozzle diameter has to be larger in contrast to the orifice diameter. If doing so the combustion chamber pressure is given by equation (6.7) which can be solved by newton's method

$$p_C \left\{ \frac{2\gamma}{\gamma-1} \frac{\langle \mathfrak{M} \rangle}{RT_C} \left(\frac{p_e}{p_C} \right)^{\frac{2}{\gamma}} \left[1 - \left(\frac{p_e}{p_C} \right)^{\frac{\gamma-1}{\gamma}} \right] \right\} = \left(\frac{4\dot{m}}{\pi d_t^2} \right)^2 \qquad (6.7)$$

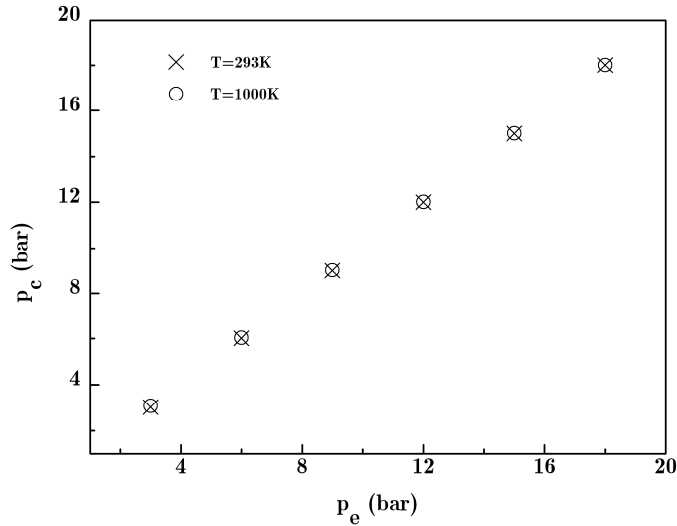Fig. 58: Combustion chamber pressure vs. back pressure

Figure 58 shows the dependency of the combustion chamber pressure vs. the back pressure for a nozzle throat diameter of 2mm, a constant mass flow of

0.3g/s and combustion chamber temperatures, T_C, of 293K respectively 1000K. The combustion chamber pressure is equal to the value of the back pressure as long as the nozzle is operated in the non choked condition.

7

EXPERIMENTAL TEST PROCEDURE

7.1 Auto ignition tests of Jet A1/H$_2$O$_2$

The primary object of the auto ignition tests was to verify the auto ignition
model which was derived in chapter 3 and thus to develop an engineering
design model for auto ignitable propulsion systems. The verification was done
in a qualitatively way by the determination of p_0-T_0 ignition diagrams for Jet-
A1/H$_2$O$_2$ mixtures.

7.1.1 Test plan overview

The ignition pressure is influenced by numerous parameters. Some of them are
intrinsic parameters of the system (Q_r, E_A, A', Φ, R) and some are given by
system requirements ($\phi \rightarrow \left\langle c_p \big|_{T_0} \right\rangle_\phi^{mix}$, $M(\phi), \dot{m}$). Thus the most accessible and at
the same time the most interested and important parameters to guide the
design of an auto-ignitable propulsion system and on the other hand to verify
the suitability of the auto ignition model are the auto ignition pressure, the
auto ignition temperature, the combustion chamber volume and diameter. For
the verification process these four parameters are considered to be variable and
the other non intrinsic parameters are supposed to be constant. Table 14 gives
the basis of the test parameters.

Measured parameter	Calculated parameter	Defined parameter	Property
Jet A1 mass flow, $\dot{m}_F$			constant
H_2O_2 mass flow, $\dot{m}_O$			constant
Initial combustion chamber pressure, p_0			variable
Initial combustion chamber temperature, T_0			variable
Wall temperature, T_w			constant
	Total mass flow, $\dot{m} = \dot{m}_F + \dot{m}_O$		constant
	Equivalence ratio, $\phi = \dfrac{\dot{m}_F / \dot{m}_O}{\left(\dot{m}_F / \dot{m}_O \right)_{stoich}}$		constant
		Combustion chamber volume, V_c	variable
		Combustion chamber diameter, D_c	variable

Tab. 14: Test parameters

7.1.1.1 Determination of the equivalence ratio

According to Dean et. al. [40] for short ignition delay times and thus for less needed ignition pressures a rich fuel/oxidizer and therefore a equivalence ratio of $\phi > 1$ is favoured. This is due to the chain branching process for large hydrocarbons which is controlled by hydrocarbon hydroperoxide species. Its production rate is directly proportional to the fuel concentration. Nevertheless it should be noted that the mean specific heat, $<c_p>(\phi)$, becomes a function of the equivalence ratio, ϕ, as well as the mole fractions given by the parameter $M(\phi)$ Therefore if the composition of the reactants is changed by changing the equivalence ratio, the mean specific heat also changes. If $\phi \to \infty$, results in $M(\phi) \to 0$ and $<c_p>(\phi) \to c_{p,F}$ thus $p_0 \to \infty$ and if $\phi \to 0$, results in $M(\phi) \to 0$ and $<c_p>(\phi) \to c_{p,O2}$ thus $p_0 \to \infty$. Furthermore high equivalence ratios lead to increased fuel fractions accompanying evaluated evaporation times and thus increased ignition pressures, p_0. As a result of this and due to the lack of

180

detailed reaction and combustion analysis of Jet $A1/O_2/H_2O$ the optimal equivalence ratio relating to the ignition condition cannot be explicitly determined. Nevertheless specific impulse calculation performed with CEA [81] showed a maximal value for the specific impulse for slightly rich fuel/oxidizer ratio $(1.11 < \phi < 1.15)$ Therefore a slightly rich equivalence ration should be chosen for the test campaign.

7.1.1.2 Determination of the fuel and oxidizer flow rates

According to equation 5.2 and assuming a propulsion system which should deliver a thrust of 1N , a equivalence ratio of 1.13, a calculated F/O value of 0.13 and a calculated specific impulse of 3139 m/s the oxidizer and the fuel mass flow rates becomes,

$$\dot{m}_{Ox} = 0.28\text{g/s} \quad \dot{m}_{F} = 0.041\text{g/s} \tag{7.1}$$

Since the mass flows are pressure feed (blow down) it is noticed that the fuel and oxidizer mass flow has to be a little increased during the start up, so that the mass flows reach the values given by equation (7.1) after transient phase (constant combustion and thrust).

7.1.1.3 Influence of the wall temperature

Since the auto-ignition behaviour of a propulsion system is influenced by the structural temperature for small combustion chamber diameters (figure 33) this parameter must be nearly held constant during the test campaign. This can be achieved by external heating of the structure during one test cycle. For rather big diameters the influence of the wall temperature can be neglected.

7.1.1.4 Determination of the combustion chamber volume and diameter

As already mentioned the combustor features a modular combustion chamber design with up to four segments of two different designs. Type A carries the injector head. Type B builds the actual combustion chamber. Hence the minimal combustor design is realized by using one segment of Type A. Tabele 15 shows the total combustion chamber volume for a given combustion chamber diameter.

D_C [mm]	A [mm³]	B [mm³]	A+B [mm³]	A+B+B [mm³]	A+B+B+B [mm³]
0	0,00	0,00	0,00	0,00	0,00
1	13,98	11,78	25,76	37,54	49,32
2	55,92	47,12	103,04	150,17	197,29
3	125,82	106,03	231,85	337,88	443,91
4	223,68	188,50	412,18	600,67	789,17
5	349,50	294,52	644,03	938,55	1233,08
6	503,28	424,12	927,40	1351,51	1775,63
7	685,02	577,27	1262,29	1839,56	2416,83
8	894,73	753,98	1648,71	2402,69	3156,67
9	1132,39	954,26	2086,65	3040,90	3995,16
10	1398,01	1178,10	2576,11	3754,20	4932,30
11	1691,59	1425,50	3117,09	4542,59	5968,08
12	2013,13	1696,46	3709,59	5406,05	7102,51
13	2362,63	1990,98	4353,62	6344,60	8335,59
14	2740,10	2309,07	5049,17	7358,24	9667,31
15	3145,52	2650,72	5796,24	8446,96	11097,68
16	3578,90	3015,93	6594,83	9610,76	12626,69
17	4040,25	3404,70	7444,95	10849,65	14254,35
18	4529,55	3817,04	8346,58	12163,62	15980,65
19	5046,81	4252,93	9299,74	13552,67	17805,60
20	5592,03	4712,39	10304,42	15016,81	19729,20

Tab. 15: Possible combustion chamber volume and diameters

7.1.2 Test procedure and firing sequence

Figure 59 shows the operation principle of the propulsion system. Hydrogen peroxide is injected into the decomposition chamber, decomposes exothermally to hot oxygen and water vapour, whereas the decomposition temperature, T_{Ox}, depends on the initial hydrogen peroxide concentration (figure 34). Afterwards the hot mixture of oxygen and water vapour is led to the swirl injector where it is mixed with the fuel (Jet A1). Then the ignitable mixture of Jet A1/O_2/H_2O is injected into the combustion chamber with the temperature, T_0, and pressure, p_0.
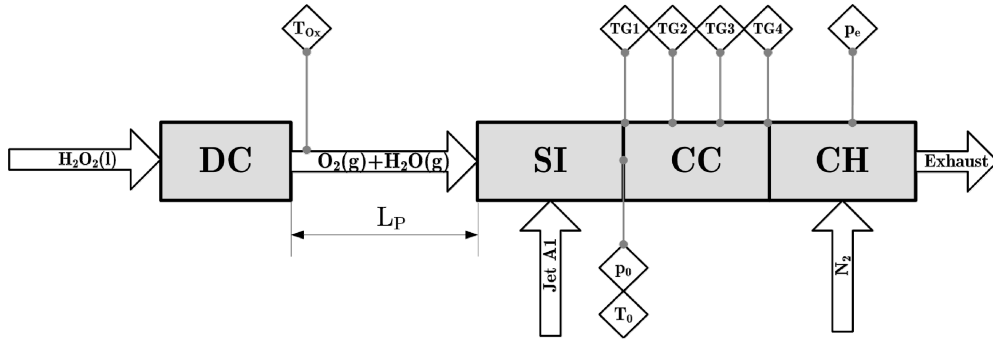

Fig. 59: Operation principle

The variation of the initial mixture temperature, T_0, is achieved by cooling the oxidizer mixture (water vapour and O_2) by a gas cooler which is given in the simplest form by a stainless steal pipe of different lengths, L_p, This is installed between the outlet of the decomposition chamber and the oxidizer inlet of the swirl injector. The oxidizer temperature is cooled down by convective heat loss whereas the minimum value of the oxidizer temperature at combustion chamber inlet is given by the pipe length and the maximum temperature is given by the decomposition temperature of hydrogen peroxide if the pipe length equals zero. The variation of the initial combustion chamber pressure, p_0, can be achieved by installing a back pressure device (choke) behind the nozzle. The back pressure, p_e, can be manually adjusted by setting a nitrogen mass flow and therefore the combustion chamber pressure is increased or decreased if the total mass flow is kept constant. It is important to note that the coupling between the back pressure and combustion chamber pressure can only be achieved if the combustor nozzle operates in the non choked condition. Otherwise the combustion chamber presser will not be affected by the back pressure and becomes primary a function of the total mass flow. Therefore the nozzle throat

diameter has to be designed in such a way to fulfil the non choked condition, nevertheless the entire propulsion system (combustor and choke) runs under choked condition. Additionally the wall temperature, T_w, of the combustor is monitored to avoid structural damage due to heat loads. The ignition sequence is shown by figure 60.
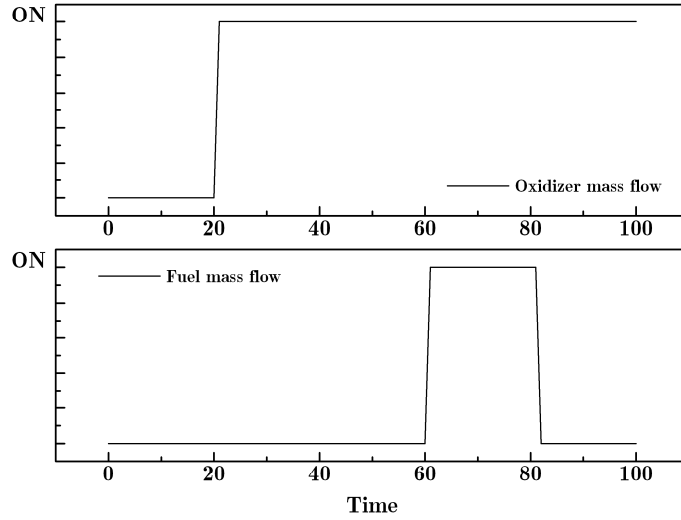

Fig. 60: Ignition sequence

Catalyst performance evaluation performed before ignition evaluation started showed that the catalyst bed requires warm-up period prior to running an auto ignition test. This was done to make sure that the bed was fully decomposing the hydrogen peroxide before any fuel was supplied to the combustor. Furthermore due to the large mass of the combustion unit the heat loss decreased the injection temperature of the fuel/oxidizer mixture significantly in the beginning of a test sequence. Thus the combustion unit was preheated by a heating device and additionally by running the combustor in mono propellant mode before injecting the fuel. Therefore the fuel injection is initiated delayed in contrast to the oxidizer flow. The firing time is limited to avoid damage of the propulsion system because the combustion chamber is designed as a pure heat sink chamber. In order to cool the combustion system after fuel injection is stopped it is necessary that the oxidizer flow is still active. This will avoid damage of the swirl injector after combustion by heat loads due to heat flux from the combustion chamber to the injector. The overall test sequence was performed in a kind of a regula falsi method (figure 61) whereas the ignition temperature, T_0, is approximated by a temperature interval with an upper and

a lower boundary where ignition occurred and failed (convergence interval given by black and white triangles). The ignition test is initiated at an arbitrary system pressure which was held constant during the test champagne. If ignition occurs the new value of the initial temperature, T_0, is adjusted in the convergence interval until the ignition temperature is determined with the required accuracy. Afterwards a new combustion chamber pressure was set and the related temperature is experimentally determined. The black triagles indicates succesfull auto ignition and the white indicates failed auto ignition.
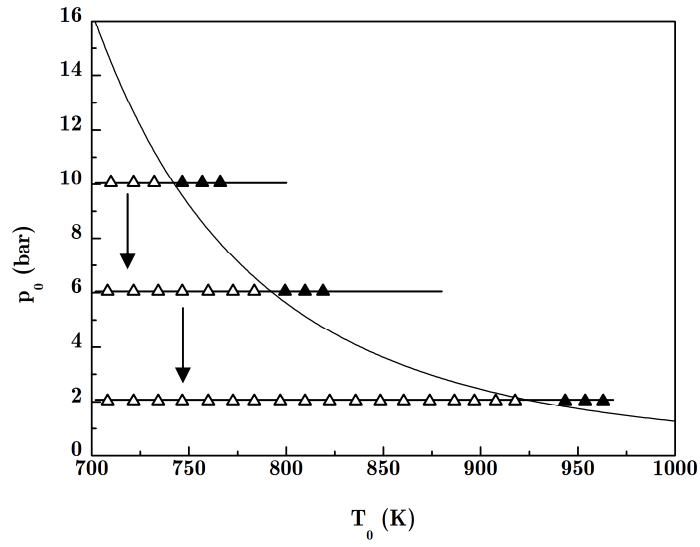

Fig. 61: Test sequence.

8

RESULTS AND DISCUSSION

8.1 Experimental results

A total of 65 tests were conducted to investigate the influence of mixture pressure and temperature on the auto ignition behaviour of Jet A1 in decomposed hydrogen peroxide with a concentration of 87.5%, a total mass flow between 0.37 and 0.44g/s, an equivalence ratio between 0.64 and 2.32, a combustion chamber diameter of 8mm and a wall temperature between 210±347°C measured at the bulk of the combustion chamber. 16 tests were conducted using a total combustion chamber volume of 1648 mm^3 and 49 tests were performed using a total combustion chamber volume of 3156 mm^3.

Test	H_2O_2 %	V_C [mm^3]	D_C [mm]	p_0 [bar]	T_0 [°C]	$\dot{m}$ [g/s]	O/F	ϕ	T_w bulk [°C]	Ignition
1	87.5	3156.67	8	8.3	372	0.39	4.6	1.61	258	Yes
2	87.5	3156.67	8	8.5	367	0.38	4.6	1.61	273	Yes
3	87.5	3156.67	8	11.4	361	0.38	6.16	1.20	251	Yes
4	87.5	3156.67	8	14.2	351	0.38	6.41	1.16	238	Yes
5	87.5	3156.67	8	14.6	347	0.37	7.36	1.01	251	Yes
6	87.5	3156.67	8	21.8	351	0.36	11.5	0.64	244	Yes
7	87.5	3156.67	8	21.6	362	0.38	6.94	1.07	255	Yes
8	87.5	3156.67	8	21.5	339	0.39	6.94	1.07	257	Yes
9	87.5	3156.67	8	21.1	342	0.39	6.94	1.07	243	Yes
10	87.5	3156.67	8	21.4	329	0.39	6.94	1.07	251	Yes
11	87.5	3156.67	8	21.2	328	0.39	6.94	1.07	253	Yes
12	87.5	3156.67	8	8.14	368	0.38	5.2	1.43	259	Yes
13	87.5	3156.67	8	6.97	379	0.40	5.26	1.41	261	Yes
14	87.5	3156.67	8	6.59	380	0.38	6.13	1.21	265	Yes
15	87.5	3156.67	8	6.66	393	0.37	5.9	1.26	282	Yes
16	87.5	3156.67	8	4.48	421	0.37	5.9	1.26	329	Yes

17	87.5	3156.67	8	4.14	425	0.39	5.9	1.26	318	Yes
18	87.5	3156.67	8	4.32	420	0.37	5.9	1.26	305	Yes
19	87.5	3156.67	8	4.53	415	0.41	5.9	1.26	291	Yes
20	87.5	3156.67	8	7.81	304	0.44	3.28	2.26	212	No
21	87.5	3156.67	8	8.07	337	0.43	3.2	2.32	230	No
22	87.5	3156.67	8	8.56	354	0.41	4.61	1.61	242	No
23	87.5	3156.67	8	11.7	309	0.39	6.16	1.20	211	No
24	87.5	3156.67	8	11.8	345	0.40	6.16	1.20	232	No
25	87.5	3156.67	8	7.15	350	0.43	3.61	2.05	270	No
26	87.5	3156.67	8	13.8	315	0.40	6.41	1.16	218	No
27	87.5	3156.67	8	14.4	335	0.39	7.16	1.03	247	No
28	87.5	3156.67	8	14.4	344	0.39	7.36	1.01	250	No
29	87.5	3156.67	8	21.3	325	0.36	11.5	0.64	229	No
30	87.5	3156.67	8	21.1	320	0.38	6.4	1.16	249	No
31	87.5	3156.67	8	21.1	326	0.38	6.37	1.16	243	No
32	87.5	3156.67	8	8.17	301	0.39	5.19	1.43	210	No
33	87.5	3156.67	8	8.29	330	0.39	5.28	1.40	224	No
34	87.5	3156.67	8	8.06	347	0.39	5.17	1.43	237	No
35	87.5	3156.67	8	8.03	359	0.38	5.2	1.43	249	No
36	87.5	3156.67	8	8.02	355	0.38	5.16	1.44	271	No
37	87.5	3156.67	8	6.88	323	0.39	5.59	1.33	229	No
38	87.5	3156.67	8	7.12	364	0.42	5.26	1.41	246	No
39	87.5	3156.67	8	7	360	0.40	5.26	1.41	265	No
40	87.5	3156.67	8	7.05	358	0.41	5.59	1.33	258	No
41	87.5	3156.67	8	7.07	367	0.40	5.58	1.33	263	No
42	87.5	3156.67	8	7.1	374	0.38	5.36	1.38	268	No
43	87.5	3156.67	8	6.09	324	0.37	5.82	1.27	222	No
44	87.5	3156.67	8	6.23	365	0.41	6.13	1.21	242	No
45	87.5	3156.67	8	6.15	373	0.39	5.79	1.28	275	No
46	87.5	3156.67	8	6.34	379	0.40	5.9	1.26	274	No
47	87.5	3156.67	8	4.28	409	0.43	5.9	1.26	285	No
48	87.5	3156.67	8	3.95	397	0.42	6	1.24	276	No
49	87.5	3156.67	8	3.74	403	0.41	5.84	1.27	276	No
50	87.5	1648.71	8	4.66	423	0.43	6.71	1.10	340	Yes
51	87.5	1648.71	8	6.89	381	0.39	4.9	1.51	304	Yes
52	87.5	1648.71	8	8.13	368	0.38	5.51	1.34	287	Yes
53	87.5	1648.71	8	8.35	368	0.38	5.67	1.31	290	Yes

54	87.5	1648.71	8	10.83	365	0.41	6.23	1.19	276	Yes
55	87.5	1648.71	8	11.3	359	0.41	6.23	1.19	278	Yes
56	87.5	1648.71	8	11.1	356	0.40	5.82	1.27	276	Yes
57	87.5	1648.71	8	3.88	413	0.43	6.71	1.10	330	No
58	87.5	1648.71	8	3.7	427	0.44	6.71	1.10	347	No
59	87.5	1648.71	8	6.21	366	0.33	4.9	1.51	295	No
60	87.5	1648.71	8	6.21	374	0.38	5.02	1.48	304	No
61	87.5	1648.71	8	6.01	376	0.32	5.31	1.40	305	No
62	87.5	1648.71	8	8.09	355	0.40	5.51	1.34	279	No
63	87.5	1648.71	8	8.12	365	0.38	5.67	1.31	290	No
64	87.5	1648.71	8	10.43	338	0.39	6.23	1.19	260	No
65	87.5	1648.71	8	10.4	354	0.40	5.82	1.27	277	No

Tab. 16: Cunducted test campaign for the investigation of the auto ignition behaviour of Jet A1/H_2O_2

Auto ignition was classified in two regimes: yes and no ignition based on recorded chamber pressure and temperature measurements. The temperature measurement sensors along the combustion chamber which recorded the combustion chamber temperature were planar fixed to the combustion chamber segments in order to prevent flame holding effects. Thus the recorded chamber temperatures were influenced by the wall temperature and therefore they were much lower than the hot gas temperature (figure 62, figure 63). Furthermore the combustion chamber pressure, mass flows and O/F ratios were recorded (figure 64). Figure 62 shows the hot gas temperature inside the combustion chamber. Five temperature elements were mounted down stream along the combustion chamber. Only TG1 was extending several millimeters into the combustion chamber. TG2-TG4 were mounted planar with the inner wall of the combustion chamber. This graph shows a successful ignition of a Jet A1/H_2O_2 mixture. The test was automatically aborted after the temperature reaches 1000°C in order to avoid damage due to excessive heat load.
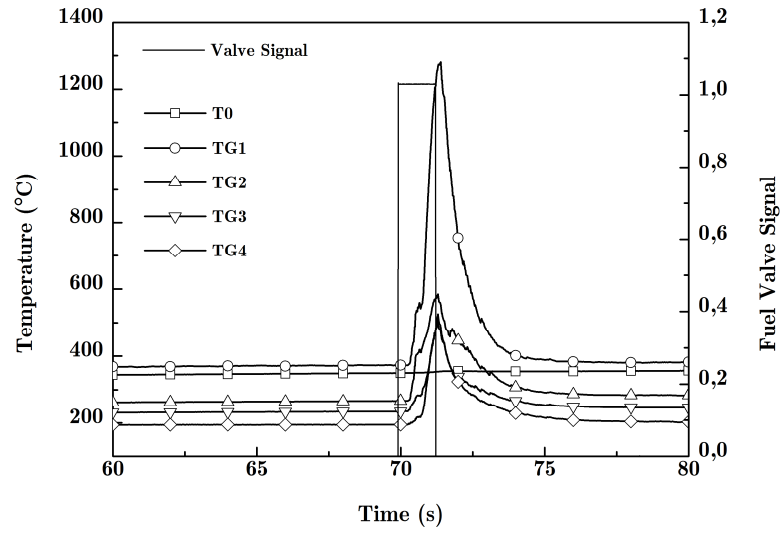
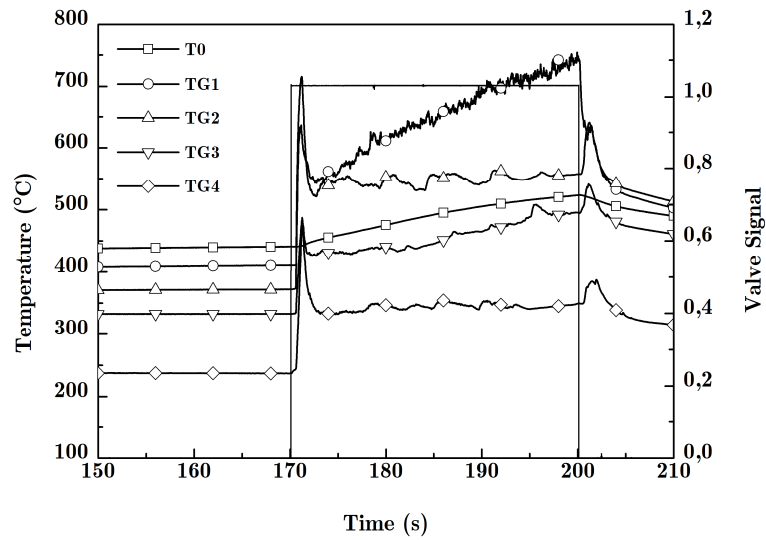Fig. 62: Hot gas temperature after successful ignition

Fig. 63: Combustion chamber temperatures during successful ignition and combustion.

Figure 63 shows a successful auto ignition occurrence as well as figure 62 but all temperature elements were mounted planar. As a consequence of the large heat sink property of the combustor due to the large mass, the recorded temperatures raised slowly in contrast to figure 62 because of the influence of the wall temperature in this setup.
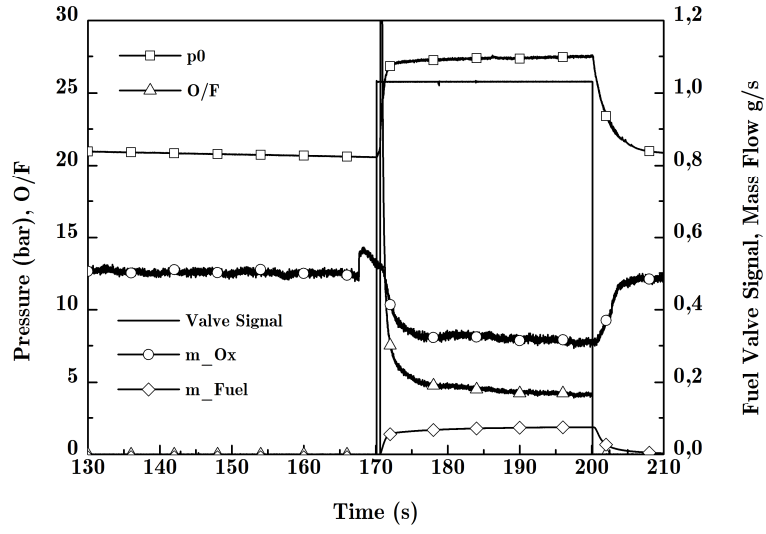
Fig. 64: Chamber pressure, mass flows and O/F ratio during successful auto ignition and combustion
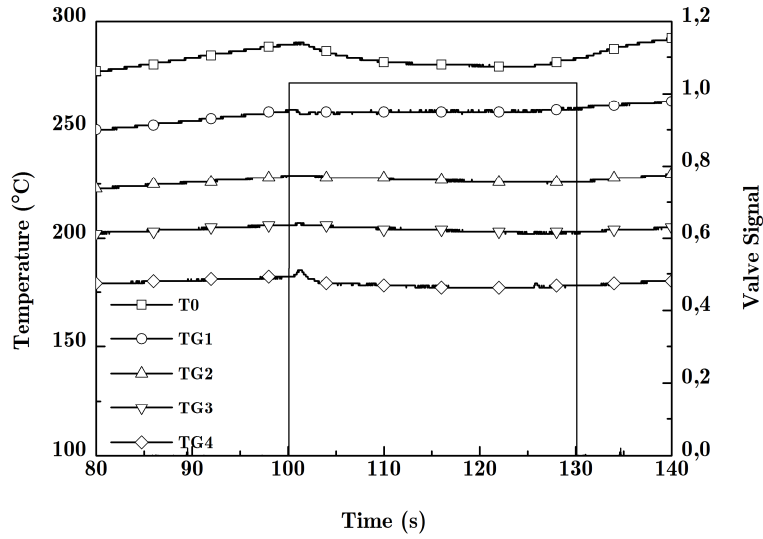

Fig. 65: Failed ignition

Figure 64 shows the combustion chamber pressure, oxidizer-fuel ratio (O/F), oxidizer mass flow, fuel mass flow and the fuel valve signal. The occurrence of auto ignition is given by an abrupt rise of the combustion chamber pressure (squares) as well as the oxidizer mass flow (circles) decreases to a stable flow rate. Figure 65 shows failed auto ignition. The cooling effect due to evaporation of the fuel is clearly visible (squares).

8.2 Correlation of auto ignition data with the auto ignition model

The correlation of the experimentally determined ignition pressure with the predicted ignition pressure by the theory will be done by equation (3.228). To correlate the test data with the auto ignition model it is important to know how many parameters are unknown. Therefore table 17 summarizes all parameters which influence the initial pressure to achieve ignition classified in known and unknown parameters,

Parameter	known	unknown
n		✓
R	✓	
T_0	✓	
Q_r	✓	
E_A		✓
A'		✓
M	✓	
$\dot{m}$	✓	
c_p	✓	
Φ		✓
V_C	✓	
D_C	✓	
χ , T_w	✓	

Tab. 17: Ignition parameters

Four parameters are unknown: n, E_A, A', Φ. Their determination via a suitable fit procedure is almost impossible because a huge set of data points will be necessary for providing a good fit. Additionally, it can be assumed that there exist several local minima in the $\mathbb{R}^4$ parameter space. Thus the fit procedure converges depending on the initial assumed values to any of these local minima. Consequently the values of the fitted parameters are not definite and many sets of the fit parameters exists which give the same fit quality. Therefore the verification of the auto ignition model will be done in a qualitatively way by the demonstration that the experimental evaluated data and theoretical data are linearly dependent by,

$$\delta' p_{0,\text{theoretical}} = p_{0,\text{data}} \tag{8.1}$$

Thus the correlated ignition conditions becomes

1$^\text{st}$ignition condition given by: $\dfrac{E_A}{RT_0}\left(1 - \dfrac{\langle T_w\rangle}{T_0}\right) \leq 1$

$$p_0 = \sqrt[n]{\frac{T_0^{(n+2)}}{E_A}\left\{\frac{P_1}{V_C}\exp\left(\frac{E_A}{RT_0}\right) + \frac{P_2}{D_C}\exp\left[\frac{E_A}{RT_0}\left(2 - \frac{\langle T_w\rangle}{T_0}\right) - 1\right]\right\}} \tag{8.2}$$

$$P_1 = \delta'\frac{R^{(n+1)}}{Q_r A'(\phi)M(\phi)}\frac{\dot{m}\left\langle c_p\big|_{T_0}\right\rangle_\phi^{mix}}{\Phi} \qquad P_2 = \delta'\frac{4\left\langle\chi\big|_{T_0}\right\rangle_\phi^{mix} R^{(n+1)}}{Q_r A'(\phi)M(\phi)}$$

2$^\text{nd}$ignition condition given by: $\dfrac{E_A}{RT_0}\left(1 - \dfrac{\langle T_w\rangle}{T_0}\right) > 1$

$$p_0 = \sqrt[n]{T_0^n\exp\left(\frac{E_A}{RT_0}\right)\left\{P_1\frac{T_0^2}{V_C E_A} + \frac{P_2}{D_C}\left[1 - \frac{\langle T_w\rangle}{T_0}\right]\right\}} \tag{8.3}$$

$$P_1 = \delta'\frac{R^{(n+1)}}{Q_r A'(\phi)M(\phi)}\frac{\dot{m}\left\langle c_p\big|_{T_0}\right\rangle_\phi^{mix}}{\Phi} \qquad P_2 = \delta'\frac{4\left\langle\chi\big|_{T_0}\right\rangle_\phi^{mix} R^n}{Q_r A'(\phi)M(\phi)}$$

where P_1 and P_2 are fit coefficients. The activation energy, E_A, and the order of the chemical reaction process, n, remain still unknown but if an adiabatic ignition process is assumed, equation (3.224), which is equivalent to the non adiabatic ignition process for the limit $D_C\to\infty$, following relation can be stated.

$$E_A = \frac{R\ln\left(\dfrac{p_{0,1}^n\, T_{0,2}^{(n+2)}}{p_{0,2}^n\, T_{0,1}^{(n+2)}}\right)}{\dfrac{1}{T_{0,1}} - \dfrac{1}{T_{0,2}}} \tag{8.4}$$

where $T_{0,1}, T_{0,2}$, $p_{0,1}$ and $p_{0,2}$ are given by the initial temperatures and pressures at which ignition occurs whereas the mass flow, equivalence ratio, combustion

chamber diameter, combustion chamber volume, the residence time factor and specific heat remain constant. Therefore the fit procedure can be performed according to figure 66.
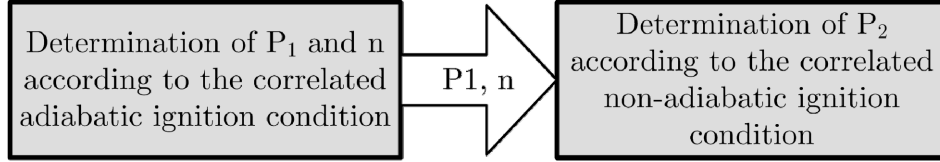

Fig. 66: Fit procedure

Since only one test campaign were conducted with a combustion chamber diameter of 8mm the proposed correlation procedure does not fit well. Therefore all four fit parameters were determined simultaneously. Thus the ignition analysis results in following p-T diagram for Jet-A1/H_2O_2.
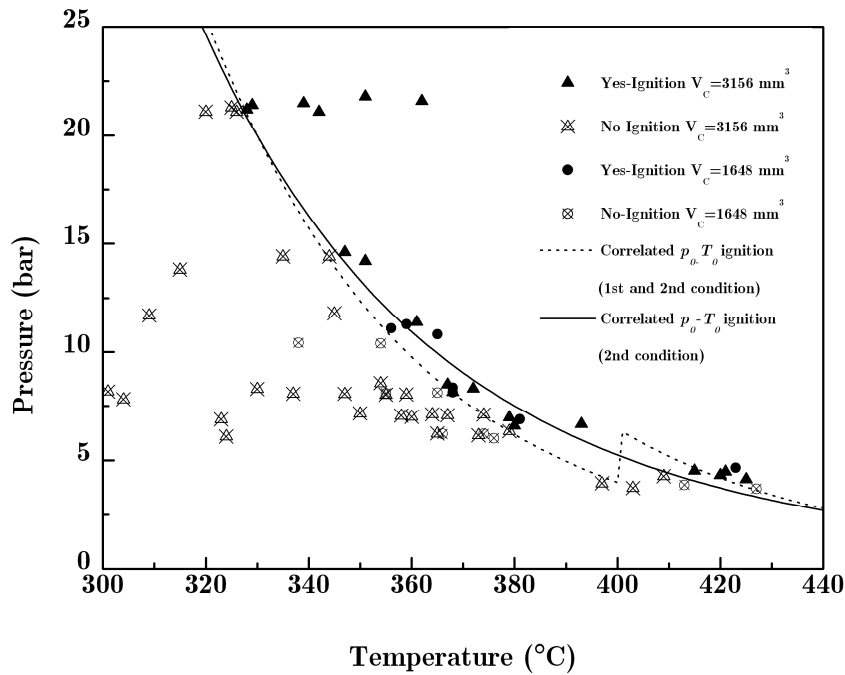

Fig. 67: Pressure-Temperature ignition behaviour of Jet A1/H_2O_2

The solid triangles and circles show a successful auto ignition and combustion for a total combustion chamber volume of 3156mm^3 and 1648mm^3 respectively. The crossed out triangles and circles show failed auto ignition. The full black line in figure 67 shows a correlation assuming auto ignition given by the 2nd ignition condition and the dashed line gives the correlation for the necessary

193

pressure to achieve ignition assuming the first ignition condition in the temperature range $T_0>400°C$ and the second ignition condition for initial temperatures less than 400°C. The discontinuity at $T_0=400°C$ is given due to the existence of two possible ignition condition depending on the relation between the wall temperature and the initial gas temperature, T_0. Additionally the experimental data showed a negligible influence of the combustion chamber volume on the pressure-temperature auto ignition behaviour at least for the magnitude of the two tested volume. The determined fit coefficients (Table 18) thus have to reflect this auto ignition characteristic. Hence the lines of the ignition boundary for the two tested combustion chamber volumes are very close together thus only one is visible.

	n	E_A	P_1	P_2
Straight line	3.54	273241	1E-18	5E-13
Dashed line	6.01	547991	1E-32	9.68E-27

Tab. 18: Fit parameters for the pressure-temperature auto ignition behaviour of Jet A1/H_2O_2 mixtures

Furthermore Figure 67 shows the corresponding characteristic chamber length, L^*, depending on the necessary initial temperature to achieve auto ignition. The black and dashed lines show the correlation of L^* with the help of the fit coefficients given by Table 18. Two basic facts can be stated. Firstly, the fit coefficient given by Table 18 provides accurate prediction of the auto ignition boundary and secondly they reflects the behaviour of nearly constant pressure-temperature auto ignition behaviour of the two tested combustion chamber volumes although the corresponding characteristic chamber length are appreciable different.
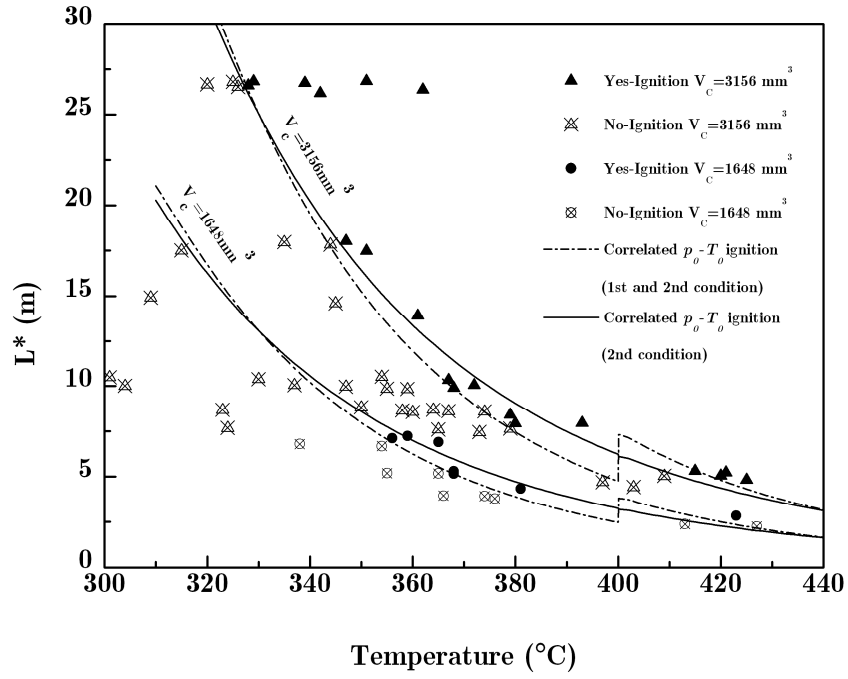
Fig. 68: Characteristic chamber length vs. initial temperature

Since the two different characteristic chamber length –temperature ignition boundaries reflect the same pressure-temperature characteristic it is assumed that the combustion chamber volume can be further decreased without influencing the pressure-temperature auto ignition behaviour significantly.

9

CONCLUSIONS AND DISCUSSION

In the case of Jet A-1 fuel the pressure-temperature correlation (black line) shows well agreement with the experimental data nevertheless marginal discrepancy exists. Several explanations for this behaviour can be stated. First, due to the higher injection temperatures which are achieved by a longer pre ignition test run, the wall temperatures at the inner combustion chamber surface becomes almost the same as the hot gas temperature. Therefore the first ignition conditions have to be utilized for the correlation. This is given by the dashed line in figure 67. Second, during the test campaign it was nearly impossible to set the equivalence ratio constant. Since it is assumed that the auto ignition behaviour of Jet A1 depends on the equivalence ratio [40, 75, 92, 93] the variance in the occurrence of successful auto ignition is based on the variance of the equivalence ratio. Third, if it is assumed that molecular transport effects, equation (3.68) of fuel and oxidizer concentration are significant reactant depletion becomes significant for the ignition process. Since the molecular diffusion flux of the reactant concentration depends on the partial pressures the loss effect becomes much more relevant for high pressures than for low pressures resulting in a much more essential non linearity than given by the case of negligible reactant depletion. Furthermore the influence of the combustion chamber volume can be assumed to be negligible for the two tested volumes. This fact seems to be contradictory considering the analytical analysis of the influence of the combustion chamber volume. But due to the swirl injector and the rearward facing step the mean residence time becomes very large and only for very small combustion chambers the influence of it becomes significant. An analytical non-adiabatic auto-ignition model of the ignition conditions for a choked and non-choked flow reactor has been developed assuming a one-step single forward chemical reaction based on the theory of residence time distributions. Special focus is laid on the pressure temperature ignition behavior in correlation to the combustion chamber geometry. The analytical model shows well accordance to the pressure-

temperature correlation function for a decomposed hydrogen peroxide/Jet-A1 fuel mixture proposed by Walder in the early 1950s whereas the ignition delay is proportional to the characteristic chamber length, L^*, of the engine. Furthermore the model shows that the constant L' in Walder's correlation function depends on the initial gas temperature as well as on the specific heat, mean molar mass and isentropic exponent of the mixture. Consequently it depends on the mixture ratio. Additionally Walder's correlation neglects the influence of the heat loss effect which is high for a high surface to volume ratios. As a result, the correlation function proposed by Walder is a priori not applicable for micro rocket combustion chambers. For the model validation, an experimental setup and a segmented combustion chamber was developed which allows to systematically investigate the auto-ignition conditions whereas the initial pressure, initial temperature and mass flow can be varied independently and with easy variation of the combustion chamber geometry.

In several test cases auto ignition of Jet-A1/O_2/H_2O was experimental investigated with a concentration of 87.5%, a total mass flow of 0.39±0.06g/s, an equivalence ratio of 1.3±0.81, a combustion chamber diameter of 8mm, a combustion chamber volume of 3156 and 1648 mm^3 and a wall temperature of 265±93°C measured at the bulk of the combustion chamber. Auto ignition and stable combustion was verified by experimental data. The pressure-temperature correlation based on the analytical auto ignition model showed excellent agreement with the experimental data. Additionally the experimental data showed that the influence of the combustion chamber volume on the pressure-temperature auto ignition behaviour is negligible at least for the magnitude of the two tested volume. This is caused by a large mean residence time due to the swirl injector and the rearward facing step which increases the turbulence intensity. Thus it is assumed that the combustion chamber volume and consequently the characteristic chamber length can be decreased further without influencing the pressure-temperature auto ignition behaviour significantly, however the exactly threshold has to be investigated in the future. Unfortunately the experimental verification of the influence of the combustion chamber diameter was not possible due to lack of time, however theoretical calculation relating to Jet A/Air mixtures results in a marginal influence of the combustion chamber diameter on the pressure-temperature auto ignition behaviour for diameters greater or equal than 10mm. Basically since there is no special assumption regarding to the chemical species of the

ignitable mixture, it can be assumed that the auto ignition model is appropriate to predict the behaviour of any ignitable mixture.

BIBLIOGRAPHY

[1] Salome R, "The propulsion system of the CNES microsatellite product line", in Proc. 3rd Internat. Conf. On Spacecraft propulsion ESA SP-465, Dec. 2000, p. 99-105.

[2] Cong Y., Zhang T., et. al., "Study on Kerosene based Fuel with Hydrogen Peroxide for Hypergolic Application", Proc. 2nd Int. Conference on Green Propellants for Space Propulsion, ESA SP-557

[3] Khan, Qasim Sawar, Baek, Seung Wook, Ghassemi Hojat, On the Auto ignition and Combustion Characteristics of Kerosene Droplets at Elevated Pressure and Temperatures, Combustion Science and Technology, 179:12, 2437-2451

[4] Chung K. Law, "Combustion Physics", Cambridge University Press, 2006

[5] Brounar M., "Reaction Dynamics", Oxford University Press, 1998

[6] Houston P. L., "Chemical Kinetics and Reaction Dynamics", Dover Publications, 2006

[7] J. F. Griffiths, W. Nimmo, "Novel experimental investigation of spontaneous ignition of gaseous hydrocarbons", Nature 322, 46 - 47 (03 July 1986)

[8] Burcat, A., Farmer, R. F., and Matula, R. A., "Shock Initiated Ignition in Heptane–Oxygen–ArgonMixtures," Proceedings of the Thirteenth International Symposium on Shock Tubes and Waves, State Univ. of NY Press, Albany, NY, 1981, pp. 826–833.

[9] Ryan, T. W., and Callahan, T. J., "Engine and Constant Volume Bomb Studies of Diesel Ignition and Combustion," Society of Automotive Engineers, SAE TP Series, Paper 881626, 1988.

[10] Vermeer, D. J., Meyer, J. W., and Oppenheim, A. K., "Auto-Ignition of Hydrocarbons Behind Re ected ShockWaves," Combustion and Flame, Vol. 18, 1972, pp. 327–336.

[11] Burwell, W. G., and Olson, D. R., "The Spontaneous Ignition of Isooctane Air Mixtures Under Steady Flow Condition," Society of Automotive Engineers, SAE Paper 650510, 1965.

[12] Ciezki, H. K., and Adomeit, G., "Shock-Tube Investigation of n-Heptane–Air Mixtures Under Engine Relevant Condition," Combustion and Flame, Vol. 93, 1993, pp. 421–433.

[13] Gray, J. A., and Westbrook, C. K., "High-Temperature Ignition of Propane with MTBE as an Additive: Shock Tube Experiments and Modeling," Journal of Chemical Kinetics, Vol. 26, 1994, pp. 757–770.

[14] Norman F., Van den Schoor F., Verplaetsen F., "Auto-ignition and upper explosion limit of rich propane-air mixtures at elevated pressures", Journal of Harzardous Materials A137 (2006), 666-671

[15] Brown, C. J., and Thomas, G. O., "Experimental Studies of Shock Induced Ignition and Transition to Detonation in Ethylene and PropaneMixtures," Combustion and Flame, Vol. 117, 1999, pp. 861–870.

[16] Coats, C.M., andWilliams, A., "Investigation of the Ignition and Combustion of n-Heptane–Oxygen Mixtures," Proceedings of the Seventeenth International Symposiumon Combustion, Combustion Inst., Pittsburgh,PA, 1979, pp. 611–621.

[17] Petersen, E. L., Davidson, D. F., and Hanson, R. K., "Ignition Delay Times of Ram Accelerator CH4/O2/Diluent Mixtures," Journal of Propulsion and Power, Vol. 15, No. 1, 1999, pp. 82–91.

[18] Burcat, A., Scheller, K., and Lifshitz, A., "Shock-Tube Investigation of Comparative Ignition Delay Times for C1 –C4 Alkanes," Combustion and Flame, Vol. 16, 1971, pp. 29–33.

[19] Burcat, A., Lifshitz, A., Scheller, K., and Skinner, G. B., "Shock-Tube Investigation of Ignition in Propane–Oxygen–Argon Mixtures," Proceedingsof the Thirteenth InternationalSymposiumon Combustion, Combustion Inst., Pittsburgh, PA, 1971, pp. 745–755.

[20] Spadaccini, L. J., and Colket, M. B., "Ignition Delay Characteristics of Methane Fuels," Progress in Energy and Combustion Science,Vol. 20, 1994, pp. 431–460.

[21] Baker, J. A., and Skinner, G. B., "Shock-Tube Studies on the Ignition of Ethylene-Oxygen-ArgonMixtures," Combustion and Flame, Vol. 19, 1972, pp. 347–350.

[22] Bhaskaran, K. A., and Srinivasa, C., "ShockTubeStudyof HighTemperature Ethylene-Oxygen Reaction," Proceedings of 4th National Conference on Internal Combustion Engines, College of Engineering, Indian Inst. of Technology,Madras, India, 1978, pp. 23–28.

[23] Yoshizawa, Y., and Kawada, H., "A Shock-Tube Study on the Ignition Lag of Gaseous Fuels," Bulletin of the Japan Society of Mechanical Engineers, Vol. 16, No. 93, 1973, pp. 576–587.

[24] Suzuki, M., Moriwaki, T., Okazaki, S., Okuda, T., and Tanzawa, T., "Oxidation of Ethylene in Shock Tube," Astronautica Acta, Vol. 18, 1973, pp. 359–365.

[25] Orr, C. R., "Combustion of Hydrocarbons Behind a Shock Wave," 9th Symposium(International) on Combustion, Academic, New York, 1963, pp. 1034–1045.

[26] Craig, R. A., "A Shock Tube Study of the Ignition Delay of Hydrogen- Air Mixtures Near the Second Explosion Limit," AFAPL-TR-66-74, WPAFB, OH, Nov. 1966.

[27] Glassman I., Yetter R. A., "Combustion", Academic Press 2008

[28] Dagaut P., Bakali A. E., Ristori A., „"The combustion of kerosene: Experimental results and kinetic modelling using 1- tp 3-component surrogate model fuels", Fuel 85 (2006) 944-956

[29] Warnatz J., "Combustion: Physical and Chemical Fundamentals, Modeling and Simulation, Experiments, Pollutant Formation", Springer, 4th ed. 2005

[30] N.N. Semenov, "Chemical Kinetics and Reactivity", vols. I and II, Princeton: Princeton University Press, 1958, 1959

[31] Cullins C. F., Foster C. D., "Application of Thermal Ignition Theory to Determination of Spontaneous Ignition Temperature Limits of Hydrocarbon-Oxygen Mixtures", Proc. R. Soc. Lond. A 1977 355, 153-165

[32] P.H. Thomas, C & F9, 369 (1965)

[33] P. Gray and P. R. Lee, "Oxidation and Combustion Review" 2, 1(1967).

[34] B. F. Gray and C. H. Yang, 11th Symp. (1967), 1057-1061

[35] Forman A. Williams, "Combustion Theory", Perseus Books, 2nd Edition, 1985

[36] Turner, J.,M.,"Rocket and Spacecraft Propulsion: Principles, Practice and New Developments", Springer 3rd ed. 2008

[37] Rosner E. Daniel, "Transport Processes in Chemically Reacting Flow Systems", Dover Publication, Inc., 2000

[38] Chapman, S., Cowling, T. G., "The Mathematical Theory of Non-Uniform Gases", Cambridge University Press 1953

[39] D. A. Frank-Kamenetskii, "Diffusion and Heat Transfer in Chemical Kinetics", New York: Plenum Press, 1969

[40] Dean, A. J., Penyazkov, O. G., Sevruk K. L., Varatharajan B., "Autoignition of surrogate fuels at elevated temperatures and pressures", Proceedings of the Combustion Institute 31 (2007) 2481-2488

[41] Yuriy I. Khavkin, "Combustion System Design- A new Approach", Pennwell Publishing Company Tulsa, Oklahoma, 1996

[42] Ian S. Metcalfe, "Chemical Reaction Engineering", Oxford Chemistry Primers, 2002

[43] Dirk Thoenes, "Chemical Reactor Development", Springer 2004

[44] Leonardi F., Larochette M., et al. ," Optimisation of extruded polymer foam by the resident time distribution approach", Proceedings of the Polymer Processing Society 24th Annual Meeting

[45] Fengquan Zhong, Xuejun Fan et al.,"Heat Transfer of Aviation Kerosene at Supercritical Conditions", AIAA Paper 2008-4615

[46] Hendricks, R. C., Simoneau, R. J. and Smith, R. V., "Survey of Heat Transfer to Neat Critical Fluids", NASA TN D-5886, 1970.

[47] Giovanetti, A. J., Spadaccini, L. J., Szetela, E. J., "Deposit Formation and Heat Transfer Characteristics of Hydrocarbon Rocket Fuels", Journal of Spacecraft，Vol.22，No.5, pp. 574-580, 1985.

[48] Meyer, M. L., "Electrically Heated Tube Investigation of Cooling Channel Geometry Effects", AIAA Paper 95-2500.

[49] Bates, R. W., Edwards, T., "Heat Transfer and Deposition Behavior of Hydrocarbon Rocket Fuels", AIAA Paper 2003-0123.

[50] Stiegemeier, B., Meyer, M. L., Taghavi, R., "A Thermal Stability and Heat Transfer Investigation of Five Hydrocarbon Fuels", AIAA Paper 2002-3873.

[51] Hu, Z-H., Chen, T-K., Luo Y-S., Zheng J-X., Tang, M., "Heat Transfer Characteristics of Kerosene at Supercritical Pressure", Journal of Xi'an Jiaotong University, Vol. 33, No.9, 1999.

[52] Weixing Zhou, Wen Bao et al., „Structural Optimization and Design of Cooling Channel Considering Heat Transfer Deterioration of Endothermic Hydrocarbon Fuel", AIAA Paper 2008-5177

[53] Humble, R. W., Henry, G. N., Larson, W. J., "Space Propulsion Analysis and Design", McGraw-Hill Companies Inc., New York, 1995.

[54] Franz Joos, "Technische Verbrennung", Springer 2000

[55] "Robust Summary of Information on Kerosene/Jet Fuel", American Petroleum Institute, 2003

[56] Edwards T. "Liquid Fuels and Propellants for Aerospace Propulsion: 1903-2003", Journal of Propulsion and Power Vol. 19, No. 6, 2003

[57] Edwards T., Maurice L. Q., "Surrogate Mixtures to Represent Complex Aviation and Rocket Fuels", Journal of Propulsion and Power, Vol. 17, No. 2, 2001

[58] Martel, C. R., "Molecular Weight and Average Composition of JP-4, JP-5, JP-8, and Jet A," Chemical Propulsion Information Agency Airbreathing Propulsion Manual CPIA/M6, Units 8 (JP-7) and 11 (JP-8), Columbia, MD, Sept. 2000.

[59] "HandbookofAviationFuel Properties," CoordinatingResearch Council Rept. 530, Coordinating Research Council, Atlanta, GA, 1983.

[60] "Survey of Jet Fuels (1990-1997)," Defense Energy Supply Center, Ft Belvoir, VA, June 1998 (annual updates thereafter).

[61] Yu, J., and Eser, S., "Determination of Critical Properties (Tc, Pc) of Some Jet Fuels," Industrial and Engineering Chemistry Research, Vol. 34, No. 1, 1995, pp. 404–409.

[62] Martel, C. R., "Air Force Aviation Fuel Thermal Oxidation Stability R&D," Jet Fuel Thermal Stability, edited byW. F. Taylor,NASATM 79231, National Aeronautics and Space Administration, Cleveland, OH, Nov. 1978.

[63] Wood, C. P., McDonell, V. G., Smith, R. A., and Samuelson, G. S., "Development and Application of a Surrogate Distillate Fuel," Journal of Propulsion and Power, Vol. 5, No. 4, 1989, pp. 399–405.

[64] Sobel, D. R., and Spadaccini, L. J., "Hydrocarbon Fuel Cooling Technologies for Advanced Propulsion," American Society of Mechanical Engineers Journal of Engineering for Gas Turbines and Power, Vol. 119, No. 2, April 1997, pp. 344–351.

[65] Freeman, G., "The Spontaneous Ignition Characteristics of Gaseous Hydrocarbon Fuel-Air Mixtures at Atmospheric Pressure," M.S. Thesis, School of Aeronautics and Astronautics, Purdue Univ., West Lafayette, IN, 1984.

[66] Spadaccini, L. J., and TeVelde, J. A., "Autoignition Characteristics of Aircraft-Type Fuels," NASA CR-159886, June 1980.

[67] Freeman, G., and Lefebvre, A. H., "Spontaneous Ignition Characteristics of Gaseous Hydrocarbon-Air Mixtures," Combustion and Flame, Vol. 58, Nov. 1984, pp. 153–162.

[68] Mestre, A., and Ducourneau, F., "Recent Studies on the Spontaneous Ignition of Rich Air-Kerosene Mixtures," Combustion Institute European Symposium, Academic Press, Inc., London, 1973, pp. 225–229.

[69] Burcat, A., Farmer, R. F., and Matula, R. A., "Shock Initiated Ignition in Heptane–Oxygen–ArgonMixtures," Proceedings of the Thirteenth International Symposium on Shock Tubes and Waves, State Univ. of NY Press, Albany, NY, 1981, pp. 826–833.

[70] Ryan, T. W., and Callahan, T. J., "Engine and Constant Volume Bomb Studies of Diesel Ignition and Combustion," Society of Automotive Engineers, SAE TP Series, Paper 881626, 1988.

[71] Vermeer, D. J., Meyer, J. W., and Oppenheim, A. K., "Auto-Ignition of Hydrocarbons Behind Re ected ShockWaves," Combustion and Flame, Vol. 18, 1972, pp. 327–336.

[72] Burwell, W. G., and Olson, D. R., "The Spontaneous Ignition of Isooctane Air Mixtures Under Steady Flow Condition," Society of Automotive Engineers, SAE Paper 650510, 1965.

[73] Colket, M. B., Spadaccini, L. J., "Scramjet Fuels Autoignition Study," Journal of Propulsion and Power, Vol. 17, No. 2, March-April 2001, pp. 315-323.

[74] Fieweger, K., Blumenthal, R., Adomeit, G., "Self- Ignition of S.I. Engine Model Fuels: A Shock Tube Investigation at High Pressure," Combustion and Flame, Vol. 109, No. 4, June 1997, pp. 599-619.

[75] Vasu, S. S., Davidson, D. F., Hanson R. K., "Jet fuel delay times: Shock tube experiments over wide conditions and surrogate model predictions", Combustion and Flame 152 (2008) 125-143

[76] TEP Version 1.5, SEA Software, Inc., Carson City, Nevada, 1999

[77] Imbert B., Lafosse F., Catoir L., Paillard C.E., Khasainov B.," Formulation reproducing the ignition delays simulated by a detailed mechanism: Application to n-heptane combustion", Combustion and Flame 155 (2008) 380-408

[78] Walder, H., and Broughton, L.W., "Thermal Ignition Tests of Hydrogen Peroxide and Kerosine in a 2200lb Thrust Rocket Motor," Royal Aircraft Establishment, RAE-TN-RPD-70, Aug. 1952.

[79] Walder, H., "An Investigation into the Thermal Ignition of Hydrogen Peroxide and Kerosine," Royal Aircraft Establishment, RAE-R-RPD 7, May 1950.

[80] Walder, H., "Further Investigations into the Thermal Ignition of Hydrogen Peroxide and Kerosine," Royal Aircraft Establishment, RAE-TNRPD-43, Dec. 1950.

[81] S. Gordon, B.J. McBride, Computer Program for Calculation of Complex Chemical Equilibrium Compositions and Applications I. Analysis, NASA Ref. Pub. 1311, 1994.

[82] Wernimont, E. J., Durant, D., "Development of a 250 lbfv Kerosene – 90% Hydrogen Peroxide Thruster", AIAA 2004-4148

[83] "Hydrogen Peroxide Handbook,", AFRPL-TR-67-144, Rocketdyne, Inc., July 1967.

[84] Sengupta D., Mazumder S., Cole J., Lowry S., "Controlling Non-Catalytic Decomposition of High Concentration Hydrogen Peroxide", CFD Research Corporation, 2004

[85] Sorge A., Turco M., Pilone G., Bagnasco G., "Decomposition of Hydrogen Peroxide on MnO2/TiO2 Catalysts", Journal of Propulsion and Power, Vol. 20, No. 6, 2004

[86] Hasan, M., Zaki, M. I., Pasupulety, L., and Kumari, K., "Promotion of the Hydrogen Peroxide Decomposition Activity of Manganese Oxide Catalysts," Applied Catalysis, A: General, Vol. 181, No. 1, 1999, pp. 171–179.

[87] Deraz, N., Allah, M., Salim, H. H., and El-Aal, A. A., "The Influence of Lithium on the Hydrogen Peroxide Decomposition Activity of Manganese-Alumina Catalysts," Materials Letter, Vol. 53, No. 1–2, 2002, pp. 102–109.

[88] Kubota N., "Propellants and Explosives: Thermochemical Aspect of Combustion", Wiley-VCH, 2007

[89] Sutton, "Rocket Propulsion Elements", Wiley & Sons, 2001

[90] Musker, A.J., Roberts, G.T., "Progress with Catalysis of Highliy Stabilized Hydrogen Peroxide", 8th International hydrogen Peroxide Propulsion Conference –Perdue University- September 18-12, 2005

[91] Wernimont E.J., Durant D., "Development of a 250 lbfv Kerosene – 90% Hydrogen Peroxide Thruster", 40th AIAA/ASME/SAE/ASEE Joint Propulsion Conference Exhibit 11-14 July 2004, Fort Lauderdale, Florida

[92] Park, G., Lim H., "Novel Ramjet Propulsion System with H2O2-Kerosene Rocket as an Initial Accelerator", 44th AIAA/ASME/SAE/ASEE Joint Propulsion Conference Exhibit 21-23 July 2008, Hartfort, CT

[93] Sisco J.C., et al. "Autoignition of Kerosene by Decomposed Hydrogen Peroxide in a Dump-Combustor Configuration", Journal of Propulsion and Power, Vol.21, No. 3, May-June 2005, pp. 450-459

[94] Huang Y., Yang V., "Modeling and Control of Combustion Dynamics in Lean-Premixed Swirl-Stabilized Combustors", Proceeding of Sixth Symposium on Smart Control of Turbulence, Japan, March 6-9,2005

[95] Zucrow M. J., Osborn, J. R., "An Experimental Study of High-Frequency Combustion Pressure Oscillations", Jet Propuilsion, Vol. 28, No. 10, pp. 649-659, October, 1958

[96] Lieuwen, T., "Experimental Investigation of Limit-Cycle Oscillations in an Unstable Gas-Turbine Combustor," Journal of Propulsion and Power, Vol.18, 2003, pp.61-67.

[97] Huang, Y., Sung, H.G., Hsieh, S.Y. and Yang, V., "Large Eddy Simulation of Combustion Dynamics of Lean-Premixed Swirl-Stabilized Combustor," Journal of Propulsion and Power, Vol.19, 2003, pp.782-794.

[98] Poinsot, T.J., Trouve, A.C., Veynante, D.P., Candel, S., and Esposito, E., "Vortex-driven Acoustically Coupled Combustion Instabilities," Journal of Fluid Mechanics, Vol.177, 1987, pp.165-292.

[99] Schadow, K.C. and Gutmark, E., "Combustion Instability Related to Vortex Shedding in Dump Combustor and Their Passive Control", Progress in Energy and Combustion Science, Vol.18, 1992, pp.117-132.

[100] Lieuwen, T. and Zinn, B.T. "The Role of Equivalence Ratio Oscillation in Driving Combustion Instabilities in Low Nox Gas Turbines", Proceedings of the Combustion Institute, Vol. 27, 1998, pp.1809-1816.

[101] Yu Y. C., Koeglmeier S. M., Sicso J.C., Anderson W. E., „Combustion Instability of Gaseous Fuels in a Continuously Variable Resonance Chamber (CVRC)", 44th AIAA/ASME/SAE/ASEE Joint Propulsion Conference & Exhibit, 21-23 July 2008, Hartfort, CT

[102] Nicoud, F., Pointsot, T., "Thermoacoustic Instabilities: Should Rayleigh Criterion be Extended to Include Entropy Changes?", Combustion and Flame, Vol. 142, 2005, pp. 153-159

[103] Gallagher, K. E., Sander, G. F., and Brink, D.F., "Characteristic Time Correlations to Liquid Fuel Ramjet Combustion Efficiency", 24th JANNAF Combustion Meeting, Vol. II, CPIA Publication 476, 1987, pp. 127-137

[104] Prior, R.C., Fowler, D.K., Mellor, A.M., "Engineering Design Models for Ramjet Efficiency and Lean Blowoff", Journal of Propulsion and Power, Vol. 11, No 1., January-February 1995, pp. 117-123

[105] Sisco J. C., "Autoignition of Kerosene by decomposed Hydrogen Peroxide in a dump combustor configuration", M.S Thesis 2003

[106] Chao, Y.C., Leu, J.H. and Huang, Y.F., "Downstream Boundary Effects on the Spectral Characteristics of a Swirling Flowfield," Experiments in Fluids, Vol.10, 1991, pp.341-348.

[107] Tuttle, J. H., Colket, M. B., Bilger, R. W., and Mellor, A. M., "Characteristic Times for Combustion and Pollutant Formation in Spray Combustion," Sixteenth Symposium (International) on Combustion, Combustion Inst., Pittsburgh, PA, 1976, p. 209-219.

[108] Blazowski, W. S., and Henderson, R. E., "Aircraft Exhaust Pollution and Its Effect on the U.S. Air Force," Air Force Aero Propulsion Lab., AFAPL-TR-74-64, Aug. 1974.

[109] Schmidt, D. A., and Mellor, A. M., "Characteristic Time Correlation for Combustion Inefficiency from Alternative Fuels," Journal of Energy, Vol. 3, No. 3, 1979, pp. 167-176.

[110] Plee, S. L., and Mellor, A. M., "Characteristic Time Correlation for Lean Blowoff of Bluff-Body-Stabilized Flames," Combust. Flame, Vol. 35, May 1979, p. 61-80.

[111] Stull, F. D., Craig, R. R., and Hojnacki, J. T., "Dump Combustor Parametric Investigations," Fluid Mechanics of Combustion, American Society of Mechanical Engineers, New York, 1974, pp. 135-154

[112] AFRPL-TR-67-144, "Hydrogen Peroxide Handbook," Rocketdyne, Inc., July 1967

[113] Drewry, J. E., "Fluid Dynamic Characterization of Sudden-Expansion Ramjet Combustor Flowfields," AIAA Journal, Vol. 16, No. 4, 1978, p. 313-319

[114] Pitz, R. W., Daily, J. W., "Combustion in a Turbulent Mixing Layer Formed at a Rearward-Facing Step," AIAA Journal, Vol. 21, No. 11, November 1983, pp. 1565-1570.

[115] Huang, R. F., Tsai, F. C., "Flow field characteristics of swirling double concentric jets", Exp. Thermal anf Fluid Sci., 25, 151-161, 2001

[116] Lefebvre, A.H., "Gas Turbine – Combustion"; Taylor & Francis, Philadelphia/London, 1999

[117] NASA, "Liquid Rocket Engine Injectors", Space Vehicle Design Criteria (Chemical Propulsion), SP-8089, March 1976

[118] Scharlemann C., Schiebl M., Marhold K., Tajmar M., "Test of a Turbo-Pump Fed Miniature Rocket Engine", AIAA-2006-4551

[119] Scharlemann C., Schiebl M., Marhold K., Tajmar M., "Development and Test of a Miniature Hydrogen Peroxide Monopropellant Thruster", AIAA-2006-4550

[120] Brahmi r., Batonneau Y., Kappenstein C., Miotti P., Tajmar M., Scharlemann C., Lang M., „Ceramic Catalysts fort he decomposition of H2O2. Influence of the wash-coat procedure and the active phase", 8th International Hydrogen Peroxide Propulsion Conference, 2005

[121] Law, C. K., Williams, F. A., "Kinetics and Convection in the Combustion of Alkane Droplets", Combustion and Flame, 19(3): 393-406 (1972)

[122] Turns, S. R., "An Introduction to Combustion. Concepts and Applications", McGraw-Hill, 2000

[123] Rutherford Sris, "Vectors, Tensors, and the Basic Equations of Fluid Mechanics", Dover Publication, 1989

[124] Brikner N. A., Protz J. M., " Modeling of the Decomposition and Combustion of Hydrogen Peroxide and Ethanol for Design of a Bipropellant Microrocket Engine", AIAA 2011-5851